UNIVERSITY OF CALIFORNIA,
IRVINE

Chemical Building Blocks and Models for Studying Peptides

DISSERTATION

submitted in partial satisfaction of the requirements
for the degree of

DOCTOR OF PHILOSOPHY

in Chemistry

by

Xingyue Li

Dissertation Committee:
Professor James S. Nowick, Chair
Professor Zhibin Guan
Professor Chris D. Vanderwal

2022

DEDICATION

To

my family

for their unconditional love and support

and to

my friends

for all the new experiences and growth

TABLE OF CONTENTS

Page

LIST OF FIGURES v

LIST OF TABLES vii

LIST OF SCHEMES viii

ACKNOWLEDGEMENTS ix

VITA x

ABSTRACT OF THE DISSERTATION xv

CHAPTER 1: An Improved Turn Structure for Inducing β-Hairpin Formation in Peptides
- Preface to Chapter 1 1
- Introduction 3
- Results and Discussion 4
- Conclusion 21
- References and Notes 23

Supplementary Information
- Table of Contents 27
- Supporting Figures and Tables 29
- MC/SD Modeling Studies 36
- Bacterial Expression and Chemical Synthesis 36
- Peptide Synthesis 45
- X-ray Crystallography 51
- Circular Dichroism Spectroscopy 52
- NMR Spectroscopy 52
- Characterization Data 56

CHAPTER 2: Enantiomeric β-sheet peptides from AB form homochiral pleated β-sheets rather than heterochiral rippled β-sheets
- Preface to chapter 2 110
- Introduction 112
- Results and Discussion 116
- Conclusion 133
- References and Notes 135

Supplementary Information
- Table of Contents 138
- Supporting Figures and Tables 140
- Peptide Synthesis 151
- ^{15}N-Labeled and Deuterated Amino Acids 154

NMR Spectroscopy 156
Characterization Data 160

CHAPTER 3: Synthesis and stereochemical determination of Novo29, a new peptide antibiotic
Preface to chapter 3 205
Introduction 207
Results and Discussion 209
Future Directions 218
References and Notes 220
Supplementary Information
Table of Contents 222
Supporting Figures and Tables 223
Chemical Synthesis 225
Peptide Synthesis 232
NMR Spectroscopy 235
MIC Assay 236
X-ray Crystallography 237
Characterization Data 240

LIST OF FIGURES

		Page
Figure 1.1	Equilibrium of unfolded and folded methylated ornithine derivatives	5
Figure 1.2	Minimum energy models of folded states	6
Figure 1.3	X-ray crystal structure of peptide **1.1b**	10
Figure 1.4	Circular dichroism spectrum of peptides **1.2a** and **1.2b**	12
Figure 1.5	NOEs of peptides **1.3**, **1.4a**, and **1.4b**	13
Figure 1.6	α-Proton chemical shifts of peptides **1.3**, **1.4a**, and **1.4b**	15
Figure 1.7	Circular dichroism spectrum of peptides **1.3**, **1.4a**, and **1.4b**	17
Figure 1.8	NOEs of peptides **1.5**, **1.6a**, and **1.6b**	18
Figure 1.9	α-Proton chemical shifts of peptides **1.5**, **1.6a**, and **1.6b**	20
Figure 1.10	Circular dichroism spectrum of peptides **1.5**, **1.6a**, and **1.6b**	21
Figure S1.1	MC/SD hydrogen bond simulations	29
Figure S1.2	X-ray crystal structure turn conformation of peptides **1.2a** and **1.2b**	30
Figure S1.3	NOESY spectra for upfield shifting of protons	31
Figure S1.4	^{1}H NMR spectra overlay of dilute and concentrated peptides	33
Figure 2.1	Pleated and rippled β-sheet alignment	113
Figure 2.2	^{1}H NMR overlay of peptide **2.1a**, *ent*-**2.1a**, and mixture	118
Figure 2.3	^{1}H,^{15}N HSQC spectra of peptide **2.2a**	120
Figure 2.4	Cartoon illustrations of mixed assembly	122
Figure 2.5	^{15}N-edited NOESY of peptide **2.2a**	124
Figure 2.6	Expected NOEs in homochiral and heterochiral assemblies	126
Figure 2.7	^{1}H,^{15}N HSQC spectra of peptide **2.3a**	128
Figure 2.8	^{1}H NMR overlay of peptide **2.1b**, *ent*-**2.1b**, and mixture	130
Figure 2.9	^{1}H,^{15}N HSQC spectra of peptide **2.2b**	133
Figure S2.1	EXSY spectrum of peptide **2.1a** with peptide *ent*-**2.1a** at 298K	140
Figure S2.2	Expanded spectrum of peptide **2.1a** with peptide *ent*-**2.1a** at 298K	141

Figure S2.3 EXSY spectrum of peptide **2.1a** with peptide *ent*-**2.1a** at 328K 142
Figure S2.4 Expanded spectrum of peptide **2.1a** with peptide *ent*-**2.1a** at 328K 143
Figure S2.5 DOSY spectrum of 8.0 mM peptide **2.1a** 144
Figure S2.6 DOSY spectrum of 8.0 mM peptide **2.1a** and 8.0 mM peptide *ent*-**2.1a** 145
Figure S2.7 DOSY spectrum of 1.0 mM peptide **2.1b** 146
Figure S2.8 DOSY spectrum of 4.0 mM peptide **2.1b** 147
Figure S2.9 DOSY spectrum of 8.0 mM peptide **2.1b** 148
Figure S2.10 DOSY spectrum of 4.0 mM peptide **2.1b** and 4.0 mM peptide *ent*-**2.1b** 149
Figure S2.11 ^{1}H NMR of commercial deuterated L-phenylalanine 150
Figure 3.1 Structures of Novo29 and teixobactin 209
Figure 3.2 ^{1}H NMR overlay of natural Novo29 and synthetic peptides 214
Figure 3.3 X-ray crystal structure of *epi*-Novo29 217
Figure S3.1 Expanded ^{1}H NMR overlay of natural Novo29 and synthetic peptides 223

LIST OF TABLES

		Page
Table S1.1	X-ray crystallography parameters for peptide **1.1b**	35
Table S2.1	Diffusion coefficients of peptides **2.1a** and *ent*-**2.1a**	144
Table S2.2	Diffusion coefficients of peptides **2.1b** and *ent*-**2.1b**	146
Table 3.1	MIC assay of natural Novo29 and synthetic peptides	216
Table S3.1	X-ray crystallography parameters for *epi*-Novo29	224

LIST OF SCHEMES

		Page
Scheme 1.1	Synthesis of N^{α}-Boc-N^{δ}-Fmoc-γ(*R*)-methyl-ornithine	7
Scheme 3.1	Synthesis of Fmoc-(*2R,3S*)-hydroxyasparagine	211
Scheme 3.2	Synthesis of (*2R,3S*)-hydroxyasparagine containing Novo29	213

ACKNOWLEDGEMENTS

My graduate school experience has been so meaningful and unforgettable; I could not have asked for a better group of people to have shared my growth with. I would like to thank my advisor and committee chair, Prof. James Nowick, for all the valuable advice that he has provided over the years. As both a student and scientist, I admire James for his passion for scientific discovery and his enthusiasm for teaching. Writing with James has been one of the most rewarding experiences for me; I am tremendously proud of the progress that I have made in writing since my first year. Thank you, James, for bearing with all my frustrations and impatience throughout our writing meetings, and I look forward to refining the foundations that you have taught me in the next step of my career.

I want to thank my thesis committee, Prof. Zhibin Guan and Prof. Chris Vanderwal, for their support and guidance throughout my journey. Prof. Guan, I enjoyed our chats whenever we met to discuss my progress, and I appreciate all the advice you have given me over the years. Prof. Vanderwal, thank you for your help and advice on my projects during our meetings together.

I would like to acknowledge undergraduate researchers who I have mentored during my time: Andrew Sabol and Stephanie Rios. Andrew, thank you for putting your faith in me and choosing to work with someone who has not even advanced to candidacy at the time. Your curiosity and tenacity pushed me to do the best that I can, and I could not be more proud to have you as my friend for all the great memories we shared together. Stephanie, thank you for all your help in my last year — without you, I could not have completed my second project in a timely manner. I have enjoyed working with you, and I wish you the best in a future career in the field of forensic science.

To my dear colleagues in the Nowick group: thank you for being the source of comfort and enjoyment. To my friends who have graduated — Dr. Mike Morris, Dr. Tuan Samdin, and Dr. Sheng Zhang — I could not have asked for a better group of seniors to go on fun restaurant adventures and share conference experiences with. To my friends who I have grown with — Maj, Gretchen, Chelsea P., and Chelsea J — I will cherish our inside jokes, sassy banter, and all the other little things that light up my day when time gets tough; you guys are the best. To my overachieving and brilliant juniors — Chris, Jason, and Jackson — I am confident that you will all make amazing discoveries during your time here, and I am excited to hear all about the experiences when we inevitably chat. I want to also thank Dr. Adam Kreutzer and Sarah who provided me with any assistance I needed for crystallography, and for being great lab co-workers.

Most importantly, I would not be where I am without my family. They are my rock. To Mom, Dad, and David, your words of cheer and positivity encourage me to be the best every day. You guys are my pride, joy, and solace; my accomplishments are equally yours as they are mine. Thank you all for being my greatest ally in life.

VITA

Xingyue Li

Chemistry Ph.D. candidate with 3 years of experience in biopharmaceutical industry. Mastery in noncanonical amino acid synthesis, peptide synthesis, and NMR spectroscopy of peptides and small molecules. Proficient in molecular modeling, and preparative HPLC purification. Detail-oriented, highly motivated, and determined problem-solver. Leadership experience in being the lead chemist on a kilo-scale industry project and as the UCI chemistry outreach coordinator.

Education and Graduate Research Experience

Department of Chemistry, UC Irvine – Ph.D. Candidate August 2017 – June 2022
Ph.D. candidate in Prof. James S. Nowick's Laboratory GPA: 3.8/4.0

Organic Synthesis:

- Modeled and developed the synthesis of a protected methylornithine amino acid as a β-turn for inducing β-sheet structure in peptide and with gram-quantity yields.
- Established biocatalysis as a viable strategy to the lab; chemoenzymatic reaction effectively sets the stereochemistry of the methyl group in the first step of the synthesis toward a protected methylornithine.
- Spearheaded and carried out the chemical synthesis of hydroxylated asparagine stereoisomers, which led to correct stereochemical determination of a peptide natural product by NMR spectroscopy.
- Co-authored an R21 grant proposal based on the synthesis of a peptide natural product and its analogues as promising drug candidates; this proposal is expected to be funded based on preliminary scoring.

***Relevant skills*:** molecular modeling, small-molecule synthesis, peptide synthesis, NMR and CD spectroscopy, normal-phase silica gel chromatography, reverse-phase peptide purification, FT-IR, recrystallizations, mass spectrometry

Biology:

- Adapted and executed bacterial transformation, bacteria growth, and protein expression of an enzyme necessary for inducing chemoenzymatic oxidation in the first step of a chemical synthesis.
- Advanced a project on the stereochemical determination of a peptide natural product by corroborating the antibiotic activity of the synthetic and natural peptide using Minimum Inhibitory Concentration (MIC) assay.

***Relevant skills*:** Bacterial transformation, protein expression, SDS-PAGE, Miniprep, MIC assay.

NMR Spectroscopy:

- Elucidated the folding and assignment of six β-hairpin peptides in aqueous conditions through 1D and 2D NMR spectroscopy; key cross-strand NOEs provided convincing evidence β-sheet formation essential for publication.
- Prepared and studied ^{15}N isotopic labeled peptides by ^{1}H,^{15}N HSQC, ^{15}N-edited TOCSY, and ^{15}N-edited NOESY to study self-assembly and co-assembly of enantiomeric peptides, resulting in one of the few in-depth characterizations of a heterochiral oligomer from amyloid β.
- Directed organic spectroscopy graduate student discussion sessions as head TA. Curated high-quality spectra of samples as exam problems. Composed online PDFs of exam problems for smooth transition to virtual format during COVID-19 shutdown.

***Relevant skills*:** ^{1}H, ^{19}F, ^{31}P, COSY, TOCSY, NOESY, ROESY, DOSY, HSQC, ^{15}N-edited TOCSY and ^{15}N-edited NOESY NMR spectroscopy, peptide synthesis, mass spectrometry, and reverse-phase HPLC.

Pharmaceutical Industry Experience

PPD – Biopharmaceutical Department – *Scientist* December 2015 – July 2017

Analytical Chemistry:

- Validated high-priority preclinical drug compounds by using capillary electrophoresis to determine protein degradation.
- Completed projects with demanding timelines, which led to my occasional assignment as a secondary operator on other projects with high-priority and strict-deadlines.

***Relevant skills*:** Capillary electrophoresis (CE), isoelectric capillary electrophoresis (iCE), reverse-phase HPLC, size exclusion chromatography, and ion exchange chromatography.

MilliporeSigma – Manufacturing – *Chemist I* July 2014 – December 2015

Process Chemistry:

- Coordinated between three manufacturing shifts and R&D scientists as the lead chemist on a kilogram-scale product, resulting in a successful and on-time completion of the project with expected yield.
- Worked intimately with both clients and team managers to oversee the success of a project, while building strong communication and presentation skills in adherence to GMP guidelines.

***Relevant skills*:** Documentation of experiments by GMP guidelines, presentation, and use of scale-up equipment such as large-scale jacketed reactors.

R&D systems – Cell Development – *Lab Assistant Internship* June 2011 – August 2011

Biology:

- Adaptable and quick to learn; I was able to independently load, run, and develop Western blots within weeks of starting my position and presented my results to the supervisor on a weekly basis.

Education and Undergraduate Research Experience

Department of Chemistry, UW Madison – Undergraduate Researcher August 2012 – August 2014

B.A. Chemistry, undergrad research with Prof. Samuel H. Gellman

GPA: 3.6/4.0

Peptide Synthesis and Purification:

- Synthesized and purified a library of α-helix peptides containing thioester backbone before the projected deadline, which allowed for more time to perform downstream studies.
- Synthesized two different unnatural amino acids in gram-scale quantities, which ensured adequate material for consistent peptide synthesis.

***Relevant skills*:** peptide synthesis, CD spectroscopy, mass-spectrometry, normal-phase silica gel chromatography, reverse-phase HPLC.

Publications

- Krumberger, M.[1]; **Li, X**.[1]; Kreutzer, A. G.; Peoples, A. J.; Nitti, A. G.; Cunningham, A. M.; Jones, C. R.; Hughes, D. E.; Nowick, J. S. *Manuscript in preparation*.
- **Li, X.**; Rios, S. E.; Nowick, J. S. Enantiomeric Peptides Derived from β-Sheets of Aβ Assemble Selectively as a Homochiral Tetramer. *Chem Sci.* **2022** *ASAP.* DOI: 10.1039/d2sc02080g.
- **Li, X.**; Sabol, A. L.; Wierzbicki, M.; Salveson, P. J.; Nowick, J. S. An Improved Turn Structure for Inducing β-Hairpin Formation in Peptides. *Angew. Chem. Int. Ed.* **2021**, *60,* 22776-22782*.*
- Yang, H; Pishenko, A. V.; **Li, X.**; Nowick, J. S. Design, Synthesis, and Study of Lactam and Ring-Expanded Analogues of Teixobactin. *J. Org. Chem*. **2020**, *85*, 1331-1339.

Leadership and Teaching Experience

Graduate Student NMR Spectroscopy Course Teaching Assistant January 2020 – March 2020

- Created exam problems using challenging heterocyclic small molecules. Samples were analyzed by ^{1}H, ^{13}C, DEPT, COSY, TOCSY, HMQC, HMBC, ROESY, and NOESY experiments. Developed a strong sense for interpreting NMR splitting patterns, and a critical eye for details.

- Orchestrated weekly discussions and additional practice sessions for discussing difficult problem sets for a class of 42 graduate students, resulting in strong communication skills.

UCI Chemistry Outreach Program Coordinator September 2018 – December 2019

- Lead a volunteer-based weekly outreach program to demonstrate chemistry to grade K-12 schools, focusing on primarily underprivileged districts in the Orange and Los Angeles County area. From September 2018 to July 2019, we reached out to approximately 4,000 children, with some demonstrations being over 100 students in an auditorium at once.

Conference Presentations

Division of Organic Chemistry Graduate Research Symposium November 2021
Poster Presentation Albuquerque, NM
Title: An Improved Turn Structure for Inducing β-Hairpin Formation in Peptides
Authors: **Li, X.**; Salveson, P. S.; Sabol, A. S.; Wierzbicki, M.; Nowick, J. S.
Presented at the University of New Mexico

Peptide Therapeutics Symposium October 2021
Poster Presentation La Jolla, CA
Title: Enantiomeric Peptides Derived from β-Sheets of Aβ Preferentially Assemble as a Homochiral Tetramer
Authors: **Li, X.**; Rios, S. E.; Nowick, J. S.
Presented at the SALK Institute of Biological Studies

University of California Chemical Symposium March 2021
Poster Presentation Virtual
Title: Development and Application of a Turn Structure for Studying β-Hairpin Peptides
Authors: **Li, X.**; Sabol, A. L.; Wierzbicki, M.; Salveson, P. J.; Nowick, J. S.

Gordon Research Conference February 2020
Poster Presentation Ventura, CA
Title: An Improved Turn Structure for Inducing β-Hairpin Formation in Peptides
Authors: **Li, X.**; Salveson, P. S.; Sabol, A. S.; Wierzbicki, M.; Nowick, J. S.
Presented at Chemistry and Biology of Peptides Gordon Research Conference (GRC)

Gordon Research Seminar February 2020
Poster Presentation Ventura, CA
Title: An Improved Turn Structure for Inducing β-Hairpin Formation in Peptides
Authors: **Li, X.**; Salveson, P. S.; Sabol, A. S.; Wierzbicki, M.; Nowick, J. S.
Presented at Chemistry and Biology of Peptides Gordon Research Seminar (GRS)

Peptide Therapeutics Symposium October 2019
Poster Presentation La Jolla, CA
Title: A Single Methylation Leads to an Improved β-Turn Mimic for Inducing

β-Hairpin Formation in Peptides
Authors: **Li, X.**; Salveson, P. J.; Sabol, A. L.; Wierzbicki, M.; Nowick, J. S.
Presented at the SALK Institute of Biological Studies

Orange County Section of American Chemical Society (OCACS) September 2017
Poster Presentation Santa Ana, CA
Title: Expanding the Ring of Teixobactin
Authors: Yang, H.; **Li, X.;** Nowick, J. S.
Presented at the Doubletree Club Hotel

Awards

- Peptide Therapeutics Symposium Travel Grant Awardee 2019
- Graduate Division Completion Fellowship 2021
- Peptide Therapeutics Symposium Travel Grant Awardee 2021

ABSTRACT OF THE DISSERTATION

Chemical Building Blocks and Models for Studying Peptides

by

Xingyue Li

Doctor of Philosophy in Chemistry

University of California, Irvine, 2022

Professor James S. Nowick, Chair

Chemical building blocks and models can serve as useful tools and surrogates for mimicking peptides in a biological system. In the following chapters of my thesis, I introduce two noncanonical amino acid building blocks that I have synthesized for incorporation into peptides and evaluate their secondary structure formation or biological activity (chapter 1 and chapter 3). I will also describe the use of chemical models derived from the β-amyloid peptide Aβ to investigate and probe the chiral selectivity in β-sheet assembly in aqueous solution (chapter 2). These three chapters of my thesis represent my passion for organic synthesis and NMR spectroscopy, and are linked by a theme of using building blocks and models to investigate peptide folding, assembly, and activity.

Chapter 1 describes the design, synthesis, and evaluation of an improved turn structure for inducing β-hairpin formation in peptides. This project builds upon a previous finding from our laboratory that δ-linked-ornithine ($^{\delta}$Orn) can be used as suitable turn unit for stabilizing macrocyclic β-sheet peptides. Development of β-turn units as peptidomimetic tools are important for stabilizing the secondary structure of peptides and

have led to the design of biomaterials and potential biomedical therapeutics. Chapter 1 details the development and characterization of γ-methylornithine — a methylated version of $^{\delta}$Orn — and shows its propensity to induce a β-hairpin conformation in comparison to the established turn, D-Pro-Gly. The utility provided by this improved turn structure will add to the existing toolbox of ways to create stabilized macrocyclic β-sheet peptides.

Chapter 2 seeks to answer a basic question: do enantiomeric β-sheet peptides prefer to self-assemble to form pleated β-sheets or co-assemble to form rippled β-sheets? In the past decade, a theory has emerged that enantiomeric β-sheets prefer to co-assemble in a heterochiral fashion to form rippled β-sheets. Our laboratory has previously found that enantiomeric β-sheet pentapeptides strongly prefer to self-assemble. To address this discrepancy, equimolar amounts of L- and D-chemical model peptides derived from Aβ were mixed and studied by solution-phase NMR spectroscopy. These NMR spectroscopic studies reveal that β-sheet peptide models derived from Aβ prefer to self-assemble in a homochiral fashion in aqueous solution. Chapter 2 ends with concluding remarks about our interpretation of the different forces that drive the formation of heterochiral rippled β-sheets vs. homochiral pleated β-sheets.

Chapter 3 is an ongoing collaborative project with members of the lab, on the synthesis and stereochemical determination of Novo29, a new Gram-positive peptide antibiotic discovered by Novobiotic Pharmaceuticals. Novo29 is an 8-residue peptide that contains a noncanonical hydroxyasparagine amino acid at position 5; the stereochemistry of this amino acid is undetermined. Chapter 3 begins with the syntheses of two diastereomers of hydroxyasparagine containing either the *R,R* or the *R,S* stereochemistry at

the α- and β-positions. Incorporation of the hydroxyasparagine amino acids into peptides enabled the stereochemical determination of the natural Novo29 through NMR spectroscopic studies and functional correlation assays. At the end of chapter 3, a 1.13 Å X-ray crystallographic structure of the synthetic peptide containing the *R,S* stereochemistry is presented and discussed in further detail. Future directions for this project will aim to generate a molecular model of the peptide containing *R,R* stereochemistry in order to provide an explanation into the potential mechanism of action of the natural Novo29 antibiotic.

CHAPTER 1

An Improved Turn Structure for Inducing β-Hairpin Formation in Peptides

Preface to Chapter 1

Chapter 1 revisits a previously reported finding of the δ-linked ornithine turn unit from our laboratory in 2003 and aims to bring a significant improvement for inducing β-sheet secondary structure in peptides. This project was initiated by Dr. Patrick Salveson, who used computational modeling to find that the introduction of a single methyl group to the side chain of ornithine dramatically increased its propensity to fold into a β-turn-like conformation. Using MacroModel, I replicated the simulations with an expanded portfolio of functional groups and developed and executed a synthesis to obtain the desired methylated ornithine amino acid. What I could not have anticipated at that time was that three and a half years later, I would be wrapping up the project by adding a diverse set of skills to my repertoire, including computational modeling, biological expression, small-molecule synthesis, and peptide NMR spectroscopy.

I am tremendously grateful to my former colleagues who have made this project possible — their contribution, advice, and guidance allowed me to put together a project that boasts a wide array of skills. Dr. Patrick Salveson worked on the early ideas of improving the ornithine turn unit through MCSD calculations in MacroModel and I feel fortunate to be able to expand on those findings after his graduation. I also got to work with

a talented peptide crystallographer, Dr. Michał Wierzbick, who helped me with solving the crystal structure of crystals that I grew containing my new and improved γ-methylornithine turn within a peptide. Finally, I am thankful for having such a dedicated undergraduate, Andrew Sabol, who assisted me in the routine biological expression in the first step of my synthesis and who pushed me to bring my best effort to lab every day.

The introduction of Chapter 1 begins with a brief history recapitulating some of the seminal works in the development of β-turns over the last decades, and lists examples of their applications in contemporary work. The results and discussion section describe the chronological sequence of experiments from the initial computational work to evaluation of peptides with the synthetic methylornithine. To evaluate the potential of the new methylornithine turn, I took meticulous effort to characterize and compare the folding of peptides containing a D-Pro-Gly, L-ornithine, and methylornithine turn unit. Based on the results of my studies, the conclusion is that the methylornithine turn presents a viable addition to the toolbox of β-turn units for stabilizing β-hairpin conformations in peptides.

Chapter 1 is adapted from and or taken verbatim from Li, X.; Sabol, A. L.; Wierzbicki, M.; Salveson, P. J.; Nowick, J. S. An Improved Turn Structure for Inducing β-Hairpin Formation in Peptides. *Angew. Chem. Int. Ed.* **2021**, *60,* 22776-22782*.*

INTRODUCTION

Although almost three decades have elapsed since initial reports of small peptides that fold to form β-hairpins in aqueous solution, there is still no universal tool to coax any small peptide to adopt a β-hairpin conformation, regardless of sequence. β-Hairpins occur widely in folded peptides and proteins and are defined by two hydrogen-bonded antiparallel β-strands connected by a short loop. Even though β-hairpins are nearly ubiquitous within proteins, most β-hairpins will not retain a folded structure in aqueous solution when excised from the protein. Instead, most peptides that fold into β-hairpins in aqueous solution require relatively specific sequences for the β-strands and loop. One approach to stabilizing β-hairpin formation in peptides involves replacing the loop region with a turn template.[1–8] The template mimics the loop and enforces proximity, hydrogen bonding, and an antiparallel alignment between the β-strands.

Early efforts to stabilize β-hairpins involved turn templates composed of either α-amino acids or other amino acid building blocks. A D-proline residue at the *i+1* position proved particularly effective for driving the formation of a β-turn. Balaram and co-workers first observed the D-Pro-L-Pro motif acting as a turn in the X-ray crystal structure of pivaloyl-D-Pro-L-Pro-L-Ala-*N*-methylamide, and later reported the crystal structure of a designed octapeptide containing a D-Pro-Gly sequence that folds as a β-hairpin.[9,10] Gellman and co-workers subsequently demonstrated that D-Pro-Gly is favorable for inducing a β-hairpin conformation in aqueous solution in several model peptide sequences.[11–13] Not all turn templates are composed of α-amino acids. Kelly and co-workers demonstrated that a dibenzofuran amino acid can induce a β-sheet structure in analogues of gramicidin S.[14] A

number of other cleverly designed templates based on aromatic and alkene scaffolds have also been described.[15–18]

Amongst the turn templates reported to date, the D-Pro-L-Pro and D-Pro-Gly turn templates have emerged as favorites for stabilizing useful β-hairpin peptides. Schneider and co-workers have developed a series of biomaterials based on MAX1, a β-hairpin peptide containing the D-Pro-L-Pro turn motif that self-assembles into a hydrogel.[19] Further investigations of MAX1 have revealed antibacterial properties for non-sterile injections and lead to other analogues with useful attributes.[20,21] Robinson and co-workers have applied the D-Pro-L-Pro turn to construct cyclic β-hairpin peptides inspired by natural antibiotics. These peptidomimetic antibiotics exhibit enhanced activity and have revealed lipopolysaccharide transport proteins as cellular targets in the outer membrane of Gram-negative bacteria.[22–24] Wetzel and co-workers have used the D-Pro-Gly turn motif to create polyglutamine-containing β-hairpin peptides as chemical models for the aggregation of polyglutamine-containing proteins in Huntington's disease.[25–26]

In 2003, our laboratory introduced δ-linked ornithine ($^{\delta}$Orn) as a new turn-forming unit to induce a β-hairpin conformation in peptides.[27] We have subsequently used the $^{\delta}$Orn turn unit to stabilize a growing repertoire of macrocyclic β-hairpin peptides — containing sequences from Aβ,[28–30] α-synuclein,[31] IAPP,[32] and β2-microglobulin[33] — to provide insight into the structures of amyloid oligomers.[34] In the current study, we set out to improve the $^{\delta}$Orn turn. Here, we report that introduction of a single methyl group at the γ-position with *R* stereochemistry substantially improves folding of the $^{\delta}$Orn turn unit.

RESULTS AND DISCUSSION

Design of an improved δ-linked ornithine turn. We hypothesized that the introduction of a methyl group into the side chain of ornithine, at the right position and with the right stereochemistry, might limit the number of unfolded conformers and thus favor a folded β-turn conformation. We used Monte Carlo Stochastic Dynamics (MC/SD) calculations to guide the design of a methylated $^{\delta}$Orn turn with improved folding properties.[35,36] We examined the equilibrium between the unfolded and folded states of the methylated ornithine derivatives shown in Figure 1.1 by MC/SD simulation in MacroModel using the MMFFs force field with GB/SA water solvation at 300 K. We explored the effect of methylation at the β-, γ-, and δ-positions and found that methylation at the γ-position with *R* stereochemistry shifts the equilibrium from 0.8% folded (for the unmethylated ornithine) to 20.3% folded — an enhancement of 2.08 kcal/mol (Figure S1.1). Molecular modeling studies suggest that other than enhanced folding, there should be little difference between the γ(*R*)-methyl-ornithine turn and the unmethylated ornithine turn, as the minimum-energy turn conformations (local minima) of the ornithine derivatives are virtually identical (Figure 1.2). These simulations provided us with the confidence to pursue the synthesis and study of turn formation by γ(*R*)-methyl-ornithine.

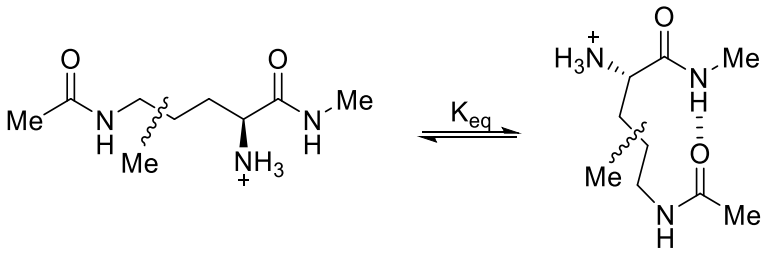

Figure 1.1. Equilibrium between unfolded and folded conformations of methylated ornithine derivatives.

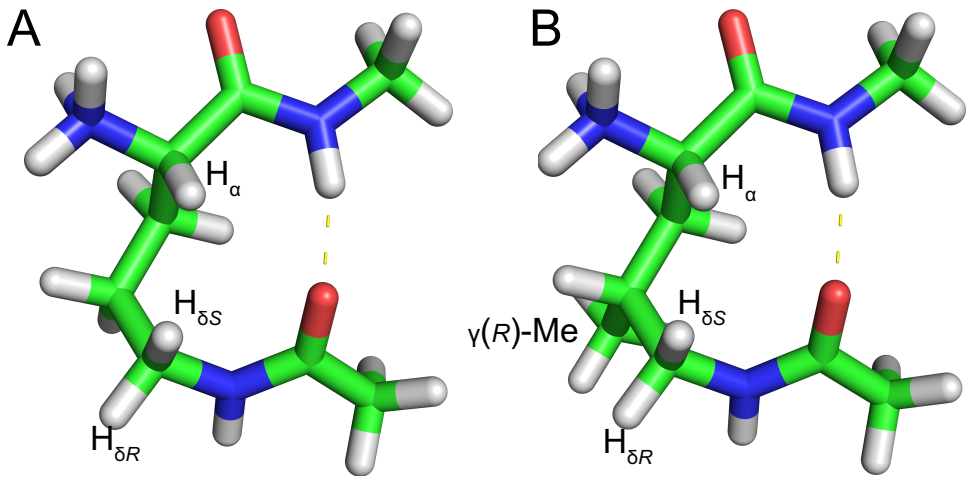

Figure 1.2. Minimum-energy models (local minima) of ornithine and γ(*R*)-methyl-ornithine derivatives Ac-$^{\delta}$Orn-NHMe (A) and Ac-$^{\delta}$MeOrn-NHMe (B) in folded conformations.

Synthesis of orthogonally protected γ(R)-methyl-ornithine. We have developed a synthesis of orthogonally protected γ(*R*)-methyl-ornithine as a building block suitable for use in standard Fmoc-based solid-phase peptide synthesis. The synthesis begins with L-leucine and relies on the recently reported finding by Renata and co-workers that L-leucine can be chemoenzymatically oxidized to 4-hydroxyleucine **1.2** with high stereoselectivity and that the resulting product can be isolated as the Boc-protected lactone **1.3**.[37]

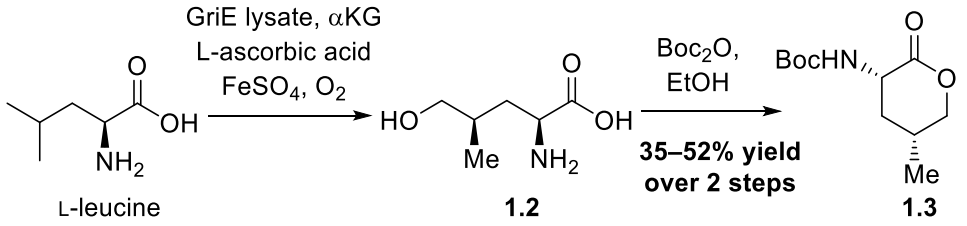

Ring opening of the lactone was achieved by treatment with *N,O*-dimethylhydroxylamine hydrochloride and trimethylaluminum to afford the Weinreb

amide (Scheme 1.1). The liberated alcohol group was then converted to the corresponding mesylate using methanesulfonyl chloride, resulting in an overall two-step transformation with 71% yield of the mesylated intermediate **1.4**. This procedure was previously reported by the Renata group en route to (*2S,4R*)-N^{α}-Boc-methylproline, but the intermediate **1.4** was not isolated.[38]

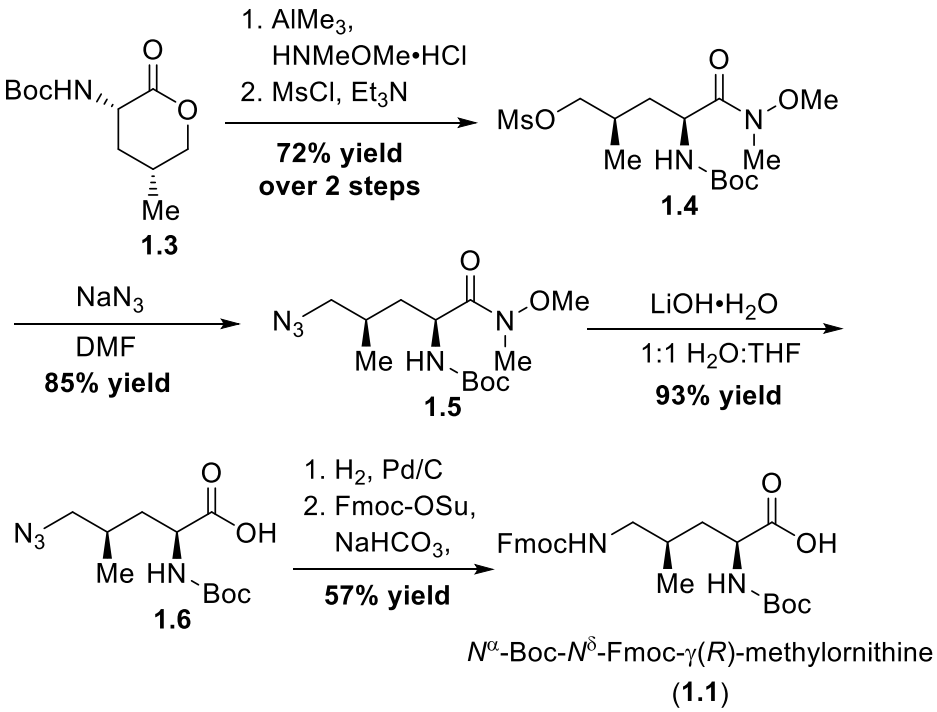

Scheme 1.1. Synthesis of N^{α}-Boc-N^{δ}-Fmoc-γ(*R*)-methyl-ornithine (**1.1**) from Boc-protected lactone **1.3**.

Displacement of the mesylate group with sodium azide afforded the Weinreb protected azidoleucine **1.5** in 85% yield. The reaction was run at 70 °C to increase solubility of sodium azide in dimethylformamide and facilitate S_N2 displacement. Subsequent hydrolysis of the Weinreb amide with lithium hydroxide at 55 °C in a 1:1

mixture of water and THF furnished the Boc-azidoleucine intermediate **1.6** in a 93% yield. Reduction of the azide group to the corresponding amine was then carried out by catalytic hydrogenation with H_2 and Pd/C, followed by Fmoc protection with Fmoc-OSu in a 1:1 mixture of water and THF to give N^{α}-Boc-N^{δ}-Fmoc-γ(*R*)-methyl-ornithine (**1.1**, Boc-MeOrn(Fmoc)-OH) in gram quantities and a yield of 57% over the two steps.

X-ray crystallographic structure of a macrocyclic β-hairpin peptide containing the $^{\delta}$*MeOrn turn*. To confirm the stereochemistry and conformation of the $^{\delta}$MeOrn turn unit within a β-hairpin motif, we turned to X-ray crystallography. Our laboratory has previously reported the X-ray crystallographic structure of a β-hairpin peptide derived from β2-microglobulin (peptide **1.1a**, PDB 4P4Z).[33] Peptide **1.1a** is a macrocyclic β-hairpin peptide containing two heptapeptide strands linked by two $^{\delta}$Orn turn units. In the X-ray crystallographic structure of peptide **1.1a**, only one of the two $^{\delta}$Orn turn units (right side) adopts the characteristic hydrogen-bonded turn conformation shown in Figure 1.2A. The other $^{\delta}$Orn turn unit (left side) does not adopt this hydrogen-bonded conformation. To visualize the $^{\delta}$MeOrn turn unit and determine whether it adopts the hydrogen-bonded conformation hypothesized in Figure 2B, we prepared homologue **1.1b** and studied its structure by X-ray crystallography (PDB 7LIB).

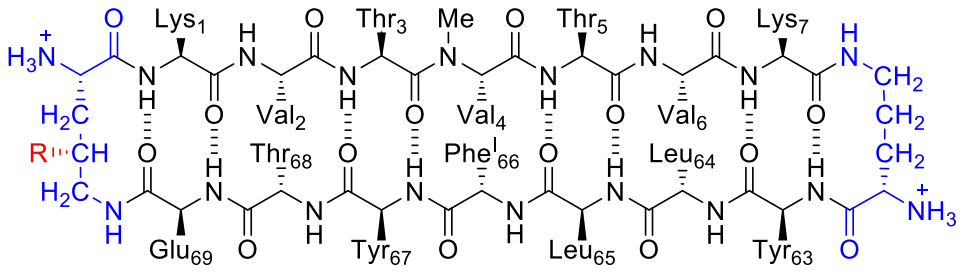

peptide **1.1a** R = H; peptide **1.1b** R = Me

We crystallized peptide **1.1b** using similar conditions to those used for peptide **1.1a** and determined the X-ray crystallographic structure at 1.1 Å. In the X-ray crystallographic structure, peptide **1.1b** adopts a well-defined macrocyclic β-hairpin conformation (Figure 1.3A). The $^{\delta}$MeOrn turn unit adopts the hypothesized hydrogen-bonded conformation, with the γ(*R*)-methyl group clearly visible in the electron density map (Figure 1.3B). The conformation of the $^{\delta}$MeOrn turn unit in peptide **1.1b** is particularly noteworthy, since the corresponding $^{\delta}$Orn turn unit in peptide **1.1a** does not adopt this well-defined hydrogen-bonded conformation (Figure S1.2). The improved folding of this turn in peptide **1.1b** corroborates the MC/SD prediction that the $^{\delta}$MeOrn turn unit is superior to the $^{\delta}$Orn turn unit.

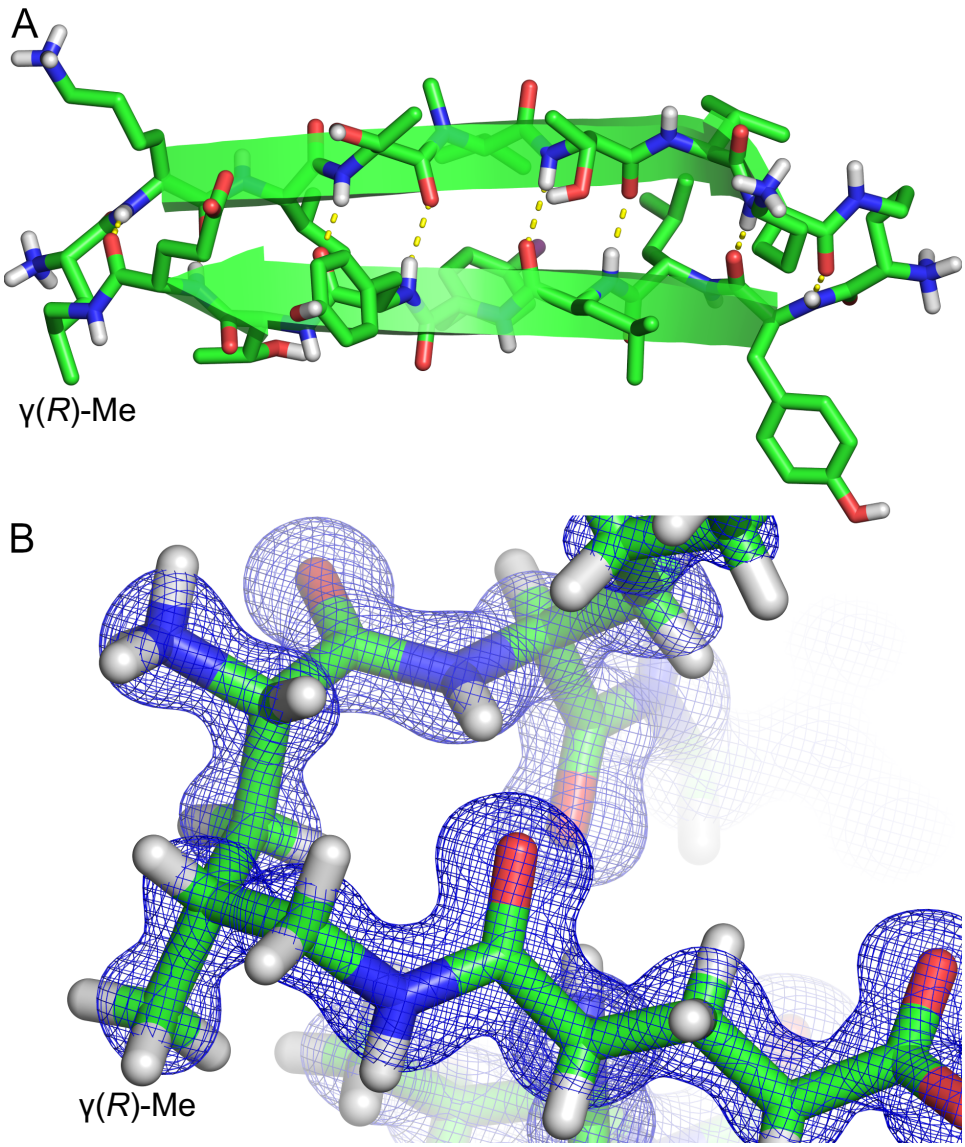

Figure 1.3. (A) X-ray crystallographic structure of peptide **1.1b**. (B) $2F_O$-F_C electron density map contoured at the 1 sigma level, showing the conformation of the $^{\delta}$MeOrn turn unit and the stereochemistry of the γ-carbon.

Circular dichroism (CD) spectroscopic studies of a macrocyclic β-hairpin peptide containing the $^{\delta}$MeOrn turn. To investigate the propensity of the $^{\delta}$MeOrn turn unit to induce β-hairpin formation in the solution state, we compared a macrocyclic β-hairpin peptide containing two $^{\delta}$MeOrn turn units to a homologue containing two $^{\delta}$Orn turn units by CD

spectroscopy. Our laboratory has previously described the X-ray crystallographic structure of a β-hairpin peptide derived from the β-amyloid peptide Aβ (peptide **1.2a**).[28] Peptide **1.2a** contains a heptapeptide strand derived from $A\beta_{17-23}$ and a heptapeptide strand derived from $A\beta_{30-36}$, which are linked by two $^{\delta}$Orn turns to form a macrocycle. The CD spectrum of peptide **1.2a** exhibits an extended region of negative ellipticity below 250 nm, with a minimum at 202 nm and an additional small minimum at 192 nm (Figure 1.4). These features reflect a predominance of random coil structure in aqueous solution, even though the peptide adopts a β-hairpin conformation in the crystal state.

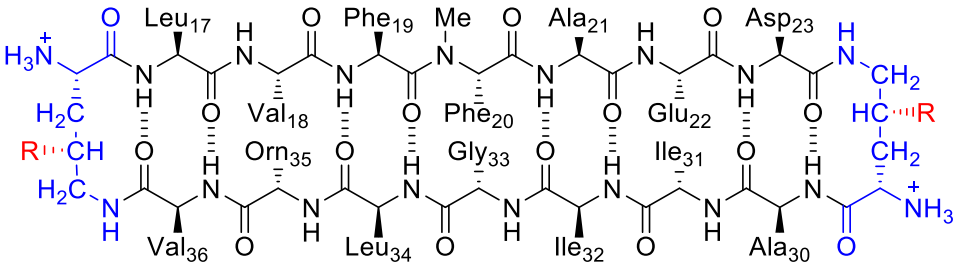

peptide **1.2a** R = H; peptide **1.2b** R = Me

Replacement of the two $^{\delta}$Orn turn units with $^{\delta}$MeOrn turn units affords peptide **1.2b**. The CD spectrum of peptide **1.2b** shows a well-defined minimum centered at 216 nm, with a maximum positive ellipticity at ca. 194 nm (Figure 1.4). These features suggest a predominance of β-sheet character. The striking difference between the CD spectra of peptides **1.2a** and **1.2b** provides additional evidence that the $^{\delta}$MeOrn turn is more effective at inducing a β-hairpin conformation than the $^{\delta}$Orn turn.

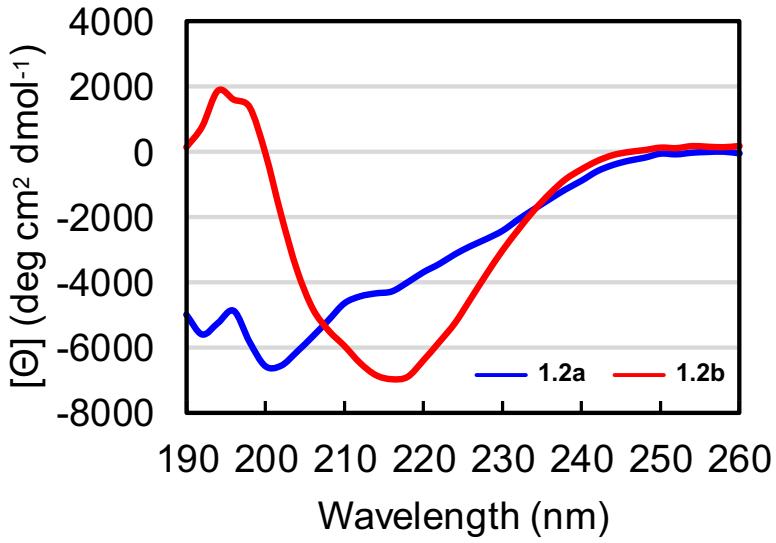

Figure 1.4. CD spectra of peptides **1.2a** (blue) and **1.2b** (red). CD spectra were acquired for each peptide at 150 μM in 10 mM phosphate buffer at pH 7.4; the ellipticity was normalized for the number of residues in each peptide.

NMR and CD spectroscopic studies of β-hairpin peptides containing D*-Pro-Gly,* $^{\delta}$*Orn, and* $^{\delta}$*MeOrn turns*. To further evaluate the propensity of the $^{\delta}$MeOrn turn unit to induce β-hairpin formation in solution, we used NMR spectroscopy to compare a set of β-hairpin peptides containing D-Pro-Gly, $^{\delta}$Orn, and $^{\delta}$MeOrn turns. In 1998, Gellman and co-workers reported that a turn comprising D-Pro-Gly induces a β-hairpin conformation in peptide **1.3**, a 12-residue linear peptide.[12] We prepared peptides **1.4a** and **1.4b** as homologues of peptide **1.3** in which the D-Pro-Gly turn is replaced by $^{\delta}$Orn and $^{\delta}$MeOrn turn units. We used TOCSY and NOESY experiments in D_2O and in 90:10 H_2O:D_2O to assign key NOE crosspeaks associated with β-hairpin folding for each of the three peptides (Figure 1.5).

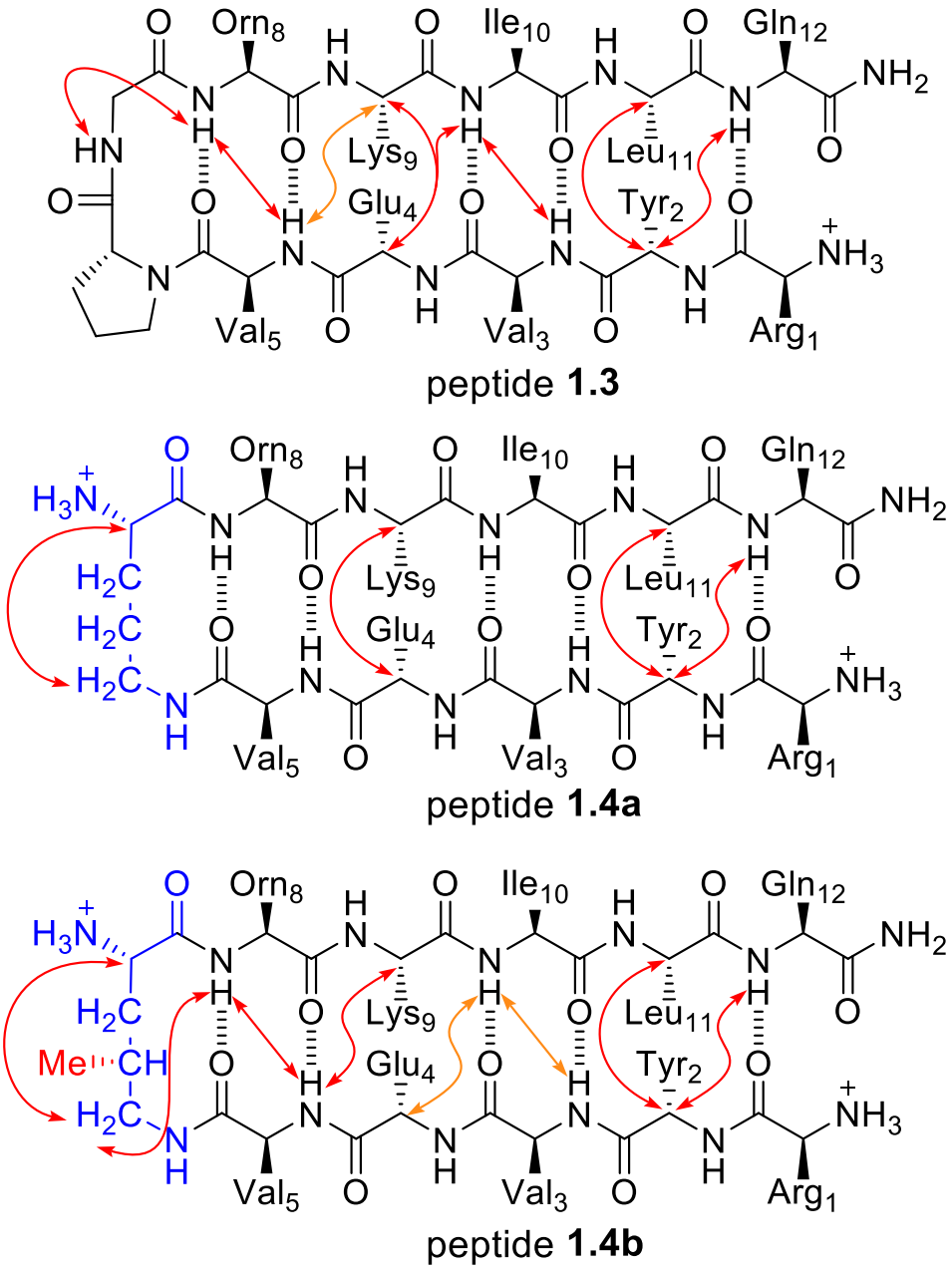

Figure 1.5. Chemical structures of peptide **1.3** and homologues **1.4a** and **1.4b**. Key NOEs associated with solution-state folding for each peptide are represented with double-headed arrows. Red arrows represent unambiguous NOEs. An orange arrow in peptide **1.3** and two orange arrows in peptide **1.4b** represent NOEs in which overlap with other resonances preclude unambiguous assignment. The resonances of the α-protons of Lys_9 and Glu_4 are nearly coincident in peptide **1.4b**, preventing identification of an NOE between these protons. NMR spectra were acquired for each peptide at 4.0 mM and 277 K in D_2O or 90:10 H_2O:D_2O, with a buffer of 100 mM CD_3COOD and 100 mM CD_3COONa.

The NOEs represented in Figure 5 for peptides **1.3**, **1.4a**, and **1.4b** suggest that all three peptides adopt a folded conformation in aqueous solution. Peptides **1.3** and **1.4b** exhibit an extensive network of cross-strand NOEs associated with hydrogen-bonded β-hairpin formation. An expected NOE between the α-protons of Lys_9 and Glu_4 could not be observed in peptide **1.4b**, because the α-proton resonances occur at very similar chemical shifts ($\Delta\delta$ = 0.03 ppm). Unlike peptides **1.3** and **1.4b**, peptide **1.4a** exhibits only three key cross-strand NOEs, which suggests that it is less well-folded than peptides **1.3** and **1.4b**.

In addition to the cross-strand NOEs, each of the peptides also exhibits key NOEs associated with turn formation (Figure 5). Peptide **1.3** exhibits an NOE between the NH protons of Orn_8 and Gly_7. Peptide **1.4b** exhibits NOEs between the NH proton of Orn_8 and the δ-protons of $^{\delta}$MeOrn. Peptide **1.4b** also displays NOEs between the α-proton and δ-protons of $^{\delta}$MeOrn. Peptide **1.4a** only exhibits NOEs between the α-proton and δ-protons of $^{\delta}$Orn. The diastereotopic δ-proton resonances of the $^{\delta}$MeOrn turn in peptide **1.4b** are separated by 0.72 ppm, reflecting the formation of a well-defined turn conformation, in which the *pro-S* δ-proton is proximal to the Val_5 carbonyl group.[39] In contrast, the diastereotopic δ-proton resonances of the $^{\delta}$Orn turn in peptide **1.4a** are only separated by 0.14 ppm, reflecting the formation of a significantly less well-defined turn structure.

To further compare the folding of peptides **1.3**, **1.4a**, and **1.4b**, we examined the chemical shifts of the α-protons, which are widely used to probe the secondary structure of peptides and proteins.[40–44] The chemical shifts of α-protons in a β-sheet are typically more downfield than those of a random coil or an α-helix. The differences between the α-proton chemical shifts of peptides **1.3**, **1.4a**, and **1.4b** and those of a random coil are plotted in

Figure 1.6. In this figure, residues 2–4 and 8–11 are grouped together, because they represent regions of the β-hairpin that can be compared in a meaningful fashion across peptides **1.3**, **1.4a**, and **1.4b**. Residues 1, 5, and 12 are grouped separately, because they either terminate the β-hairpin are attached to the differing turn units.[45,46]

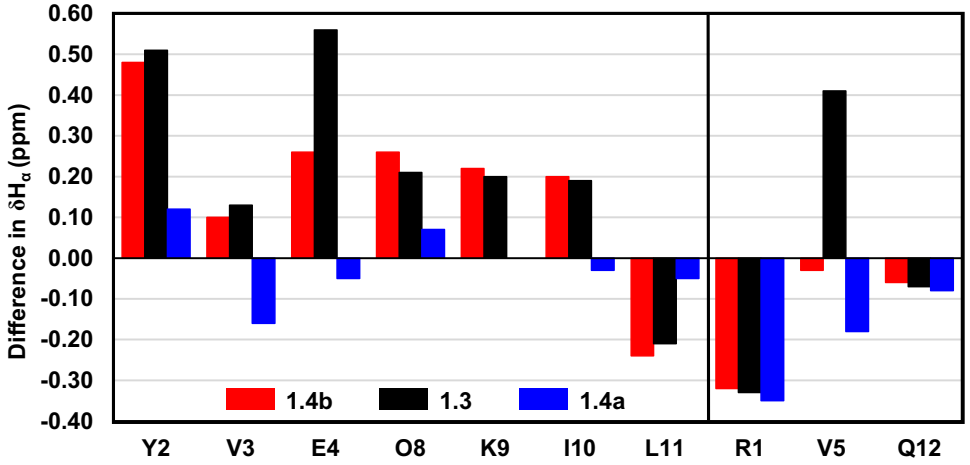

Figure 1.6. Chemical shift differences between the α-protons of each residue in peptides **1.3** (black), **1.4a** (blue), and **1.4b** (red) and random coil values reported by Wüthrich.[44] NMR spectra were acquired for each peptide at 4.0 mM and 277 K in D_2O in a buffer of 100 mM CD_3COOD and 100 mM CD_3COONa with 0.06 mM DSA as a reference standard.[47]

The difference in α-proton chemical shifts relative to random coil values for residues 2–3 and 8–11 of peptide **1.4b** are similar to those of peptide **1.3**, with all but residue 11 shifted substantially downfield. This downfield shifting reflects β-hairpin formation and suggests that both peptides exhibit comparable degrees of β-hairpin folding. The α-protons of Leu_{11} in peptides **1.3** and **1.4b** are shifted upfield by ca. 0.2 ppm, which may result from the proximity of the aromatic ring of Tyr_2. The α-proton of Glu_4 in peptide

1.3 is substantially downfield to that of peptide **1.4b** ($\Delta\delta$ = 0.30 ppm), suggesting subtle differences in the folded β-hairpin conformations of the two peptides.

The chemical shifts of the α-protons of peptide **1.4a** are similar to those observed for a random coil (Figure 6), suggesting that peptide **1.4a** does not form a well-folded β-hairpin. This result seems to contradict the NOEs observed for peptide **1.4a** (Figure 1.5) and may reflect that peptide **1.4a** adopts an ensemble of poorly folded β-hairpin conformations, with significant cross-strand proximity between Leu_{11} and Tyr_2 and between Lys_9 and Glu_4. Taken together, the NOE and chemical shift data suggest that peptide **1.4a** exhibits substantially less β-hairpin formation than peptides **1.3** and **1.4b**.

The CD spectrum of peptide **1.3** exhibits a well-defined negative ellipticity centered at 215 nm and a maximum positive ellipticity centered at 201 nm, reflecting a β-sheet-like conformation (Figure 1.7). The CD spectrum of peptide **1.4b** has a broader minimum at ca. 205–220 nm and a second minimum centered at 196 nm, indicating a mixture of β-sheet and random coil conformations. The CD spectrum of peptide **1.4a** displays a strong minimum at 197 nm, with a small inflection at ca. 217 nm, suggesting a predominance of random coil conformation. These observations corroborate the substantial improvement of the $^{\delta}$MeOrn turn over the $^{\delta}$Orn turn in inducing β-hairpin formation in peptides, while also suggesting that the D-Pro-Gly turn is superior to the $^{\delta}$MeOrn turn.

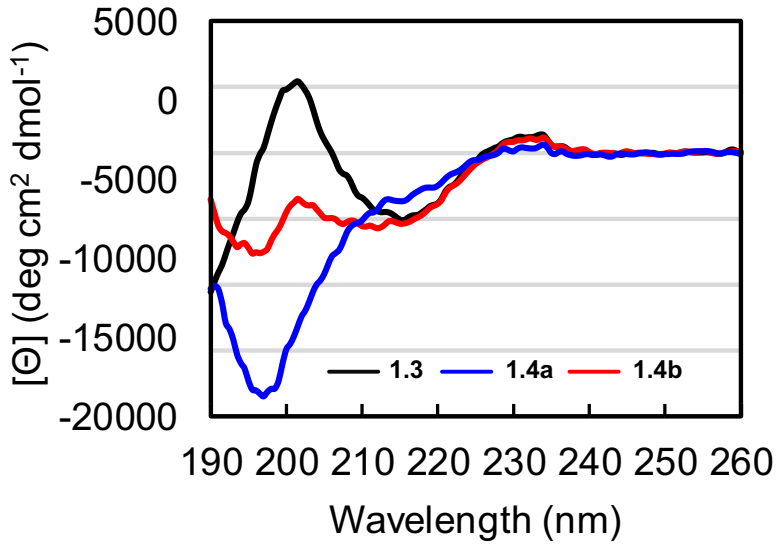

Figure 1.7. CD spectra of peptides **1.3** (black), **1.4a** (blue), and **1.4b** (red). CD spectra were acquired for each peptide at 100 μM in 10 mM phosphate buffer at pH 7.4; the ellipticity was normalized for the number of residues in each peptide.

NMR and CD spectroscopic studies of a second set of β-hairpin peptides. We further investigated the effect of the $^{\delta}$MeOrn turn with a second β-hairpin peptide reported by the Gellman group, peptide **1.5**.[13] We prepared peptides **1.6a** and **1.6b** as homologues of peptide **1.5** in which the D-Pro-Gly turn is replaced by $^{\delta}$Orn and $^{\delta}$MeOrn turn units. The NOEs represented in Figure 8 for peptides **1.5**, **1.6a**, and **1.6b** suggest that all three peptides adopt a folded conformation in aqueous solution. All three peptides exhibit an extensive network of cross-strand NOEs associated with hydrogen-bonded β-hairpin formation. An expected NOE between the NH protons of Thr_{10} and Gln_3 could not be observed in peptides **1.6a** and **1.6b**, because the NH proton resonances occur at very similar chemical shifts ($\Delta\delta$ = 0.03 ppm).

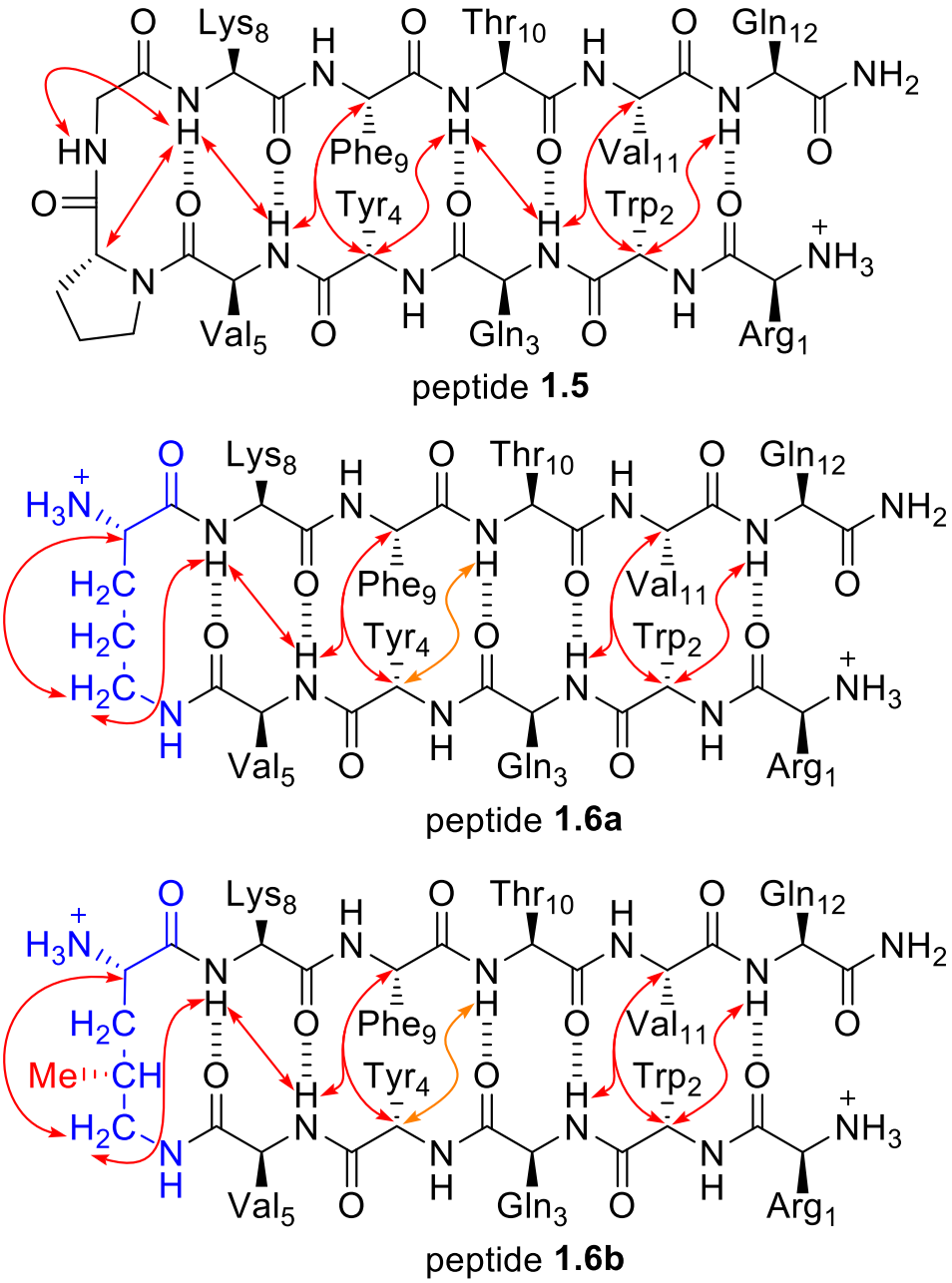

Figure 1.8. Chemical structures of peptide **1.5** and homologues **1.6a** and **1.6b**. Key NOEs associated with solution-state folding for each peptide are shown with double-headed arrows. An orange arrow in peptides **1.6a** and **1.6b** represent NOEs in which overlap with other resonances preclude unambiguous assignment. The resonances of the NH protons of Thr_{10} and Gln_3 are nearly coincident in peptides **1.6a** and **1.6b**, preventing identification of an NOE between these protons. NMR spectra were acquired for each peptide at 4.0 mM and 277 K in D_2O or 90:10 H_2O:D_2O, with a buffer of 100 mM CD_3COOD and 100 mM CD_3COONa.

Peptides **1.5**, **1.6a**, and **1.6b** each show NOE patterns associated with turn formation. Peptide **1.5** exhibits NOEs between the NH proton of Lys_8 and both the NH proton of Gly_7 and α-proton of $D\text{-}Pro_6$ (Figure 1.8). Peptide **1.6a** displays NOEs between the NH proton of Lys_8 and the δ-protons of $^{\delta}Orn$. Peptide **1.6a** also displays NOEs between the α-proton and δ-protons of $^{\delta}Orn$. Peptide **1.6b** has the same pattern of NOEs associated with the $^{\delta}MeOrn$ turn. The diastereotopic δ-proton resonances of the $^{\delta}MeOrn$ turn in peptide **1.6b** are separated by 0.89 ppm, indicating that the turn is well-folded, while the diastereotopic δ-proton resonances of the $^{\delta}Orn$ turn in peptide **1.6a** are separated by 0.35 ppm, reflecting only moderate folding.[39]

The α-proton chemical shifts of peptides **1.5**, **1.6a**, and **1.6b** suggest that peptides **1.6a** and **1.6b** fold in a similar fashion to each other but a different fashion from peptide **1.5** (Figure 1.9). In both peptides **1.6a** and **1.6b**, the α-protons of Trp_2, Gln_3, Lys_8, Phe_9, and Thr_{10} are shifted downfield, while the α-protons of Tyr_4 and Val_{11} are shifted upfield. The downfield shifting for Trp_2, Gln_3, Lys_8, Phe_9, and Thr_{10} is greater in peptide **1.6b** than in **1.6a**, reflecting a greater degree of folding for peptide **1.6b**. Peptide **1.5** exhibits a somewhat different pattern of chemical shifts, with the α-proton of Gln_3 showing only slight downfield shifting, the α-proton of Phe_9 showing slight upfield shifting, and the α-proton of Tyr_4 showing substantial downfield shifting. These differences may result from subtle differences in the β-hairpin conformations of the peptides, with the magnetic anisotropies from the aromatic rings of Trp_2, Tyr_4, and Phe_9 affecting the chemical shifts of many of the α-protons (Figure S1.3).

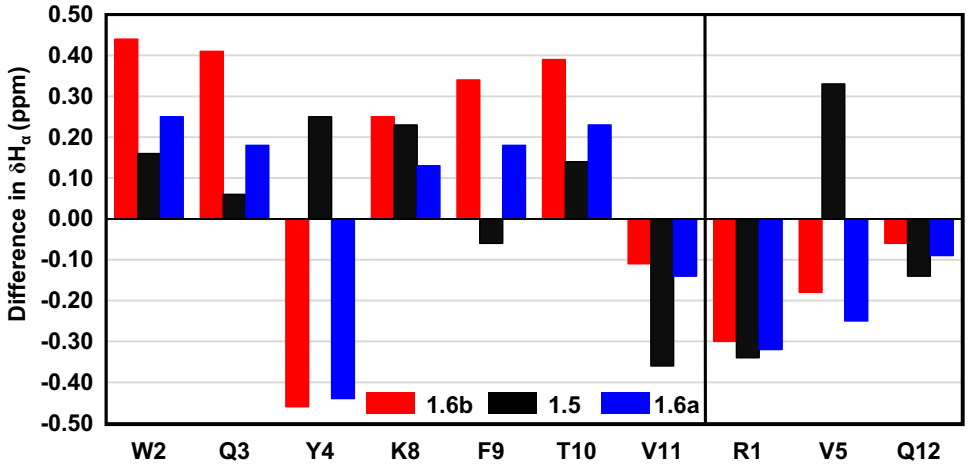

Figure 1.9. Chemical shift differences between the α-protons of each residue in peptides **1.5** (black), **1.6a** (blue), and **1.6b** (red) and random coil values reported by Wüthrich.[44] NMR spectra were acquired for each peptide at 4.0 mM and 277 K in D_2O in a buffer of 100 mM CD_3COOD and 100 mM CD_3COONa with 0.06 mM DSA as a reference standard.[47]

The CD spectrum of peptide **1.5** has a maximum at 230 nm, a broad minimum at ca. 210–220 nm and a second more intense minimum at 200 nm, reflecting a mixture of β-sheet and random coil conformations (Figure 1.10). The CD spectrum of peptide **1.6b** is similar to peptide **1.5**, but with a more intense minimum at ca. 204–208 nm instead of ca. 210–220 nm. The combination of minima at 200 nm and at ca. 204–208 nm in peptide **1.6b** suggest a mixture of β-sheet and random coil conformations, with the shifted minimum at ca. 204–208 nm reflecting significant contributions from the packing of the aromatic residues. The CD spectrum of peptide **1.6a** exhibits a pair of small minima at 196 nm and 200 nm, reflecting a predominance of random coil conformations. These observations stand in agreement with our findings that the $^{\delta}$MeOrn turn is more effective than the $^{\delta}$Orn turn in inducing β-hairpin formation in peptides.

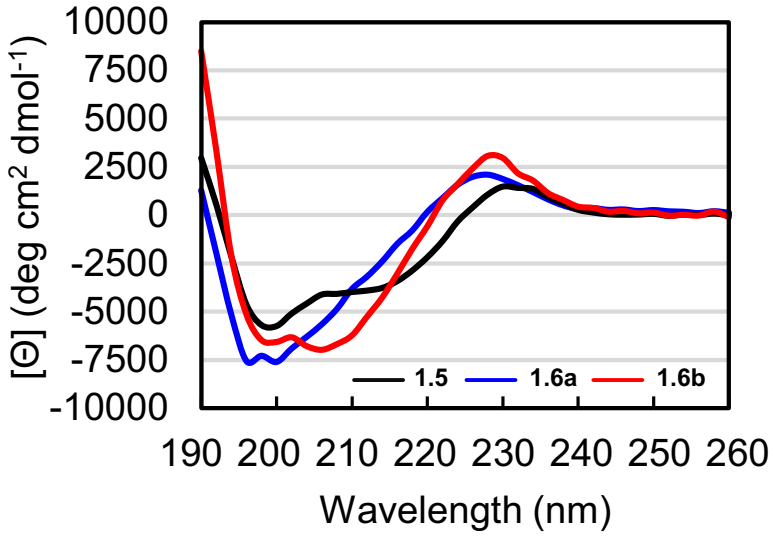

Figure 1.10. CD spectra of peptides **1.5** (black), **1.6a** (blue), and **1.6b** (red). CD spectra were acquired for each peptide at 100 μM in 10 mM phosphate buffer at pH 7.4; the ellipticity was normalized for the number of residues in each peptide.

CONCLUSION

Stereospecific incorporation of a single methyl group substantially enhances the propensity of δ-linked ornithine to induce β-hairpin formation in peptides. A recently reported chemoenzymatic hydroxylation of L-leucine selectively sets the *R* stereochemistry of the methyl group at the γ-position and enables the subsequent gram-scale synthesis of the protected γ(*R*)-methyl-ornithine derivative, Boc-MeOrn(Fmoc)-OH. This derivative bears orthogonal protecting groups compatible with solid-phase peptide synthesis and can be readily incorporated into different peptide sequences.

The X-ray crystallographic structure of peptide **1.1b** unambiguously confirms the stereochemistry of the methyl group and the predicted hydrogen-bonded conformation of the $^{\delta}$MeOrn turn. CD spectroscopic studies of peptides **1.2a** and **1.2b** reveal a distinct improvement in β-hairpin folding when both the $^{\delta}$Orn turns are replaced with $^{\delta}$MeOrn

turns. NMR and CD spectroscopic studies of β-hairpin peptides **1.3**–**1.6** also indicate a substantial improvement in β-hairpin folding induced by $^{\delta}$MeOrn. NMR and CD spectroscopic studies further indicate comparable β-hairpin folding induced by $^{\delta}$MeOrn and D-Pro-Gly, with the latter perhaps being somewhat superior.

The improved β-hairpin formation provided by the $^{\delta}$MeOrn turn places it in the same league as the popular D-Pro-L-Pro and D-Pro-Gly turns and opens the door to useful applications. We anticipate using it in our own laboratory to improve the mimicry of amyloid oligomers composed of β-hairpins.[34] We also envision that the free α-amino group of the $^{\delta}$MeOrn turn will offer advantages over the D-Pro-L-Pro and D-Pro-Gly turns in solubility and could also serve as a handle for further functionalization.[30,38] Although there is still no universal tool to coax any small peptide — polyalanine, for example — to adopt a β-hairpin conformation, the $^{\delta}$MeOrn turn represents a worthy addition to the toolbox of turn templates. MC/SD calculations predict that β(*R*),γ(*R*)-dimethyl-ornithine may be even better at inducing β-hairpin formation in peptides (Figure S1.1). We look forward to future synthetic advances or clever application of existing methodology that enable the facile preparation of derivatives of β(*R*),γ(*R*)-dimethyl-ornithine suitable for use in solid-phase peptide synthesis, so that this hypothesis can be tested.

REFERENCES AND NOTES

[1] Moriuchi, T.; Hirao, T. *Chem. Soc. Rev.* **2004**, *33* (5), 294–301.

[2] Khakshoor, O.; Nowick, J. S. *Curr. Opin. Chem. Biol.* **2008**, *12* (6), 722–729.

[3] Robinson, J. A. *Acc. Chem. Res.* **2008**, *41* (10), 1278–1288.

[4] Marcelino, A. M. C.; Gierasch, L. M. *Biopolymers* **2008**, *89* (5), 380–391.

[5] Fuller, A. A.; Du, D.; Liu, F.; Davoren, J. E.; Bhabha, G.; Kroon, G.; Case, D. A.; Dyson, H. J.; Powers, E. T.; Wipf, P.; Martin, G.; Kelly, J. W. *Proc. Natl. Acad. Sci. U. S. A.* **2009**, *106* (27), 11067–11072.

[6] Nair, R. V.; Baravkar, S. B.; Ingole, T. S.; Sanjayan, G. J. *Chem. Commun.* **2014**, *50* (90), 13874–13884

[7] Horne, W. S.; Grossmann, T. N. *Nat. Chem.* **2020**, *12* (4), 331–337.

[8] Lenci, E.; Trabocchi, A. *Chem. Soc. Rev.* **2020**, *49* (11), 3262–3277.

[9] Nair, C. M.; Vijayan, M.; Venkatachalapathi, Y. V. Balaram, P. *J.C.S. Chem. Comm*. **1979**, 1183–1184.

[10] Karle, I. L.; Awasthi, S. K.; Balaram, P. *Proc. Natl. Acad. Sci. U. S. A.* **1996**, *93* (16), 8189–8193.

[11] Haque, T. S.; Gellman, S. H. *J. Am. Chem. Soc.* **1997**, *119* (9), 2303–2304.

[12] Stanger, H. E.; Gellman, S. H. *J. Am. Chem. Soc.* **1998**, *120* (17), 4236–4237.

[13] Espinosa, J. F.; Gellman, S. H. *Angew. Chem. Int. Ed*. **2000**, *11* (13), 2330–2333.

[14] Díaz, H.; Tsang, K. Y.; Choo, D.; Espina, J. R.; Kelly, J. W. *J. Am. Chem. Soc.* **1993**, *115* (9), 3790–3791.

[15] Kemp, D. S.; Li, Z. Q. *Tetrahedron Lett.* **1995**, *36* (24), 4175–4178.

[16] Kemp, D. S.; Li, Z. Q. *Tetrahedron Lett.* **1995**, *36* (24), 4179–4180.

[17] Schopfer, U.; Stahl, M.; Brandl, T.; Hoffman, R. W. Angew. Chem. Int. Ed. 1997, 36 (16), 1745–1747.

[18] Gardner, R. R.; Liang, G. B.; Gellman, S. H. *J. Am. Chem. Soc.* **1999**, *121* (9), 1806–1816.

[19] Schneider, J. P.; Pochan, D. J.; Ozbas, B.; Rajagopal, K.; Pakstis, L.; Kretsinger, J. *J. Am. Chem. Soc.* **2002**, *124* (50), 15030–15037.

[20] Haines-Butterick, L.; Rajagopal, K.; Branco, M.; Salick, D.; Rughani, R.; Pilarz, M.; Lamm, M. S.; Pochan, D. J.; Schneider, J. P. *Proc. Natl. Acad. Sci. U. S. A.* **2007**, *104* (19), 7791–7796.

[21] Salick, D. A.; Kretsinger, J. K.; Pochan, D. J.; Schneider, J. P. *J. Am. Chem. Soc.* **2007**, *129* (47), 14793–14799.

[22] Shankaramma, S. C.; Athanassiou, Z.; Zerbe, O.; Moehle, K.; Mouton, C.; Bernardini, F.; Vrijbloed, J. W.; Obrecht, D.; Robinson, J. A. *ChemBioChem* **2002**, *3* (11), 1126–1133.

[23] Srinivas, N.; Jetter, P.; Ueberbacher, B. J.; Werneburg, M.; Zerbe, K.; Steinmann, J.; Van Der Meijden, B.; Bernardini, F.; Lederer, A.; Dias, R. L. A.; Mission, P. E.; Henze, H.; Zumbrunn, J.; Gombert, F. O.; Obrecht, D.; Hunziker, P.; Schauer, S.; Ziegler, U.; Käch, A.; Eberl, L.; Riedel, K.; DeMarco, S. J.; Robinson, J. A. *Science.* **2010**, *327* (5968), 1010–1013.

[24] Andolina, G.; Bencze, L. C.; Zerbe, K.; Müller, M.; Steinmann, J.; Kocherla, H.; Mondal, M.; Sobek, J.; Moehle, K.; Malojčić, G.; Wollscheid, B.; Robinson, J. A. *ACS Chem. Biol.* **2018**, *13* (3), 666–675.

[25] Kar, K.; Hoop, C. L.; Drombosky, K. W.; Baker, M. A.; Kodali, R.; Arduini, I.; Van Der Wel, P. C. A.; Horne, W. S.; Wetzel, R. *J. Mol. Biol.* **2013**, *425* (7), 1183–1197.

[26] Kar, K.; Baker, M. A.; Lengyel, G. A.; Hoop, C. L.; Kodali, R.; Byeon, I. J.; Horne, W. S.; van der Wel, P. C. A.; Wetzel, R. *J. Mol. Biol.* **2017**, *429* (2), 308–323.

[27] Brower, J. O.; Nowick, J. S. *J. Am. Chem. Soc.* **2003**, *125* (4), 876–877.

[28] Spencer, R. K.; Li, H.; Nowick, J. S. *J. Am. Chem. Soc.* **2014**, *136* (15), 5595–5598.

[29] Kreutzer, A. G.; Hamza, I. L.; Spencer, R. K.; Nowick, J. S. *J. Am. Chem. Soc.* **2016**, *138* (13), 4634–4642.

[30] Samdin, T. D.; Wierzbicki, M.; Kreutzer, A. G.; Howitz, W. J.; Valenzuela, M.; Smith, A.; Sahrai, V.; Truex, N. L.; Klun, M.; Nowick, J. S. *J. Am. Chem. Soc.* **2020**, *142* (26), 11593–11601.

[31] Salveson, P. J.; Spencer, R. K.; Nowick, J. S. *J. Am. Chem. Soc.* **2016**, *138* (13), 4458–4467.

[32] Wang, Y.; Kreutzer, A. G.; Truex, N. L.; Nowick, J. S. *J. Org. Chem.* **2017**, *82* (15), 7905–7912.

[33] Spencer, R. K.; Kreutzer, A. G.; Salveson, P. J.; Li, H.; Nowick, J. S. *J. Am. Chem. Soc.* **2015**, *137* (19), 6304–6311.

[34] Kreutzer, A. G.; Nowick, J. S. *Acc. Chem. Res.* **2018**, *51* (3), 706–718.

[35] McDonald, Q. D.; Still, C. W. *Tetrahedron Lett.* **1992**, *33* (50), 7747–7750.

[36] McDonald, Q. D.; Still, C. W. *J. Am. Chem. Soc.* **1994**, *116* (25), 11550–11553.

[37] Zwick, C. R.; Renata, H. *J. Am. Chem. Soc.* **2018**, *140* (3), 1165–1169.

[38] Zwick, C. R.; Renata, H. *J. Org. Chem.* **2018**, *83* (14), 7407–7415.

[39] Woods, R. J.; Brower, J. O.; Castellanos, E.; Hashemzadeh, M.; Khakshoor, O.; Russu, W. A.; Nowick, J. S. *J. Am. Chem. Soc.* **2007**, *129* (9), 2548–2558.

[40] Wishart, D. S.; Sykes, B. D.; Richards, F. M. *J. Mol. Biol.* **1991**, *222* (2), 311–333.

[41] Wishart, D. S.; Sykes, B. D.; Richards, F. M. *Biochemistry* **1992**, *31* (6), 1647–1651.

[42] Wishart, D. S.; Sykes, B. D. *Meth. Enzymol.* **1994**, *239* (1982), 363–392.

[43] Wishart, D. S.; Case, D. A. *Meth. Enzymol.* **2002**, *338*, 3–34.

[44] The random coil values that we used to calculate for the difference between observed α-proton chemical shifts in peptides **3–6b** and those of a random coil are taken from: Wüthrich, K. NMR of Proteins and Nucleic Acids, Wiley: New York, 1986.

[45] Nowick, J. S.; Khakshoor, O.; Hashemzadeh, M.; Brower, J. O. *Org. Lett.* **2003**, *5* (19), 3511–3513.

Table of Contents

Supplementary information 27
Figure S1.1 29
Figure S1.2 30
Figure S1.3 31
Figure S1.4 33
Supplementary Table 1.1 35
Modeling of the δ-linked turn units 36
Modeling Parameters. 36
Bacterial expression and chemical synthesis 36
Bacterial Expression of GriE from DNA plasmid 36
Chemoenzymatic transformation of L-leucine 37
Chemical synthesis 39
Synthesis of macrocyclic peptides 1.1–1.2 45
Peptide synthesis procedure. 45
Synthesis of β-hairpin peptides 1.3–1.6 48
Peptide synthesis procedure. 48
X-ray crystallography of peptide 1.1b 51
Crystallization of peptide **1.1b**. 51
Data collection, data processing, and structure determination 51
Circular dichroism spectroscopy 52
Sample preparation, data collection, and data processing 52
NMR spectroscopy 52
Sample preparation, data collection, and data processing 52

Characterization Data 56
Analytical HPLC trace and MALDI mass spectrum of peptides 56
Analytical HPLC trace and MALDI mass spectrum of peptide **1.1a** 56
Analytical HPLC trace and MALDI mass spectrum of peptide **1.1b** 57

Analytical HPLC trace and MALDI mass spectrum of peptide **1.2a** 59
Analytical HPLC trace and MALDI mass spectrum of peptide **1.2b** 61
Analytical HPLC trace and MALDI mass spectrum of peptide **1.3** 63
Analytical HPLC trace and MALDI mass spectrum of peptide **1.4a** 65
Analytical HPLC trace and MALDI mass spectrum of peptide **1.4b** 67
Analytical HPLC trace and MALDI mass spectrum of peptide **1.5** 69
Analytical HPLC trace and MALDI mass spectrum of peptide **1.6a** 71
Analytical HPLC trace and MALDI mass spectrum of peptide **1.6b** 73

NMR spectra of isolated compounds 75
^{1}H NMR and ^{13}C NMR spectra of lactone **1.3** 75
^{1}H NMR and ^{13}C NMR spectra of mesylate **1.4** 77
^{1}H NMR and ^{13}C NMR spectra of azide **1.5** 79
^{1}H NMR and ^{13}C NMR spectra of Boc-azidoleucine **1.6** 81
^{1}H NMR and ^{13}C NMR spectra of N^{α}-Boc-N^{δ}-Fmoc-γ(*R*)-methyl-ornithine (**1.1**) 83
EXSY spectrum of N^{α}-Boc-N^{δ}-Fmoc-γ(*R*)-methyl-ornithine (**1.1**) 85

NMR spectroscopic studies of β-hairpin peptides 1.3–1.6 86
^{1}H NMR, TOCSY, and NOESY spectra of peptide **1.3** 86
^{1}H NMR, TOCSY, and NOESY spectra of peptide **1.4a** 90
^{1}H NMR, TOCSY, and NOESY spectra of peptide **1.4b** 94
^{1}H NMR, TOCSY, and NOESY spectra of peptide **1.5** 98
^{1}H NMR, TOCSY, and NOESY spectra of peptide **1.6a** 104
^{1}H NMR, TOCSY, and NOESY spectra of peptide **1.6b** 106

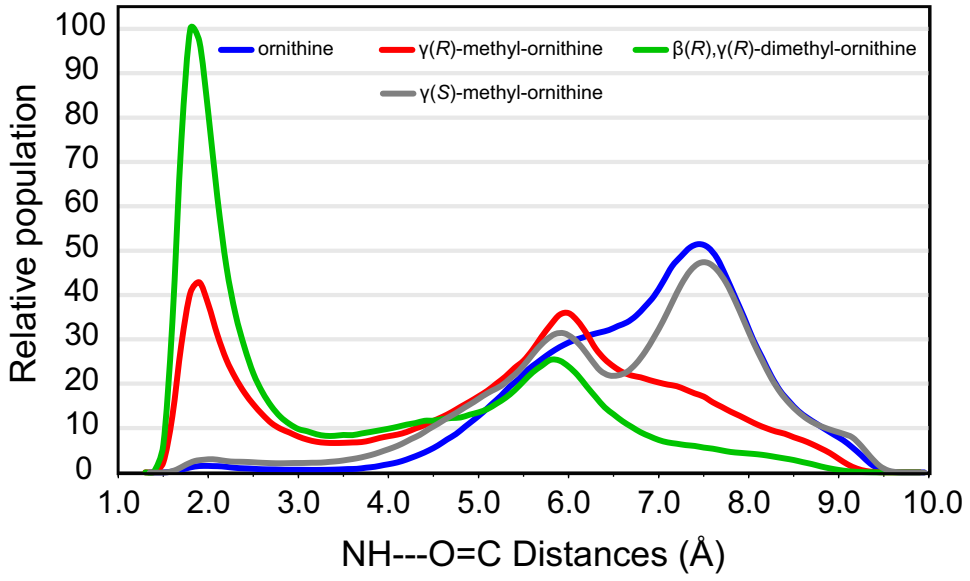

Figure S1.1. Folding of Ac-$^{\delta}$Orn-NHMe, and methylated analogues predicted by MC/SD simulation in MacroModel.[1,2] The distribution of NH—O=C distances for ornithine, γ(*R*)-methyl-ornithine, γ(*S*)-methyl-ornithine, and β(*R*),γ(*R*)-dimethyl-ornithine is plotted above. The percentage of hydrogen-bonded conformations was determined to be 0.77%, 20.28%, 1.64%, and 44.05%, respectively.

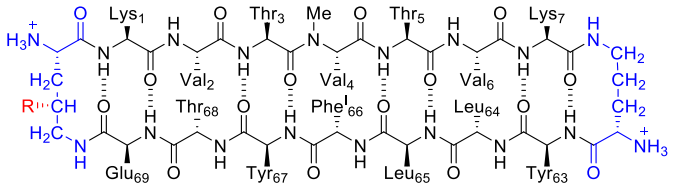

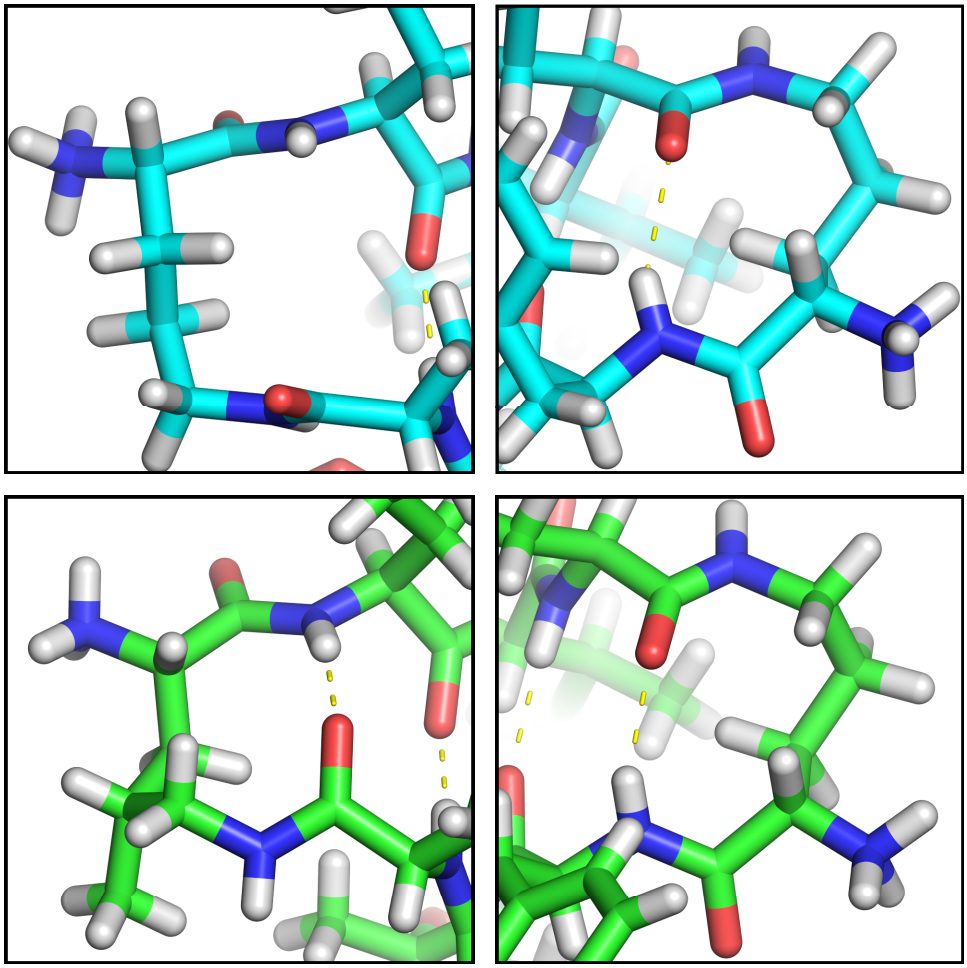

Figure S1.2. An example of the left and right $^{\delta}$Orn turns in peptide **1.1a** (cyan); the left and right $^{\delta}$MeOrn turns in peptide **1.1b** (green). [**1.1a**, PDB 4P4Z, 12 peptide molecules in the asymmetric unit; **1.1b**, PDB 7LIB, 1 peptide molecule in the asymmetric unit.] In peptide **1.1a**, only the $^{\delta}$Orn on the right side adopts the characteristic hydrogen-bonded turn conformation, while the left side does not. In peptide **1.2b**, both the right and left $^{\delta}$MeOrn turn units adopt the hypothesized hydrogen-bonded conformation.

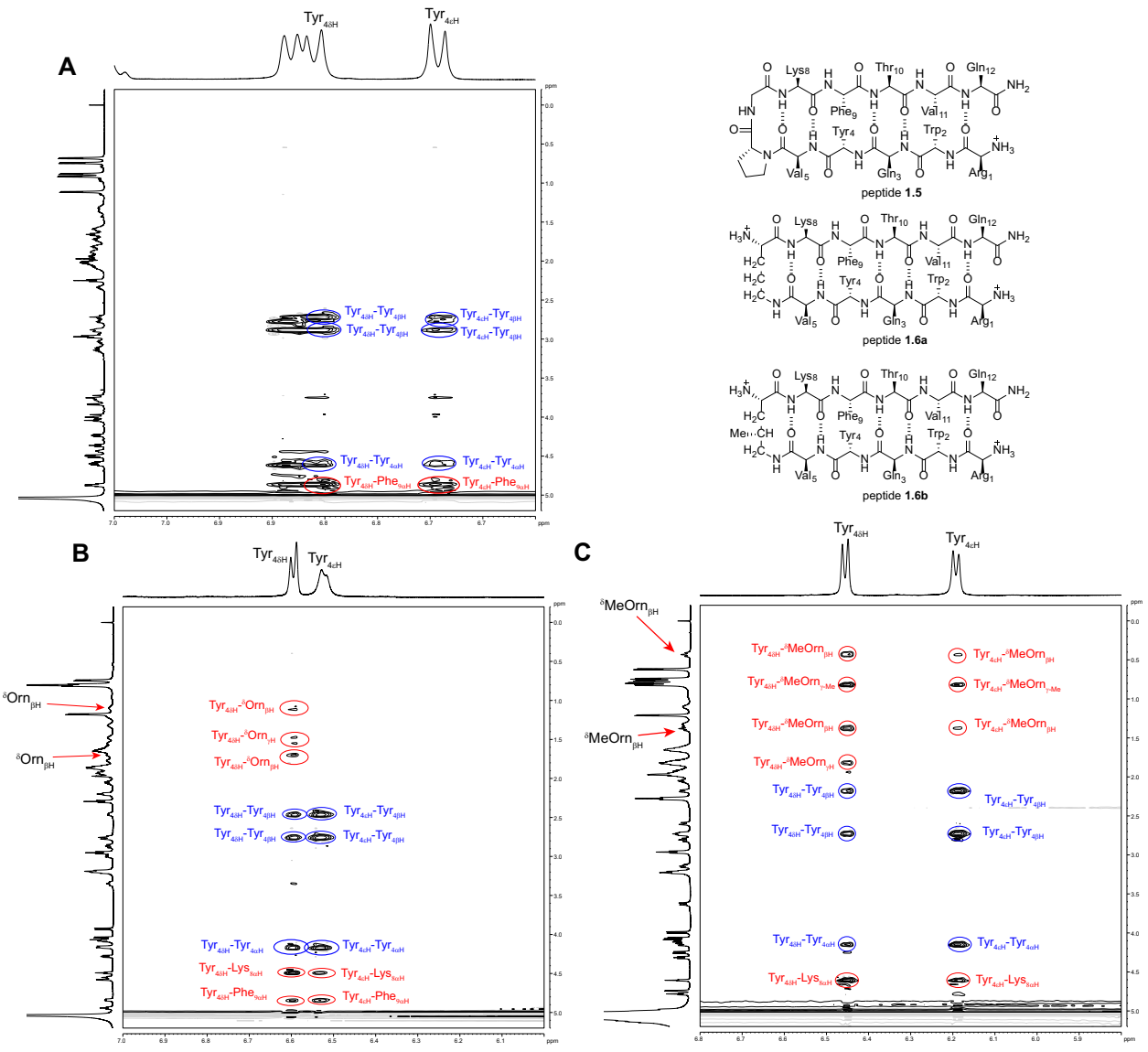

Figure S1.3. 2D NOESY spectra of peptide **1.5** (A), peptide **1.6a** (B), and peptide **1.6b** (C) depicting the NOEs associated with the aromatic protons of Tyr_4. Expected NOEs between the aromatic protons and the α- and β-protons of Tyr_4 are labeled in blue. NOEs between the aromatic protons of Tyr_4 and the protons of other residues within the peptide are labeled in red. Each spectrum was acquired at 277 K in D_2O in a buffer of 100 mM CD_3COOD and 100 mM CD_3COONa with 0.06 mM DSA as a reference standard.

In the NOESY spectrum of peptide **1.6b**, the β-protons, the γ-methyl, and the γ-proton of the $^{\delta}$MeOrn turn all have crosspeaks with the aromatic protons of Tyr_4. One of the two diastereotopic β-protons of the $^{\delta}$MeOrn is significantly upfield shifted and appears at

0.43 ppm. The upfield shifting of $^{\delta}$MeOrn and the NOEs with Tyr_4 indicate that the $^{\delta}$MeOrn turn is packed against the aromatic ring of Tyr_4. The NOESY spectrum of peptide **1.6a** shows less packing between the $^{\delta}$Orn turn and the aromatic ring of Tyr_4: the NOE crosspeaks between the sidechain of $^{\delta}$Orn and the aromatic protons of Tyr_4 are weaker, and there is no significant upfield shifting of the β-protons. In contrast, peptide **1.5** shows no NOE crosspeaks between D-Pro or Gly and Tyr_4 and no significant upfield shifting of the protons of D-Pro or Gly

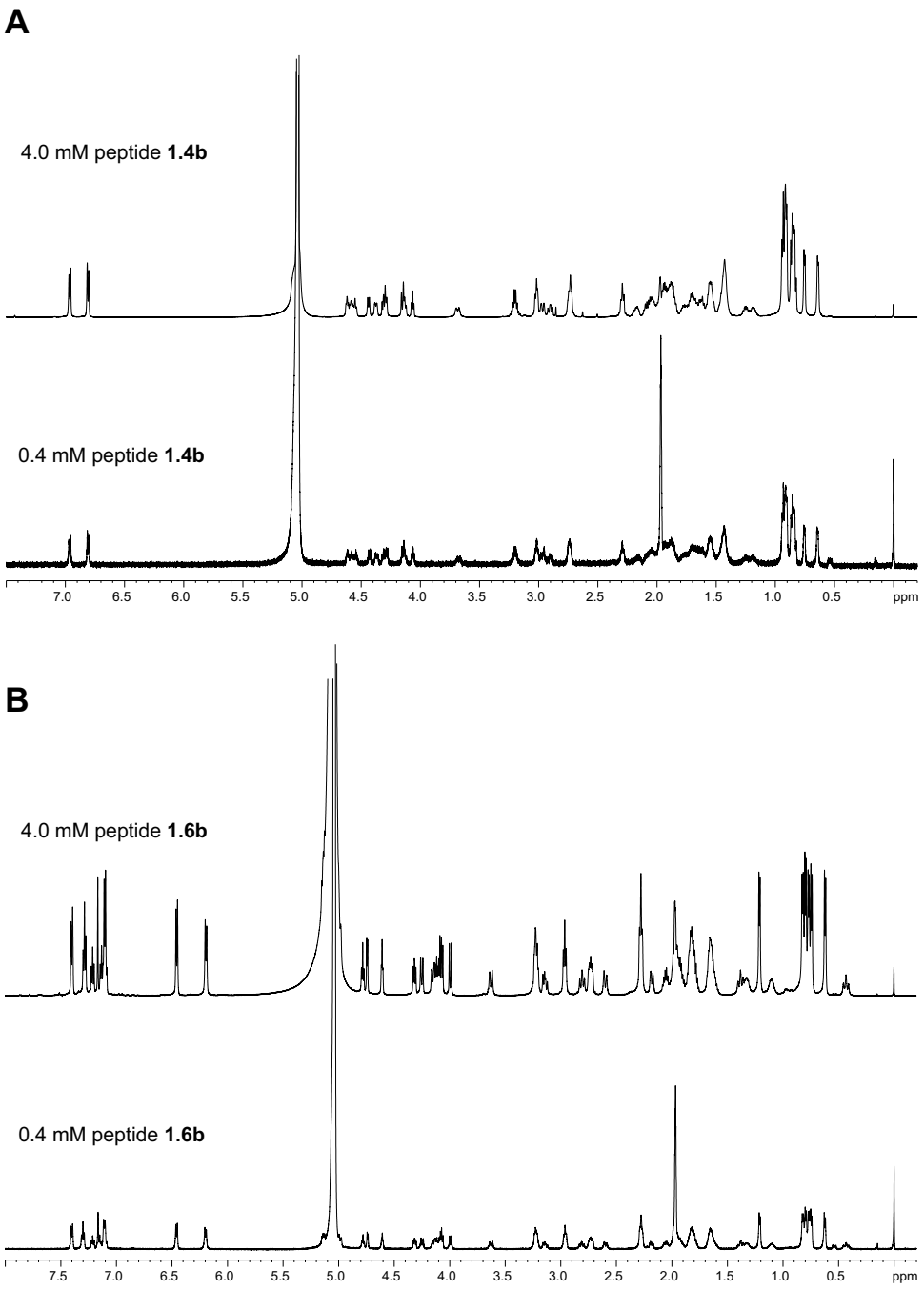

Figure S1.4. ^{1}H NMR spectra overlay of peptide **1.4b** (A) and peptide **1.6b** (B) at 0.4 mM and 4.0 mM concentrations; each spectrum was acquired at 277 K in D_2O in a buffer of 100 mM CD_3COOD and 100 mM CD_3COONa with 0.06 mM DSA as a reference standard.

The ^{1}H NMR spectra of peptide **1.4b** shows no significant differences in chemical shift between 4.0 and 0.4 mM (≤0.02 ppm), indicating that the peptide does not self-associate at the low-millimolar concentrations used for the NMR studies. The ^{1}H NMR spectra of peptide **1.6b** also shows no significant differences in chemical shift between 4.0 and 0.4 mM (≤0.02 ppm), indicating that the peptide does not self-associate at the low-millimolar concentrations used for the NMR studies.

Supplementary Table 1.1. Crystallographic properties, crystallization conditions, data collection, and model refinement statistics for the calcium salt of peptide **1.1b** (PDB 7LIB).

peptide	**1.1b**
PDB ID	7LIB
Crystallization conditions	0.1 M SPG buffer (pH 10.5), w/v PEG 1500
Wavelength / Å	1.0000
Resolution range / Å	27.28 – 1.100 (1.139 – 1.100)
Space group	I422
Unit cell parameters	38.5738 38.5738 34.9252 90
Total reflections	109961 (4440)
Unique reflections	5410 (405)
Multiplicity	20.3 (10.9)
Completeness / %	96.27 (74.04)
Mean I/σ(I)	24.68 (9.46)
Wilson B-factor	9.56
R_{merge}	0.07663 (0.4137)
R_{meas}	0.07872 (0.4337)
R_{pim}	0.01726 (0.1256)
$CC_{1/2}$	0.997 (0.965)
CC*	0.999 (0.991)
Reflections used in	5413 (405)
Reflections used for R_{free}	271 (18)
R_{work}	0.1773 (0.2463)
R_{free}	0.2084 (0.2640)
$CC_{(work)}$	0.950 (0.878)
$CC_{(free)}$	0.964 (0.870)
Number of non-hydrogen	172
macromolecules	142
ligands (Ca^{2+})	41
solvent (H_2O)	12
Protein residues	16
RMS(bonds)	0.016
RMS(angles)	1.86
Ramachandran favored (%)	100.00
Ramachandran allowed (%)	0.00
Ramachandran outliers (%)	0.00
Rotamer outliers (%)	0.00
Clashscore	5.90
Average B-factor	12.40
macromolecules	11.96
ligands	12.11
solvent	18.00

Modeling of the δ-linked turn units

Modeling parameters. MacroModel with Maestro user interface was used to create the unfolded structures of Ac-$^{\delta}$MeOrn-NHMe and Ac-$^{\delta}$MeOrn-NHMe. Energy minimized conformations (global minima) of each turn were then generated using the conformational search function with the MMFFs force field and GB/SA water. The equilibrium between the unfolded and folded states of Ac-$^{\delta}$MeOrn-NHMe and Ac-$^{\delta}$MeOrn-NHMe and related derivatives was calculated by Monte Carlo Stochastic Dynamics (MC/SD) with GB/SA water at 300 K and MMFFs force field.[1,2] Simulations were run for 50 ns to ensure convergence, with monitoring of hydrogen bonding between the Ac and NHMe groups. The distance was also monitored between the acetyl carbonyl oxygen atom and the methyl amide hydrogen atom (Figure S1.1).

Bacterial expression and chemical synthesis

Expression of GriE enzyme.[4] Sequence-verified pET22b(+) plasmids encoding GriE[1] were transformed into BL21 DE3 competent *E. coli* cells through heat shock method. The cell cultures were spread on LB agar plates containing carbenicillin[2]. Single colonies were picked to inoculate overnight cultures; the colonies were suspended in 3 mL of LB media supplemented with carbenicillin and shaken at 225 rpm and 37 °C for ca. 16–18 h.[3]

[1]The pET22b(+) plasmids encoding for the GriE enzyme was provided to us as a generous gift from Professor Hans Renata.
[2]The carbenilicin was added as a 50 mg/mL solution in water, and in a 1:1000 ratio of carbenilicin to final volume.
[3]Glycerol stocks of BL21 DE3 competent *E. coli* cells bearing the plasmid were also made from the inoculated cultures, and stored at -80 °C for future use.

(Colonies were picked to inoculate two overnight cultures at a time). The next day, each overnight culture (3 mL) was transferred to a 2 L baffled Erlenmeyer flask containing Terrific Broth (TB, 400 mL) culture media supplemented with carbenicillin and shaken at 225 rpm and 37 °C. When the optical density of cells reached an OD_{600} of 0.7–1.0 (ca. 4 h), the cultures were cooled on ice for 20 minutes. Protein expression of each culture was induced by the addition of IPTG (2 mL, 0.5 mM). The cells were incubated for 20 h at 20 °C, shaken at 225 rpm, and harvested by centrifugation (4 °C, 15 min, 3,000x*g*). The cell pellets were frozen at -20 °C or below for at least 2 h.

The frozen cell pellets were thawed at room temperature and suspended in 100 mL of 50 mM potassium phosphate buffer at pH 7.0, to give an OD_{600} of ca. 30. (The absorbance was checked by taking 50 uL of the suspension, diluting with 1450 uL of potassium phosphate buffer, and back calculating the OD_{600}). The cells were lysed by sonication (3x1 min, 50% duty cycle, 40% power) and pelleted by centrifugation (4 °C, 15 min, 4,000 rpm). The supernatant was decanted and stored at -20 °C until further use.

Chemoenzymatic oxidation of l-leucine

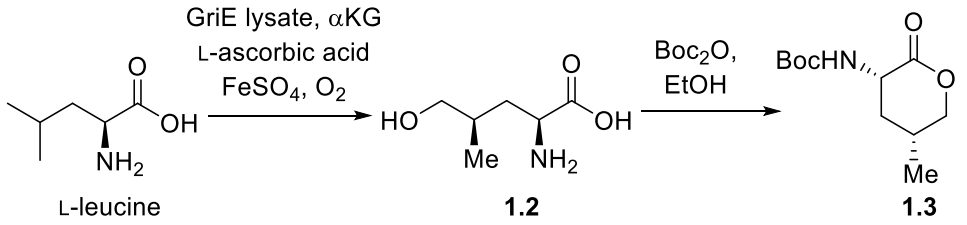

Lactone 1.3.[4] A 2 L baffled Erlenmeyer flask was charged with L-leucine (1.31 g, 10 mmol, 1.0 equiv), L-ascorbic acid (1.76 g, 10 mmol, 1.0 equiv), α-ketoglutaric acid

(disodium salt dihydrate, 6.78 g, 30 mmol, 3.0 equiv), $FeSO_4$ (heptahydrate, 111 mg, 0.4 mmol, 0.04 equiv), and 50 mM potassium phosphate buffer (pH 7.0, 100 mL). To this suspension, the thawed supernatant containing the GriE lysate (100 mL) was added, and the flask was shaken for 7 h at 20 °C and 225 rpm. The reaction was stopped by the addition of 1 M HCl (20 mL), and the mixture was centrifuged (4 °C, 15 min, 4,000 rpm). The resulting supernatant was concentrated to dryness by rotary evaporation and used without further purification.

The dry lysate was then suspended in 20 mL of 2 M NaOH. The resulting brown suspension was adjusted to a pH of approximately 9 (by addition of 1 M HCl if necessary) using a pH meter, and diluted with an additional 30 mL of H_2O. A solution of Boc_2O (7.63 g, 35 mmol, 3.5 equiv) dissolved in 50 mL of EtOH was added, and the mixture was stirred at room temperature for 4 h. The reaction mixture was acidified to a pH of 2.0–3.0 (monitoring by a pH meter) by addition of 1 M HCl and then concentrated by rotary evaporation to remove EtOH (ca. 50 mL distillate). CH_2Cl_2 (100 mL) was added, and the biphasic mixture was stirred at room temperature for 16–20 h. The layers were separated, and the aqueous layer was extracted with CH_2Cl_2 (2 x 200 mL). The combined organic extracts were washed with sat. aq NaCl (150 mL), dried over $MgSO_4$, filtered, and concentrated by rotary evaporation. The resulting residue was purified by column chromatography on silica gel (elution with 40:60 EtOAc:hexanes) to afford lactone **1.3** as a white solid. In typical experiments, yields ranging from 0.8 to 1.2 g (35–52%) of lactone **1.3** were obtained from 1.31 g of leucine. ^{1}H NMR (500 MHz, $CDCl_3$): δ 5.32 (s, 1 H), 4.35 (dd, *J* = 11.1, 4.5 Hz, 1 H), 4.24 (br s, 1 H), 3.96 (dd, *J* = 11.3, 7.0 Hz, 1 H), 2.57 (br s, 1 H), 2.32–2.21 (m, 1 H), 1.43 (s, 9 H), 1.38–1.30 (m, 1 H), 1.02 (d, *J* = 6.7 Hz, 3 H). ^{13}C NMR (125 MHz,

$CDCl_3$): δ 171.97, 155.52, 80.28, 74.18, 50.04, 35.19, 28.40, 27.83, 18.35. HRMS (ESI-TOF) *m/z*: $[M + Na]^+$ calcd for $C_{11}H_{19}NO_4Na^+$ 252.1212, found 252.1205.

Chemical synthesis

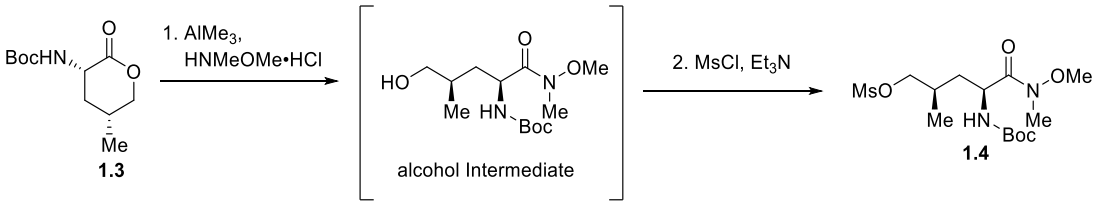

Mesylate 1.4.[5] [CAUTION: Trimethylalumnimum (2 M in toluene) is pyrophoric and should be handled by placing the solution under a blanket of nitrogen prior to use.] An oven dried 500-mL, three-necked, round-bottom flask equipped with a nitrogen inlet adapter, two septa, and a magnetic stirring bar was charged with *N,O*-dimethylhydroxylamine hydrochloride (3.85 g, 39.4 mmol, 3.0 equiv) and 40 mL of anhydrous THF. The resulting suspension was cooled to 0 °C using an ice bath, and $AlMe_3$ (2 M in toluene, 19.8 mL, 39.4 mmol, 3.0 equiv) was added in drops via syringe over 30 min. The ice bath was removed, and the reaction mixture was stirred for 1 h at room temperature (ca. 23°C). The solution was cooled to -30 °C using a dry ice/acetone bath. A separate solution of lactone **1.3** (3.01 g, 13.1 mmol, 1.0 equiv) in 26 mL anhydrous THF (0.5 M) was added in drops via syringe over 10 min. The solution was stirred at -30 °C for 1 h. A 30% (w/w) aqueous solution of Rochelle's salt (120 mL) was added, followed by Et_2O (120 mL). The resulting white suspension was stirred at room temperature for 1.5 h, diluted with 100 mL H_2O, and filtered through Celite. The Celite was washed with additional Et_2O. The layers were separated, and the aqueous layer was extracted with Et_2O

(3 x 150 mL). The combined organic extracts were washed with sat. aq NaCl (150 mL), dried over $MgSO_4$, filtered, and concentrated to dryness by rotary evaporation to give the alcohol intermediate as a yellow oil.

An oven dried 250-mL, three-necked, round-bottom flask equipped with a nitrogen inlet adapter, two septa, and a magnetic stirring bar was charged with a solution of the alcohol intermediate in 66 mL anhydrous THF (0.2 M), and chilled to -78 °C using a dry ice/acetone bath. To this solution, Et_3N (3.7 mL, 26.3 mmol, 2.0 equiv) was added, and MsCl (1.1 mL, 14.5 mmol, 1.1 equiv) was then added in drops via syringe over approximately 5 min. The solution was stirred for 2.5 h at -78 °C and then allowed to warm to room temperature. The solution was then filtered through Celite and washed with additional Et_2O. The filtered solution was transferred to a separatory funnel and shaken with 100 mL of H_2O. The layers were separated, and the aqueous layer was extracted with Et_2O (3 x 150 mL). The combined organic extracts were washed with sat. aq NaCl (150 mL), dried over $MgSO_4$, filtered, and concentrated to dryness by rotary evaporation. The resulting residue was purified by column chromatography on silica gel (elution with 60:40 EtOAc:hexanes) to afford mesylate **1.4** as a white solid (3.48 g, 72 % yield over two steps). ^{1}H NMR (600 MHz, $CDCl_3$): δ 5.22 (d, *J* = 8.5 Hz, 1 H), 4.76 (br t, *J* = 10.0, 1 H), 4.25 (dd, *J* = 9.5, 5.5 Hz, 1 H), 4.17 (dd, *J* = 9.4, 4.3 Hz, 1 H), 3.79 (s, 3 H), 3.20 (s, 3 H), 3.03 (s, 3 H), 2.08–2.00 (m, 1 H), 1.80 (ddd, *J* = 13.9, 8.8, 4.2 Hz, 1 H), 1.47–1.44 (m, 1 H), 1.42 (s, 9 H), 1.06 (d, *J* = 6.8 Hz, 3 H). ^{13}C NMR (150 MHz, $CDCl_3$): δ 172.87, 155.75, 79.95, 73.40, 61.90, 48.52, 37.20, 36.55, 32.24, 29.82, 28.46, 17.78. HRMS (ESI-TOF) *m/z*: $[M + Na]^+$ calcd for $C_{14}H_{28}N_2O_7SNa^+$ 391.1515, found 391.1502.

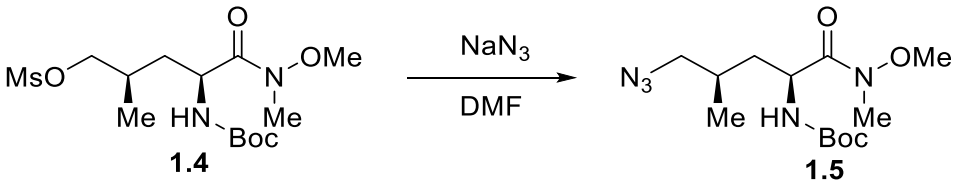

Azide 1.5. A 250-mL, single-necked, round-bottom flask equipped with a magnetic stirring bar and a condenser fitted with a nitrogen inlet adapter was charged with a solution of mesylate **1.4** (3.48 g, 9.44 mmol, 1.0 equiv) in 63 mL of anhydrous DMF (0.15 M). To this solution, NaN_3 (1.37 g, 37.8 mmol, 4.0 equiv) was added. The resulting suspension was heated to 70 °C, stirred for 22 h, and allowed to cool to room temperature (ca. 23°C). The reaction solution was then transferred to a separatory funnel, and the flask was rinsed with 100 mL H_2O and 150 mL Et_2O. The layers were separated, and the aqueous layer was extracted with Et_2O (3 x 150 mL). The combined organic extracts were washed with sat. aq NaCl (150 mL), dried with $MgSO_4$, filtered, and concentrated to dryness by rotary evaporation. The resulting residue was purified by column chromatography on silica gel (elution with 40:60 EtOAc:hexanes) to afford azide **1.5** as a yellow oil (2.52 g, 85% yield). ^{1}H NMR (600 MHz, $CDCl_3$): δ 5.17 (d, *J* = 9.2 Hz, 1 H), 4.74 (br t, *J* = 9.9 Hz 1 H), 3.79 (s, 3 H), 3.40 (dd, *J* = 12.1, 3.9 Hz, 1 H), 3.29 (dd, *J* = 11.3, 5.8 Hz, 1 H), 3.21 (s, 3 H), 1.92–1.83 (m, 1 H), 1.78–1.71 (m, 1 H), 1.43 (s, 9 H), 1.42–1.36 (m, 1 H), 1.01 (d, *J* = 6.8 Hz, 3 H). ^{13}C NMR (150 MHz, $CDCl_3$): δ 173.13, 155.69, 79.82, 61.78, 56.33, 48.52, 37.41, 32.19, 30.15, 28.41, 18.69. HRMS (ESI-TOF) *m/z*: $[M + H]^+$ calcd for $C_{13}H_{25}N_5O_4H^+$ 316.1985, found 316.1986.

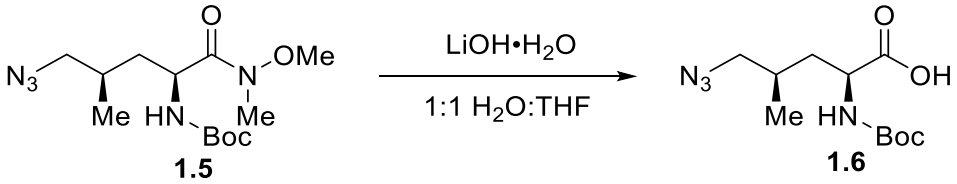

Boc-azidoleucine 1.6. A 250-mL, single-necked, round-bottom flask equipped with a magnetic stirring bar and a condenser fitted with a nitrogen inlet adapter was charged with a solution of azide **1.5** (2.52 g, 8.00 mmol, 1.0 equiv) in 20 mL of THF. A solution of LiOH•H_2O (1.01 g, 24.0 mmol, 3.0 equiv) in 20 mL H_2O was added to the flask. (The reaction was run at ca. 0.2 M concentration of the azide **1.5**). The mixture was heated in an oil bath and stirred for 24 h at 55 °C and then allowed to cool to room temperature (ca. 23 °C). The solution was then transferred to a separatory funnel, and the round-bottom flask was rinsed with 75 mL H_2O and 75 mL Et_2O. The layers were separated, and the organic layer was set aside. The aqueous layer was extracted with Et_2O (1 x 75 mL). The combined organic extracts were extracted with H_2O (1 x 75 mL). The combined aqueous extracts were acidified with 1 M HCl to a pH of 2.0–3.0 (monitoring with a pH meter) and extracted with Et_2O (3 x 150 mL). The combined organic extracts were washed with sat. aq NaCl (150 mL), dried with Na_2SO_4, filtered, and concentrated to dryness by rotary evaporation to afford Boc-azidoleucine **1.6** as a yellow oil (2.02g, 93% yield). A 2:1 mixture of rotamers was observed in the ^{1}H NMR spectrum. ^{1}H NMR (600 MHz, $CDCl_3$): δ 8.93 (br. s, 1 H), 6.58 (s, 0.32 H), 5.00 (d, *J* = 8.0 Hz, 0.65 H), 4.30 (appar q, *J* = 5.1 Hz, 0.67 H), 4.12 (appar q, *J* = 5.0 Hz, 0.32 H), 3.29–3.20 (m, 1H), 3.20–3.13 (m, 1 H), 1.90–1.82 (m, 2 H), 1.53–1.44 (m, 1 H), 1.39 (s, 9 H), 0.97 (d, *J* = 6.5 Hz, 3H). ^{13}C NMR (150 MHz, $CDCl_3$): □ 177.09 (major rotamer), 176.61 (minor rotamer) 156.59 (major rotamer), 155.74 (minor rotamer), 82.12 (minor rotamer), 80.69 (major rotamer), 57.24 (minor rotamer), 56.80 (major rotamer),

52.81 (minor rotamer), 51.57 (major rotamer), 37.41 (minor rotamer), 37.06 (major rotamer), 30.44, 28.43, 18.20. HRMS (ESI-TOF) *m/z*: $[M + Na]^+$ calcd for $C_{11}H_{20}N_4O_4Na^+$ 295.1382, found 295.1390.

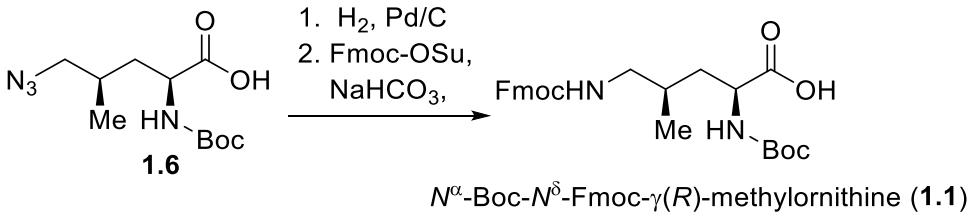

***N*$^{\alpha}$-Boc-*N*$^{\delta}$-Fmoc-γ(*R*)-methyl-ornithine (1.1).** [CAUTION: Hydrogenation is highly hazardous and the catalyst can ignite solvent vapors. Always perform hydrogenation in an uncluttered fume hood, and keep only the minimal volume of solvent needed for the reaction and filtration procedures in the hood. If fire occurs, cover the flask or filter funnel with a watch glass.] A 250-mL, three-necked, round-bottom flask equipped with a magnetic stirring bar, a nitrogen inlet adapter, an inlet adapter fitted with a hydrogen balloon, and a rubber septum was charged with a solution of Boc-azidoeleucine **1.6** (2.02 g, 7.43 mmol, 1.0 equiv) in 37 mL of anhydrous MeOH. (The reaction was run at 0.2 M concentration of the Boc-azidoleucine **1.6**). The flask was evacuated and back filled with nitrogen, and 10 % Pd/C (50% wet with H_2O, 1.01 g) was added. A balloon containing H_2 gas was fitted to an inlet adapter and the system was evacuated and back filled with H_2 gas. The resulting suspension was stirred for 5 h, filtered through Celite, and washed with 300 mL of additional MeOH. The resulting solution was concentrated by rotary evaporation to afford the amine intermediate as a white solid.

A 250-mL, single-necked, round-bottom flask containing the amine intermediate (1.73 g, 7.03 mmol, 1.0 equiv) was equipped with a nitrogen inlet adapter and a magnetic stirring bar. A solution of $NaHCO_3$ (1.77 g, 21.1 mmol, 3.0 equiv) in 35 mL of H_2O was added. The resulting solution was cooled to 0 °C using an ice bath, and a separate preparation of Fmoc-OSu (2.02 g, 5.98 mmol, 0.85 equiv) in 35 mL THF was added to the flask in a single portion. (The reaction was run at 0.1 M concentration of the amine). The reaction mixture was stirred for 1 h in an ice bath, and then for an additional 25 h at room temperature (ca. 23 °C). The solution was then transferred to a separatory funnel, and the round-bottom flask was rinsed with 75 mL H_2O. The resulting solution was extracted with Et_2O (2 x 150 mL). The aqueous layer was acidified with 1 M phosphoric acid to a pH of 3.5–4.0 (monitoring with a pH meter), and extracted with Et_2O (2 x 150 mL) and EtOAc (1 x 150 mL). The combined organic extracts were washed with sat. aq NaCl (150 mL), dried with Na_2SO_4, filtered, and concentrated by rotary evaporation to yield a white foam.

The white foam was dissolved in 150 mL CH_2Cl_2 and extracted with water (2 x 75 mL) to remove residual impurities. The combined organic extracts were concentrated by rotary evaporation, and the resulting residue was purified by column chromatography on silica gel (elution with 12:1:1:0.5 EtOAc:MeOH:acetone:H_2O). The fractions containing the product were combined and concentrated by rotary evaporation. The product was then redissolved in 150 mL CH_2Cl_2 and extracted with H_2O (1 x 100 mL) to remove deprotected impurities that had formed from the silica gel column. The aqueous layer was extracted with additional CH_2Cl_2 (2 x 150 mL). The combined organic extracts were washed with sat. aq NaCl (150 mL), dried with Na_2SO_4, filtered, and concentrated by rotary evaporation to furnish the N^{α}-Boc-N^{δ}-Fmoc-γ(*R*)-methyl-ornithine **1.1** as a white foam (1.81 g, 57% yield

over two steps). A mixture of rotamers (ca. 6:1) was observed in the ^{1}H NMR spectrum. ^{1}H NMR (600 MHz, DMSO-d_6): δ 12.40 (br s, 1 H), 7.89 (d, J = 7.7 Hz, 2 H), 7.69 (d, J = 7.7 Hz, 1.69 H), 7.64–7.60 (m, 0.28 H), 7.41 (t, J = 7.4, 2 H), 7.33 (t, J = 7.5 Hz 2.70 H), 7.08 (d, J = 8.1 Hz, 0.87 H), 6.91–6.86 (m, 0.10 H), 6.70 (d, J = 6.4 Hz, 0.14 H), 4.30–4.24 (m, 2 H), 4.23–4.19 (m, 1 H), 3.97–3.92 (m, 0.80 H), 3.88–3.83 (m, 0.19 H), 2.96–2.91 (m, 0.83 H), 2.90–2.87 (m, 0.11 H), 2.85–2.80 (m, 0.88 H), 2.76–2.70 (m, 0.11 H), 1.72–1.63 (m, 1.53 H), 1.63–1.57 (m, 0.28 H), 1.38 (s, 9 H), 1.35 (m, 1 H), 0.85 (d, J = 6.3 Hz, 2.31 H), 0.76 (br s, 0.35 H). ^{13}C NMR (150 MHz, DMSO-d_6): δ 174.37, 156.34, 155.47, 143.95, 143.91, 140.72, 127.59, 127.05, 125.19, 120.10, 77.96, 65.28, 51.76, 46.76, 45.56, 35.26, 30.45, 28.22 (major rotamer), 27.96 (minor rotamer). HRMS (ESI-TOF) *m/z*: $[M + Na]^+$ calcd for $C_{11}H_{20}N_4O_4Na^+$ 491.2158 found 491.2143.

Synthesis of macrocyclic β-sheet peptides 1.1–1.2

Peptide synthesis procedure.[6] Macrocyclic peptides **1.1b**, **1.2a**, and **1.2b** were synthesized by manual solid-phase peptide synthesis of the corresponding linear peptide on 2-chlorotrityl resin, followed by solution-phase cyclization, deprotection, and purification. A step-by-step procedure is detailed below.

a. Loading the resin. 2-Chlorotrityl chloride resin (300 mg, 1.6 mmol/g) was added to a Bio-RAD Poly-Prep chromatography column (10 mL). Dry CH_2Cl_2 (8 mL) was used to suspend and swell the resin for 30 min with gentle rocking. After draining the solution from the resin, a separate solution of either N^{α}-Boc-N^{δ}-Fmoc-L-ornithine (Boc-Orn(Fmoc)-OH, 0.6 equiv, 130 mg) or N^{α}-Boc-N^{δ}-Fmoc-γ(*R*)-methyl-ornithine (Boc-MeOrn(Fmoc)-OH, 0.6 equiv, 135 mg) in 6% (v/v) 2,4,6-collidine in dry CH_2Cl_2 (8 mL) was added depending on which peptide was being made, and the suspension was gently rocked for 6–14 h. The

solution was then drained and a mixture of CH_2Cl_2/MeOH/*N*,*N*-diisopropylethylamine (DIPEA) (17:2:1, 8 mL) was added immediately. The resin was gently rocked for 1 h, to cap the unreacted 2-chlorotrityl chloride resin sites. The resin was then washed three times with dry CH_2Cl_2 and dried by passing nitrogen through the vessel. This procedure typically yields 0.15–0.20 mmol of loaded resin using either Boc-Orn(Fmoc)-OH or Boc-MeOrn(Fmoc)-OH.

b. Manual peptide coupling. The loaded resin was suspended in dry DMF and then transferred to a solid-phase peptide synthesis vessel. Each residue was manually coupled using Fmoc-protected amino acid building blocks. The coupling cycle consisted of *i*. Fmoc-deprotection with of 20% (v/v) piperidine in DMF (5 mL) for 5–10 min at room temperature, *ii*. washing with dry DMF (4 x 5 mL), *iii*. coupling of the amino acid (4 equiv) with HCTU (4 equiv) in 20% (v/v) 2,4,6-collidine in dry DMF (5 mL) for 20–30 min, and *iv.* washing with dry DMF (4 x 5 mL). *v.* After the last amino acid was coupled, and its Fmoc protecting group deprotected, the resin was transferred from the solid-phase peptide synthesis vessel to a new BioRad Poly-Prep chromatography column. The resin was washed with CH_2Cl_2 (3 x 5mL) and dried by passing nitrogen through the column. In the synthesis of macrocyclic peptide **1.1b**, Fmoc-N(Me)-Val-OH was introduced using normal coupling times and conditions (20–30 min coupling with HCTU) and the subsequent amino acid, Fmoc-Thr(*t*-Bu)-OH, was introduced by double coupling with HOAt (4 equiv), HATU (4 equiv), and 1 h coupling times. [This modification ensured complete amino acid coupling onto a more sterically hindered, secondary amine.] In addition, the Boc-MeOrn(Fmoc)-OH (2 equiv) was introduced into peptide **1.1b** by coupling with HOAt (2 equiv) and HATU (2 equiv) for 1 h, and the subsequent amino acid, Fmoc-Glu-OH, was introduced by coupling

for 1 h with HOAt (4 equiv), HATU (4 equiv). In the synthesis of macrocyclic peptides **1.2a** and **1.2b**, Fmoc-N(Me)-Phe-OH was introduced using normal coupling times and conditions (20 min coupling with HCTU) and the subsequent amino acid, Fmoc-Phe-OH, was introduced by double coupling with HOAt (4 equiv), HATU (4 equiv), and 1 h coupling times. In peptide **1.2b** the Boc-MeOrn(Fmoc)-OH was both loaded onto the 2-chlorotrityl resin and introduced into the sequence (2 equiv) by coupling with HOAt (2 equiv) and HATU (2 equiv) for 1 h.

c. *Cleavage of the linear peptide from chlorotrityl resin*. The linear peptide was cleaved from the resin by rocking the resin in a solution of 20% (v/v) 1,1,1,3,3,3-hexafluoroispropanol (HFIP) in CH_2Cl_2 (8 mL) for 1 h. The suspension was filtered, and the filtrate was collected in a 250-mL round-bottomed flask. The resin was washed with additional cleavage solution (8 mL) for 30 min and filtered. The combined filtrates were concentrated by rotary evaporation and further dried by vacuum pump to afford the crude protected linear peptide, which was cyclized without further purification.

d. *Cyclization of the linear peptide*. The crude protected linear peptide was dissolved in dry DMF (125 mL). HOBt (6 equiv) and HBTU (6 equiv) were dissolved in 8 mL of dry DMF in a test tube to which 300 μL of 4-methylmorpholine was added and the solution mixed until homogenous. The solution was then added to the round-bottom flask containing the dissolved peptide and the mixture was stirred under nitrogen at room temperature for 48 h. The reaction mixture was concentrated by rotary evaporation and further dried by vacuum pump to afford the crude protected cyclized peptide, which was immediately subjected to global deprotection.

e. Global deprotection of the cyclic peptide. The protected cyclic peptide was dissolved in TFA:triisopropylsilane (TIPS):H2O(18:1:1, 8 mL) in a 250-mL round-bottomed flask equipped with a stir bar. The solution was stirred for 1 h under nitrogen. During the 1 h deprotection, two 50-mL conical tubes containing 40 mL of dry Et_2O each were chilled on ice. Following the 1 h time, the peptide solution was split between the two conical tubes of Et_2O. The tubes were then centrifuged at 500x*g* for 15 min, decanted, and washed with fresh Et_2O. This process of decanting and washing was repeated for two more times. The pelleted peptides were dried under nitrogen for 15–20 min. The deprotected cyclic peptide was then purified by reverse-phase HPLC (RP-HPLC).

f. Reverse-phase HPLC purification. The peptide was dissolved in 20% CH_3CN in H_2O (5 mL) and pre-purified on a Biotage Isolera One flash chromatography instrument equipped with a Biotage Sfär Bio C18 D column. The solution of crude cyclic peptide was injected at 20% CH_3CN and eluted with a gradient of 20–50% CH_3CN. Fractions containing the desired peptide was concentrated by rotary evaporation, diluted in 20% CH_3CN, injected on a Rainin Dynamax instrument, and eluted over a gradient of 20–50% CH_3CN over 90 min. The collected fractions were analyzed by analytical HPLC and MALDI-TOF, and the pure fractions were concentrated by rotary evaporation and lyophilized. This synthesis yielded 20 mg for peptide **1.1b**, 20 mg for peptide **1.2a**, and 11 mg for peptide **1.2b**, with each peptide isolated as the TFA salt.

Synthesis of β-hairpin peptides 1.3–1.6.

Peptide synthesis procedure.[6] Linear peptides **1.3–1.6** were synthesized by manual solid-phase peptide synthesis of the corresponding linear peptide on Rink amide resin, followed by solution-phase cleavage, deprotection and purification. A step-by-step procedure is detailed below.

a. Loading the resin. Rink amide resin (300 mg, 0.51 mmol/g) was added to a Bio-RAD Poly-Prep chromatography column (10 mL). Dry DMF (8 mL) was used to suspend and swell the resin for 1 h. After draining the DMF, the resin was rocked in 20% (v/v) piperidine in dry DMF (7 mL) for 1 h to remove the Fmoc protecting group. The solution was then drained and rinsed with DMF (3 x 5 mL). To the column, a solution of Fmoc-Gln(Trt)-OH (5 equiv), HATU (4.5 equiv), and HOAt (4.5 equiv) dissolved in 20% (v/v) 2,4,6-collidine in dry DMF (8 mL) was added. The resin was gently rocked for ca. 4 h. The resin was then washed three times with dry DMF and dried by passing nitrogen through the vessel. A solution of acetic anhydride and pyridine (6:4, 8 mL) was then added to the resin and rocked for 30 min at room temperature to cap the unreacted Rink amide resin sites. After capping, the solution was drained, and the column was rinsed with dry DMF (4 x 5 mL). This procedure typically yields 0.11–0.15 mmol of loaded resin using Fmoc-Gln(Trt)-OH.

b. Manual peptide coupling. The loaded resin was suspended in dry DMF and then transferred to a solid-phase peptide synthesis vessel. Each residue was coupled using Fmoc-protected amino acid building blocks. The coupling cycle consisted of *i*. Fmoc-deprotection with of 20% (v/v) piperidine in DMF (5 mL) for 5–10 min at room temperature, *ii*. washing with dry DMF (4 x 5 mL), *iii*. coupling of the amino acid (4 equiv) with HCTU (4 equiv) in 20% (v/v) 2,4,6-collidine in dry DMF (5 mL) for 20–30 min, and *iv.*

washing with dry DMF (4 x 5 mL). *v.* After the last amino acid was coupled, and its Fmoc protecting group deprotected, the resin was transferred from the solid-phase peptide synthesis vessel to a new BioRad Poly-Prep chromatography column. The resin was washed with CH_2Cl_2 (3 x 5mL), and dried by passing nitrogen through the column. In the synthesis of linear peptides **1.3**–**1.6** Boc-MeOrn(Fmoc)-OH (2 equiv) was introduced into a peptide by coupling with HOAt (2 equiv) and HATU (2 equiv) for 1 h.

c. *Cleavage of the linear peptide from Rink amide resin*. The linear peptide was cleaved from the resin by rocking the resin in a solution of TFA:triisopropylsilane (TIPS):H2O(18:1:1, 8 mL) for 1–1.5 h. The suspension was filtered, and the filtrate was collected in a 250-mL round-bottomed flask. During the cleavage, two 50-mL conical tubes containing 40 mL of dry Et_2O each were chilled on dry ice. Following the filtration into the 250 mL round-bottom flask, the peptide solution was split between the two conical tubes of Et_2O. The tubes were then centrifuged at 500x*g* for 15 min, decanted, and washed with fresh Et_2O. This process of decanting and washing was repeated for two more times. The pelleted peptides were dried under nitrogen for 15–20 min. The deprotected cyclic peptide was then purified by reverse-phase HPLC (RP-HPLC).

d. Reverse-phase HPLC purification. The peptide was dissolved in 15% CH_3CN in H_2O (5 mL) and pre-purified on a Biotage Isolera One flash chromatography instrument equipped with a Biotage Sfär Bio C18 D column. The solution of crude cyclic peptide was injected at 15% CH_3CN and eluted with a gradient of 15–40% CH_3CN. Fractions containing the desired peptide was concentrated by rotary evaporation, diluted in 15% CH_3CN, injected on a Rainin Dynamax instrument, and eluted over a gradient of 15–40% CH_3CN

over 75 min. The collected fractions were analyzed by analytical HPLC and MALDI-TOF, and the pure fractions were concentrated by rotary evaporation and lyophilized. This synthesis yielded ca. 25 mg of peptides **1.3–1.6**, with each peptide isolated as the TFA salt.

X-ray crystallography of peptide 1.1b

*Crystallization of peptide **1.1b**.*[6] Crystallization conditions for peptide **1.1b** were optimized based on the conditions previously reported for peptide **1.1a**,[7] using a 4 x 6 matrix Hampton 24-well plate. For peptide **1.1b**, the 0.1 M SPG buffer was varied in each row in increments of 0.5 pH units (9.0, 9.5, 10.0, and 10.5). The concentration of PEG in each column was varied in increments of 2% w/v (27%, 29%, 31%, 33%, 35%, 37%). Three hanging-drops were prepared on borosilicate glass slides by combing a 10 mg/mL solution of peptide **1.1b** in deionized water with the well solution in the following amounts: 1 µL:1 µL, 2 µL:1 µL, and 1 µL:2 µL. Slides were inverted and pressed firmly against the silicone grease surrounding each well. Crystals were harvested with a nylon loop attached to a copper or steel pin, and flash frozen in liquid nitrogen prior to data collection. The optimized crystallization conditions for peptide **1.1b** are summarized Supplementary Table 1.1.

Data collection, data processing, and structure determination. Diffraction data for peptide **1.1b** were collected at the Stanford Synchrotron Radiation Lightsource beamline 9-2 up to a resolution of 1.03 Å. The dataset was indexed and integrated with XDS[8] and scaled and merged with pointless and aimless in CCP4.[9] A high-resolution cutoff was applied to the dataset at 1.10 Å. The crystallographic phase determination was done with Autosol.[10]

The structure was refined using phenix.refine,[11] with manipulation of the model performed using Coot.[12] Data collection and refinement statistics are shown below in Supplementary Table 1.1.

Circular dichroism spectroscopy

Sample preparation, data collection, and data processing. Solutions of peptides **1.2a** and **1.2b** at 150 μM solution of were prepared by diluting a 5 mM stock solution of peptide dissolved in water with 10 mM sodium phosphate buffer at pH 7.4. Solutions of peptides **1.3**–**1.6** at 100 μM solution of were prepared by diluting a 5 mM stock solution of peptide dissolved in water with 10 mM sodium phosphate buffer at pH 7.4. Each solution was transferred to a 1 mm quartz cuvette for data acquisition. Data were collected using 2.0 nm intervals from 260 nm to 190 nm and averaged over five accumulations without smoothing for peptides **1.2a** and **1.2b**, and peptides **1.5**, **1.6a**, and **1.6b**. Data were collected using 0.5 nm intervals from 260 nm to 190 nm and averaged over five accumulations and were processed with five-point smoothing for peptides **1.3**, **1.4a**, and **1.4b**.

NMR spectroscopy

Sample preparation, data collection, and data processing.[13] ^{1}H NMR experiments of β-hairpin peptides **1.3**–**1.6** were performed using a 600 MHz spectrometer at 4.0 mM concentration and 277 K in D_2O and in a buffer of 100 mM CD_3COOD and 100 mM CD_3COONa, with 0.06 mM DSA[1] as a reference standard. Samples were prepared gravimetrically, based on the molecular weight of the corresponding trifluoracetate (TFA) salt and dissolved in an appropriate volume of solvent. 2D TOCSY and 2D NOESY spectra of

peptides **1.3**–**1.6** were acquired with 2048 data points in the *f*2 domain and 512 data points in the *f*1 domain. TOCSY spectra were acquired with a 200-ms spin-lock mixing time. NOESY spectra were acquired with a 250-ms mixing time. The data were collected and processed with the Bruker TopSpin software.

In order to observe amide resonances for further resonance assignments, ^{1}H NMR studies of β-hairpin peptides **1.3**–**1.6** were performed using a 600 MHz spectrometer with WATERGATE. Peptides were studied at 4.0 mM concentration and 277 K in a 90:10 H_2O:D_2O mixture and in a buffer of 100 mM CD_3COOD and 100 mM CD_3COONa, with 0.06 mM DSA[1] as a reference standard. 2D TOCSY and 2D NOESY spectra of peptides **1.3**–**1.6** in 90:10 H_2O:D_2O were acquired with 2048 data points in the *f*2 domain and 512 data points in the *f*1 domain. TOCSY spectra were acquired with a 200-ms spin-lock mixing time. NOESY spectra were acquired with a 250-ms mixing time. The data were collected and processed with the Bruker TopSpin software.

References

[1] McDonald, Q. D.; Still, C. W. An AMBER*. *Tetrahedron Lett.* **1992**, *33* (50), 7747–7750.

[2] McDonald, Q. D.; Still, C. W.. *J. Am. Chem. Soc.* **1994**, *116* (25), 11550–11553.

[3] Nowick, J. S.; Khakshoor, O.; Hashemzadeh, M.; Brower, J. O. *Org. Lett*. **2003**, 5 (19), 3511–3513.

[4] Zwick, C. R.; Renata, H. *J. Am. Chem. Soc*. **2018**, *140* (3), 1165–1169. The procedures described for the bacteria expression and chemoenzymatic hydroxylation of L-leucine are adapted from this publication.

[5] Zwick, C. R.; Renata, H. *J. Org. Chem.* **2018**, *83* (14), 7407–7415. The procedure described for the synthesis of the mesylate intermediate **4** are adapted from this publication.

[6] General procedures for peptide synthesis and X-ray crystallography were either adapted from or taken verbatim from: Samdin, T. D.; Wierzbicki, M.; Kreutzer, A. G.; Howitz, W. J.; Valenzuela, M.; Smith, A.; Sahrai, V.; Truex, N. L.; Klun, M.; Nowick, J. S. *J. Am. Chem. Soc.* **2020**, *142* (26), 11593–11601 and Howitz, W. J.; Wierzbicki, M.; Cabanela, R. W.; Saliba, C.; Motovalli, A.; Tran, N.; Nowick, J. S. *J. Am. Chem. Soc.* **2020**, *142*, 15870–15875.

[7] Spencer, R. K.; Kreutzer, A. G.; Salveson, P. J.; Li, H.; Nowick, J. S. *J. Am. Chem. Soc.* **2015**, *137* (19), 6304–6311.

[8] Kabsch, W. XDS. *Acta Crystallogr., Sect. D: Biol. Crystallogr.* **2010**, *66*, 125–132.

[9] Winn, M. D.; Ballard, C. C.; Cowtan, K. D.; Dodson, E. J.; Emsley, P.; Evans, P. R.; Keegan, R. M.; Krissinel, E. B.; Leslie, A. G. W.; McCoy, A.; McNicholas, S. J.; Murshudov, G. N.; Pannu, N. S.; Potterton, E. A.; Powell, H. R.; Read, R. J.; Vagin, A.; Wilson, K. S. *Acta Crystallogr., Sect. D: Biol Crystallogr.* **2011**, *67*, 235–242.

[10] Terwilliger, T. C.; Adams, P. D.; Read, R. J.; McCoy, A. J.; Moriarty, N. W.; Grosse-Kunstleve, R. W.; Afonine, P. V.; Zwart, P. H.; Hung, L. W. *Acta Crystallogr., Sect. D: Biol. Crystallogr.* **2009**, *65*, 582–601.

[11] Phenix : Adams, P. D.; Afonine, P. V.; Bunkoczi, G.; Chen, V. B.; Davis, I. W.; Echols, N.; Headd, J. J.; Hung, L. W.; Kapral, G. J.; Grosse-Kunstleve, R. W.; McCoy, A. J.; Moriarty, N. W.; Oeffner, R.; Read, R. J.; Richardson, D. C.; Richardson, J. S.; Terwilliger, T. C.; Zwart, P. H. *Acta Crystallogr., Sect. D: Biol. Crystallogr.* **2010**, *66*, 213–221.

[12] Emsley, P.; Lohkamp, B.; Scott, W. G.; Cowtan, K. *Acta Crystallogr., Sect. D: Biol. Crystallogr.* **2010**, *66*, 486–501.

[13] General procedures for NMR spectroscopic experiments were either adapted from or taken verbatim from: Pham, J. D.; Demeler, B.; Nowick, J. S. *J. Am. Chem. Soc.* **2014**, *136* (14), 5432–5442.

Characterization of ***Peptide 1.1a***

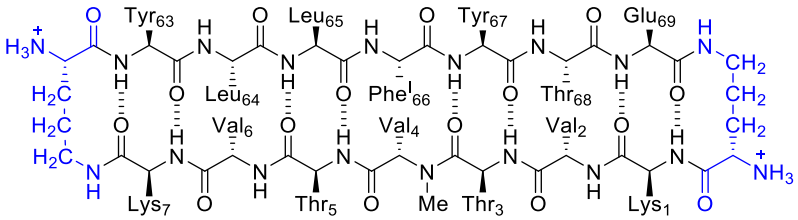

The chemical structure characterization of Peptide **1.1a** (PDB 4P4Z) has been previously described in detail and reported in our laboratory.[7]

Characterization of ***Peptide 1.1b***

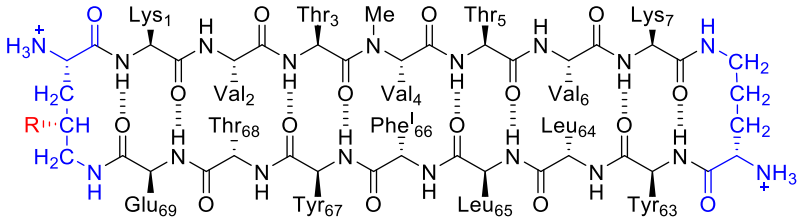

peptide **1.1a** R = H; peptide **1.1b** R = Me

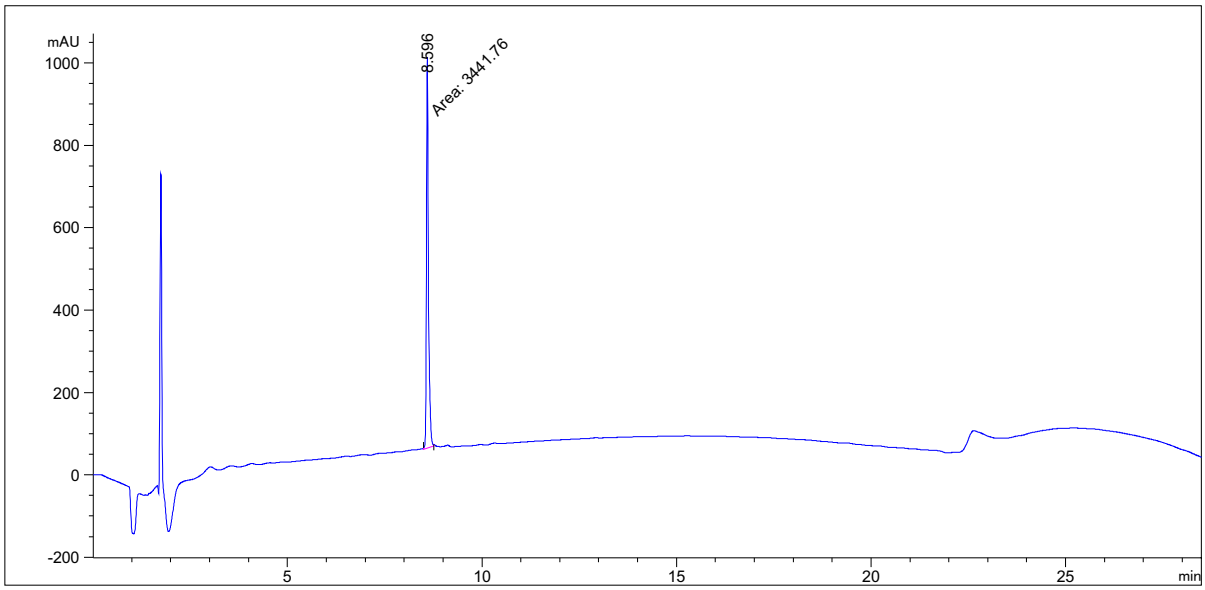

Signal 1: MWD1 A, Sig=214,4 Ref=off

Peak #	RetTime [min]	Type	Width [min]	Area [mAU*s]	Height [mAU]	Area %
1	8.596	MM	0.0602	3441.75635	952.98712	100.0000

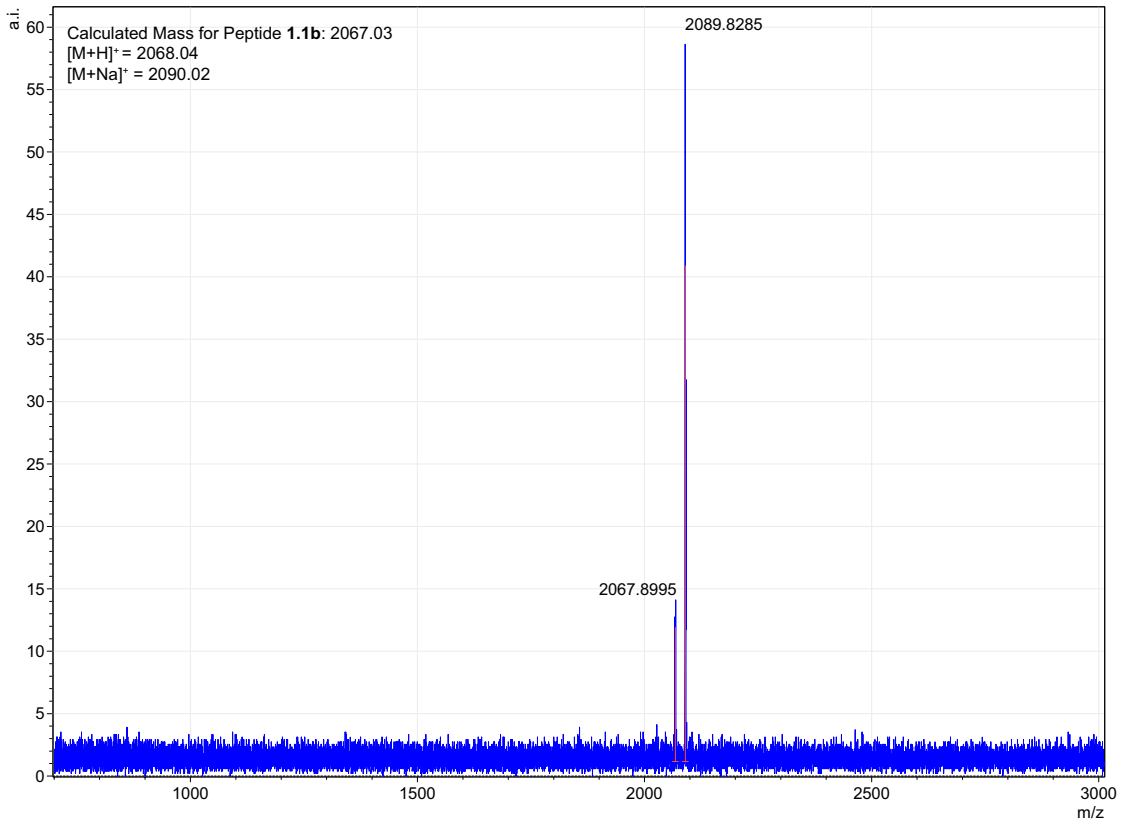
Calculated Mass for Peptide **1.1b**: 2067.03
[M+H]+ = 2068.04
[M+Na]+ = 2090.02
2089.8285
2067.8995
a.i.
m/z

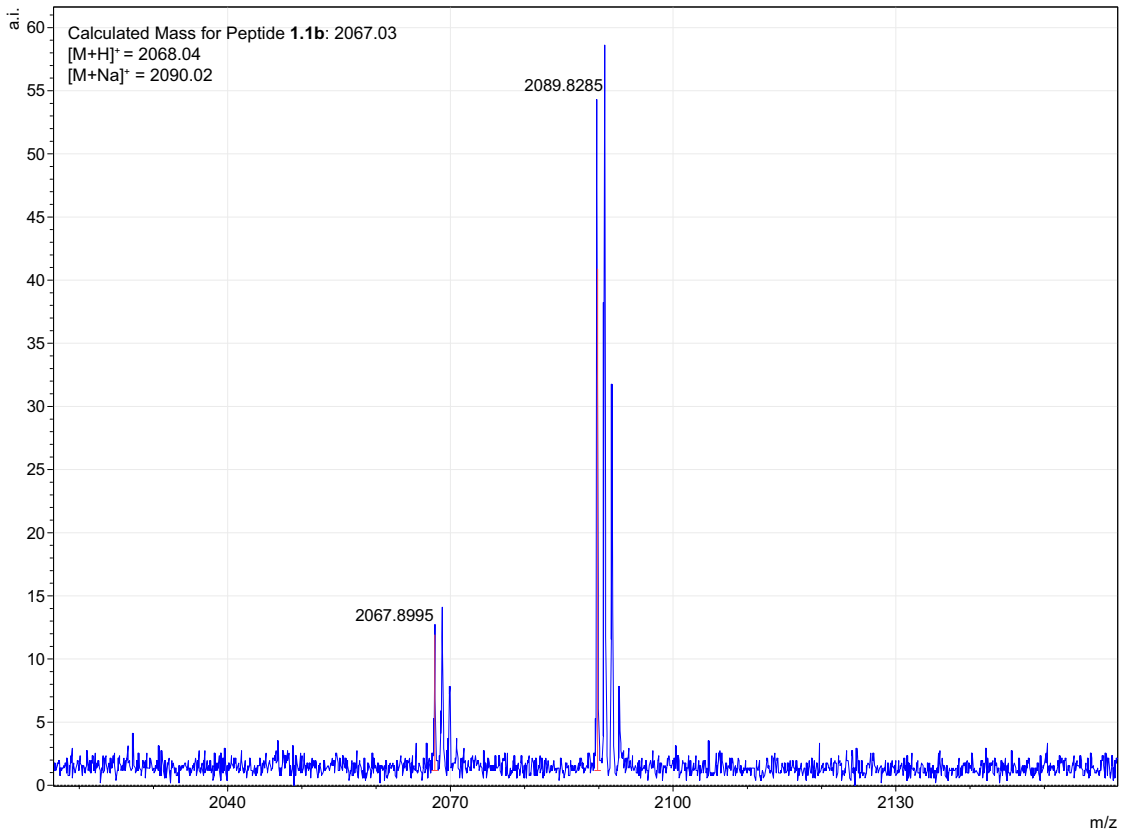
Calculated Mass for Peptide **1.1b**: 2067.03
[M+H]+ = 2068.04
[M+Na]+ = 2090.02
2089.8285
2067.8995
a.i.
m/z

Characterization of ***Peptide 1.2a***

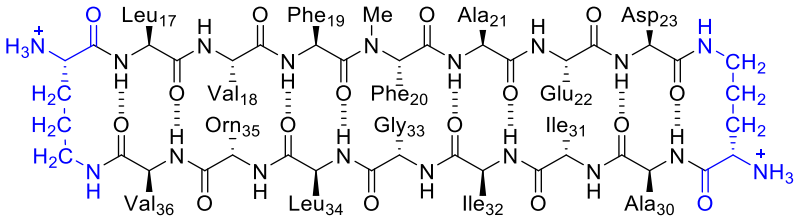

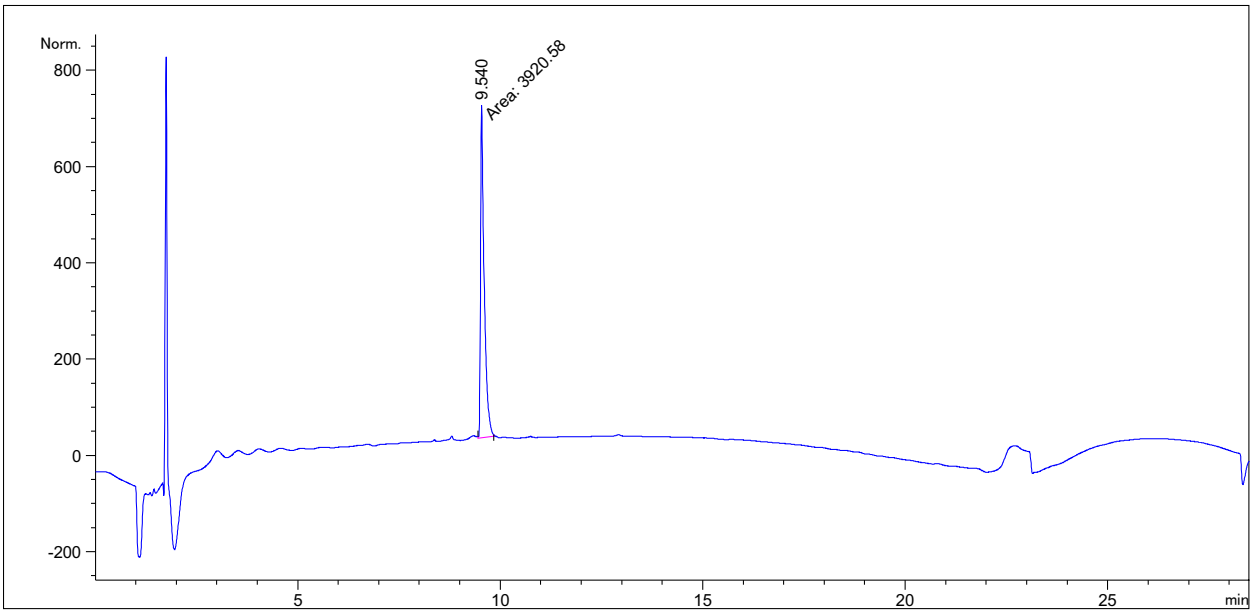

Signal 1: MWD1 A, Sig=214,4 Ref=off

Peak #	RetTime [min]	Type	Width [min]	Area [mAU*s]	Height [mAU]	Area %
1	9.540	MM	0.1046	3920.57837	624.91919	100.0000

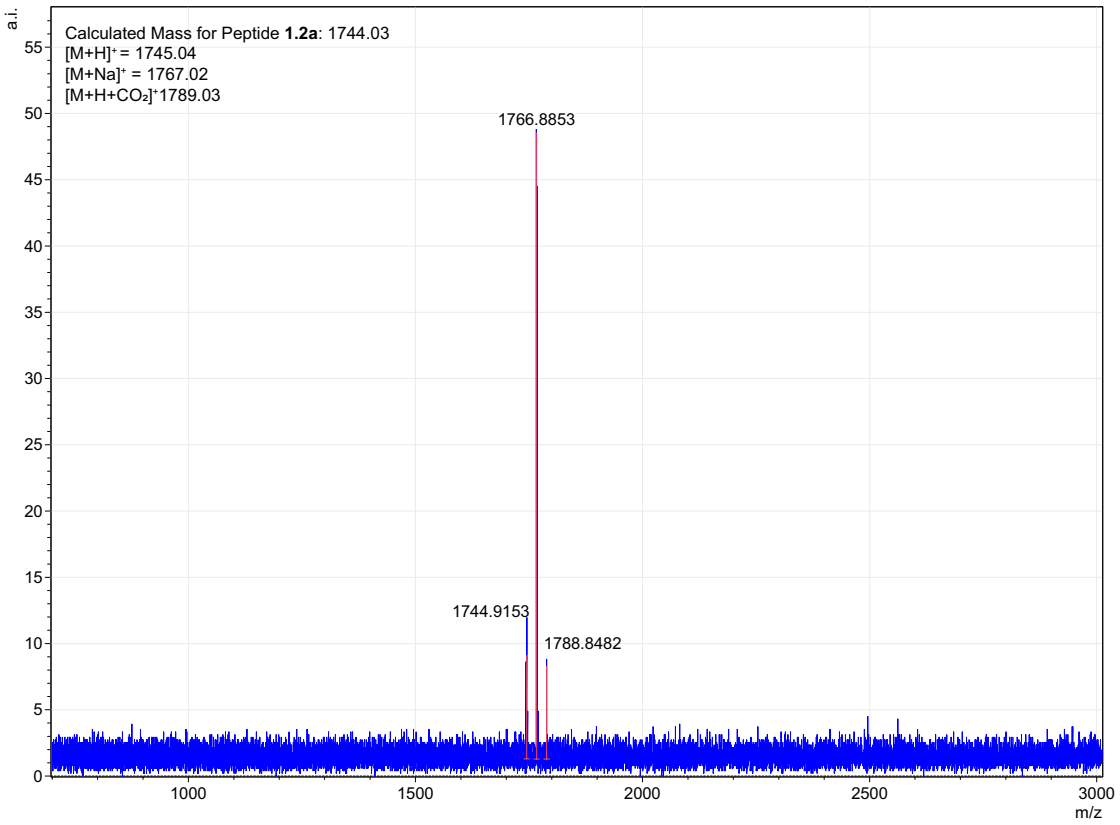
Calculated Mass for Peptide **1.2a**: 1744.03
[M+H]+ = 1745.04
[M+Na]+ = 1767.02
[M+H+CO2]+1789.03
1766.8853
1744.9153
1788.8482
a.i.
m/z

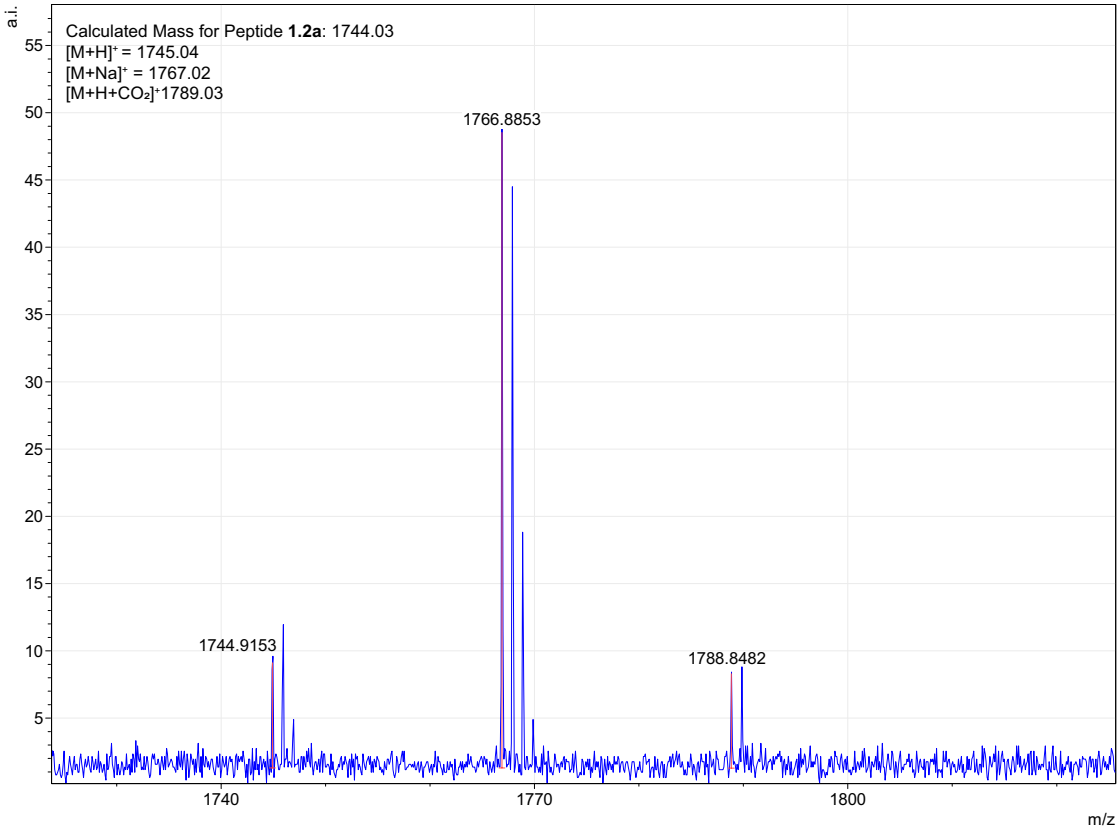
Calculated Mass for Peptide **1.2a**: 1744.03
[M+H]+ = 1745.04
[M+Na]+ = 1767.02
[M+H+CO2]+1789.03
1766.8853
1744.9153
1788.8482
a.i.
m/z

Characterization of ***Peptide 1.2b***

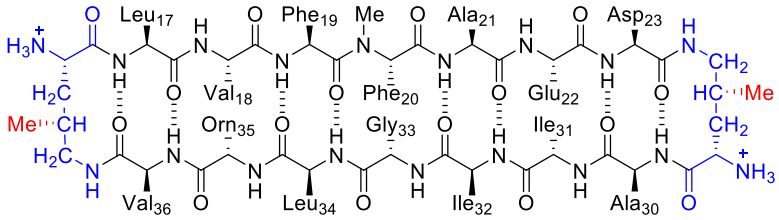

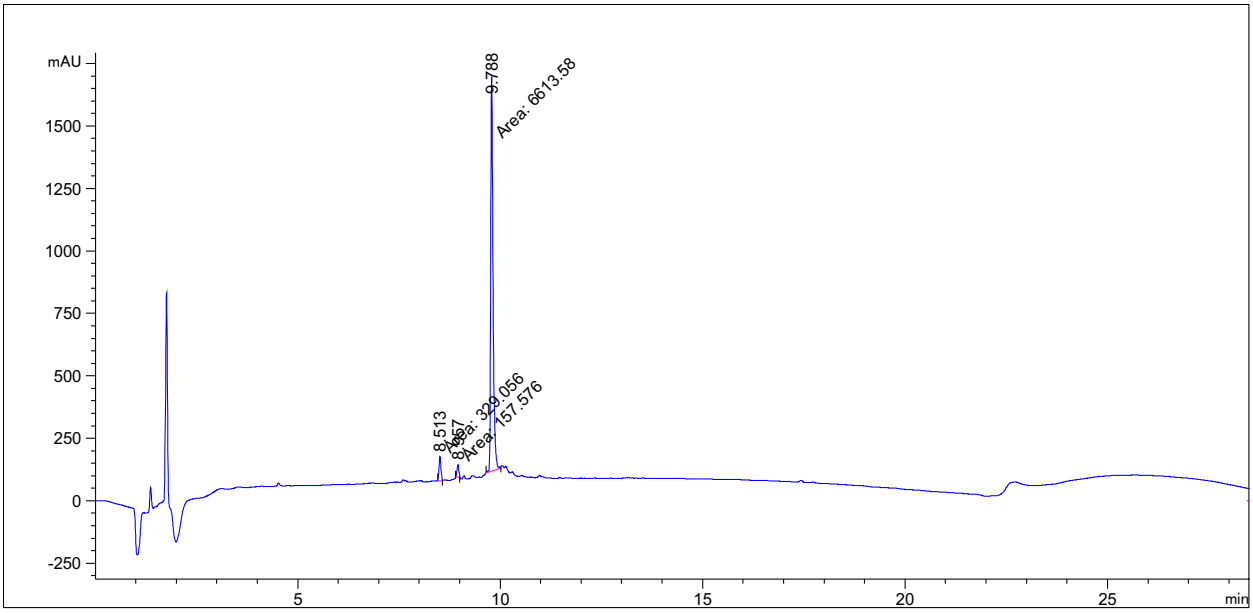

Signal 1: MWD1 A, Sig=214,4 Ref=off

Peak #	RetTime [min]	Type	Width [min]	Area [mAU*s]	Height [mAU]	Area %
1	8.513	MM	0.0556	329.05609	98.68935	4.6345
2	8.957	MM	0.0526	157.57594	49.94323	2.2193
3	9.788	MM	0.0694	6613.57959	1589.05005	93.1462

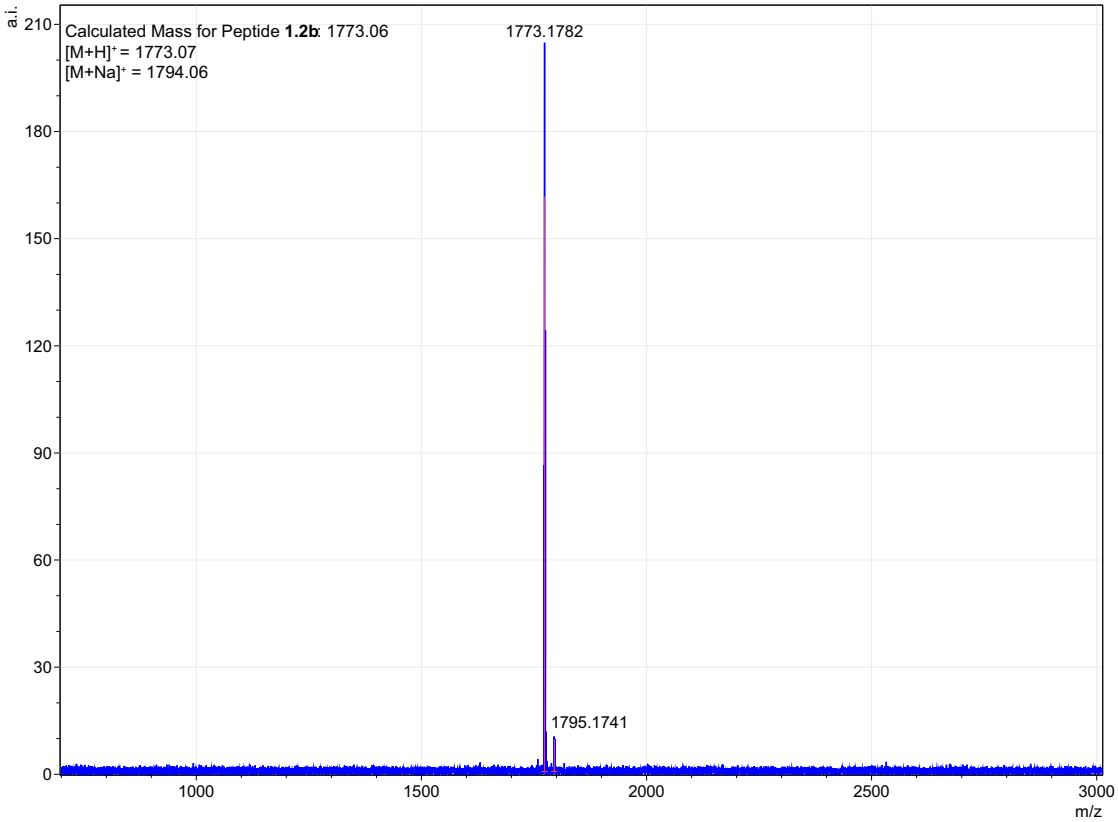
a.i.
Calculated Mass for Peptide **1.2b**: 1773.06
[M+H]+ = 1773.07
[M+Na]+ = 1794.06
1773.1782
1795.1741
m/z

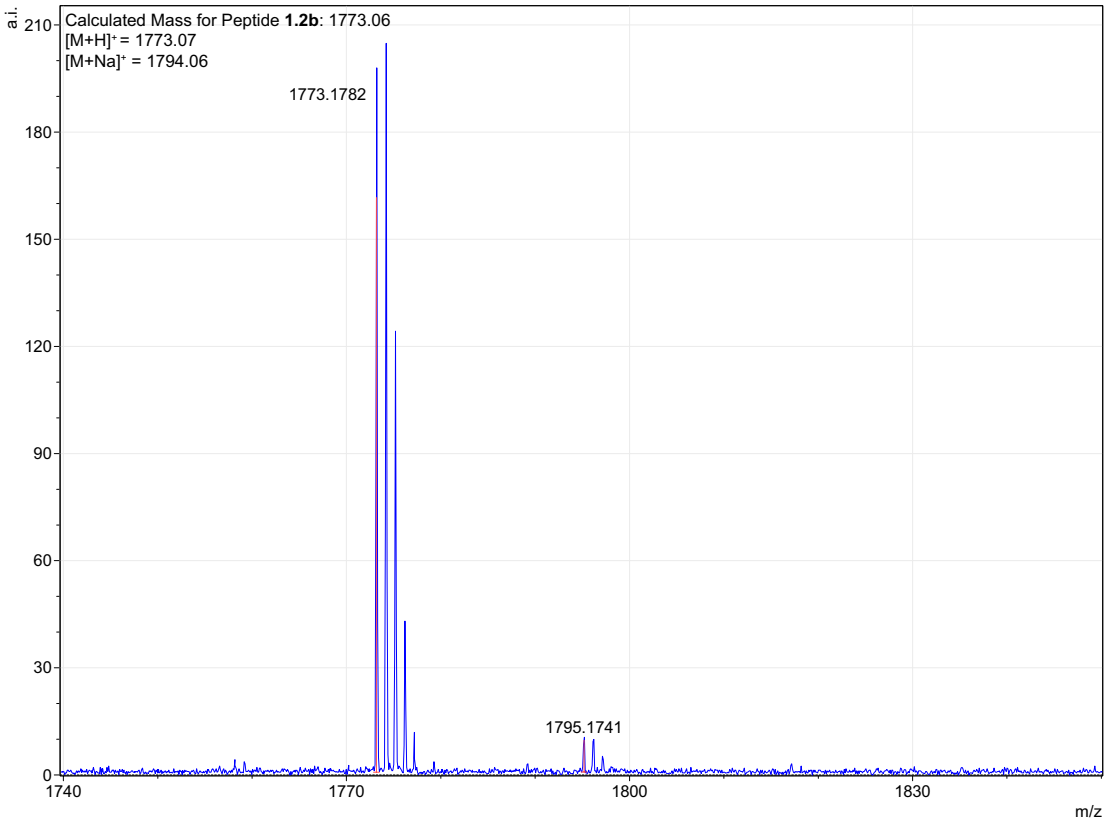
a.i.
Calculated Mass for Peptide **1.2b**: 1773.06
[M+H]+ = 1773.07
[M+Na]+ = 1794.06
1773.1782
1795.1741
m/z

Characterization of ***Peptide 1.3***

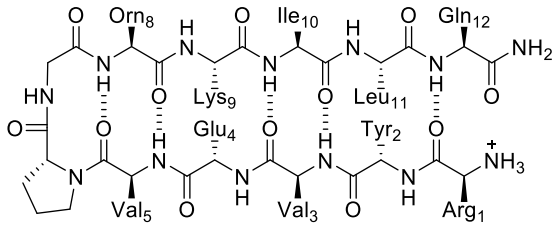

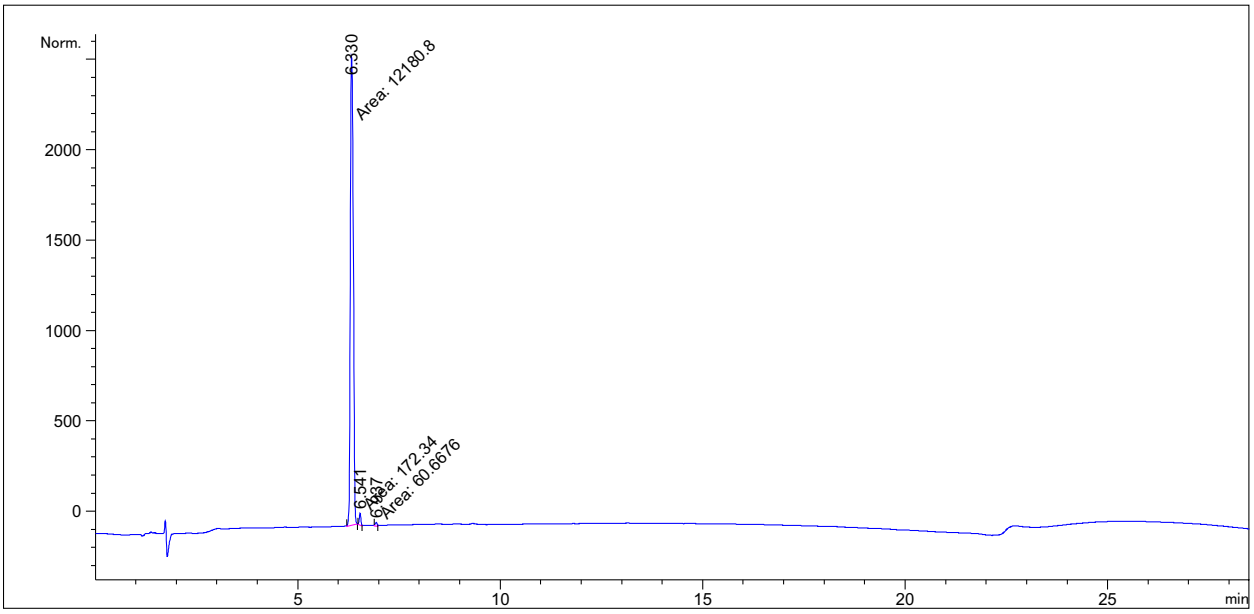

Signal 1: MWD1 A, Sig=214,4 Ref=off

Peak #	RetTime [min]	Type	Width [min]	Area [mAU*s]	Height [mAU]	Area %
1	6.330	MM	0.0867	1.21808e4	2341.82910	98.1230
2	6.541	MM	0.0480	172.34038	59.83568	1.3883
3	6.937	MM	0.0557	60.66758	18.15911	0.4887

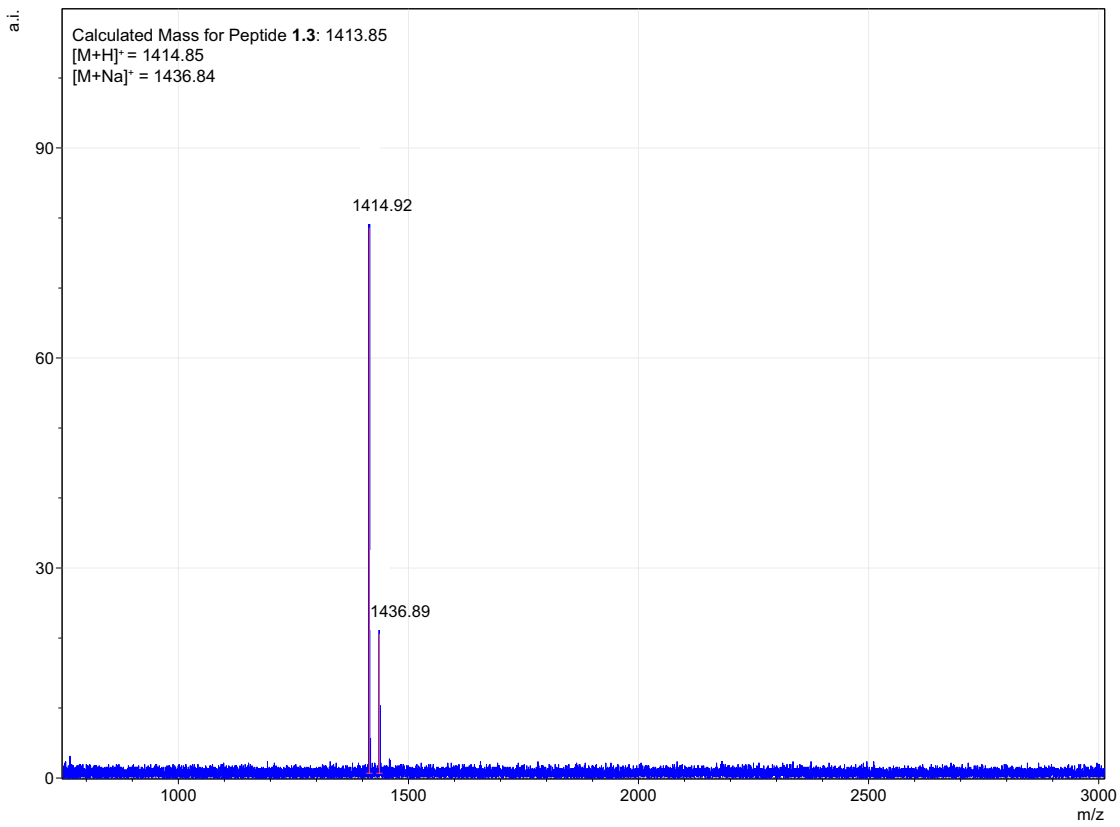
a.i.
Calculated Mass for Peptide **1.3**: 1413.85
[M+H]+ = 1414.85
[M+Na]+ = 1436.84
1414.92
1436.89
90
60
30
0
1000
1500
2000
2500
3000
m/z

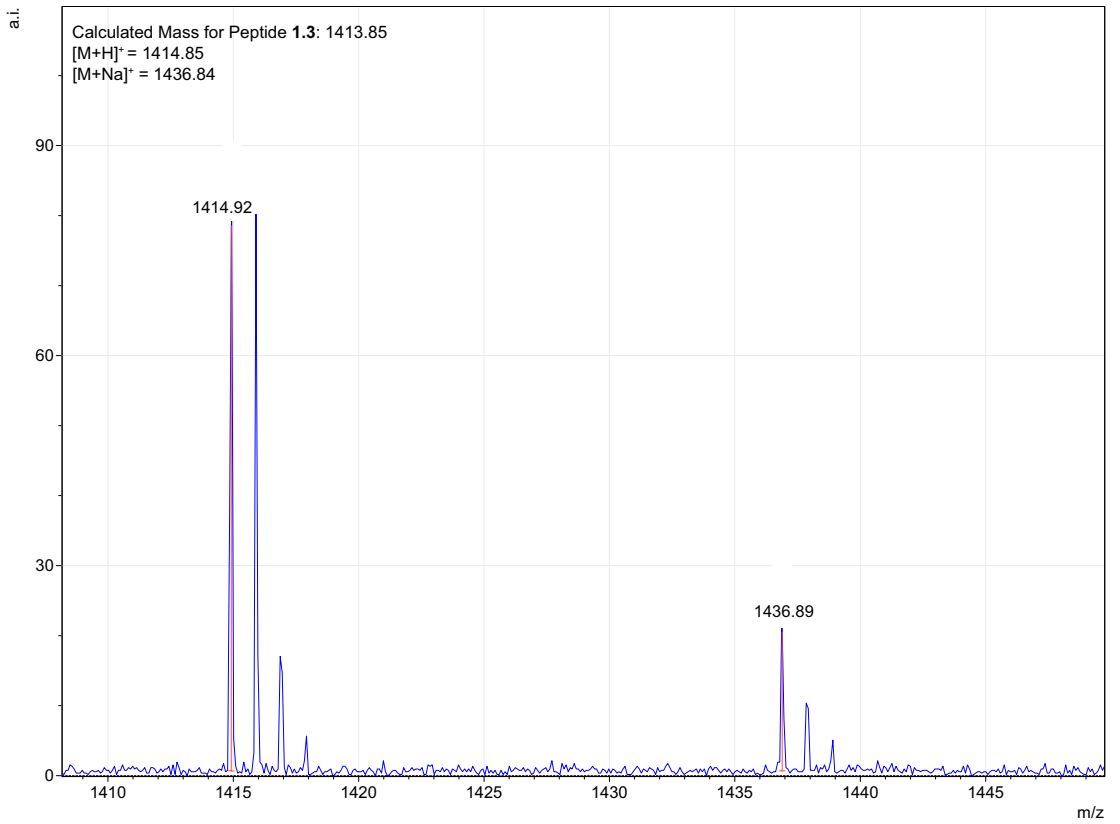
a.i.
Calculated Mass for Peptide **1.3**: 1413.85
[M+H]+ = 1414.85
[M+Na]+ = 1436.84
1414.92
1436.89
90
60
30
0
1410
1415
1420
1425
1430
1435
1440
1445
m/z

Characterization of ***Peptide 1.4a***

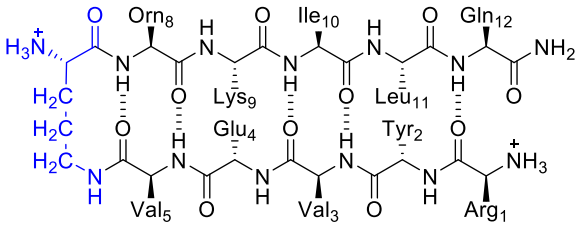

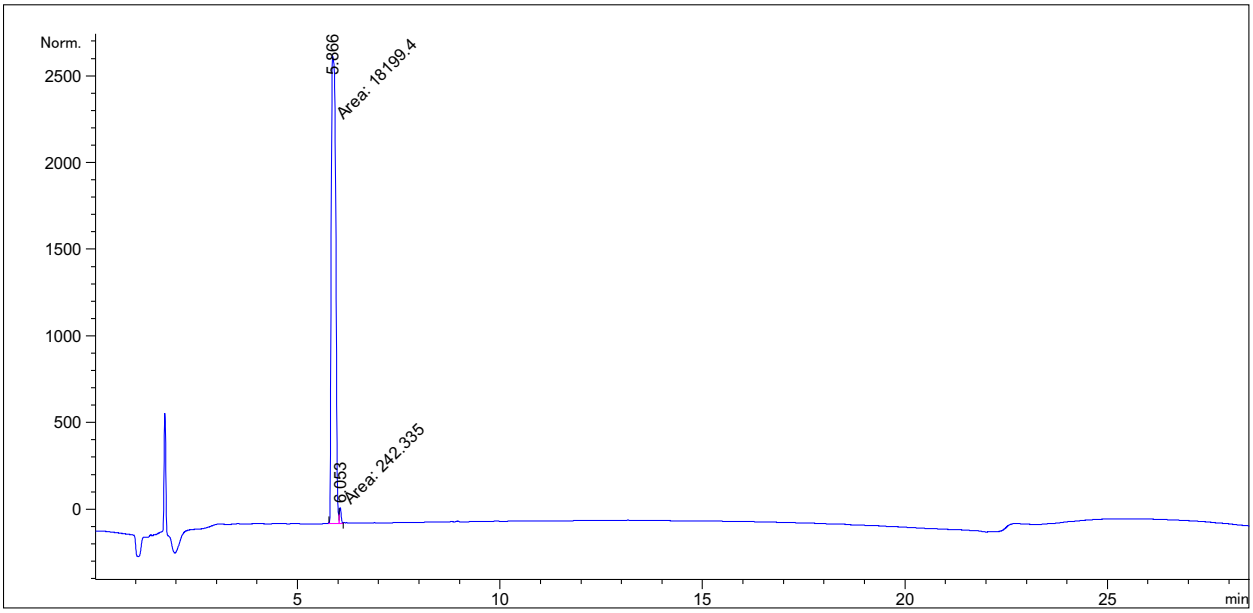

Signal 1: MWD1 A, Sig=214,4 Ref=off

Peak #	RetTime [min]	Type	Width [min]	Area [mAU*s]	Height [mAU]	Area %
1	5.866	MF	0.1247	1.81994e4	2432.17993	98.6859
2	6.053	FM	0.0483	242.33511	83.53979	1.3141

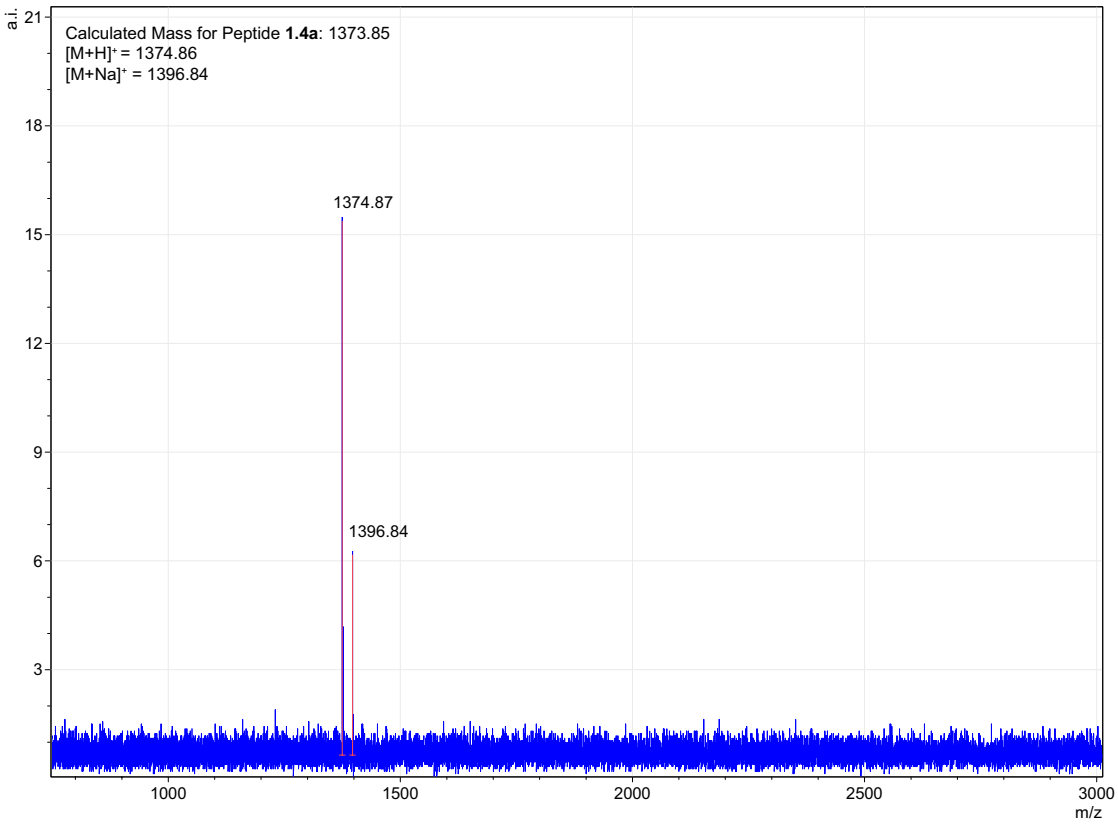
a.i.
Calculated Mass for Peptide **1.4a**: 1373.85
[M+H]+ = 1374.86
[M+Na]+ = 1396.84
1374.87
1396.84
m/z

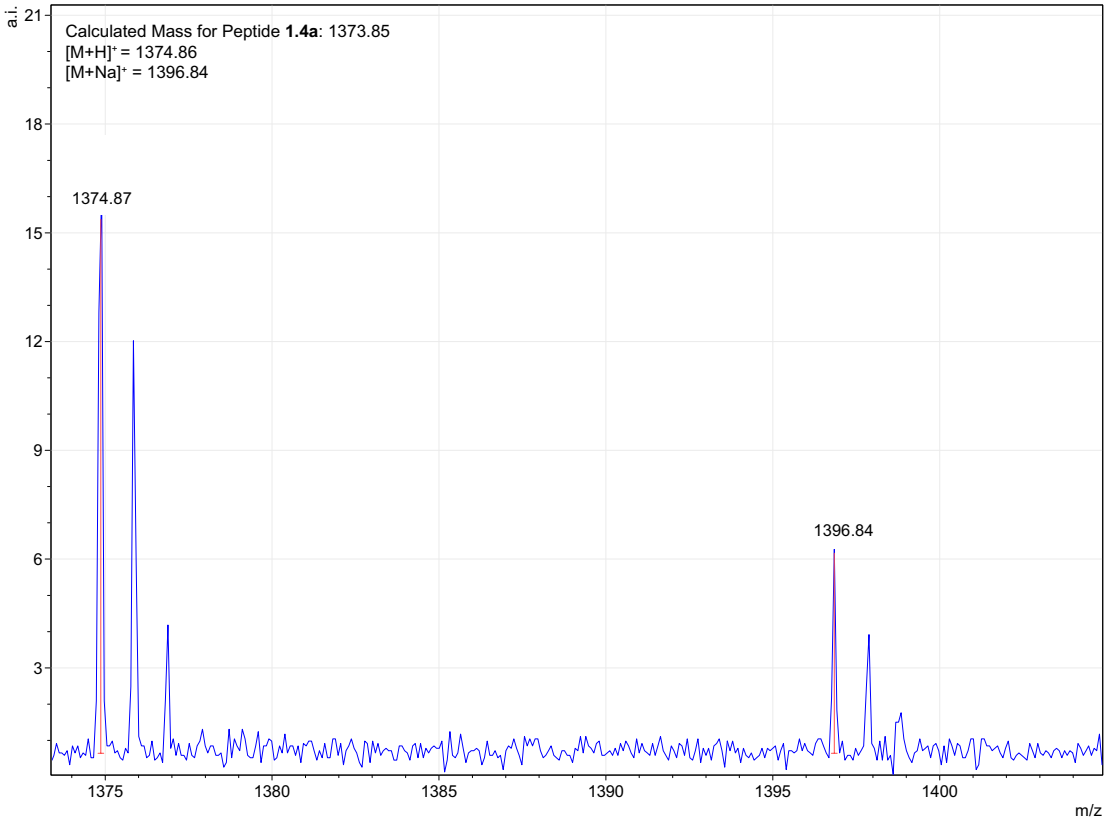
a.i.
Calculated Mass for Peptide **1.4a**: 1373.85
[M+H]+ = 1374.86
[M+Na]+ = 1396.84
1374.87
1396.84
m/z

Characterization of ***Peptide 1.4b***

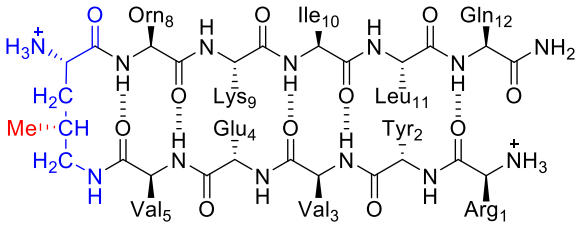

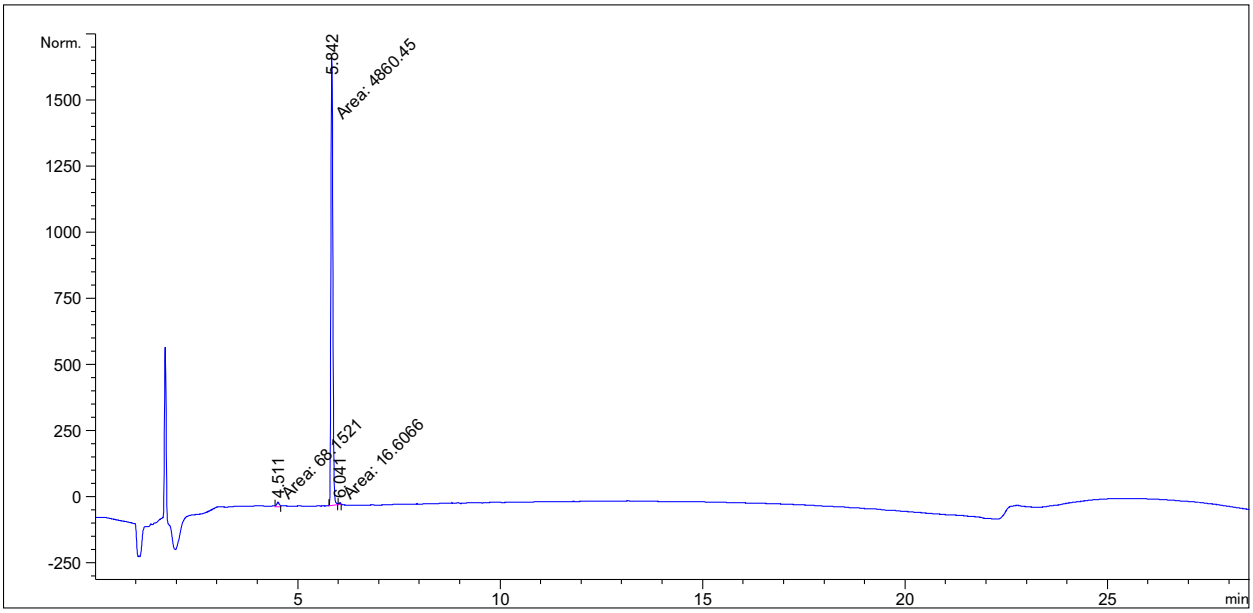

Signal 1: MWD1 A, Sig=214,4 Ref=off

Peak #	RetTime [min]	Type	Width [min]	Area [mAU*s]	Height [mAU]	Area %
1	4.511	MM	0.0780	68.15206	14.56390	1.3781
2	5.842	MM	0.0525	4860.45313	1544.15430	98.2860
3	6.041	MM	0.0464	16.60662	5.96049	0.3358

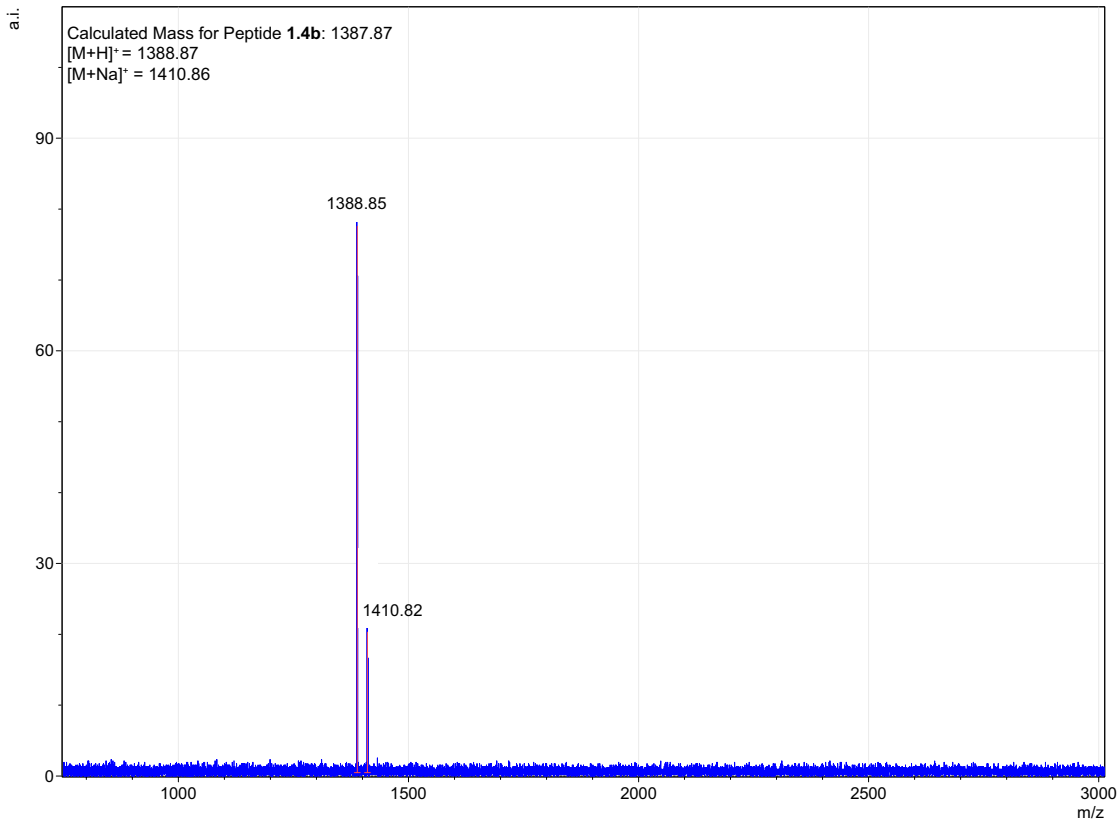
Calculated Mass for Peptide **1.4b**: 1387.87
[M+H]+ = 1388.87
[M+Na]+ = 1410.86
a.i.
90
60
30
0
1388.85
1410.82
1000
1500
2000
2500
3000
m/z

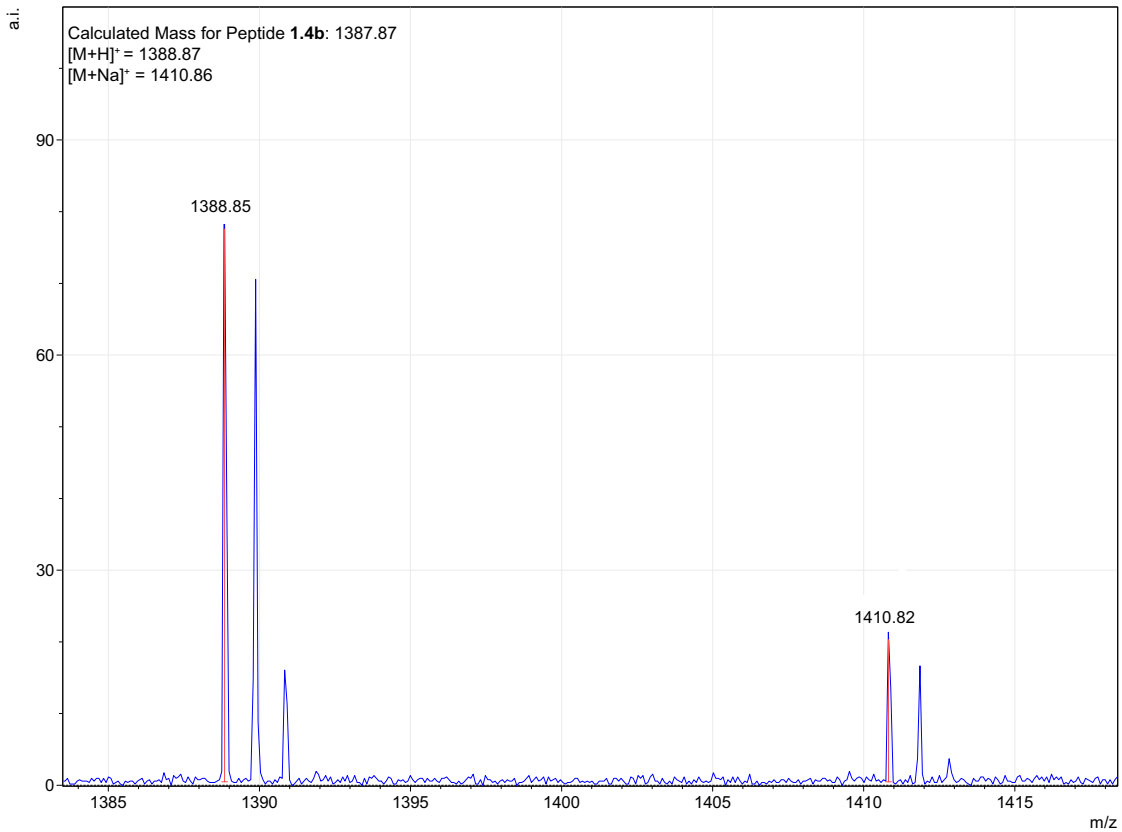
Calculated Mass for Peptide **1.4b**: 1387.87
[M+H]+ = 1388.87
[M+Na]+ = 1410.86
a.i.
90
60
30
0
1388.85
1410.82
1385
1390
1395
1400
1405
1410
1415
m/z

Characterization of ***Peptide 1.5***

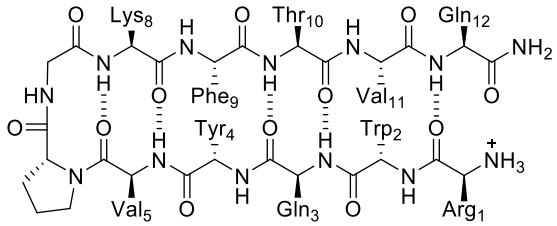

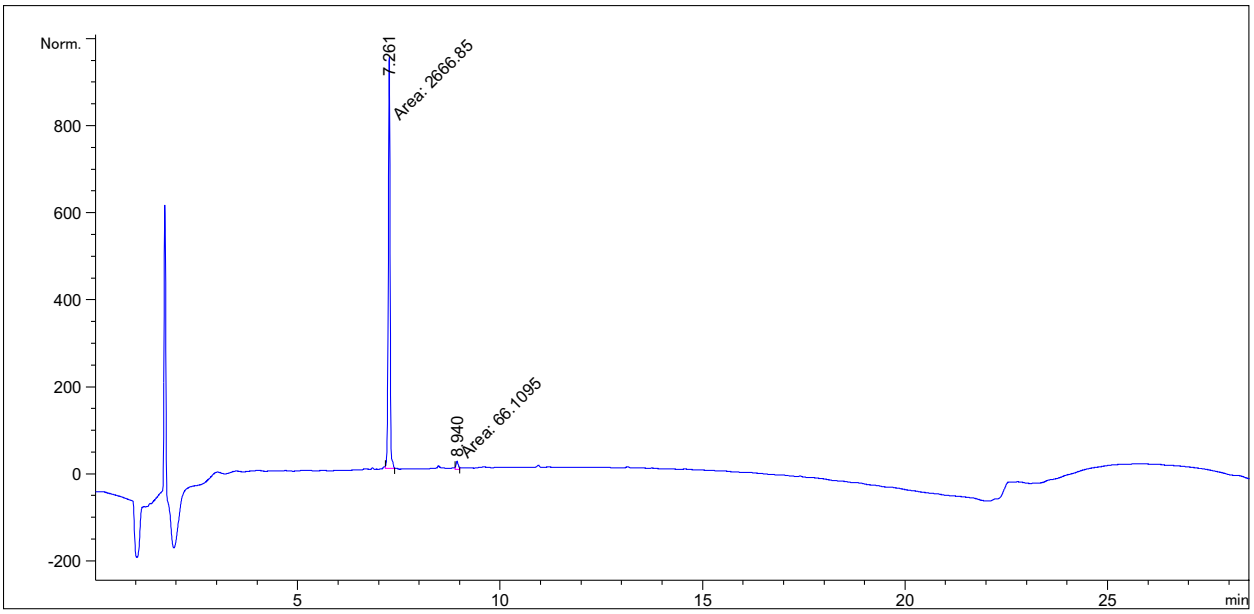

Signal 1: MWD1 A, Sig=214,4 Ref=off

Peak #	RetTime [min]	Type	Width [min]	Area [mAU*s]	Height [mAU]	Area %
1	7.261	MM	0.0516	2666.84766	862.12610	97.5810
2	8.940	MM	0.0669	66.10948	16.46899	2.4190

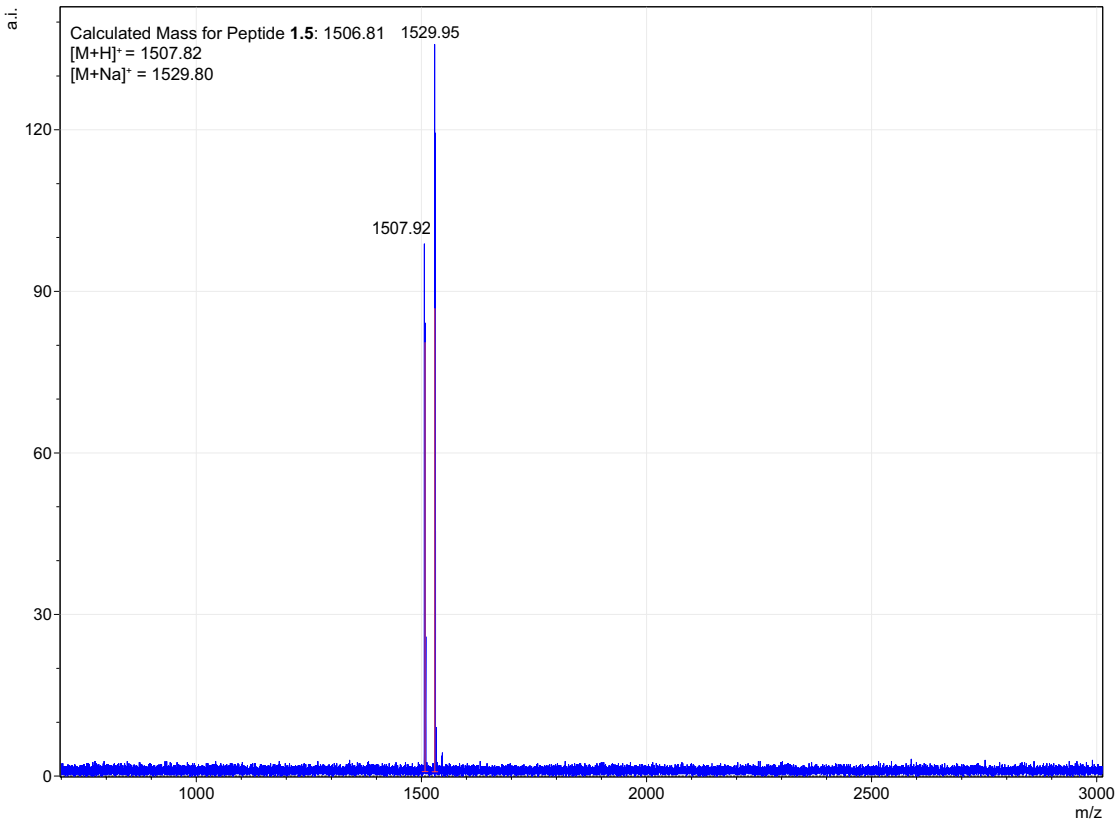
a.i.
Calculated Mass for Peptide **1.5**: 1506.81
[M+H]+ = 1507.82
[M+Na]+ = 1529.80
1529.95
1507.92
120
90
60
30
0
1000
1500
2000
2500
3000
m/z

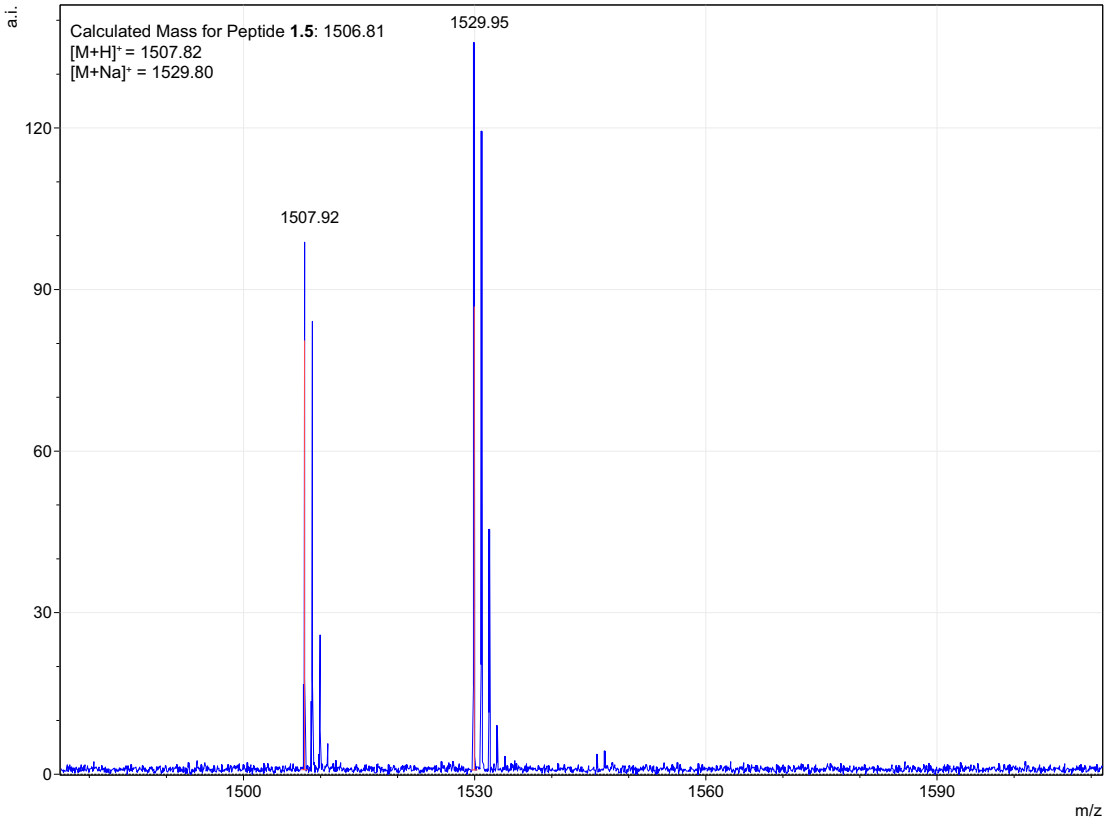
a.i.
Calculated Mass for Peptide **1.5**: 1506.81
[M+H]+ = 1507.82
[M+Na]+ = 1529.80
1529.95
1507.92
120
90
60
30
0
1500
1530
1560
1590
m/z

Characterization of ***Peptide 1.6a***

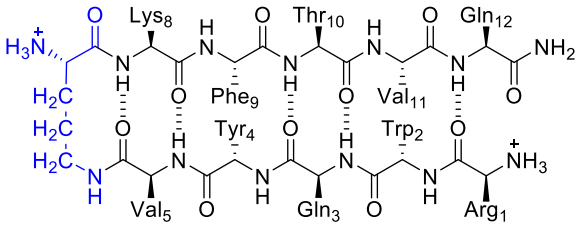

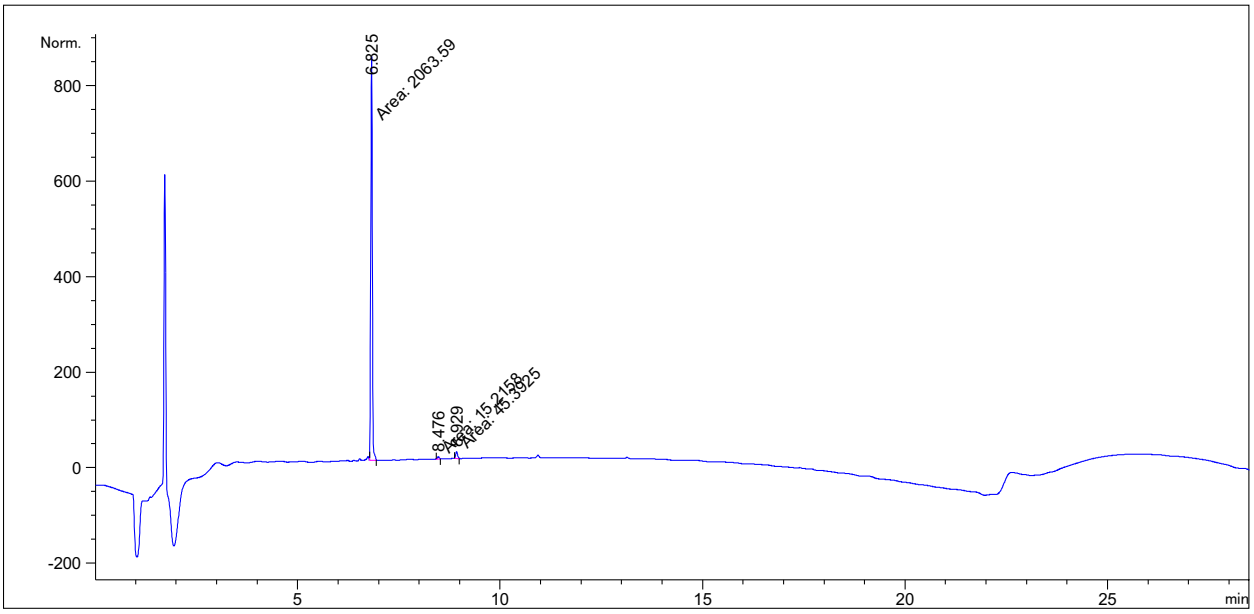

Signal 1: MWD1 A, Sig=214,4 Ref=off

Peak #	RetTime [min]	Type	Width [min]	Area [mAU*s]	Height [mAU]	Area %
1	6.825	MM	0.0448	2063.58545	767.19025	97.1468
2	8.476	MM	0.0535	15.21583	4.73603	0.7163
3	8.929	MM	0.0567	45.39245	13.35438	2.1369

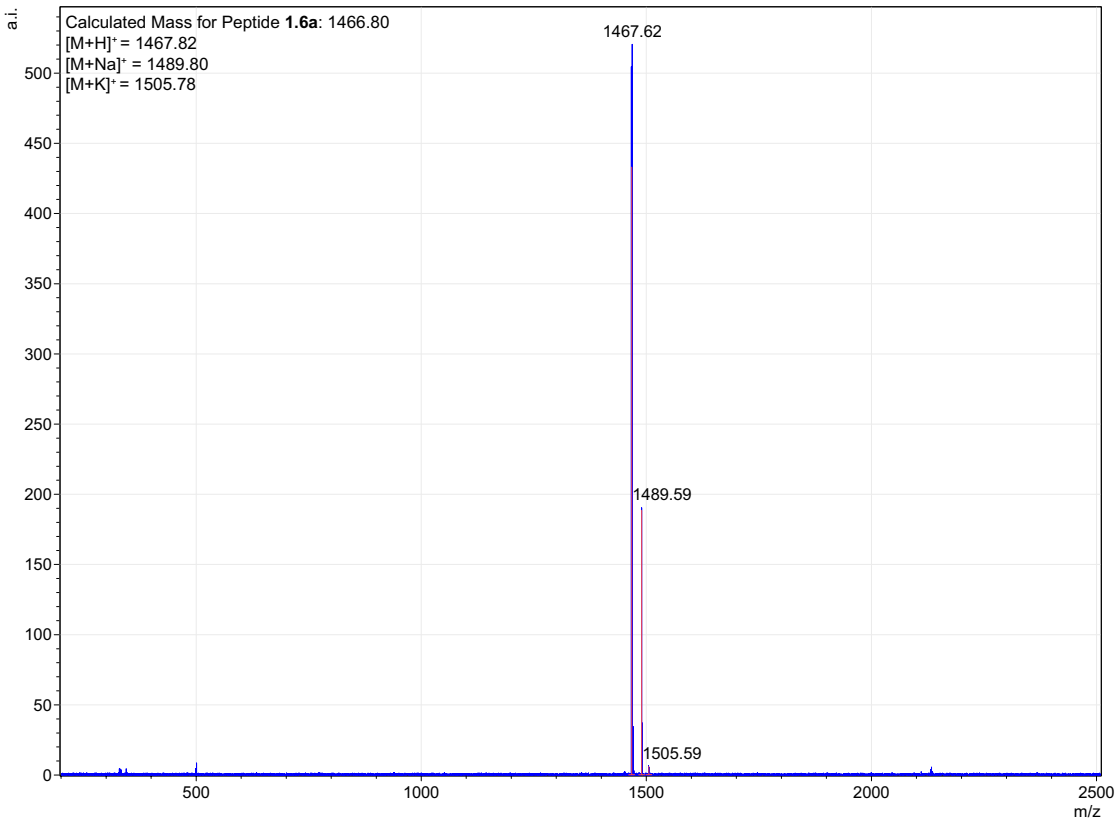
Calculated Mass for Peptide **1.6a**: 1466.80
[M+H]+ = 1467.82
[M+Na]+ = 1489.80
[M+K]+ = 1505.78
1467.62
1489.59
1505.59
a.i.
m/z

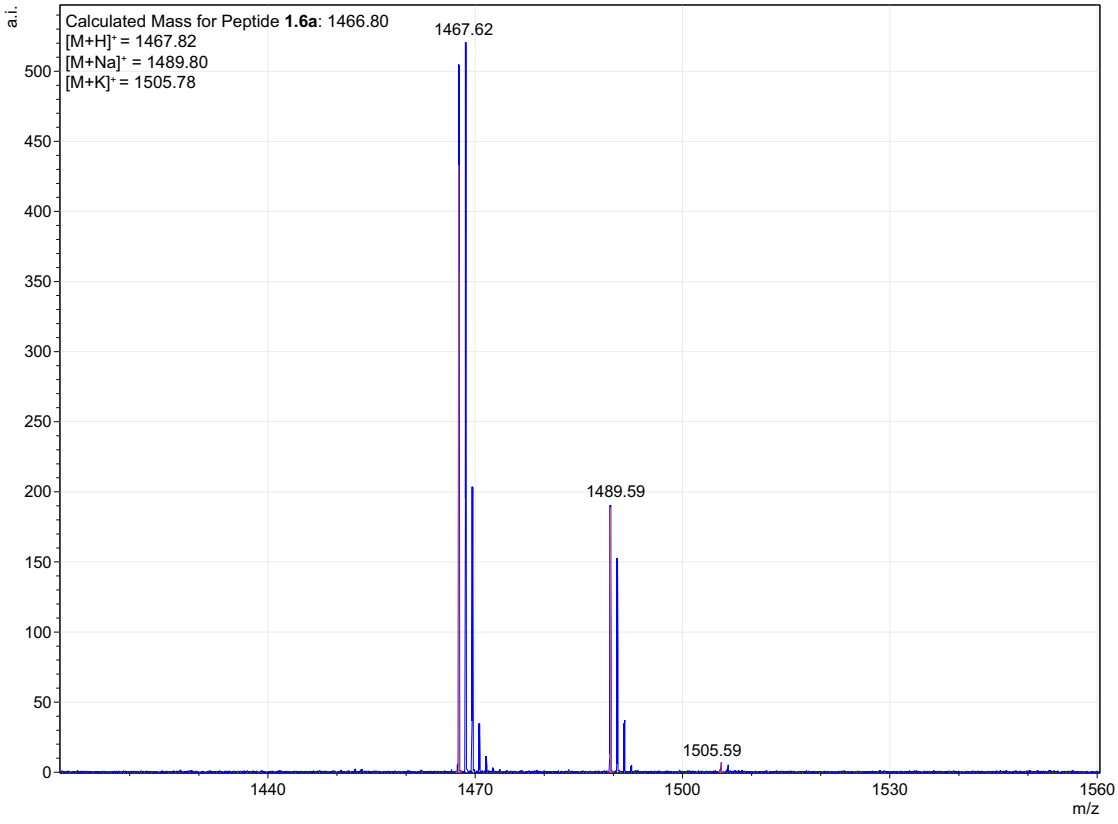
Calculated Mass for Peptide **1.6a**: 1466.80
[M+H]+ = 1467.82
[M+Na]+ = 1489.80
[M+K]+ = 1505.78
1467.62
1489.59
1505.59
a.i.
m/z

Characterization of ***Peptide 1.6b***

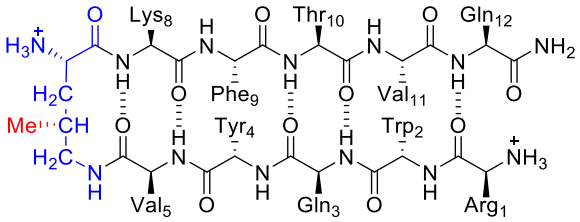

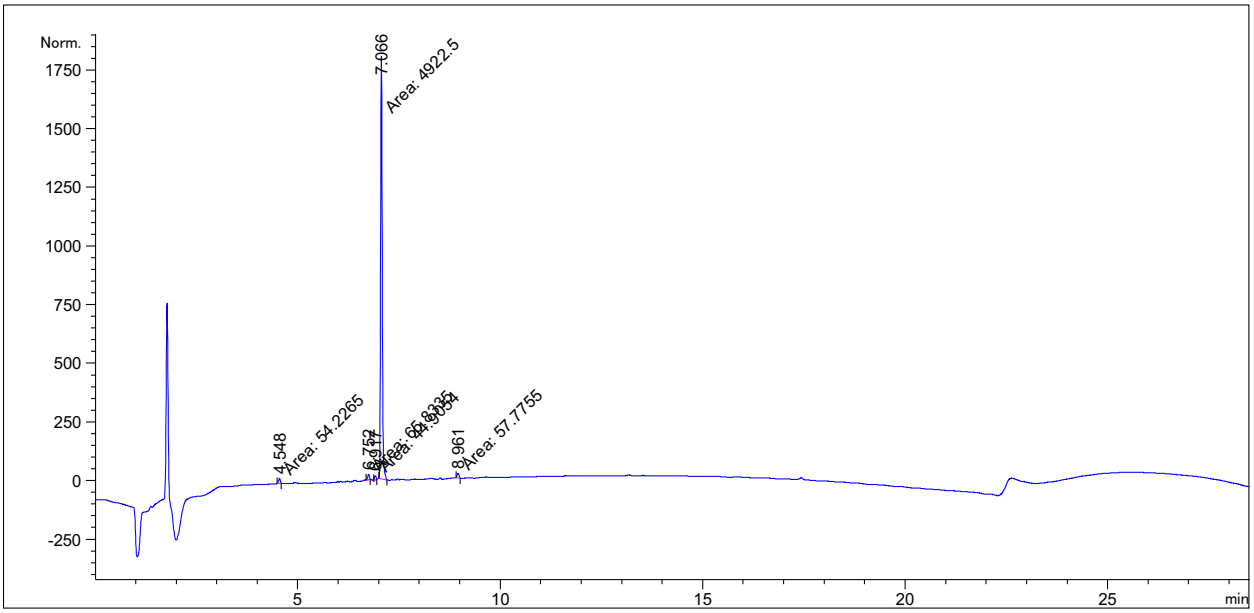

Signal 1: MWD1 A, Sig=214,4 Ref=off

Peak #	RetTime [min]	Type	Width [min]	Area [mAU*s]	Height [mAU]	Area %
1	4.548	MM	0.0495	54.22652	18.26375	1.0539
2	6.752	MM	0.0528	65.83348	20.77038	1.2795
3	6.917	MM	0.0450	44.90536	16.63755	0.8728
4	7.066	MM	0.0500	4922.50439	1642.43701	95.6709
5	8.961	MM	0.0545	57.77552	17.67418	1.1229

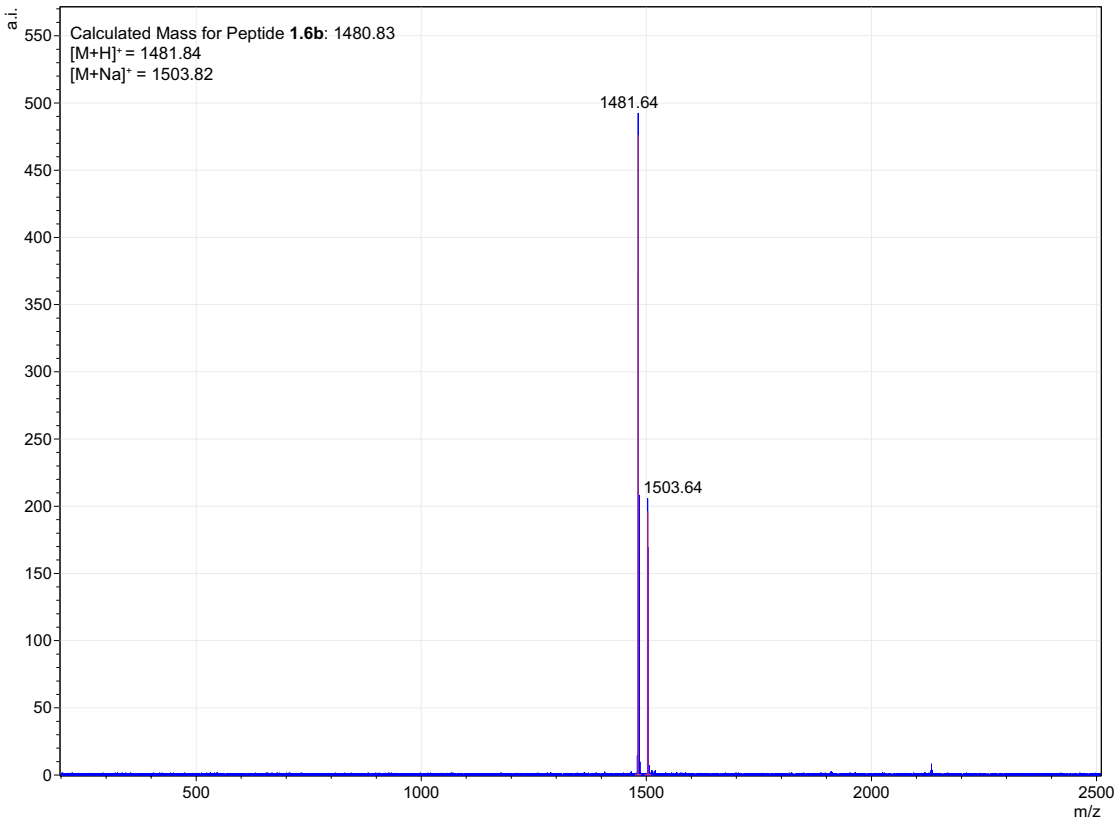
a.i.
Calculated Mass for Peptide **1.6b**: 1480.83
[M+H]+ = 1481.84
[M+Na]+ = 1503.82
1481.64
1503.64
m/z

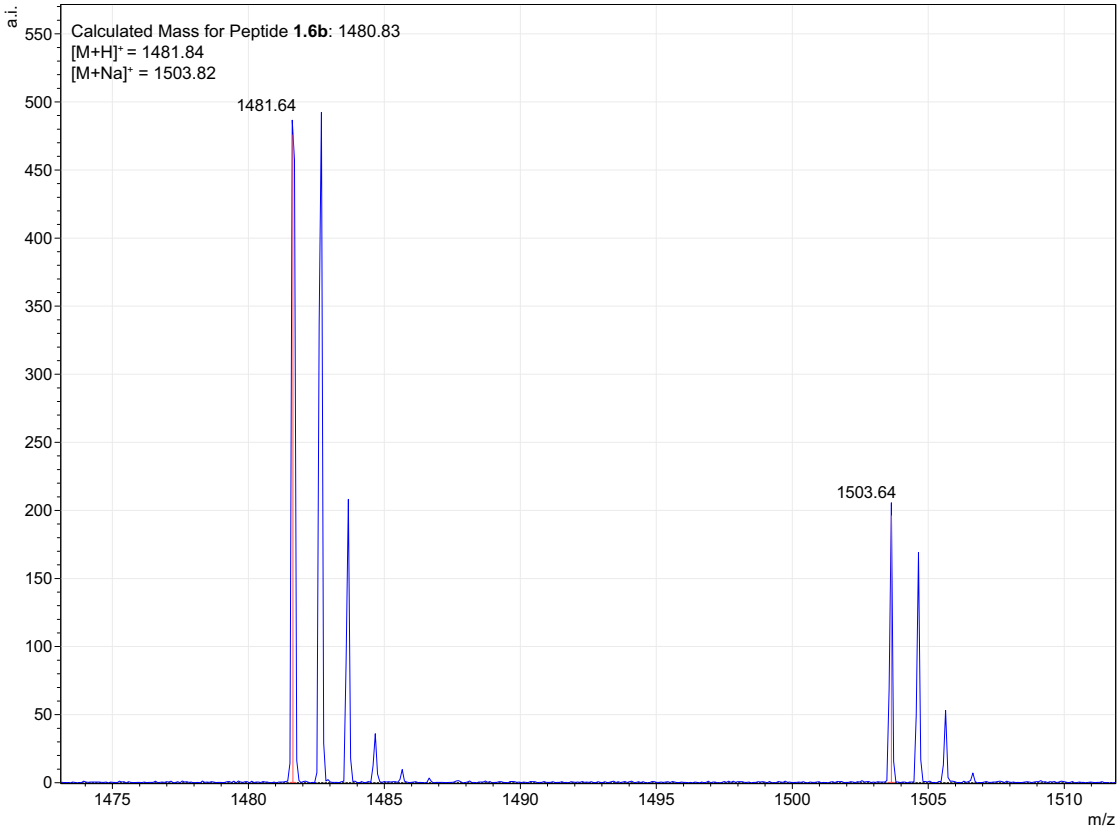
a.i.
Calculated Mass for Peptide **1.6b**: 1480.83
[M+H]+ = 1481.84
[M+Na]+ = 1503.82
1481.64
1503.64
m/z

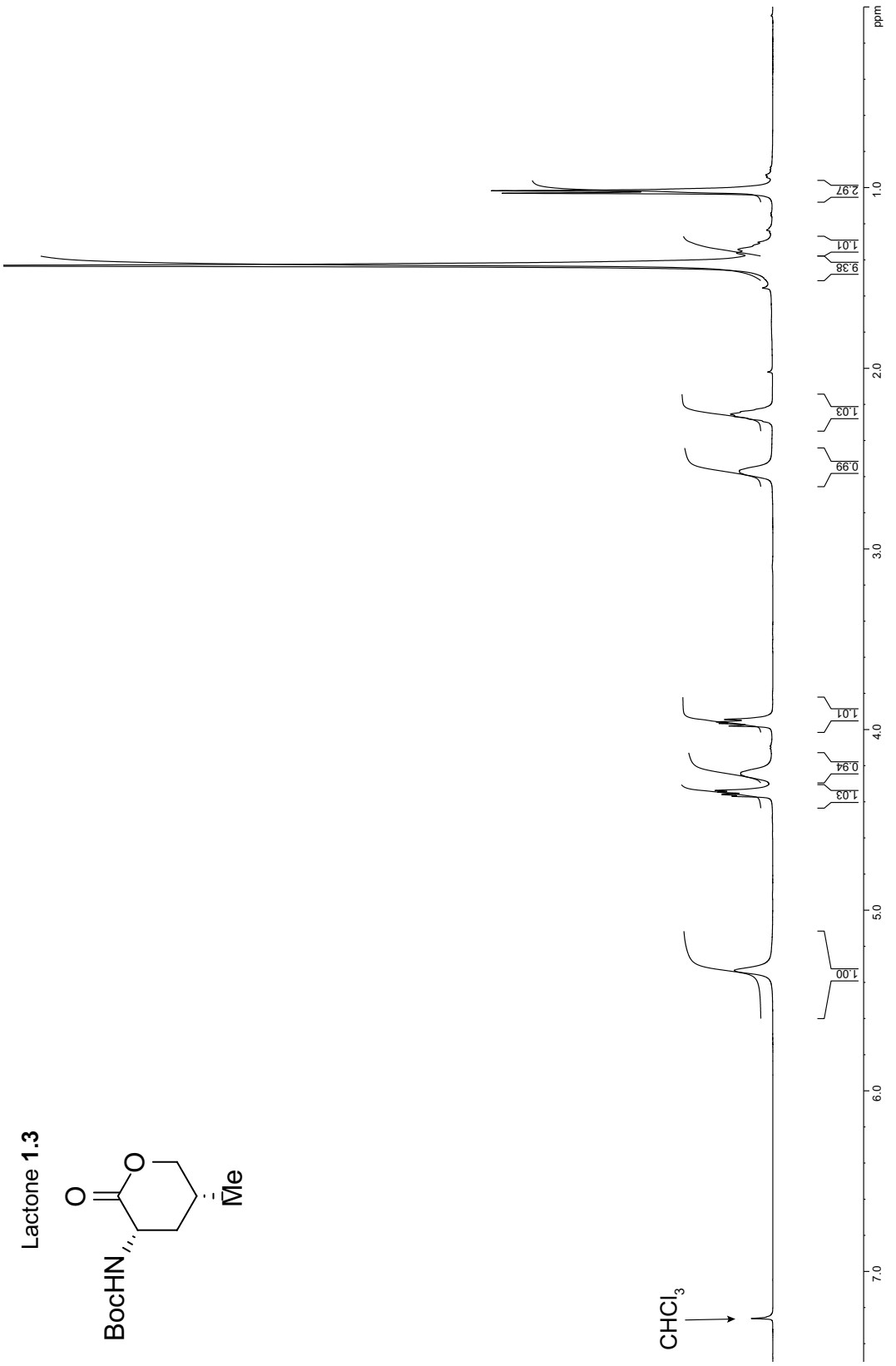
Lactone 1.3
BocHN
O
O
Me
CHCl3
ppm
1.00
1.03
0.94
1.01
1.03
0.99
1.01
9.38
2.97

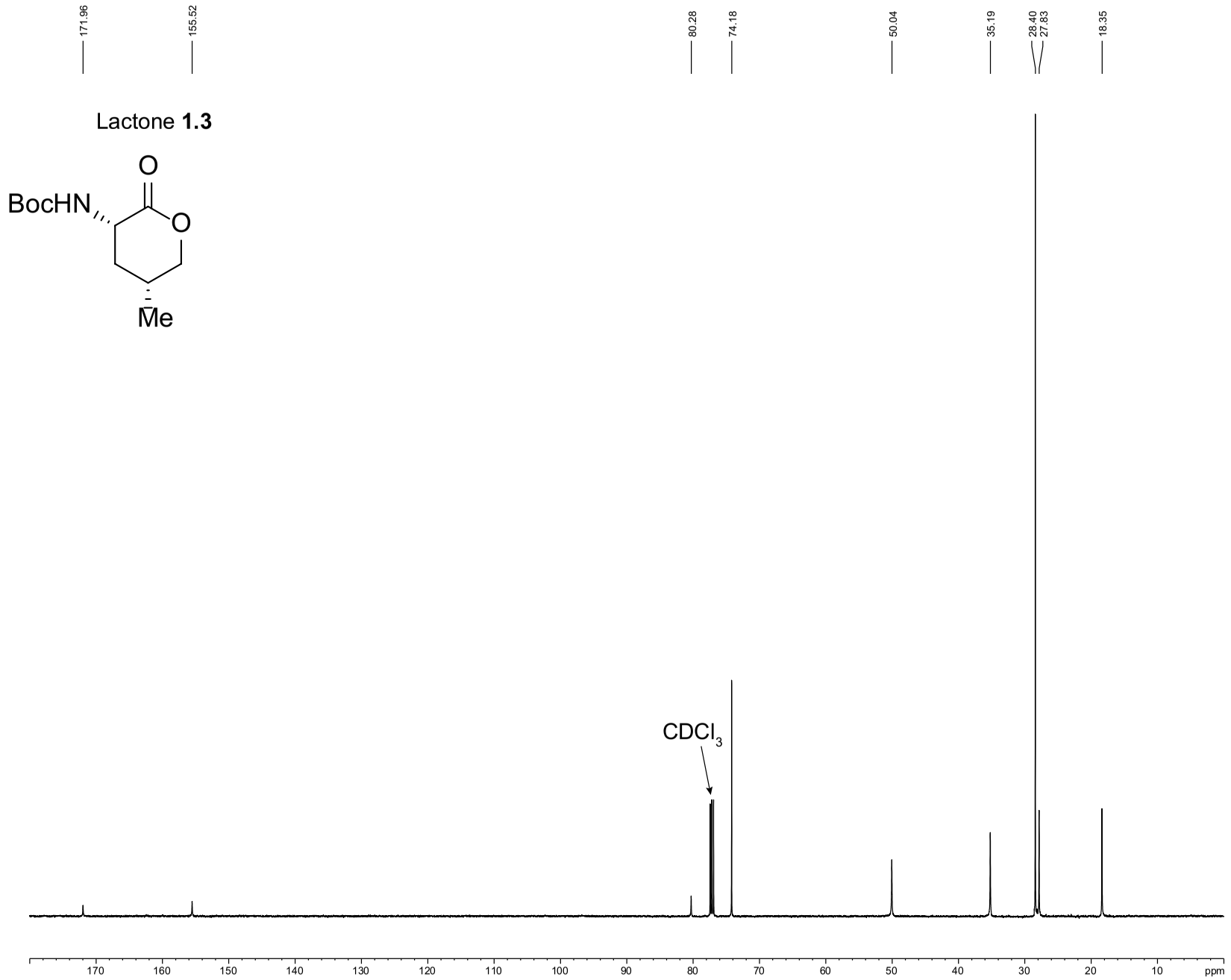
171.96
155.52
80.28
74.18
50.04
35.19
28.40
27.83
18.35
Lactone **1.3**
O
BocHN
O
Me
CDCl3
170
160
150
140
130
120
110
100
90
80
70
60
50
40
30
20
10
ppm

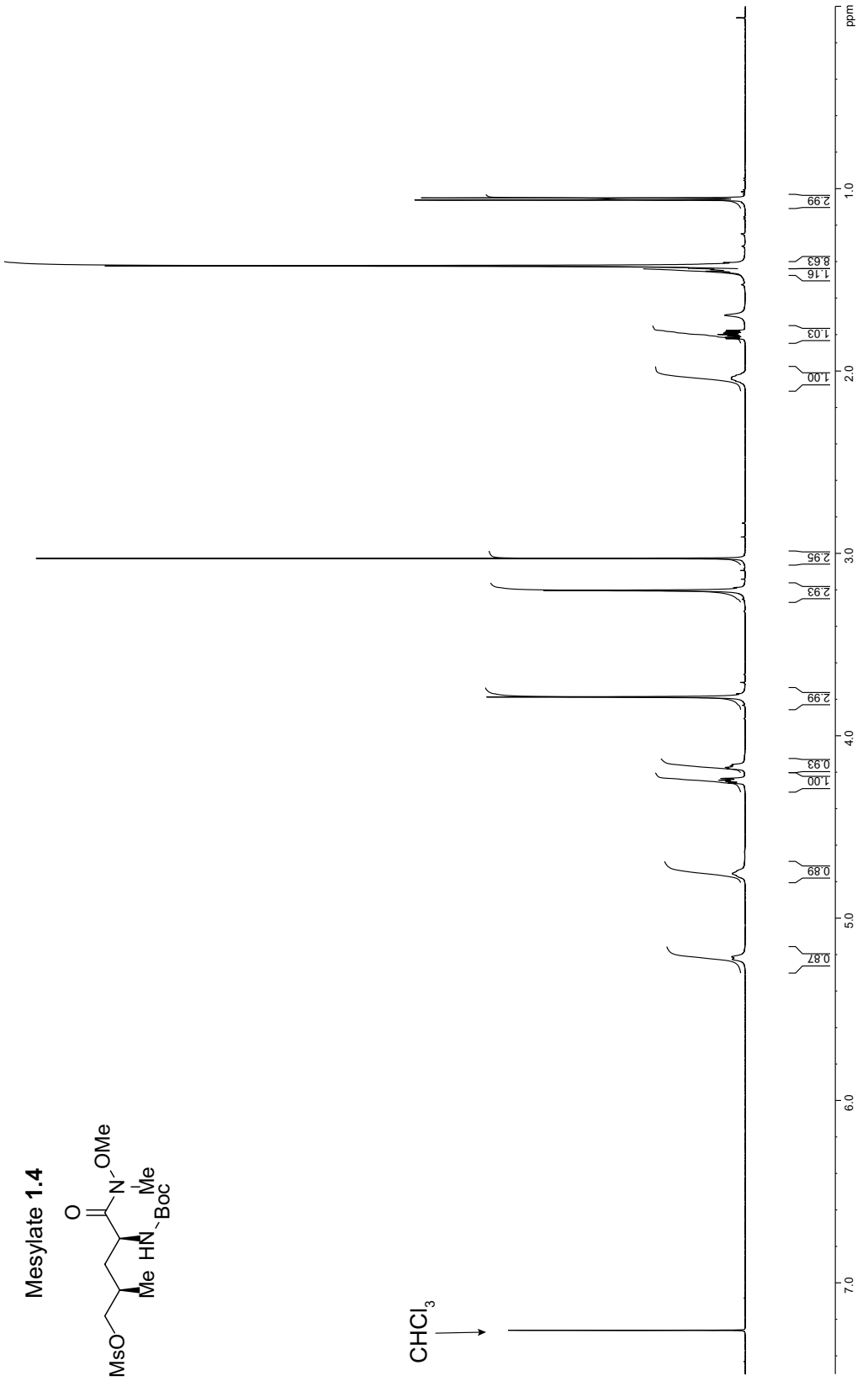
Mesylate 1.4
O
OMe
N
Me
Me HN
Boc
MsO
CHCl3
2.99
8.63
1.16
1.03
1.00
2.95
2.93
2.99
0.93
1.00
0.89
0.87
ppm
1.0
2.0
3.0
4.0
5.0
6.0
7.0

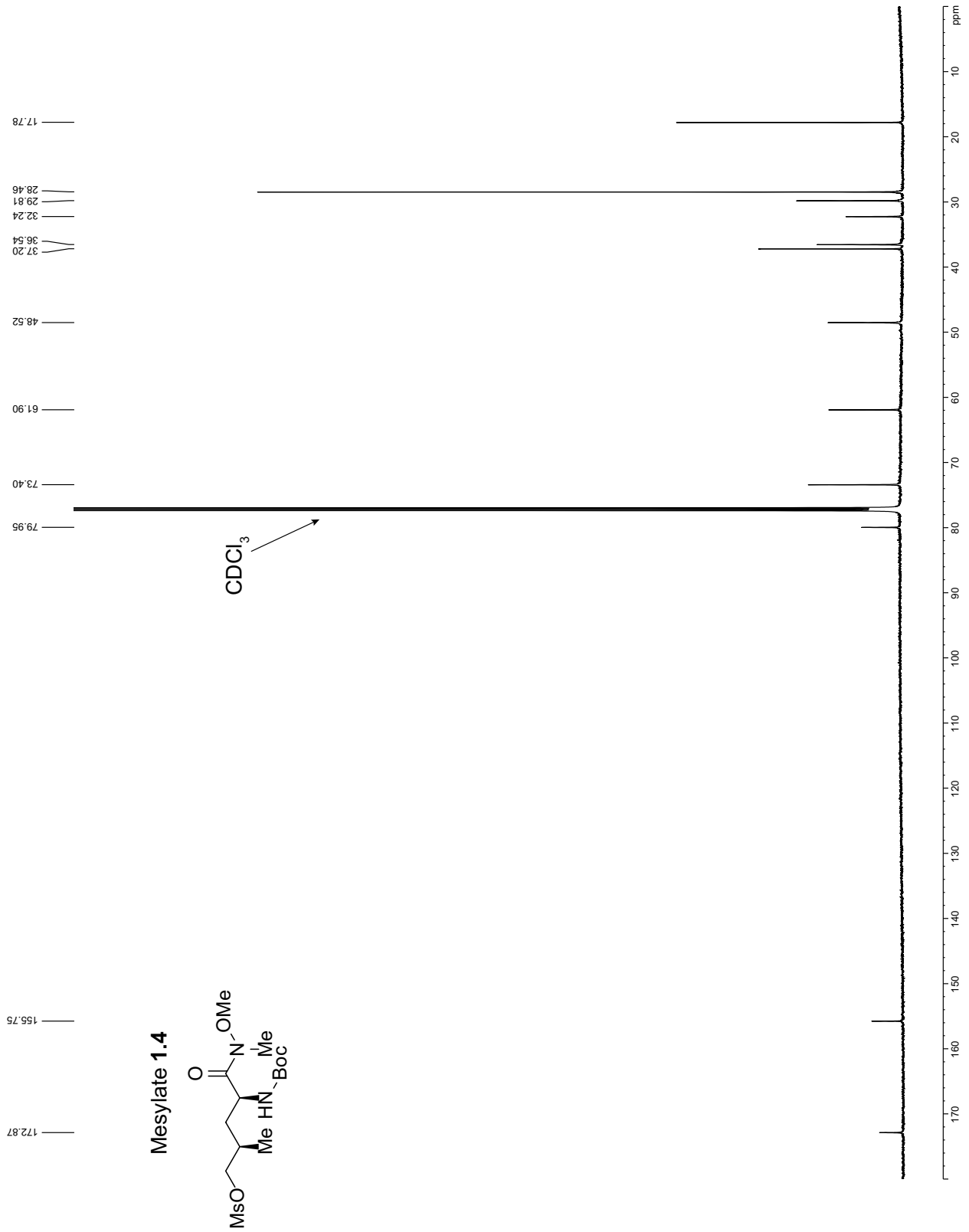
Mesylate 1.4
MsO
Me
HN
Boc
Me
N
OMe
O
CDCl3
172.87
155.75
79.95
73.40
61.90
48.52
37.20
36.54
32.24
29.81
28.46
17.78
ppm

Azide **1.5**

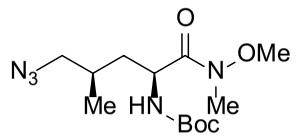
O
N3
OMe
N
Me
HN
Me
Boc

CHCl3
0.91
0.97
3.00
1.02
1.07
2.87
1.00
1.01
8.76
1.05
2.96
7.0
6.0
5.0
4.0
3.0
2.0
1.0
ppm

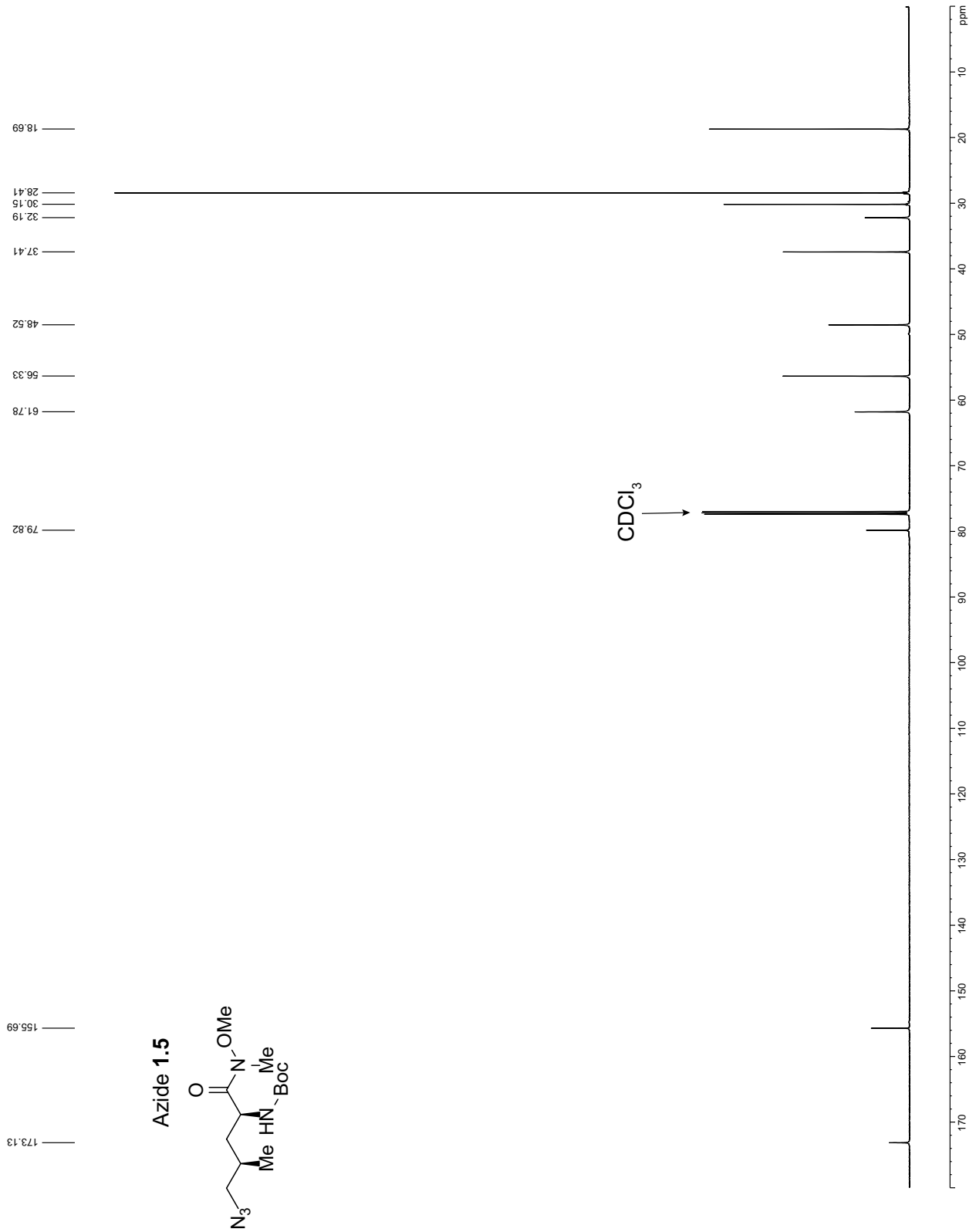
Azide 1.5
CDCl3
155.69
173.13
79.82
61.78
56.33
48.52
37.41
32.19
30.15
28.41
18.69
ppm

Boc-azidoleucine **1.6**

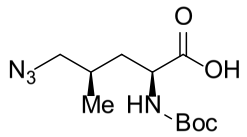

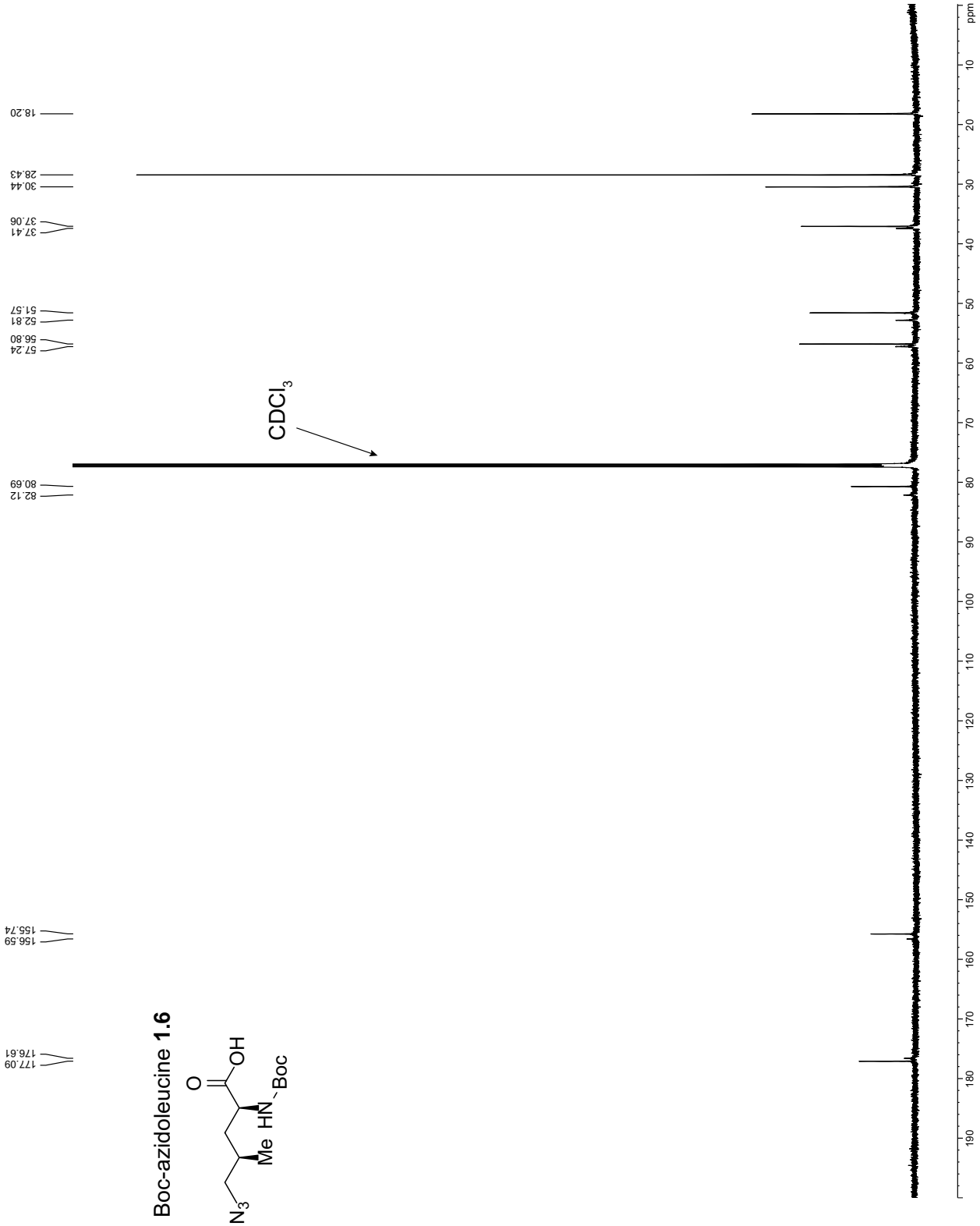
Boc-azidoleucine 1.6
O
OH
Me
HN
Boc
N3
CDCl3
177.09
176.61
156.59
155.74
82.12
80.69
57.24
56.80
52.81
51.57
37.41
37.06
30.44
28.43
18.20
ppm
10
20
30
40
50
60
70
80
90
100
110
120
130
140
150
160
170
180
190

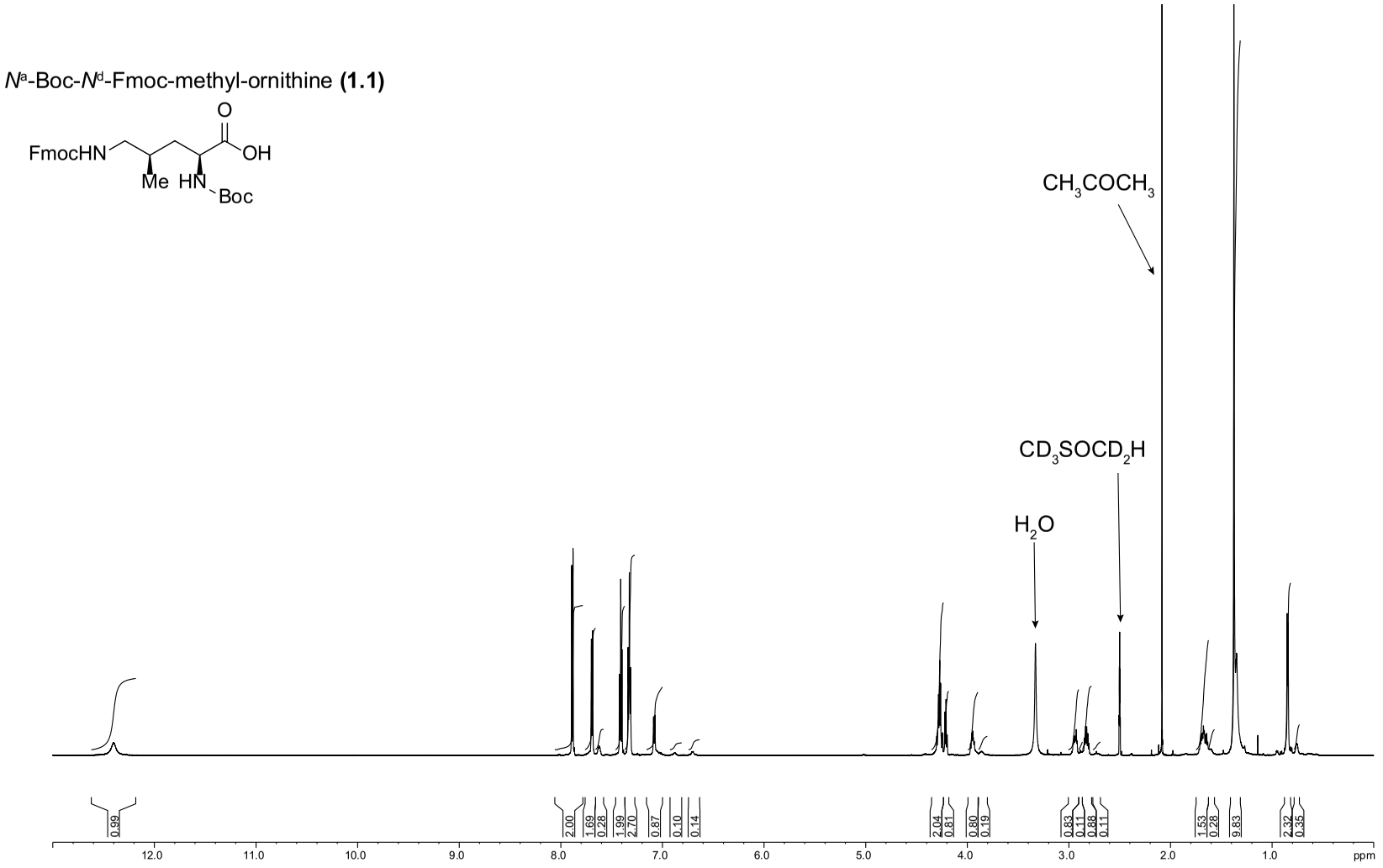
N^a-Boc-N^d-Fmoc-methyl-ornithine **(1.1)**
FmocHN
Me
HN
Boc
O
OH
CH_3COCH_3
CD_3SOCD_2H
H_2O
0.99
2.00
1.69
0.28
1.99
2.70
0.87
0.10
0.14
2.04
0.81
0.80
0.19
0.83
0.41
0.88
0.11
1.53
0.28
9.83
2.32
0.35
12.0
11.0
10.0
9.0
8.0
7.0
6.0
5.0
4.0
3.0
2.0
1.0
ppm

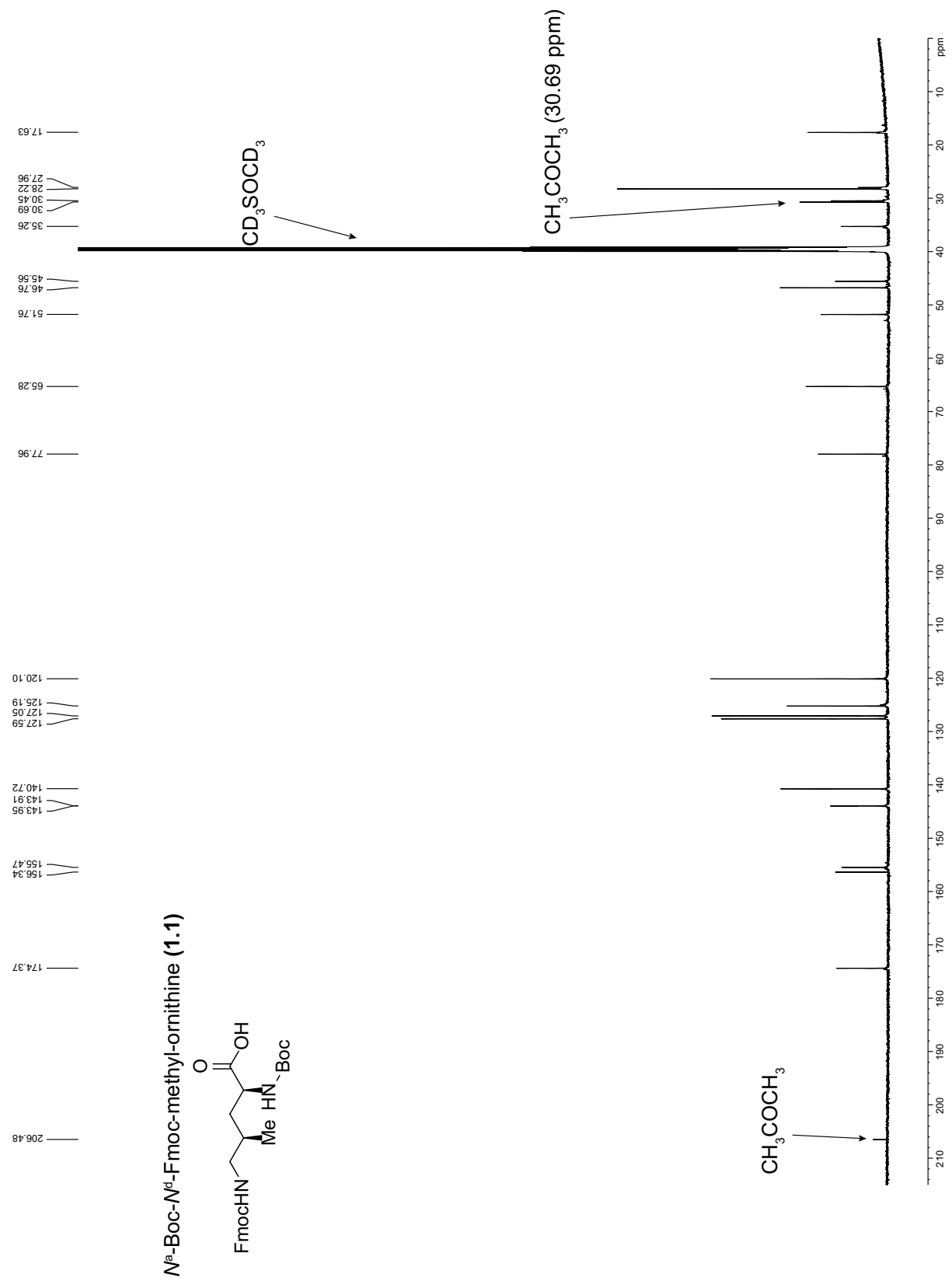
N^{a}-Boc-N^{d}-Fmoc-methyl-ornithine (1.1)
FmocHN
Me HN
Boc
O
OH
CD_3SOCD_3
CH_3COCH_3 (30.69 ppm)
CH_3COCH_3
206.48
174.37
156.34
155.47
143.95
143.91
140.72
127.59
127.05
125.19
120.10
77.96
65.28
51.76
46.76
45.56
35.26
30.69
30.45
28.22
27.96
17.63
ppm

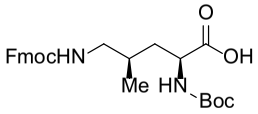

600 MHz NOESY spectrum of N^a-Boc-N^d-Fmoc-methyl-ornithine **(1.1)**
500-ms mixing time in DMSO-d_6, 298 K
Full spectrum (A) and zoom-in spectra (B, C, D) are shown.
Exchange of protons from rotamers are circled in red.
Major and minor rotamer pairs are indicated by the double-headed red arrows.

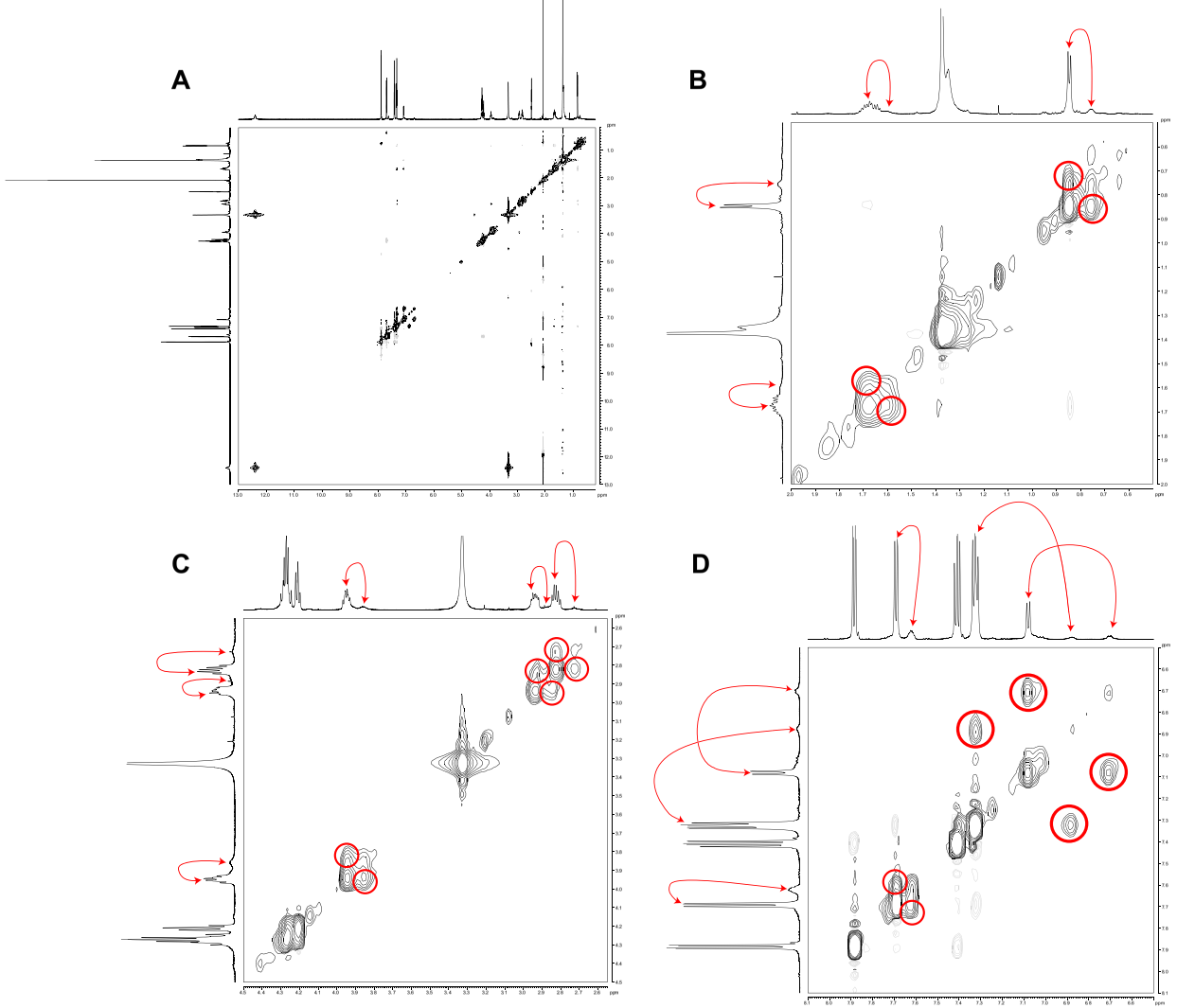

Note: small peaks associated with the cis-proline rotamer (ca. 4%) are observed.

^{1}H NMR taken at 4.0 mM peptide in D_2O, at 277 K

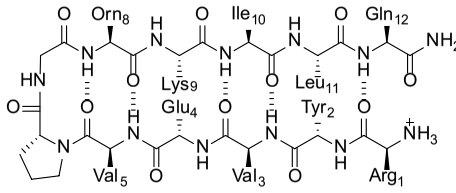

peptide **1.3**

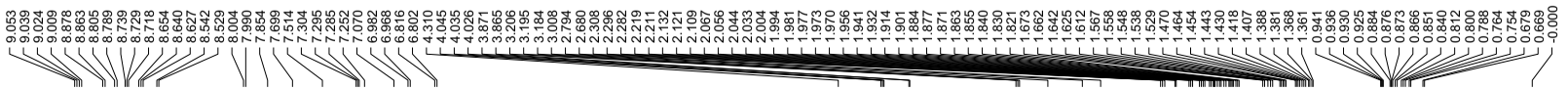

Note: small peaks associated with the cis-proline rotamer (ca. 4%) are observed.

^{1}H NMR taken at 4.0 mM peptide in 90:10 H_2O:D_2O, at 277 K

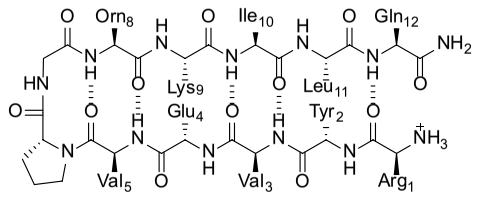

peptide **1.3**

600 MHz TOCSY spectrum of peptide **1.3**
4.0 mM in D_2O
200-ms spin-lock mixing time, at 277 K

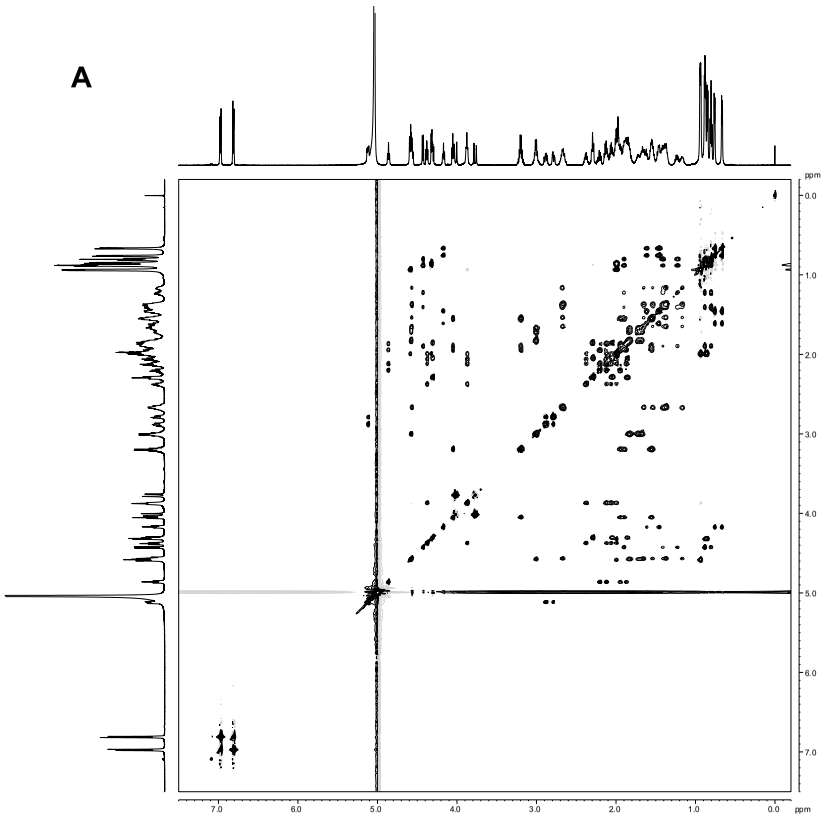

600 MHz TOCSY spectrum of peptide **1.3**
4.0 mM in 90:10 H_2O:D_2O
200-ms spin-lock mixing time, at 277 K

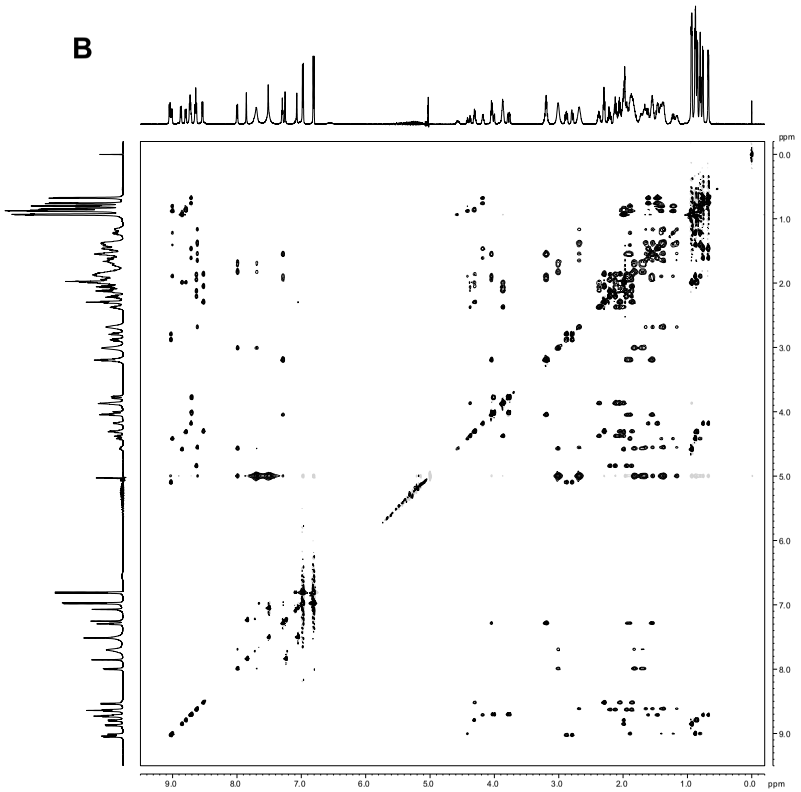

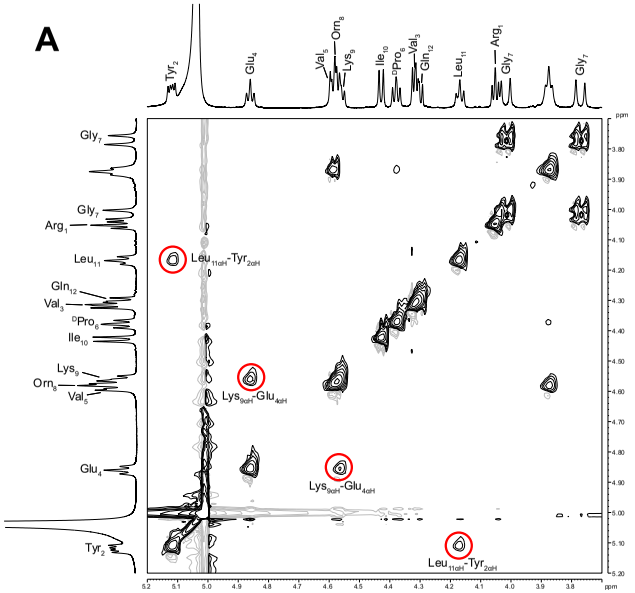

600 MHz NOESY spectrum of peptide **1.3**
4.0 mM in (A) D_2O and (B, C) 90:10 H_2O:D_2O
250-ms mixing time, at 277 K

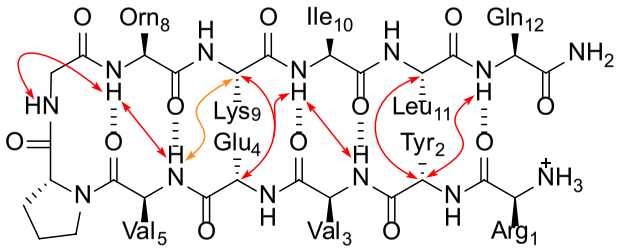

peptide **1.3**

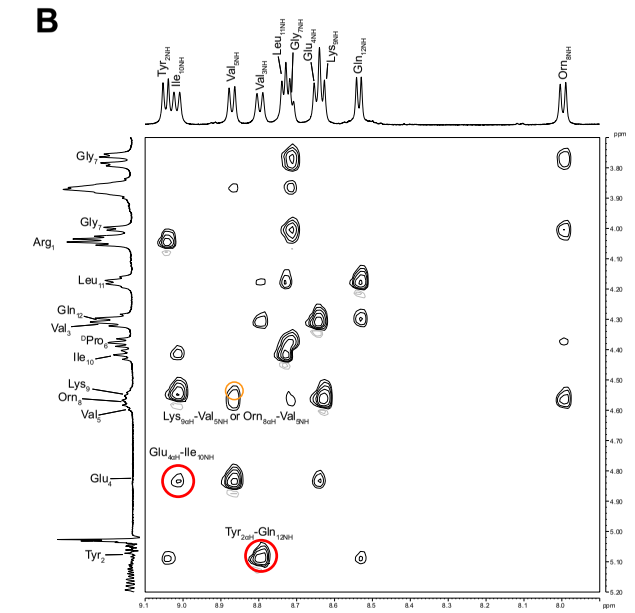

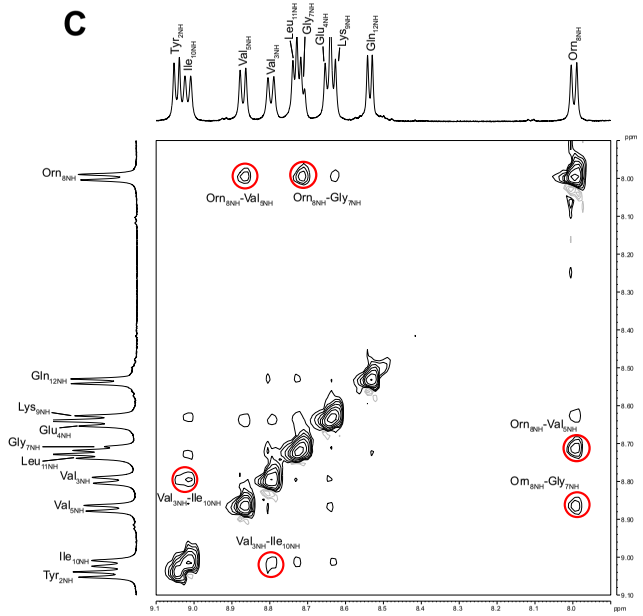

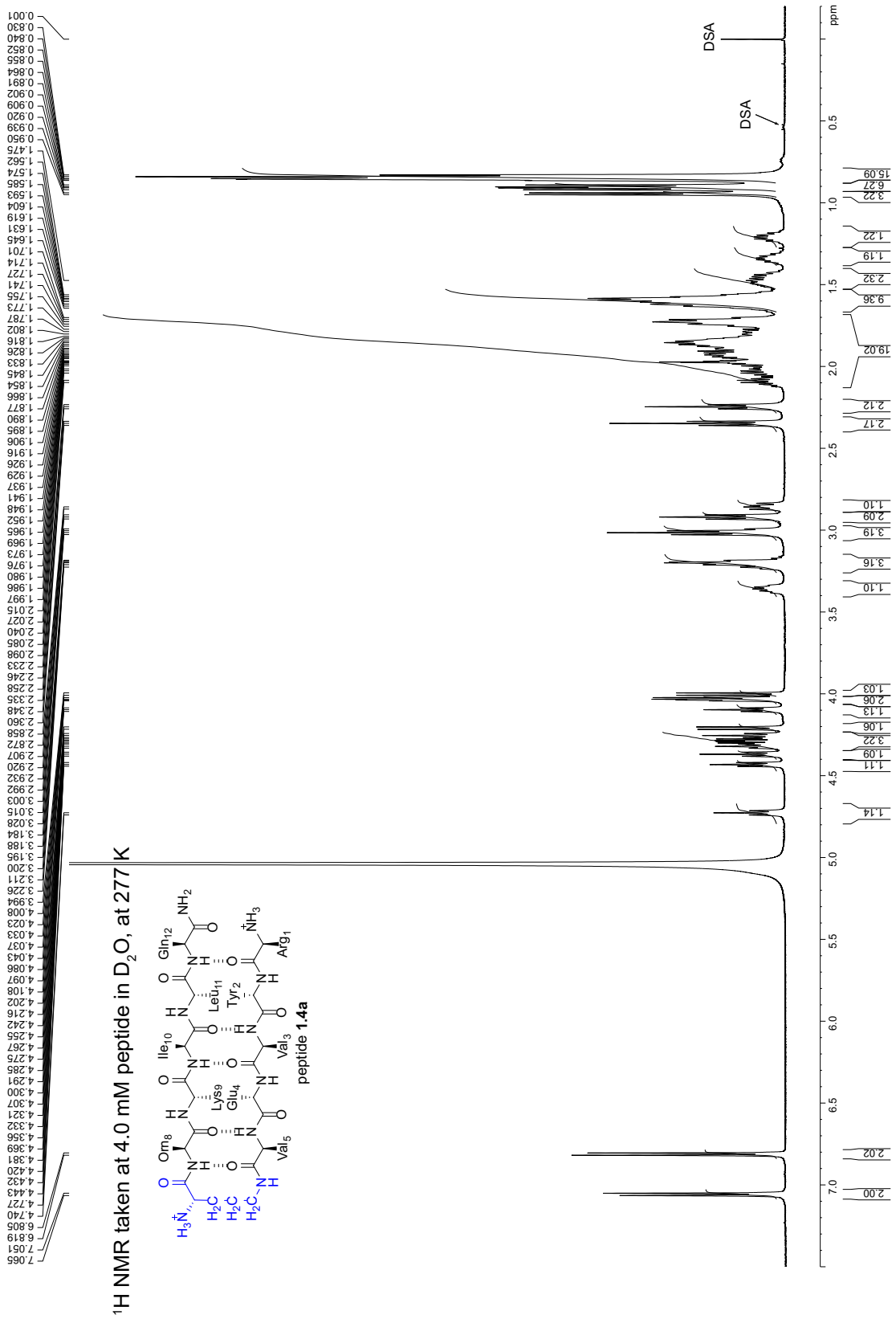
^{1}H NMR taken at 4.0 mM peptide in D_2O, at 277 K
peptide **1.4a**
DSA
DSA
ppm

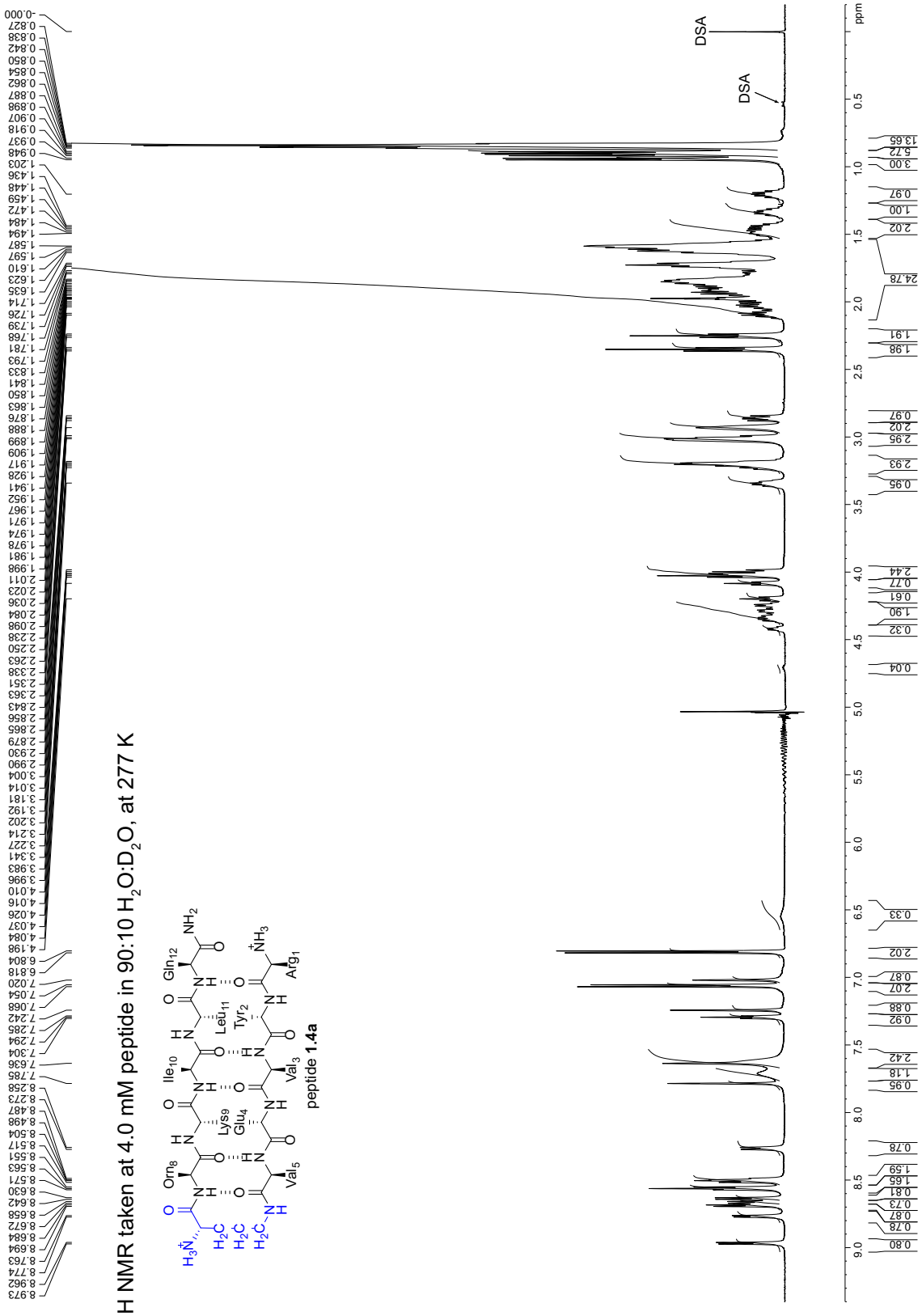

^{1}H NMR taken at 4.0 mM peptide in 90:10 H_2O:D_2O, at 277 K

600 MHz TOCSY spectrum of peptide **1.4a**
4.0 mM in D_2O
200-ms spin-lock mixing time, at 277 K

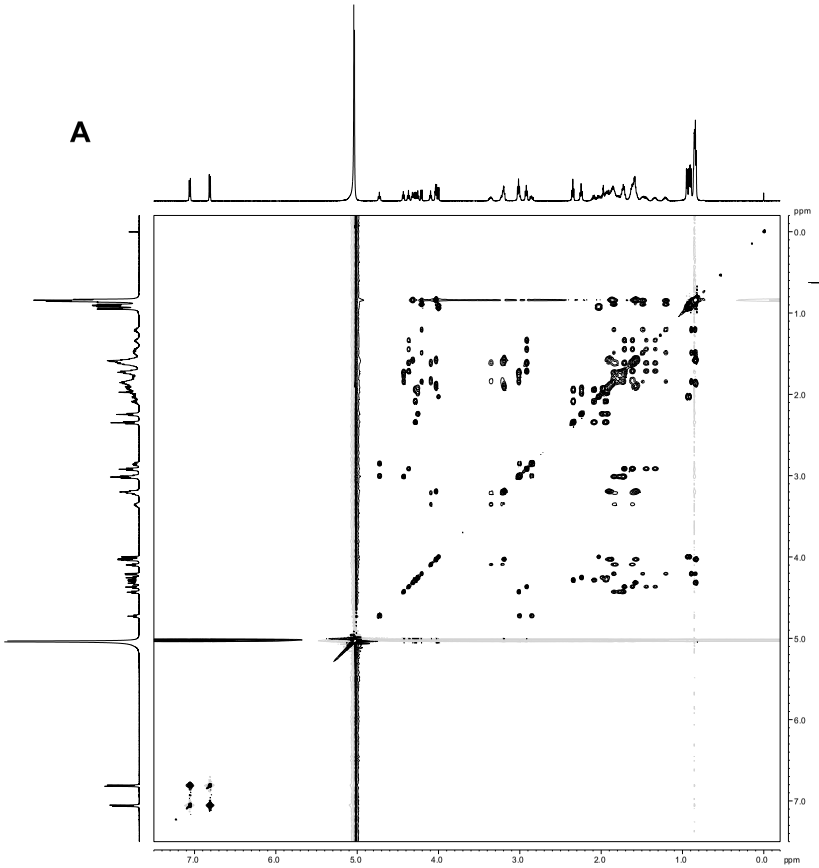

600 MHz TOCSY spectrum of peptide **1.4a**
4.0 mM in 90:10 H_2O:D_2O
200-ms spin-lock mixing time, at 277 K

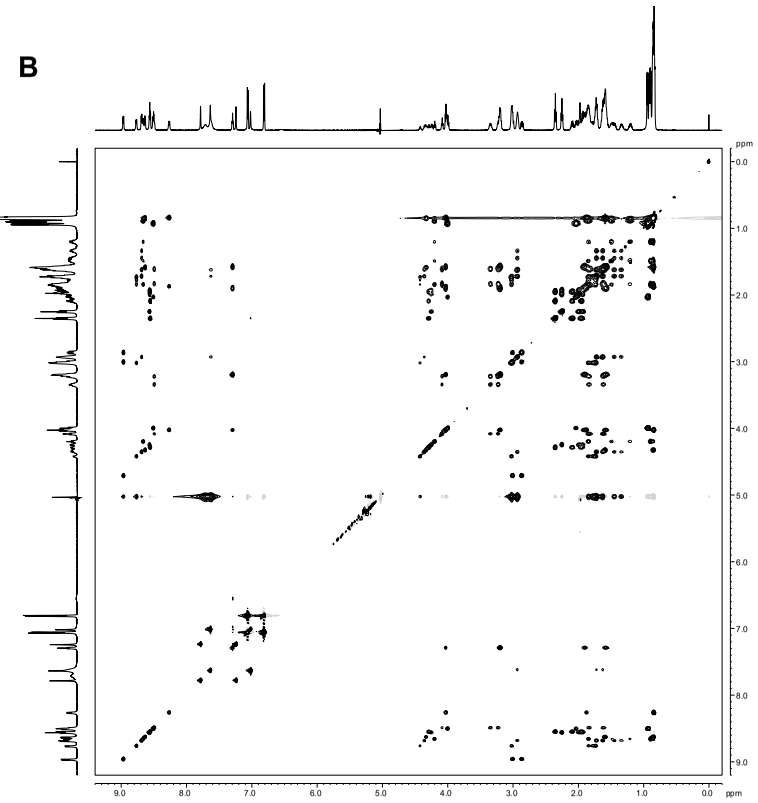

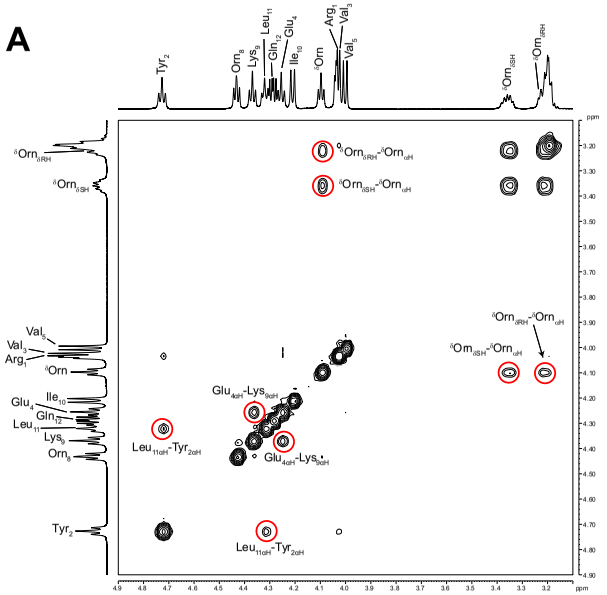

600 MHz NOESY spectrum of peptide **1.4a**
4.0 mM in (A) D_2O and (B, C) 90:10 H_2O:D_2O
250-ms mixing time, at 277 K

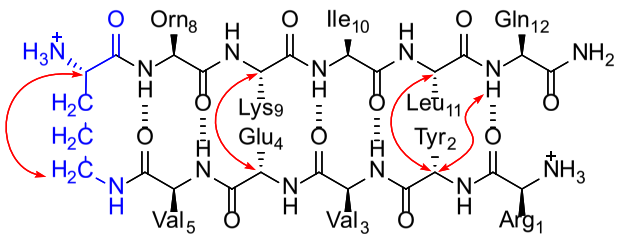

peptide **1.4a**

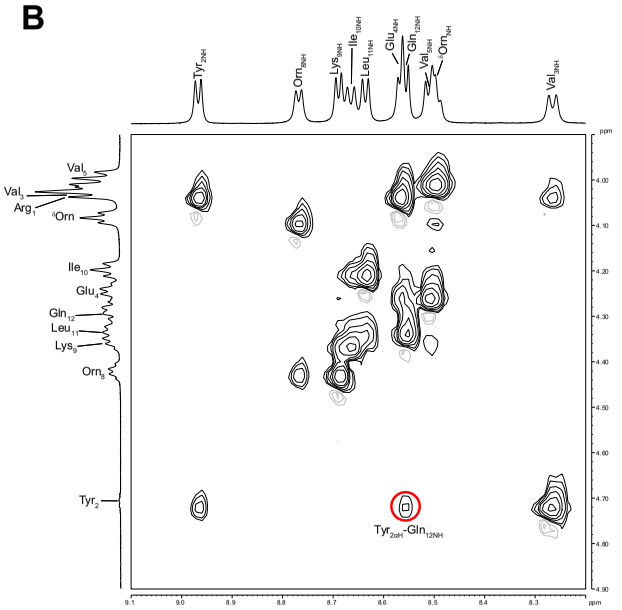

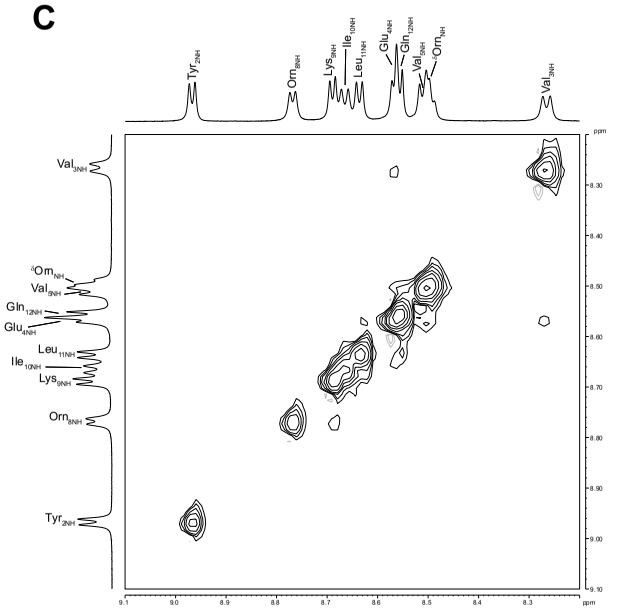

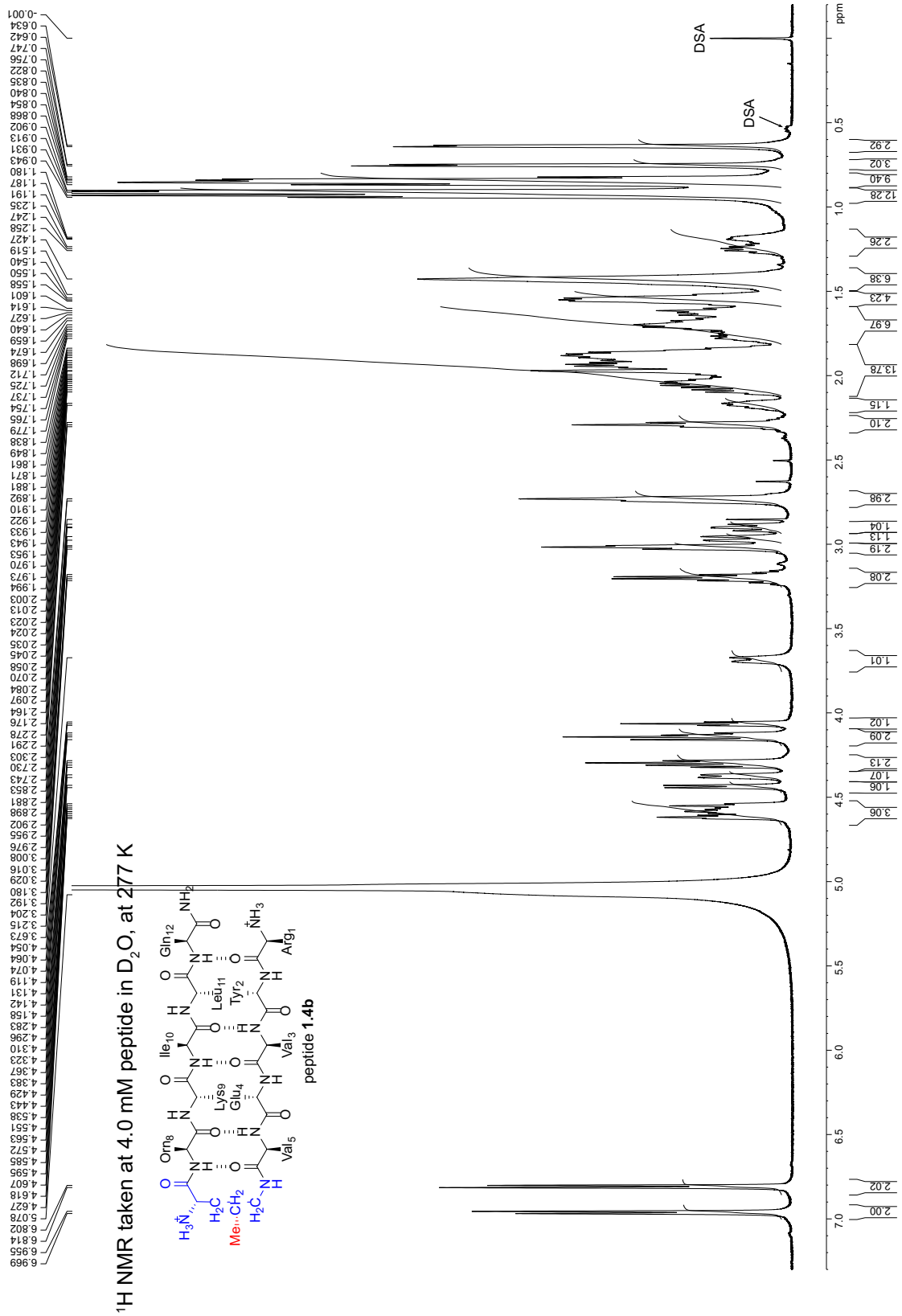
^{1}H NMR taken at 4.0 mM peptide in D_2O, at 277 K
peptide **1.4b**
DSA
DSA
ppm

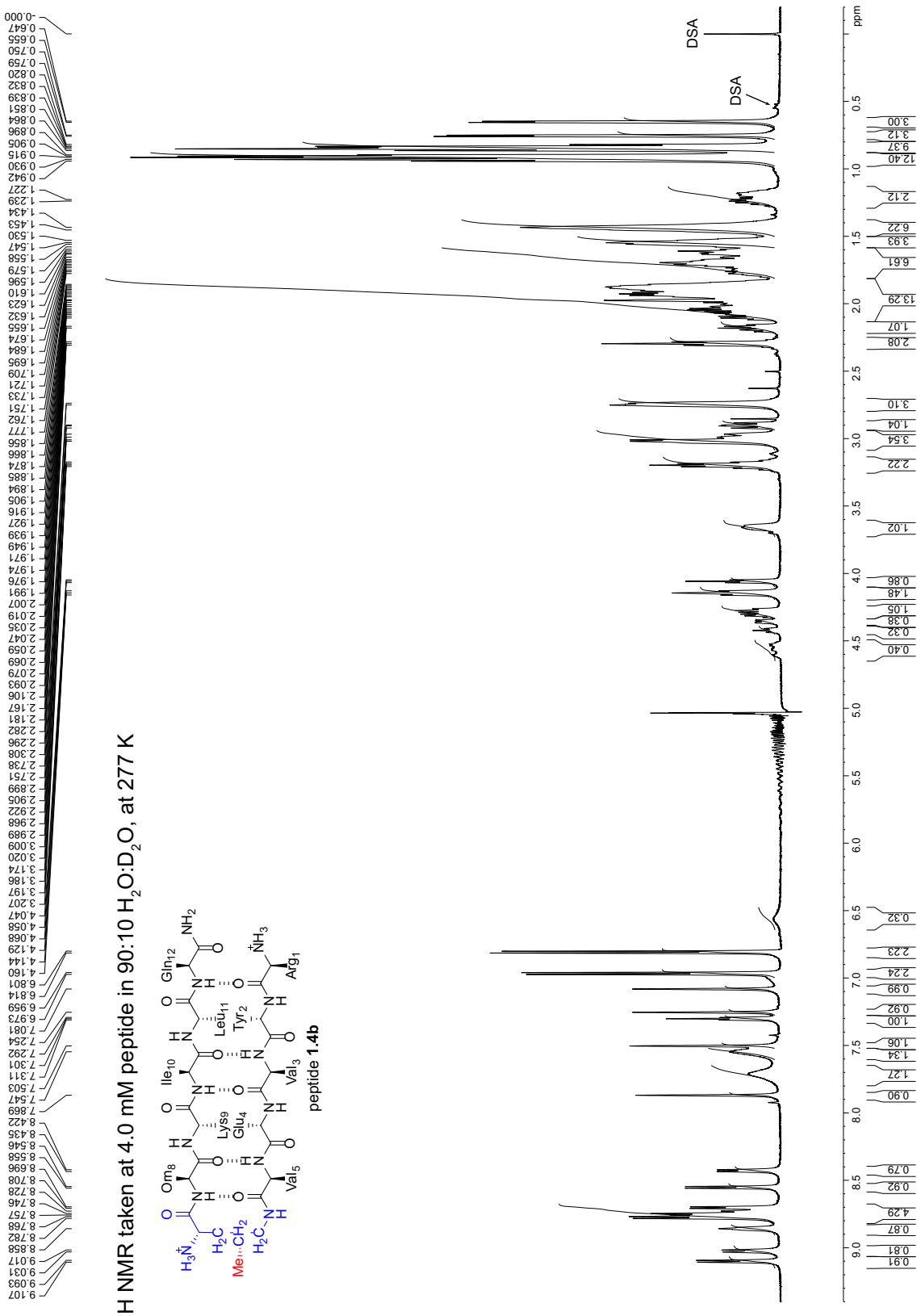
^{1}H NMR taken at 4.0 mM peptide in 90:10 H_2O:D_2O, at 277 K
peptide **1.4b**
DSA
DSA
ppm

600 MHz TOCSY spectrum of peptide **1.4b**
4.0 mM in D_2O
200-ms spin-lock mixing time, at 277 K

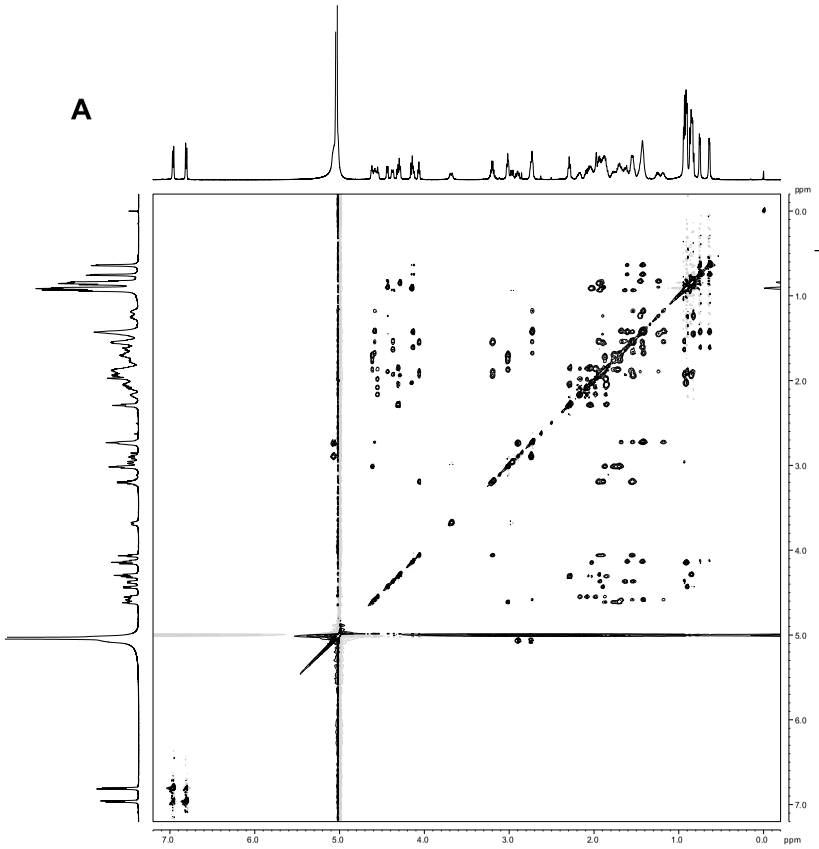

600 MHz TOCSY spectrum of peptide **1.4b**
4.0 mM in 90:10 H_2O:D_2O
200-ms spin-lock mixing time, at 277 K

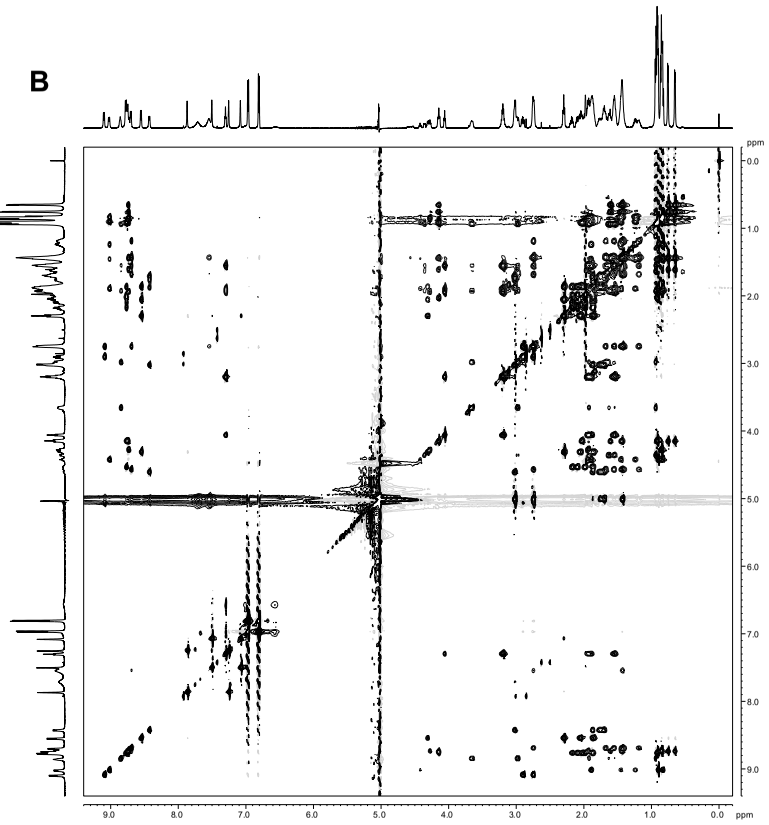

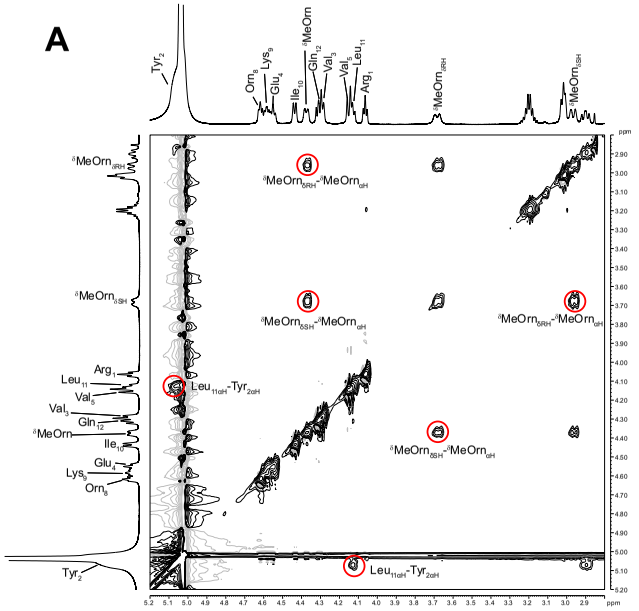

600 MHz NOESY spectrum of peptide **1.4b**
4.0 mM in (A) D_2O and (B, C) 90:10 H_2O:D_2O
250-ms mixing time, at 277 K

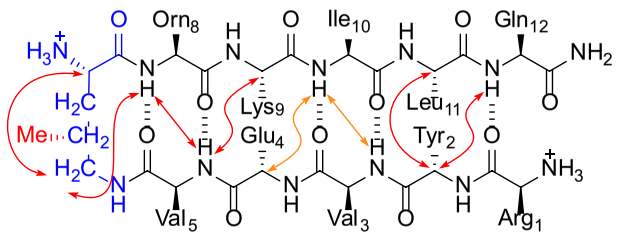

peptide **1.4b**

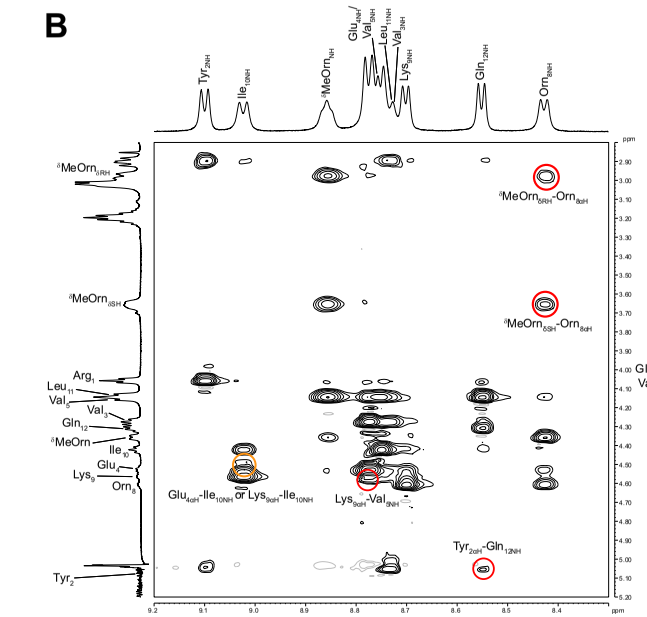

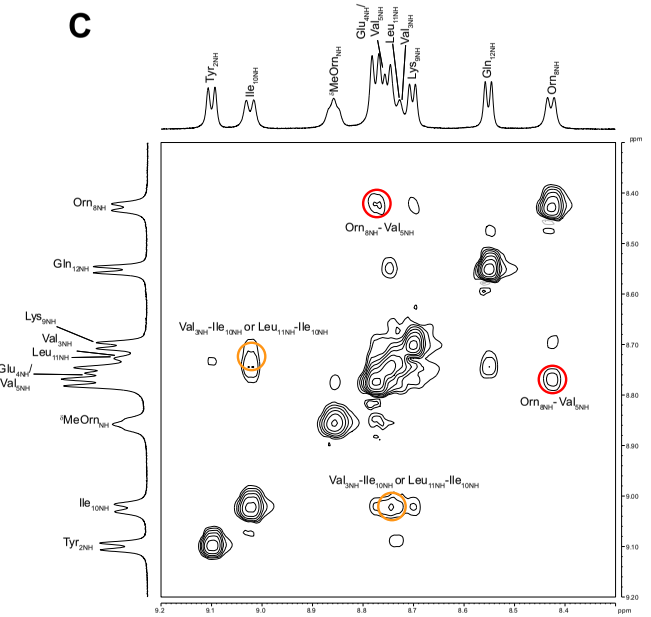

Note: small peaks associated with the cis-proline rotamer (ca. 9%) are observed.
^{1}H NMR taken at 4.0 mM peptide in D_2O, at 277 K

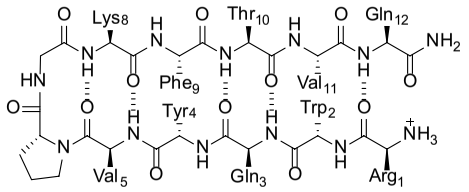

peptide **1.5**

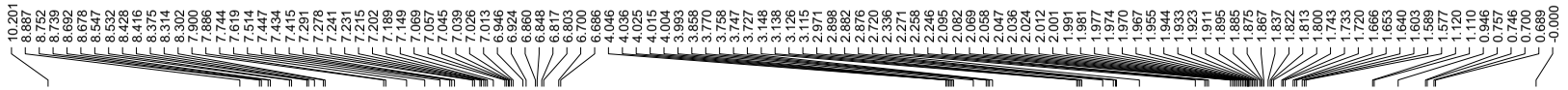

Note: small peaks associated with the cis-proline rotamer (ca. 9%) are observed.
^{1}H NMR taken at 4.0 mM peptide in 90:10 H_2O:D_2O, at 277 K

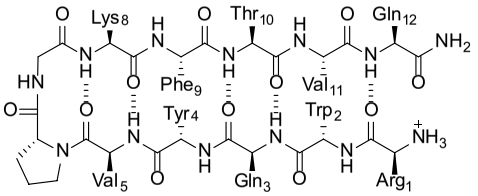

peptide **1.5**

600 MHz TOCSY spectrum of peptide **1.5**
4.0 mM in D_2O
200-ms spin-lock mixing time, at 277 K

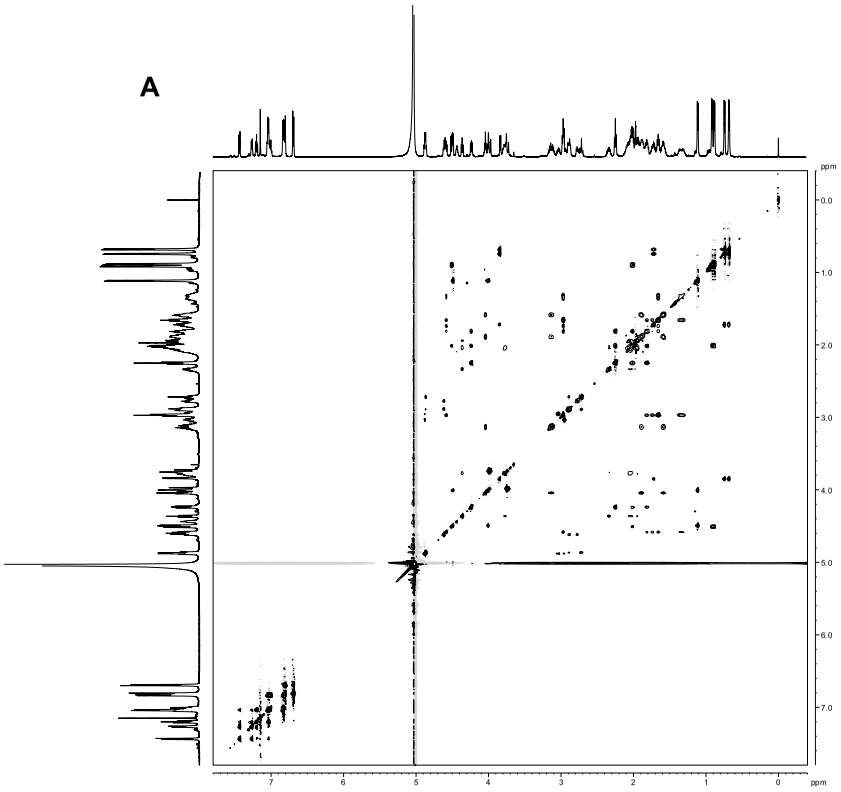

600 MHz TOCSY spectrum of peptide **1.5**
4.0 mM in 90:10 H_2O:D_2O
200-ms spin-lock mixing time, at 277 K

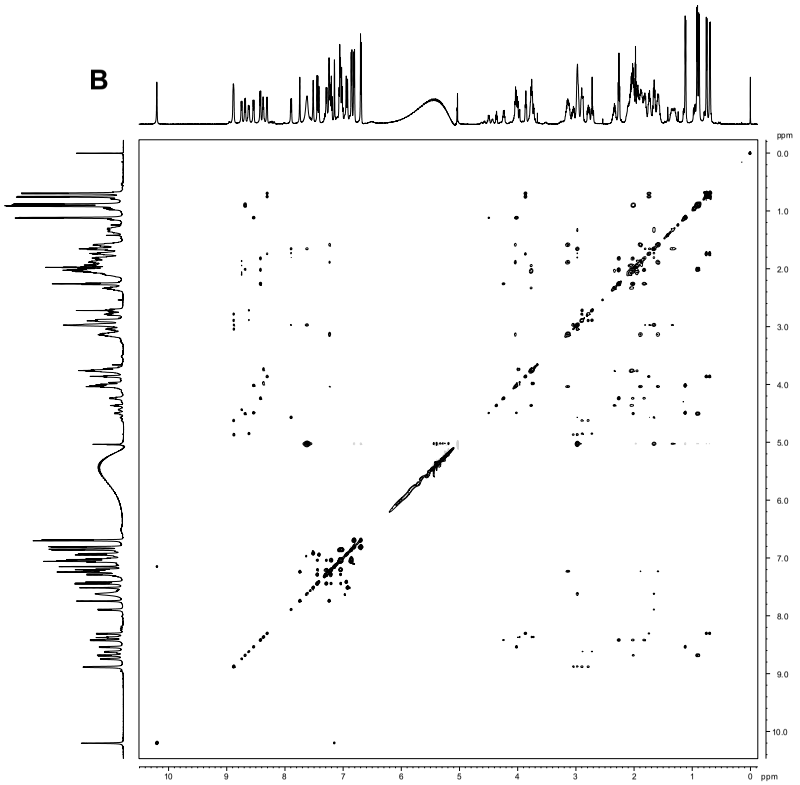

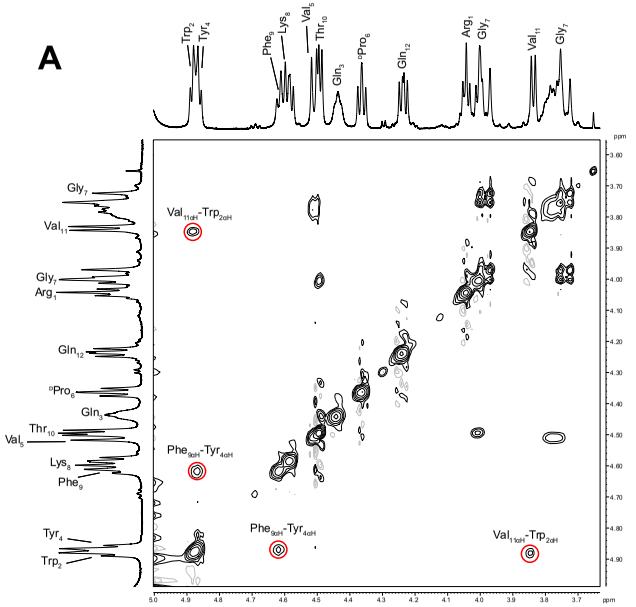

600 MHz NOESY spectrum of peptide **1.5**
4.0 mM in (A) D_2O and (B, C) 90:10 H_2O:D_2O
250-ms mixing time, at 277 K

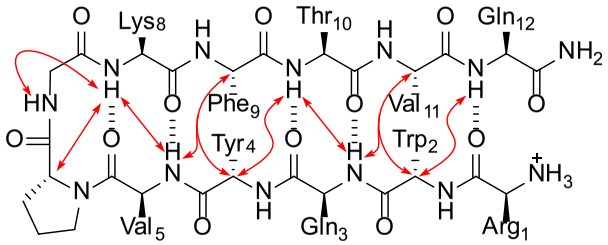

peptide **1.5**

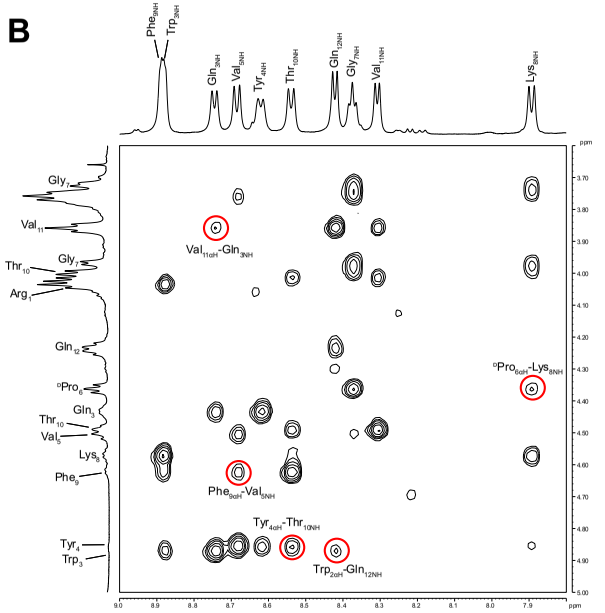

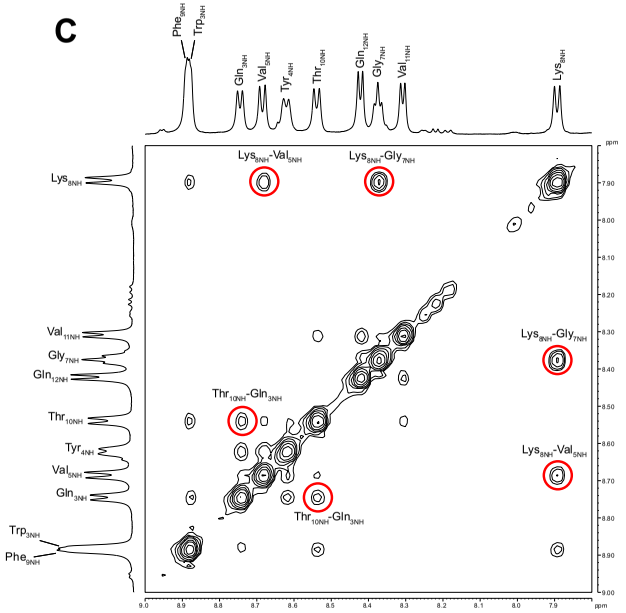

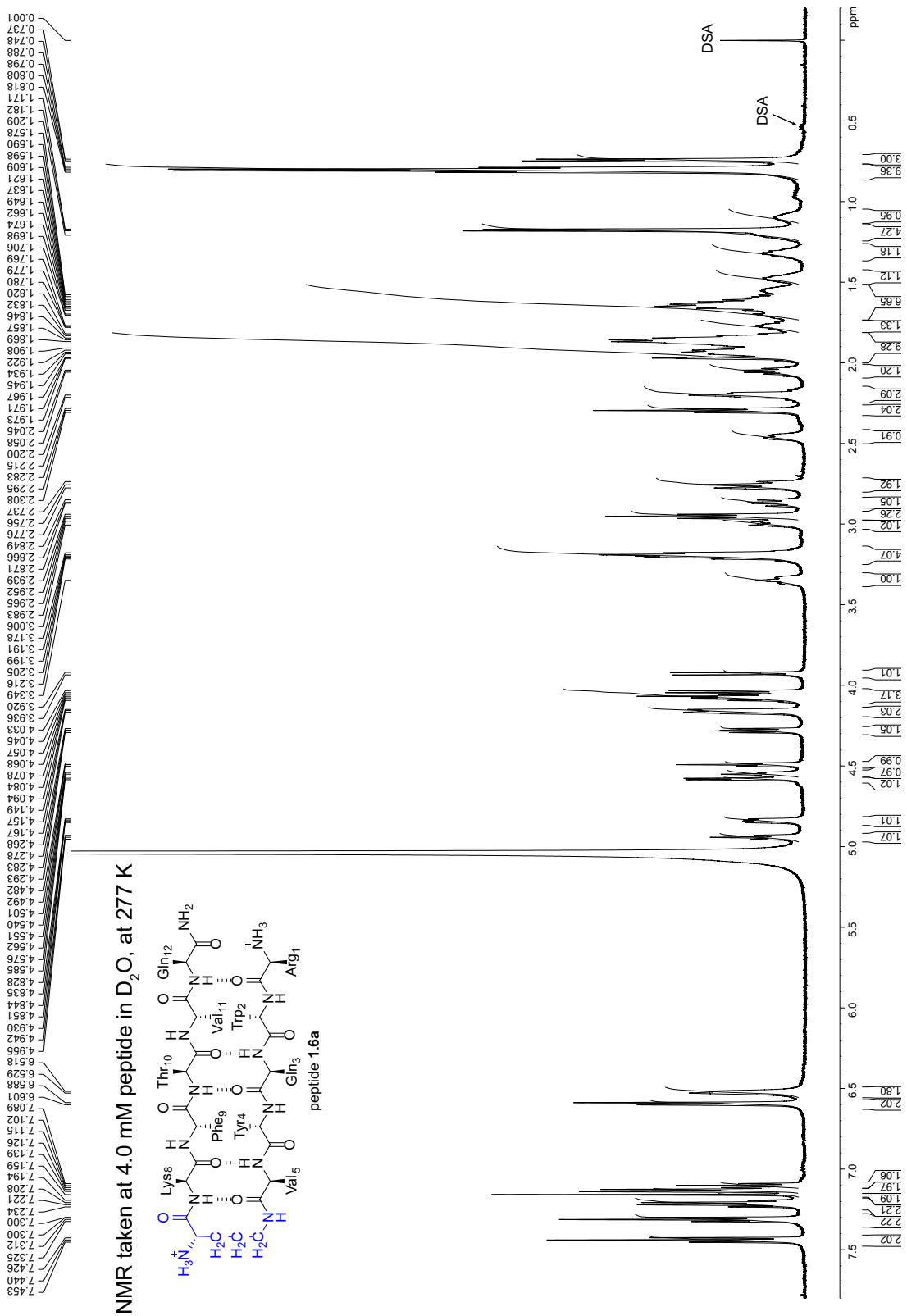
^{1}H NMR taken at 4.0 mM peptide in D_2O, at 277 K
peptide **1.6a**
DSA
DSA
ppm

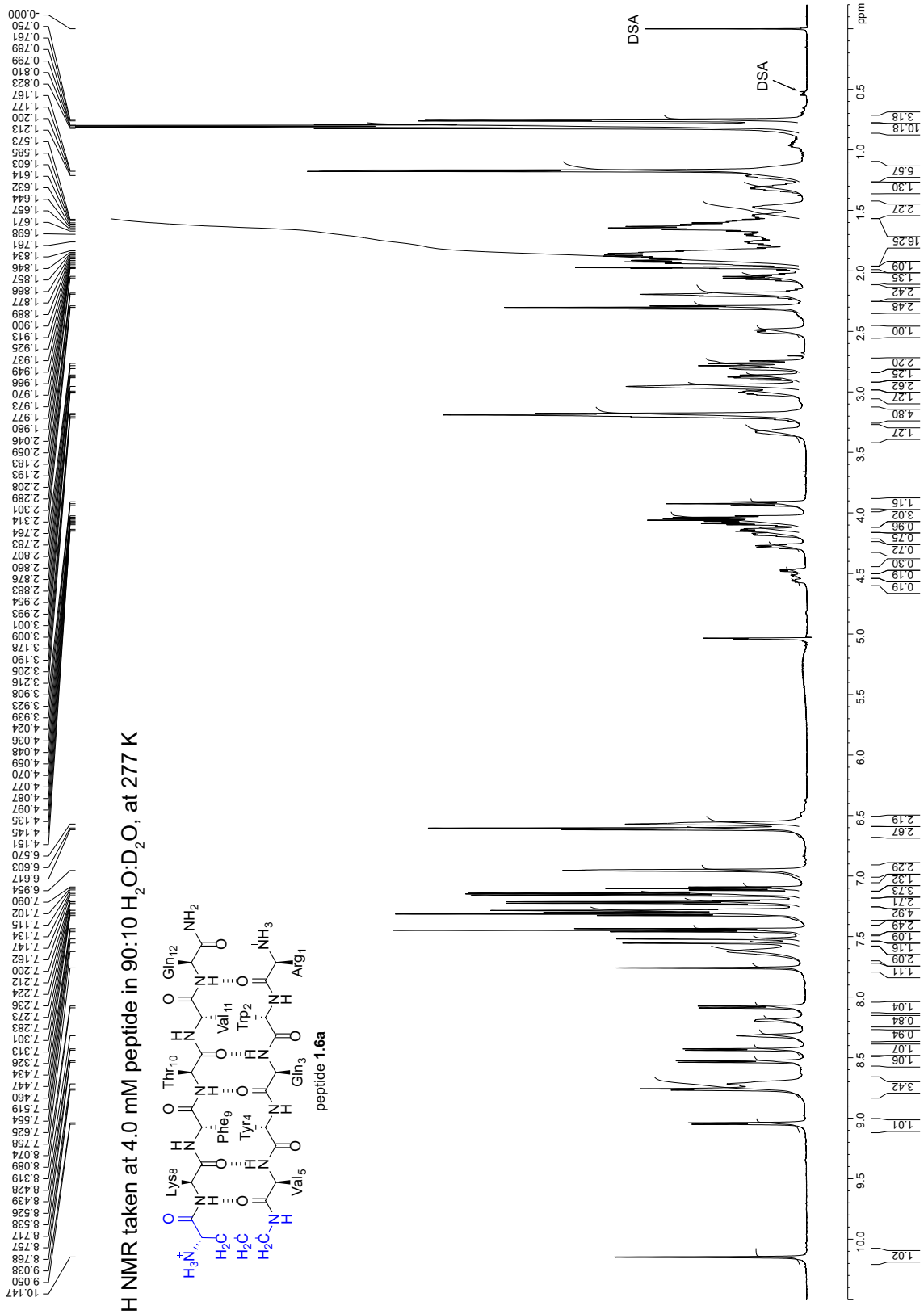

^{1}H NMR taken at 4.0 mM peptide in 90:10 H_2O:D_2O, at 277 K

600 MHz TOCSY spectrum of peptide **1.6a**
4.0 mM in D_2O
200-ms spin-lock mixing time, at 277 K

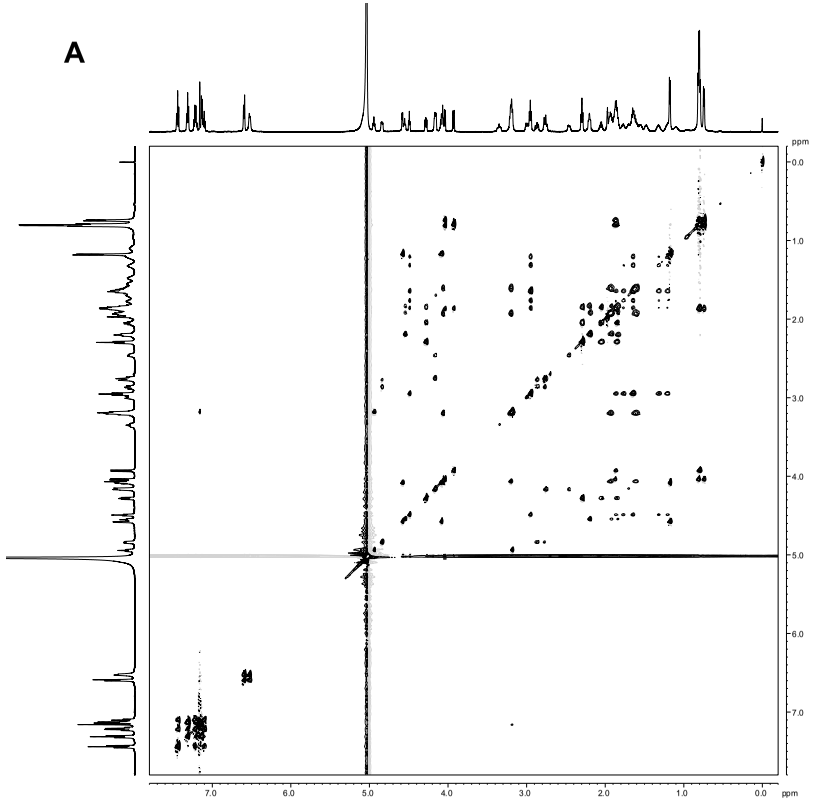

600 MHz TOCSY spectrum of peptide **1.6a**
4.0 mM in 90:10 H_2O:D_2O
200-ms spin-lock mixing time, at 277 K

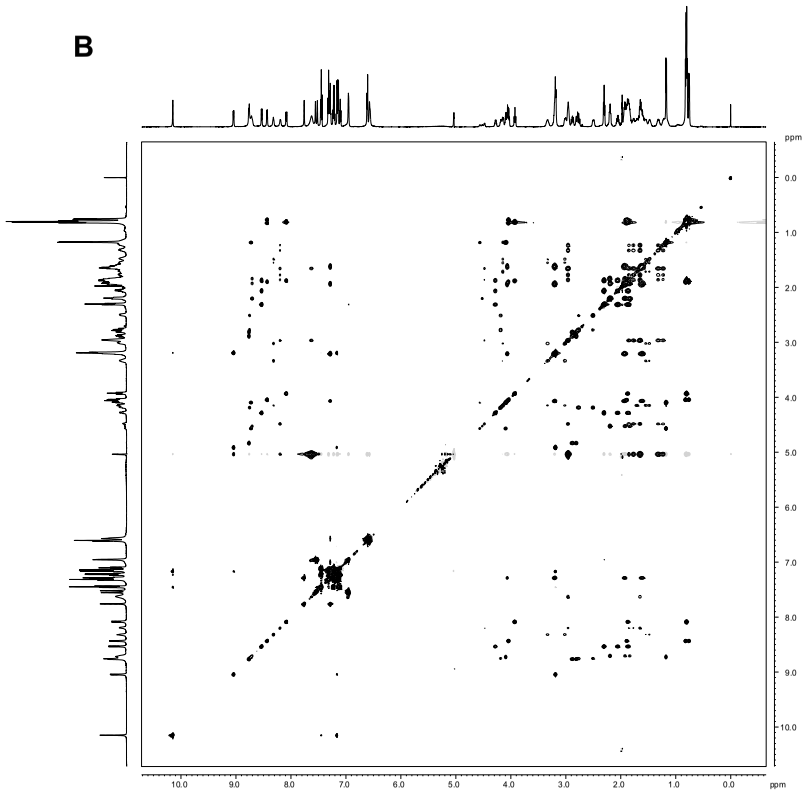

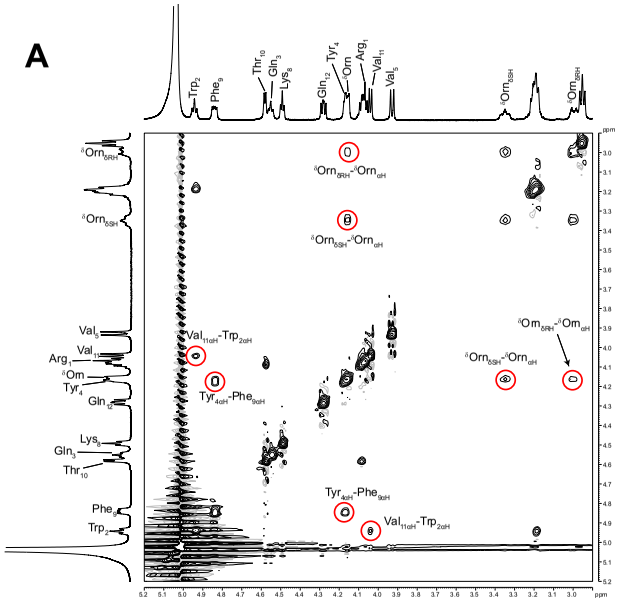

600 MHz NOESY spectrum of peptide **1.6a**
4.0 mM in (A) D_2O and (B, C) 90:10 H_2O:D_2O
250-ms mixing time, at 277 K

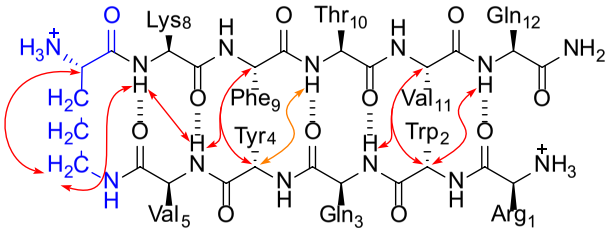

peptide **1.6a**

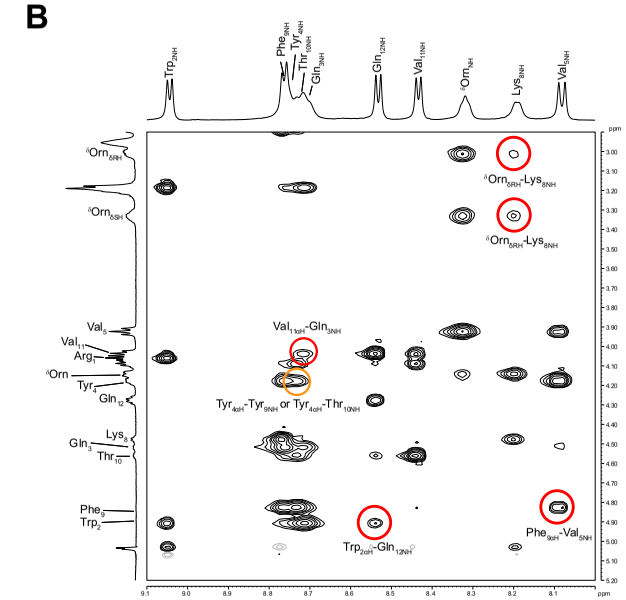

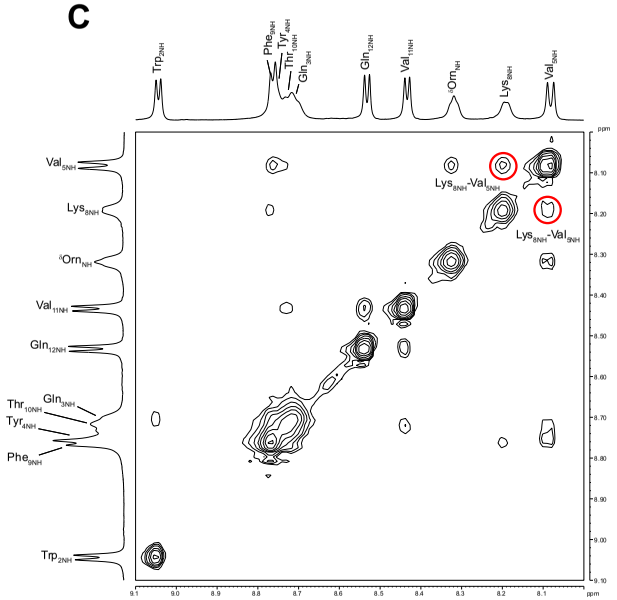

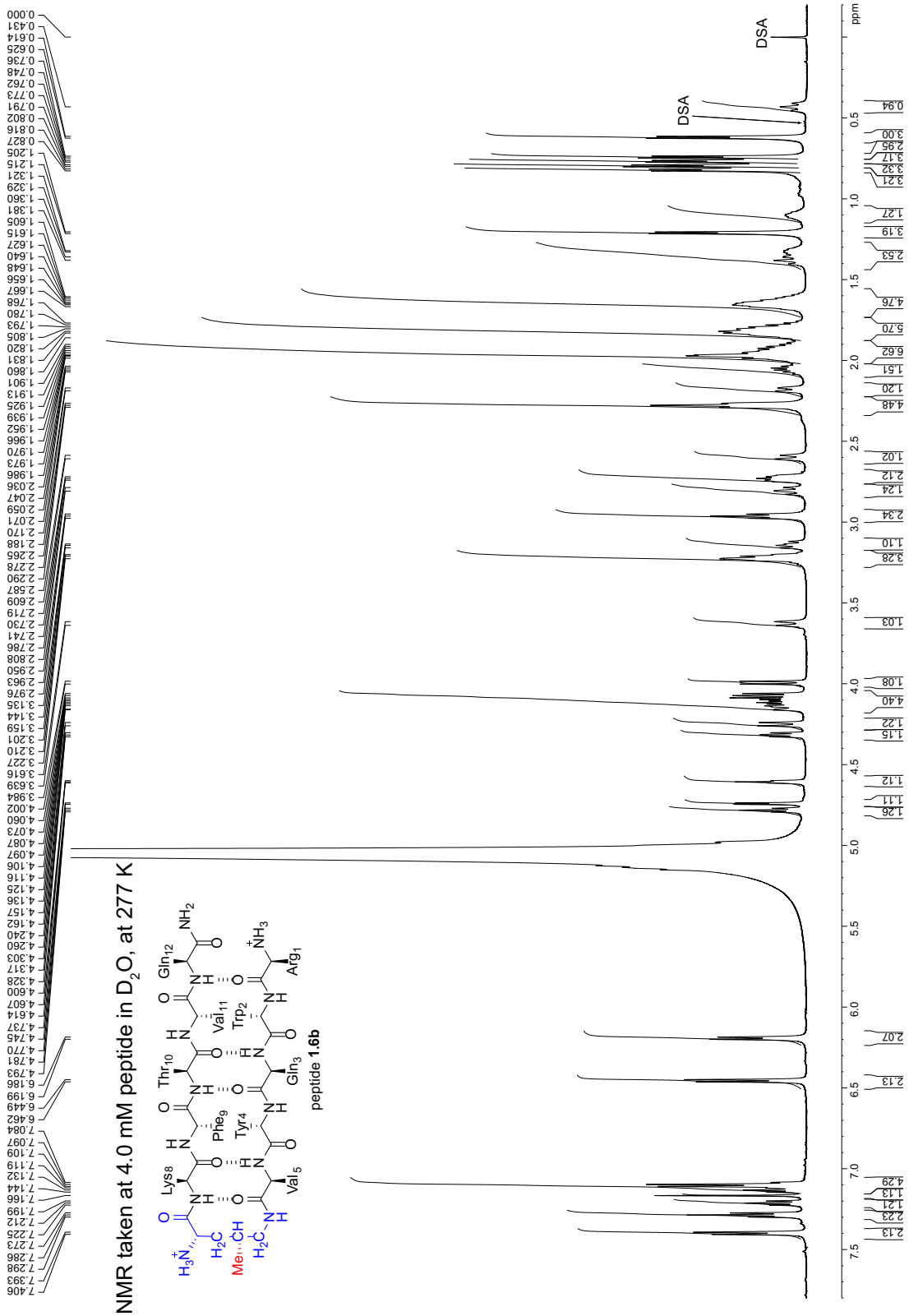
^{1}H NMR taken at 4.0 mM peptide in D_2O, at 277 K
peptide **1.6b**
DSA
DSA
ppm

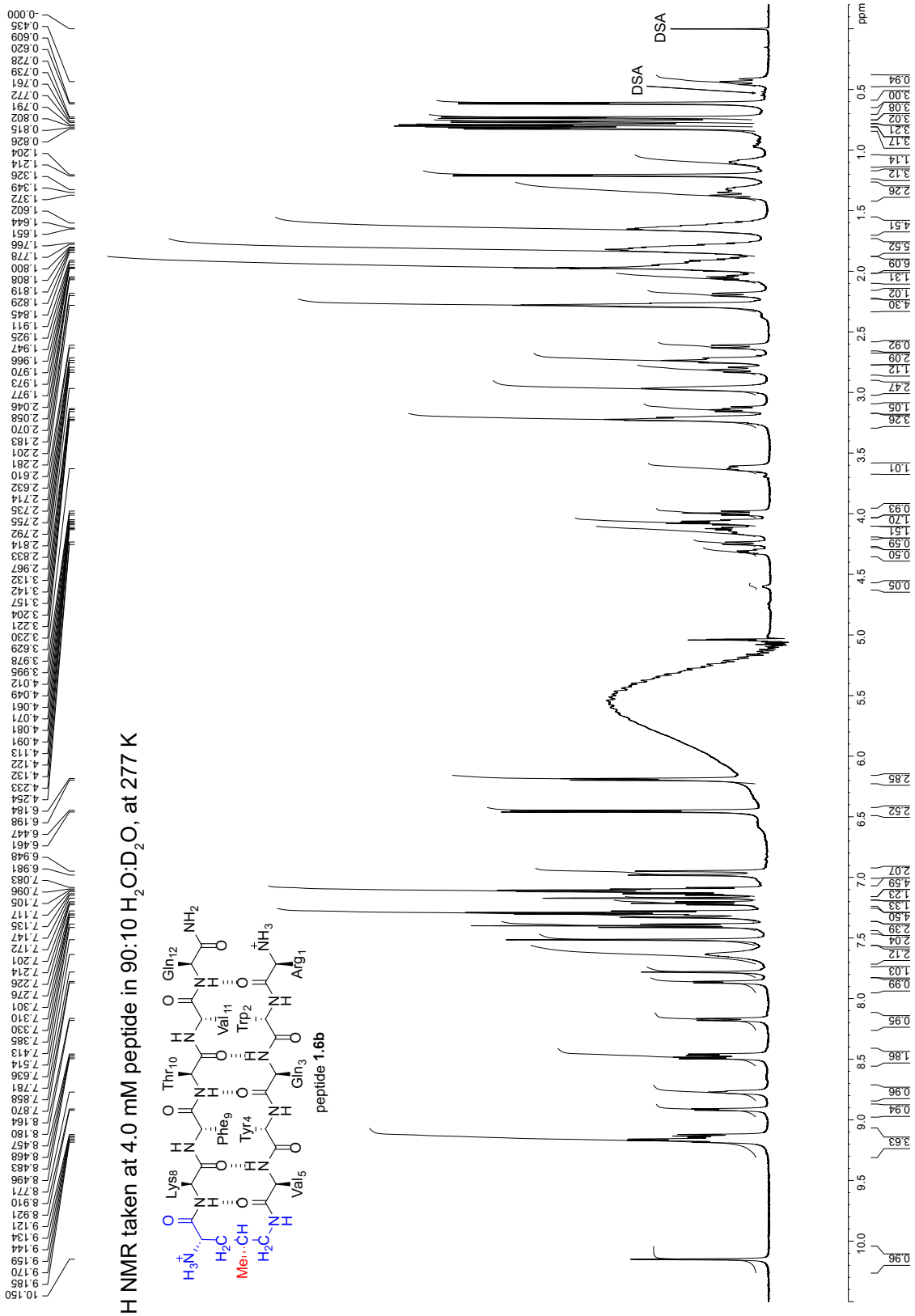
^{1}H NMR taken at 4.0 mM peptide in 90:10 H_2O:D_2O, at 277 K
peptide **1.6b**
DSA
DSA
ppm

600 MHz TOCSY spectrum of peptide **1.6b**
4.0 mM in D_2O
200-ms spin-lock mixing time, at 277 K

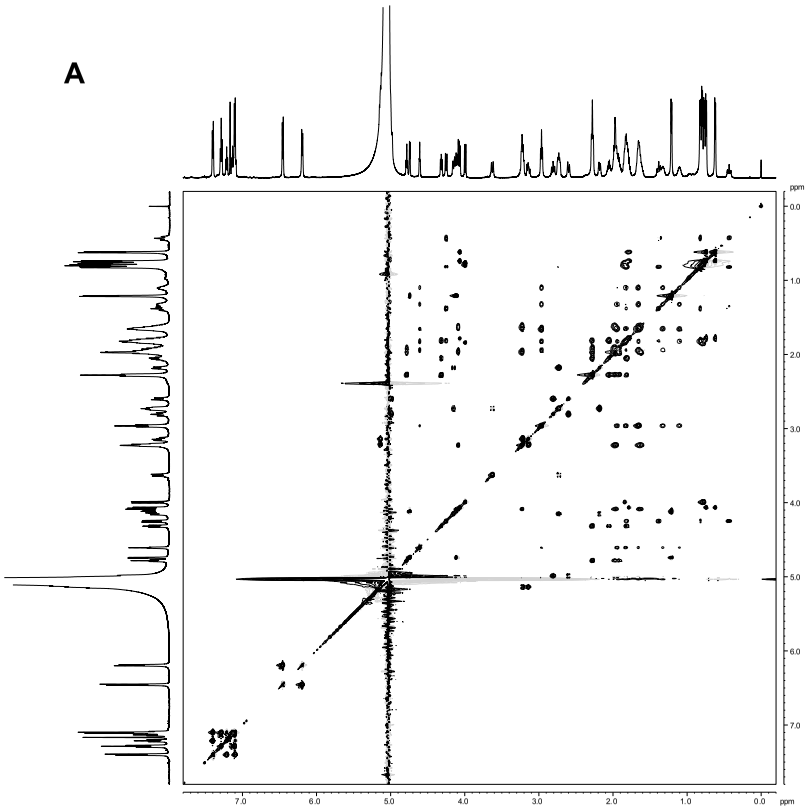

600 MHz TOCSY spectrum of peptide **1.6b**
4.0 mM in 90:10 H_2O:D_2O
200-ms spin-lock mixing time, at 277 K

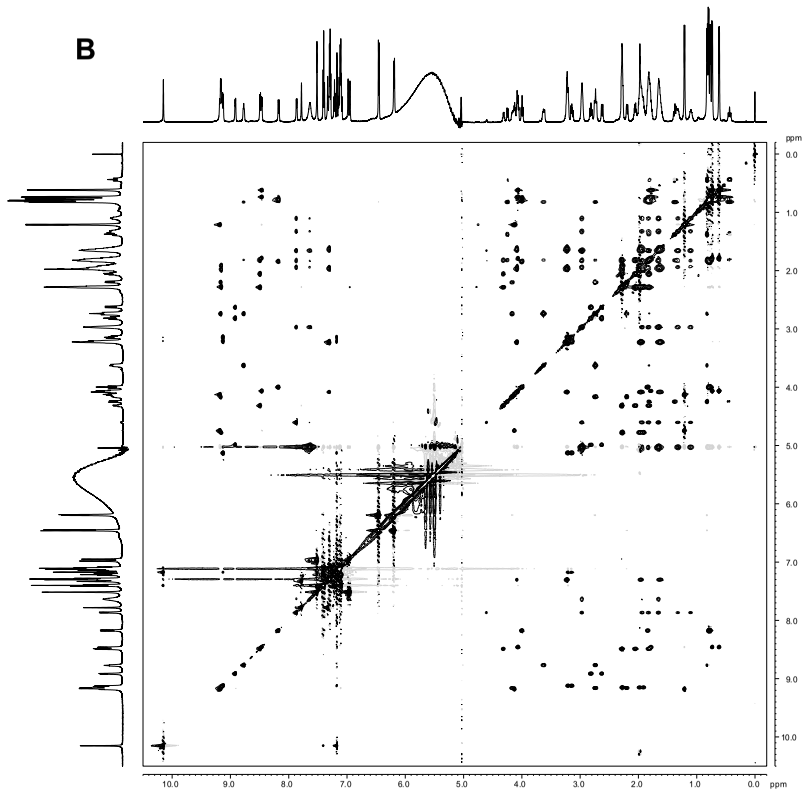

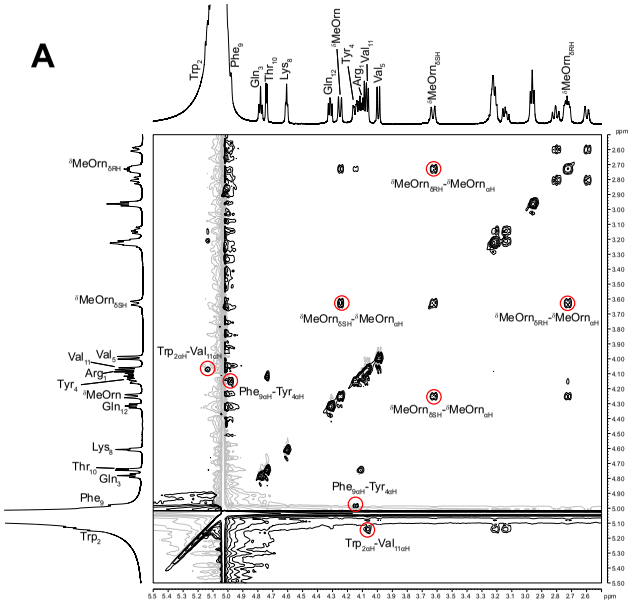

600 MHz NOESY spectrum of peptide **1.6b**
4.0 mM in (A) D_2O and (B, C) 90:10 H_2O:D_2O
250-ms mixing time, at 277 K

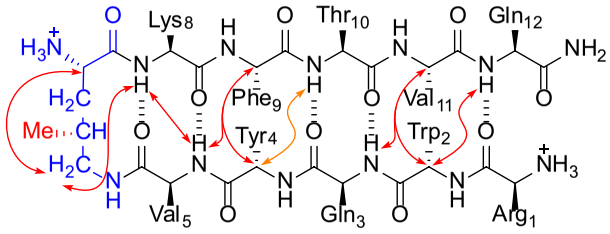

peptide **1.6b**

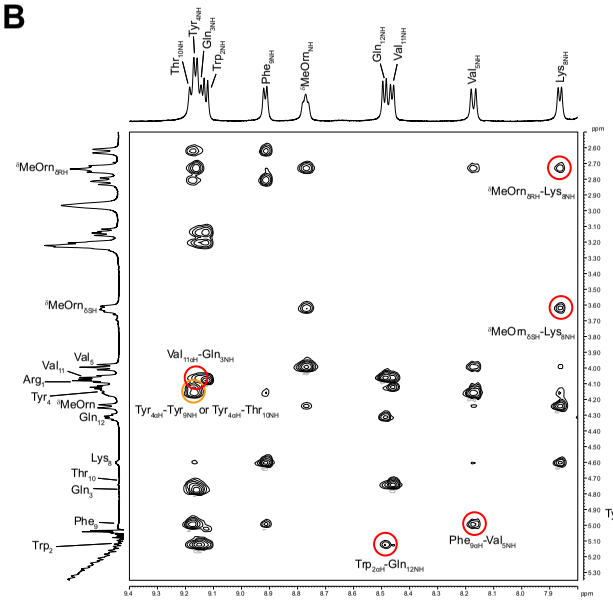

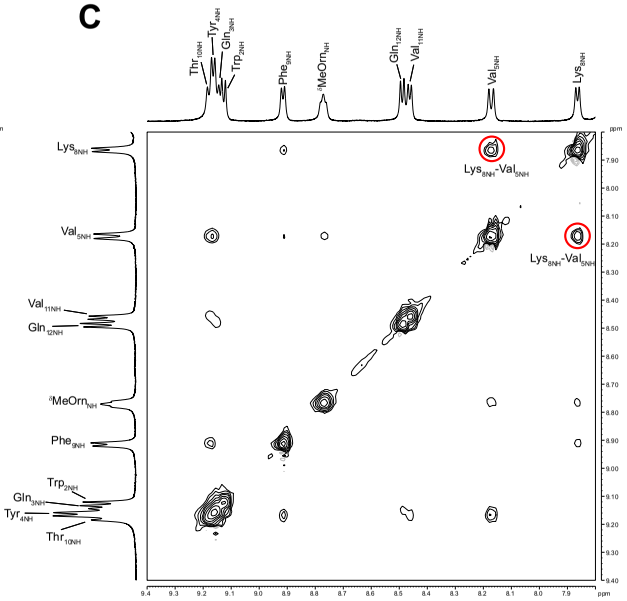

CHAPTER 2

Enantiomeric β-Sheet Peptides from Aβ Form Homochiral Pleated β-Sheets Rather than Heterochiral Rippled β-Sheets

Preface to Chapter 2

Chapter 2 seeks to address a controversy regarding two different types of β-sheet assembly: homochiral pleated β-sheets and heterochiral rippled β-sheets. The project was inspired by a curiosity to reconcile the difference between previous findings from our laboratory that β-sheet pentapeptides strongly prefer to form homochiral pleated β-sheet dimers and recent reports for the preference of heterochiral rippled β-sheets formation. In order to study the effects of chirality on β-sheet assembly, I took a peptide model system that our laboratory has previously reported to assemble as tetramers, and studied the effects of mixing the original L-peptide with equimolar amounts of the D-enantiomer. This project focuses solely on using NMR spectroscopic techniques to elucidate peptide assembly; my results indicate that homochiral β-sheet assembly is significantly more preferred than the heterochiral assembly.

This project was as much curious as it was interesting to see what type of assembly would be favored. I enjoyed taking the leading role in this project — from brainstorming early studies to designing specialized isotopically labelled experiments — I am grateful to Prof. James Nowick for giving me the chance to grow as a writer in telling the story and allowing me to explore experiments as an independent chemist. I would like to also thank my undergraduate student, Stephanie Rios, for assisting in the

syntheses of the L- and D-peptides reported in Chapter 2. Dr. Philip Dennison was extremely helpful with teaching me how to run DOSY and ^{15}N isotope NMR experiments; I was able to obtain high quality spectra because of his guidance. I would also like to thank Dr. Nicholas Truex for his feedback on the NMR spectroscopic studies.

The background of Chapter 2 dates back to the 1950s, with Pauling and Corey postulating on two types of β-sheet assembly — the pleated β-sheet and the rippled β-sheet. Although pleated β-sheets are found naturally and have been reported, structures of the rippled β-sheet have only recently begun to emerge. In the introduction, I discuss some of the key players investigating rippled β-sheets and present previous findings from our laboratory in contradiction to the idea that rippled β-sheet assembly is more favored in a mixture of L- and D-peptides. The results and discussion detail in-depth NMR spectroscopic studies using a model system derived from Aβ to elucidate the interactions between enantiomeric β-sheet peptides. Chapter 2 concludes with our interpretation for the discrepancy between preferences in rippled β-sheets reported by others and pleated β-sheets found in our studies.

Chapter 2 is adapted from or taken verbatim from: Li, X.; Rios, S. E.; Nowick, J. S. Enantiomeric Peptides Derived from β-Sheets of Aβ Assemble Selectively as a Homochiral Tetramer. *Chem. Sci.* **2022** *ASAP*. DOI: 10.1039/d2sc02080g.

INTRODUCTION

Do enantiomeric β-sheet peptides prefer to self-assemble in a homochiral fashion or co-assemble in a heterochiral fashion? In the early 1950s, Pauling and Corey introduced the terms "pleated" β-sheets and "rippled" β-sheets to describe two types of β-sheet assembly.[1–3] In both a pleated β-sheet and a rippled β-sheet, adjacent peptide strands hydrogen bond through edge-to-edge interactions (Figure 2.1). Pleated β-sheets are composed of peptide strands of the same chirality (all L-peptide strands or all D-peptide strands), while peptide strands of opposite chirality (L-peptide strands and D-peptide strands) are required to form rippled β-sheets. In a pleated β-sheet, the side chains of sequential residues are oriented up-down-up-down and those of the adjacent peptide strands are also oriented up-down-up-down (Figure 2.1A). In a rippled β-sheet, however, the side chains of sequential residues are oriented up-down-up-down and those of the adjacent peptide strands are oriented down-up-down-up (Figure 2.1B). Although pleated β-sheets are a near ubiquitous feature of proteins, rippled β-sheets are not found in nature, because ribosomal proteins and peptides are composed only of L-amino acids.

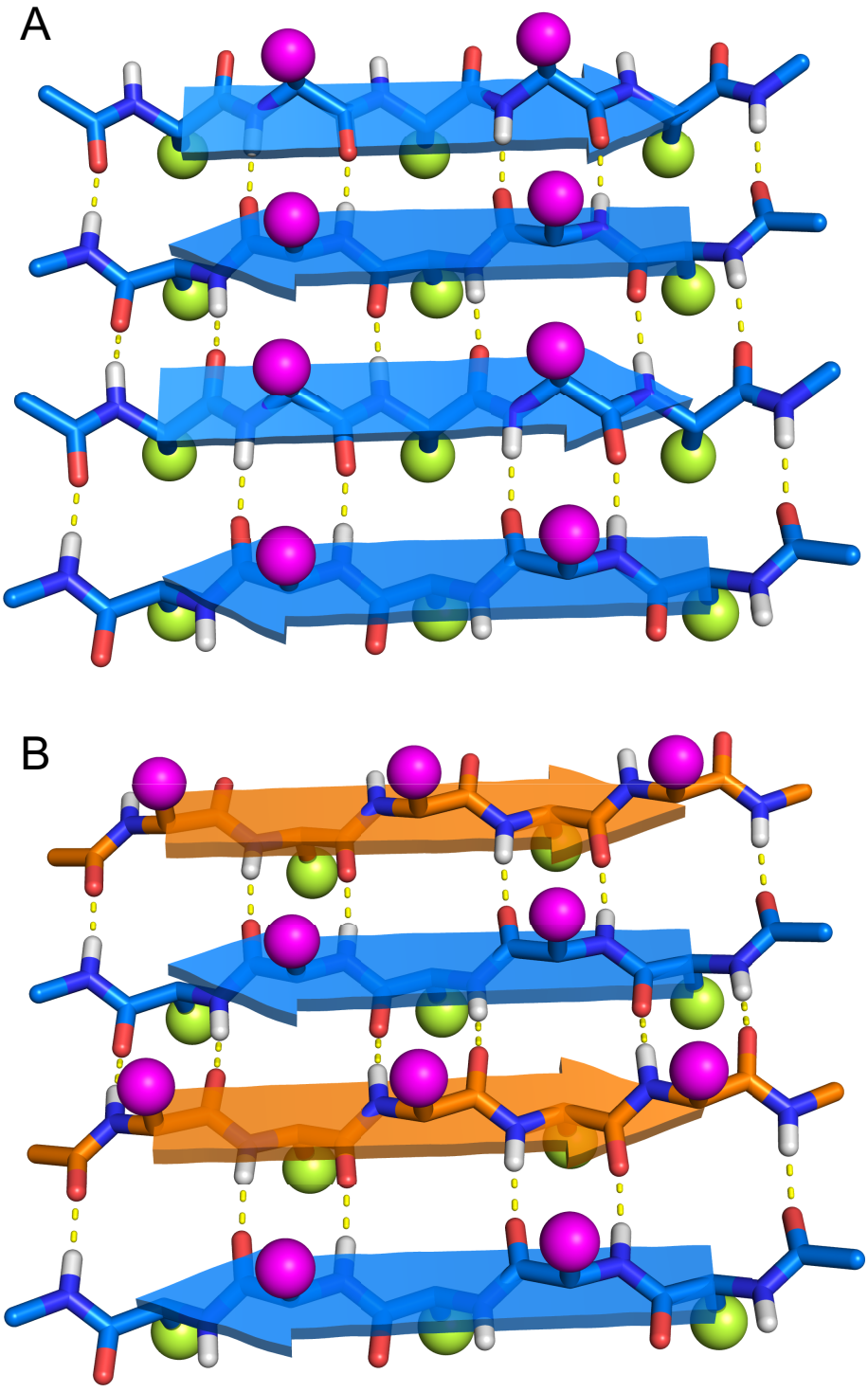

Figure 2.1. Molecular models of (A) pleated β-sheets formed from L-peptide strands (blue) and (B) rippled β-sheets formed from a mixture of L-peptide and D-peptide strands (orange). Amino acid side chains are depicted as balls, with magenta balls on the top face and yellow balls on the bottom face of the β-sheets.

Rippled β-sheets, formed by mixing D- and L-peptides, have recently attracted considerable interest as biomaterials and for other biomedical applications.[4–6] Schneider and co-workers demonstrated the effects of chirality with the hydrogel-forming peptide MAX1. When MAX1 was mixed with an equimolar amount of its enantiomer, the resulting hydrogel showed four times greater rigidity than that of the enantiopure MAX1 peptide.[7,8] Nilsson and co-workers demonstrated by isotope-edited IR spectroscopy and FRET studies that mixtures of enantiomeric peptides L-Ac-$(FKFE)_2$-NH_2 and D-Ac-$(FKFE)_2$-NH_2 form rippled β-sheet fibrils. The authors further demonstrated by isothermal titration calorimetry (ITC) that the resulting heterochiral assembly is more thermodynamically favored than the homochiral assembly.[9] In a subsequent paper, the authors reported that the hydrogel formed by the heterochiral rippled β-sheets is stronger and more resistant to proteolytic degradation than the hydrogel formed by the homochiral L-pleated β-sheets.[10]

The co-assembly of enantiomeric β-sheet peptides is not limited to designed biomaterials, and has also been used to characterize and study fibril formation of $Aβ_{40}$ and $Aβ_{42}$. Nilsson and co-workers demonstrated by isotope-edited IR spectroscopy and solid-state NMR spectroscopy that L- and D-$Aβ_{16-22}$ heptapeptides co-assemble to give rippled β-sheets and showed that the heterochiral assembly is more thermodynamically favorable.[11] Raskatov and co-workers observed that mixing D-$Aβ_{42}$ with L-$Aβ_{42}$ led to accelerated non-toxic fibril formation and attenuated cytotoxicity by suppressing oligomer formation.[12] Raskatov subsequently proposed "Aβ chiral inactivation" as a potential therapeutic strategy for Alzheimer's disease.[6,13] Recently, structures of the rippled β-sheet assembly have been reported. Tycko and Raskatov used solid-

state NMR spectroscopy to elucidate ^{15}N,^{13}C-labeled D,L-$A\beta_{40}$ fibril polymorphs in rippled β-sheets consisting of three different registrations in the hydrogen-bonded antiparallel alignment.[14] Raskatov and co-workers also reported the X-ray crystallographic structure of a rippled β-sheet formed from a mixture of L- and D-triphenylalanine.[15] DFT calculations have further supported a model in which heterochiral rippled β-sheets are favored over homochiral pleated β-sheets.[16,17] From these studies, a theory has emerged in which mixtures of enantiomeric β-sheet peptides are thought to prefer to co-assemble in a heterochiral fashion to form rippled β-sheets, rather than self-assemble in a homochiral fashion to form pleated β-sheets.

In 2004, our laboratory reported that enantiomeric β-sheet pentapeptides strongly prefer to form homochiral pleated β-sheet dimers in $CDCl_3$ solution, rather than heterochiral rippled β-sheet dimers, with a selectivity of 3.1–4.2 kcal/mol.[18] Recently Gellman and co-workers have studied homochiral and heterochiral β-sheet formation in aqueous solution using a β-hairpin model system and have found that peptides containing homochiral peptide strands fold to form β-hairpins, while peptides containing heterochiral peptide strands do not.[19] Intrigued by the conflicting reports of preferred homochiral and heterochiral β-sheet assembly, we set out to reconcile these findings using a minimal aqueous model system that recapitulates both the edge-to-edge hydrogen-bonding interactions that occur in β-sheet formation and additional face-to-face packing interactions that occur in gel and fibril formation. The model system consists of two well characterized β-sheet peptides derived from $A\beta_{17–23}$ and $A\beta_{30–36}$, peptides **2.1a** and **2.1b**.[20,21] Peptides **2.1a** and **2.1b** both form tetramers comprising sandwiches of β-sheet dimers. Using NMR spectroscopy,

we identify and characterize the different tetramers formed by mixing peptides **2.1a** and **2.1b** with their respective D-enantiomers, *ent*-**2.1a** and *ent*-**2.1b**. Through these studies, we find that homochiral pairing to form pleated β-sheets is preferred over heterochiral pairing to form rippled β-sheets.

RESULTS AND DISCUSSION

^{1}H NMR spectroscopy shows that mixing peptides 2.1a and ent-2.1a gives a new assembly. Enantiomerically pure peptide **2.1a** forms a homochiral tetramer in aqueous solution at millimolar concentrations. Peptide **2.1a** is a macrocyclic β-hairpin peptide containing two heptapeptide strands linked by two $^{\delta}$Orn turn units.[22] The upper strand of peptide **2.1a** is derived from $A\beta_{17-23}$, and the lower strand contains a Hao amino acid flanked by two dipeptides to promote solubility and prevent uncontrolled aggregation.[23] The tetramer formed by peptide **2.1a** consists of a sandwich of β-sheet dimers. Hydrogen-bonding interactions between the edges of the β-strands stabilize the dimers, and hydrophobic packing of the side chains further stabilizes the tetrameric assembly.

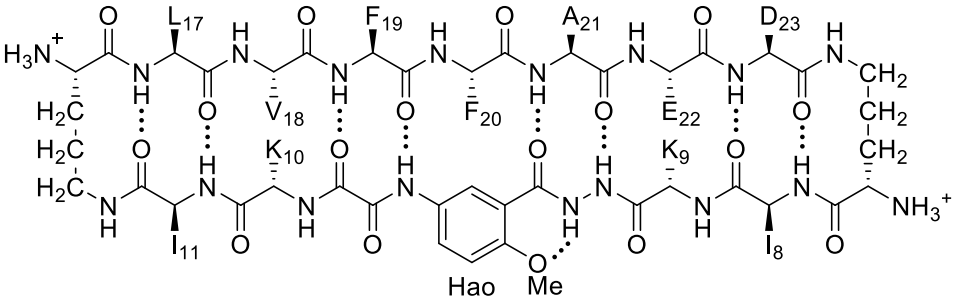

peptide **2.1a**

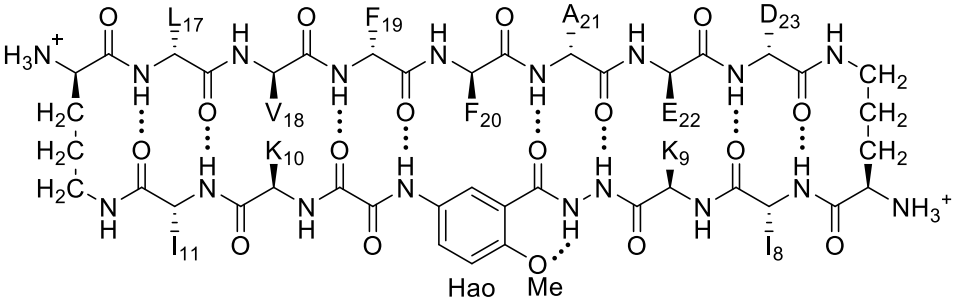

ent-**2.1a**

The ^{1}H NMR spectrum of peptide **2.1a** at 8.0 mM in D_2O at 298 K displays a predominant set of resonances associated with a homochiral tetramer, and a smaller set of resonances (4%) associated with the monomer. When peptides **2.1a** and *ent*-**2.1a** are mixed in equal concentrations (16.0 mM total), new resonances (29%) emerge that were previously unobserved for each enantiopure peptide (Figure 2.2). An EXSY experiment at 328 K shows that these new resonances exchange with the homochiral tetramer and monomer and thus correspond to a new heterochiral assembly (Figures S2.1–S2.4).[24]

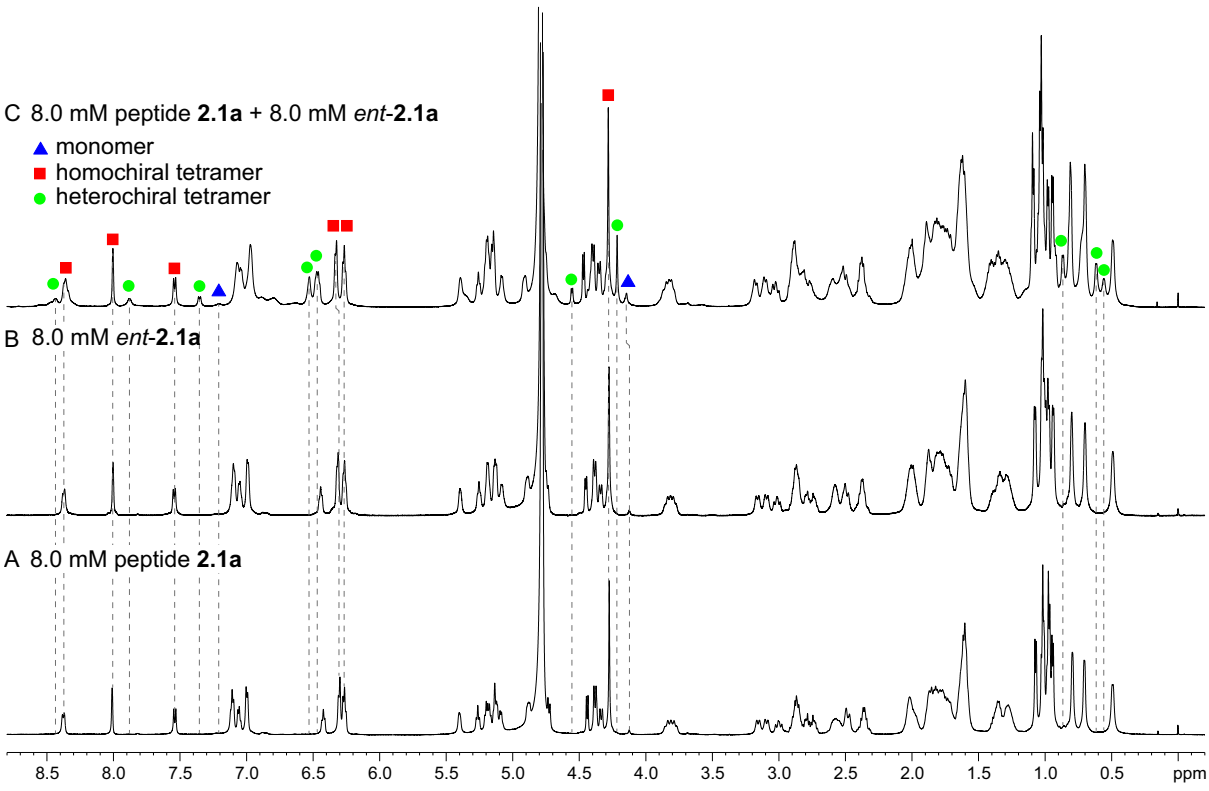

Figure 2.2. ^{1}H NMR spectra of (A) 8.0 mM peptide **2.1a**, (B) 8.0 mM peptide *ent*-**2.1a**, and (C) 8.0 mM peptide **2.1a** and 8.0 mM peptide *ent*-**2.1a** in D_2O at 600 MHz and 298 K with 0.06 mM DSA as an internal standard.[25]. Dashed lines mark key resonances associated with the monomer, homochiral tetramer, and heterochiral tetramer. These resonances are designated as follows: blue triangle, monomer; red square, homochiral tetramer; green circle, heterochiral tetramer.

$^{1}H,^{15}N$ HSQC and DOSY studies reveal a heterochiral tetramer. HSQC studies using ^{15}N isotopic labeling corroborate the formation of the new assembly observed in the 1D ^{1}H NMR spectrum. $^{1}H,^{15}N$ HSQC experiments give a unique crosspeak for each species containing an ^{15}N isotope, readily allowing the identification of the different isotopically labeled species present.[20,21] We thus prepared an isotopologue of peptide **2.1a** containing an ^{15}N label on Phe_{20} — peptide **2.2a** — and studied its mixture with peptide *ent*-**2.1a** by $^{1}H,^{15}N$ HSQC.

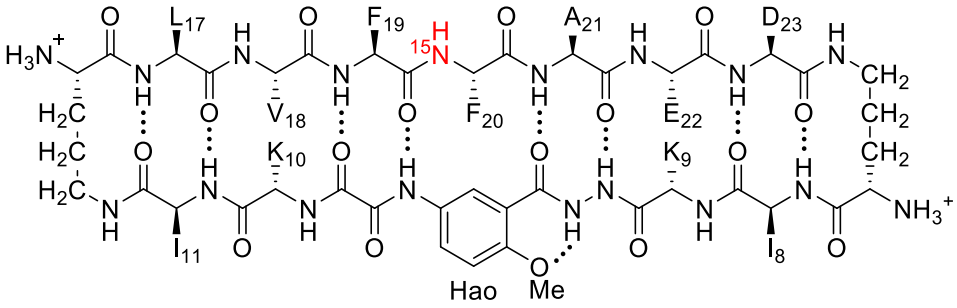

peptide **2.2a**

The $^{1}H,^{15}N$ HSQC spectrum of 8.0 mM peptide **2.2a** in 9:1 H_2O:D_2O solution shows two crosspeaks — one associated with the homochiral tetramer and the other with the monomer (Figure 2.3A).[20] The tetramer has a crosspeak that appears at 8.56 ppm in the ^{1}H dimension and 121.4 ppm in the ^{15}N dimension; the monomer has a crosspeak that appears at 8.30 ppm in the ^{1}H dimension and 122.8 ppm in the ^{15}N dimension. When peptide **2.2a** is mixed with peptide *ent*-**2.1a** (16.0 mM total), the crosspeak of the monomer is no longer observed, and a new crosspeak appears at 8.63 ppm in the ^{1}H dimension and 122.5 ppm in the ^{15}N dimension (Figure 2.3B). This crosspeak is not observed in the $^{1}H,^{15}N$ HSQC spectrum of the enantiomerically pure peptide **2.2a** and is thus associated with the formation of a heterochiral species. The weaker intensity of this new

crosspeak indicates that the homochiral tetramer forms preferentially under the conditions of the experiment.

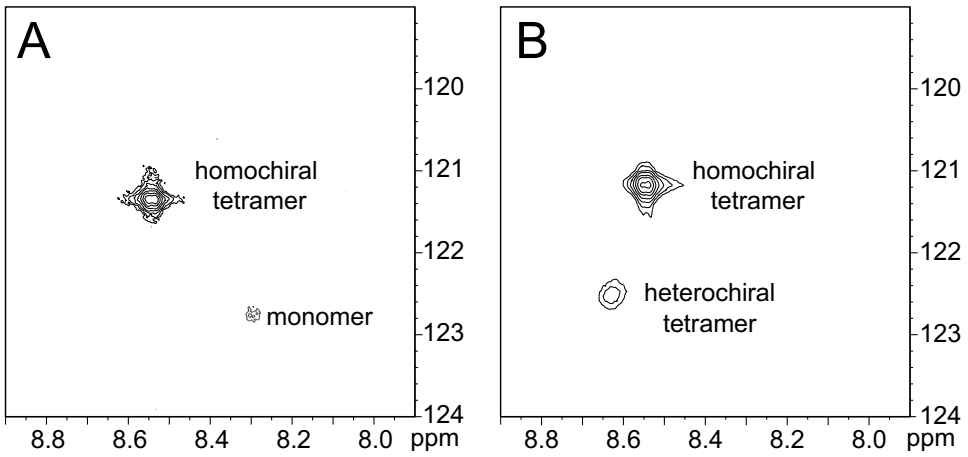

Figure 2.3. $^{1}H,^{15}N$ HSQC spectra of (A) 8.0 mM peptide **2.2a** and (B) 8.0 mM peptide **2.2a** and 8.0 mM peptide *ent*-**2.1a** in 9:1 H_2O:D_2O at 500 MHz and 298 K.

Diffusion-ordered spectroscopy (DOSY) studies suggest that the new heterochiral species is a tetramer. The DOSY spectrum of 8.0 mM peptide **2.1a** in D_2O shows a diffusion coefficient of 11.6 ± 0.9 x 10^{-11} m^2/s for the tetramer (Figure S2.5). This value is similar to what we have previously reported for peptide **2.1a** at 8.0 mM and 298 K.[20] In the DOSY spectrum of the mixture of peptides **2.1a** and *ent*-**2.1a** (8.0 mM each), the resonances corresponding to the homochiral tetramer show a diffusion coefficient of 10.7 ± 0.7 x 10^{-11} m^2/s, and the resonances corresponding to the heterochiral tetramer show a diffusion coefficient of 10.2 ± 0.7 x 10^{-11} m^2/s (Figure S2.6). The small differences among the diffusion coefficients may reflect transient non-specific interactions among the tetramers at the higher concentration (16.0 mM total) of the mixing experiment leading to a lower diffusion coefficient.[26]

Supramolecular assembly of the heterochiral tetramer. Through NOESY studies of peptide **2.1a**, our laboratory previously established that the tetramer formed by peptide **2.1a** consists of sandwiches of β-sheet dimers.[20,21] The heterochiral tetramer formed by peptides **2.1a** and *ent*-**2.1a** can adopt a similar structure, in which two dimers form a sandwich-like tetramer. Peptides **2.1a** and *ent*-**2.1a** can come together in two different ways to form heterochiral tetramers in 2:2 stoichiometry — either as an L_2D_2 topological isomer, in which the sandwich consists of L•L and D•D homochiral dimers, or as an $(LD)_2$ topological isomer, in which the sandwich consists of two L•D heterochiral dimers (Figure 2.4). The L_2D_2 tetramer should give one set of resonances in the ^{1}H NMR spectrum, distinct from those of the L_4 and D_4 homochiral tetramers, which collectively should give one set of resonances. The $(LD)_2$ tetramer should also give one set of resonances in the ^{1}H NMR spectrum. Peptides **2.1a** and *ent*-**2.1a** could also come together to give heterochiral tetramers in 3:1 and 1:3 stoichiometry, L_3D_1 and L_1D_3, which should give four sets of resonances in the ^{1}H NMR spectrum. The observation of a single set of new resonances in the ^{1}H NMR spectra of the mixture thus indicates the formation of a single heterochiral tetramer with a 2:2 stoichiometry as either the L_2D_2 or the $(LD)_2$ topological isomer.

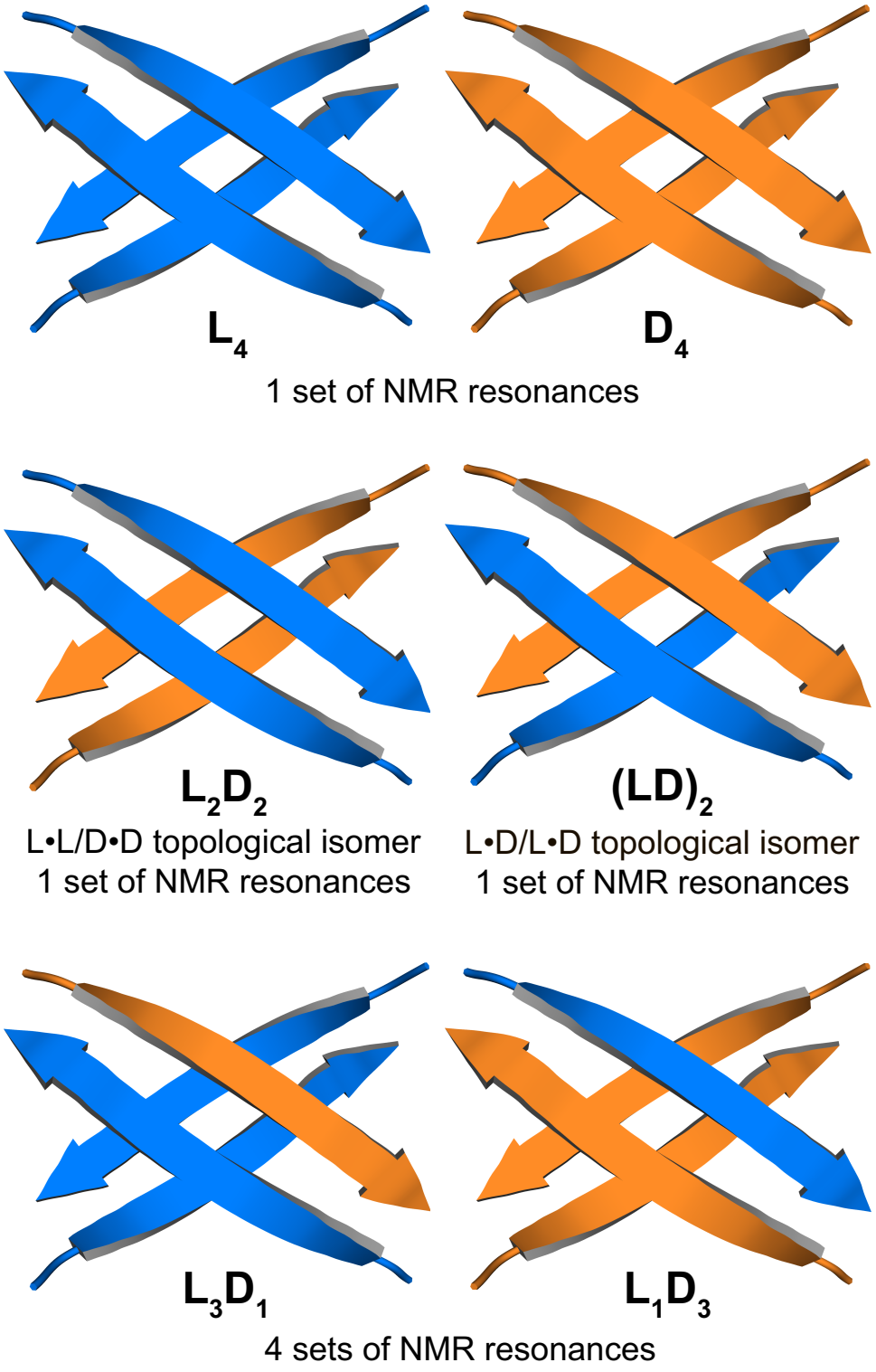

Figure 2.4. Cartoon illustrations representing the possible combinations of homochiral and heterochiral tetramers formed from a mixture of peptides **2.1a** and *ent*-**2.1a**. Macrocyclic peptide **2.1a** is represented by a blue arrow and macrocyclic peptide *ent*-**2.1a** is represented by an orange arrow.

^{15}N-Edited NOESY studies reveal homochiral dimers within the heterochiral tetramer. The ^{15}N-edited NOESY spectrum of ^{15}N-labeled enantiomerically pure peptide **2.2a** shows three NOE crosspeaks associated with close contacts in the homochiral tetramer (Figure 2.5B). The Phe_{20} ^{15}NH proton of the tetramer shows an interstrand NOE with the Ala_{21} α-proton in its dimerization partner, as well as a strong intrastrand NOE with the Phe_{19} α-proton and a weaker intrastrand NOE with the Phe_{20} α-proton. This pattern of NOEs is characteristic of the proximities observed in β-sheet structure (Figure 2.5A).[28,29]

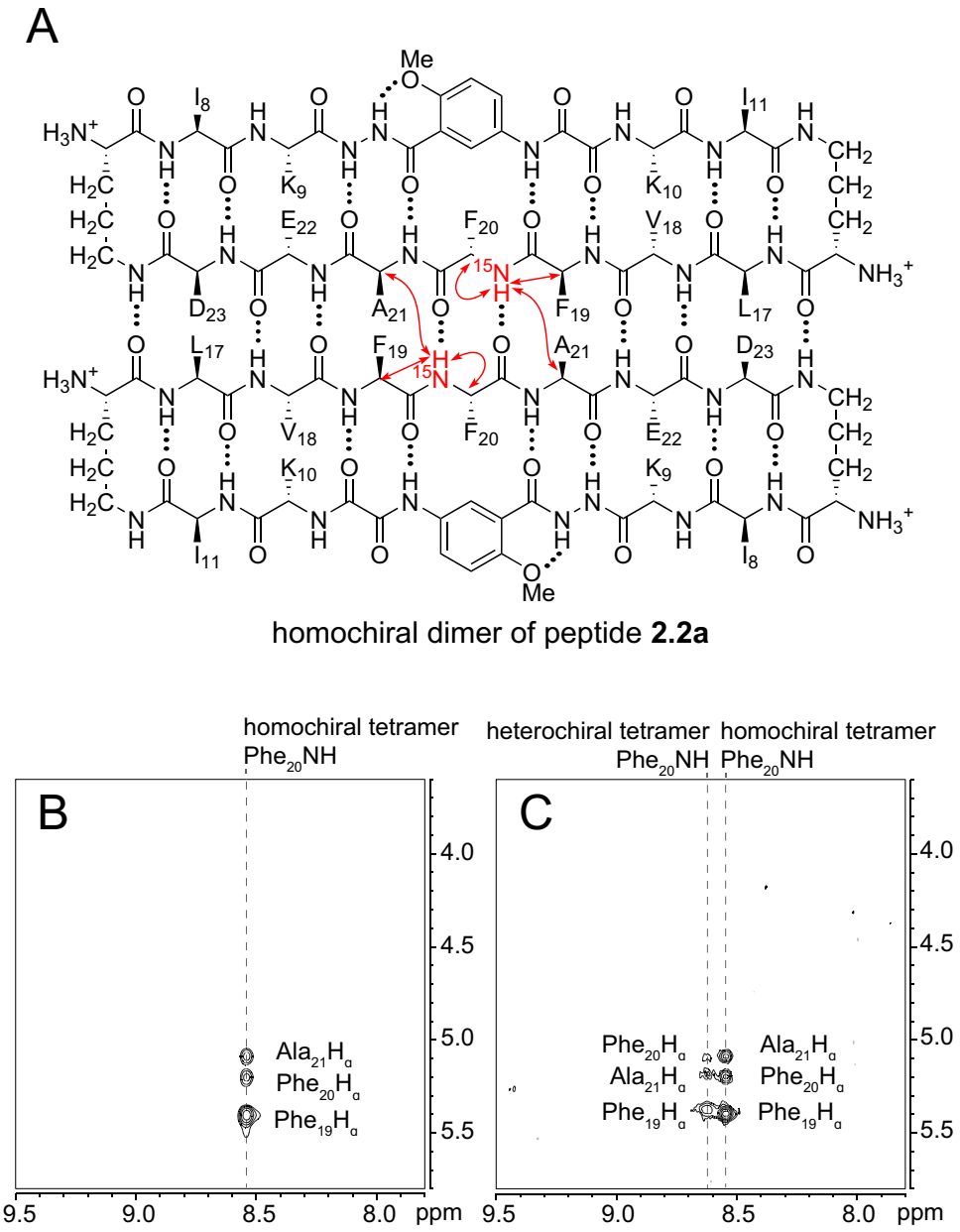

Figure 2.5. (A) Structure of the homochiral dimer subunit of the tetramer formed from ^{15}N-labeled peptide **2.2a**. Red arrows represent NOEs observed in the ^{15}N-edited NOESY spectrum. (B) ^{15}N-edited NOESY spectrum of 8.0 mM peptide **2.2a** in 9:1 H_2O:D_2O at 500 MHz and 298 K. (C) ^{15}N-edited NOESY spectrum of 8.0 mM peptide **2.2a** and 8.0 mM peptide *ent*-**2.1a** in 9:1 H_2O:D_2O at 500 MHz and 298 K.

When ^{15}N-labeled peptide **2.2a** is mixed with unlabeled peptide *ent*-**2.1a**, a new set of weaker NOE crosspeaks associated with the heterochiral tetramer emerges, in addition to the NOE crosspeaks associated with the homochiral tetramer (Figure 2.5C). In the set of NOE crosspeaks from the heterochiral

tetramer, the Phe_{20} ^{15}NH proton shows an interstrand NOE with the Ala_{21} α-proton in its dimerization partner, as well as a relatively strong intrastrand NOE with the Phe_{19} α-proton and a weaker intrastrand NOE with the Phe_{20} α-proton. Although the observation of a new set of crosspeaks establishes the formation of a heterochiral tetramer, it does not distinguish between the L_2D_2 and the $(LD)_2$ topological isomers.

To differentiate between the L_2D_2 and the $(LD)_2$ topological isomers, we strategically incorporated two deuterated residues (d_8-Phe_{19} and d_4-Ala_{21}) into ^{15}N-labeled peptide **2.2a**, to create peptide **2.3a**, and we studied its interaction with unlabeled *ent*-**2.1a** by ^{15}N-edited NOESY experiments. A homochiral dimer in which peptide **2.3a** is paired with itself should not exhibit an interstrand NOE between the ^{15}NH proton of Phe_{20} and the α-proton of d_4-Ala_{21}, because the α-proton has been replaced with deuterium (Figure 2.6A). In contrast, a heterochiral dimer in which peptide **2.3a** is paired with peptide *ent*-**2.1a** should exhibit an interstrand NOE between the ^{15}NH proton of Phe_{20} in peptide **2.3a** and the α-proton of Ala_{21} in peptide *ent*-**2.1a** (Figure 2.6B).

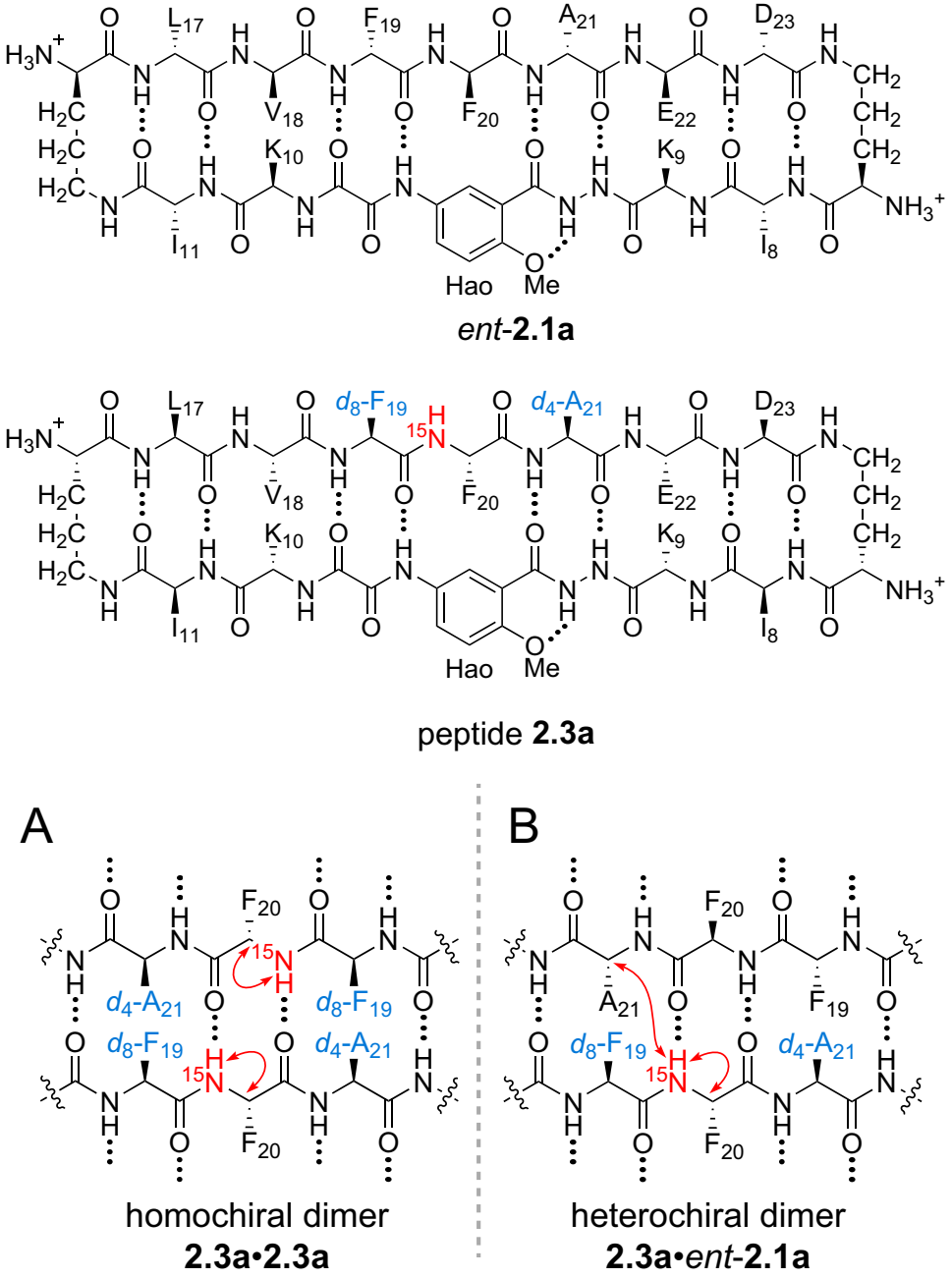

Figure 2.6. Structures of peptide *ent*-**2.1a** and triply labeled peptide **2.3a**. (A) Expected NOEs in the ^{15}N-edited NOESY spectrum of a homochiral dimer subunit. (B) Expected NOEs in the ^{15}N-edited NOESY spectrum of a heterochiral dimer subunit.

^{15}N-Edited NOESY studies of the mixture of peptides **2.3a** and *ent*-**2.1a** reveal a weak crosspeak associated with a heterochiral tetramer composed of homochiral dimers, in addition to crosspeaks associated with the homochiral tetramer. Enantiomerically pure peptide **2.3a** exhibits the expected intrastrand

NOE crosspeak between the ^{15}NH proton and the α-proton of Phe$_{20}$ and an unexpected weaker NOE crosspeak to the α-proton of d_8-Phe$_{19}$ (Figure 2.7A). This weaker NOE results from incomplete deuterium labeling at the α-position of the d_8-Phe$_{19}$.[30] In the mixture of peptides **2.3a** and *ent*-**2.1a**, a new NOE crosspeak between the ^{15}NH proton and the α-proton of Phe$_{20}$ associated with the heterochiral tetramer is observed (Figure 2.7B). No additional NOE crosspeaks are observed for the heterochiral tetramer. The presence of only an intrastrand NOE crosspeak in the ^{15}N-edited NOESY spectrum of the mixture indicates that peptides **2.3a** and *ent*-**2.1a** are not dimerization partners and shows that the heterochiral tetramer is composed of two homochiral dimer subunits.

Collectively the 1D, ^{1}H,^{15}N HSQC, DOSY, and ^{15}N-edited NOESY studies establish that peptides **2.1a** and *ent*-**2.1a** preferentially form the L$_4$ and D$_4$ homochiral tetramers, in addition to a smaller amount of the L$_2$D$_2$ heterochiral tetramer (Figure 2.4). The formation of the L$_2$D$_2$ heterochiral tetramer rather than the (LD)$_2$ heterochiral tetramer demonstrates that even within heterochiral assemblies, enantiomeric β-sheet peptides prefer to self-assemble in a homochiral fashion. Thus, the formation of the L$_2$ and D$_2$ pleated β-sheets is preferred over the formation of the LD rippled β-sheets.

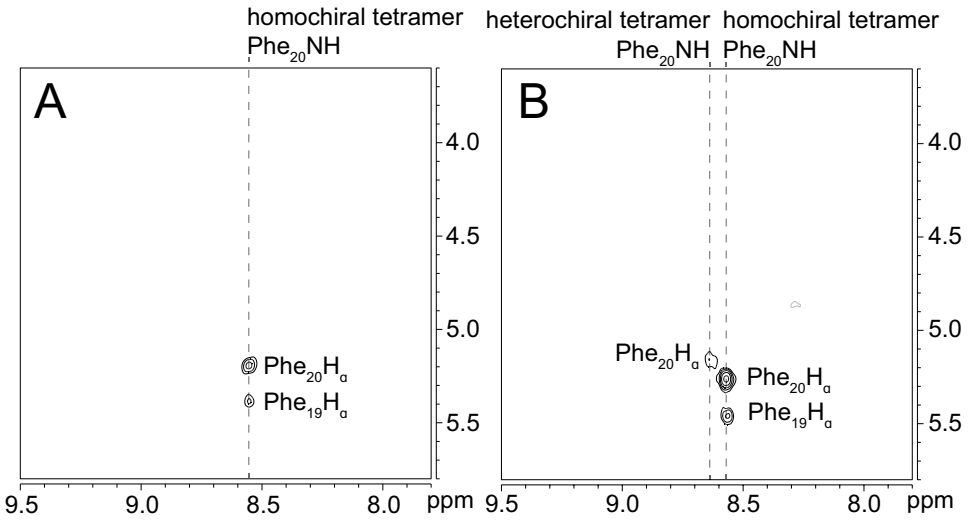

Figure 2.7. ^{15}N-Edited NOESY spectra of (A) 8.0 mM triply labeled peptide **2.3a** and (B) 8.0 mM peptide **2.3a** and 8.0 mM unlabeled peptide *ent*-**2.1a** in 9:1 H_2O:D_2O at 500 MHz and 298 K.

^{1}H NMR spectroscopy shows that mixing peptides 2.1b and ent-2.1b does not result in heterochiral assembly. To assess the preferences for homochiral or heterochiral assembly in a different β-sheet peptide, we studied the assembly of peptides **2.1b** and *ent*-**2.1b**.[20] Peptide **2.1b** is a homologue of peptide **2.1a** that contains $A\beta_{30-36}$ instead of $A\beta_{17-23}$. We had previously found that peptide **2.1b** also assembles to form a tetramer at millimolar concentrations, albeit with an equilibrium that favors the tetramer less strongly.

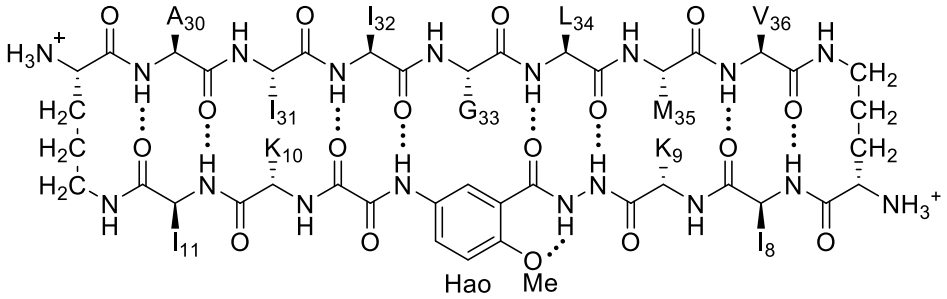

peptide **2.1b**

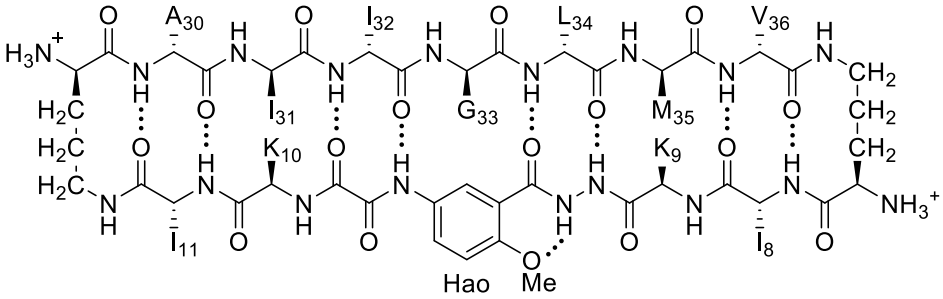

ent-**2.1b**

When peptide **2.1b** is mixed with peptide *ent*-**2.1b**, no evidence of heterochiral tetramer formation is observed. The ^{1}H NMR spectrum of peptide **2.1b** at 4.0 mM in D_2O at 298 K displays sets of resonances associated with both the monomer and the homochiral tetramer (Figure 2.8A). The 4.0 mM ^{1}H NMR spectrum of peptide *ent*-**2.1b** is identical to that of peptide **2.1b** (Figure 2.8B). At 8.0 mM, the spectrum of peptide **2.1b** displays a shift in equilibrium toward the tetramer (Figure 2.8C). The spectrum broadens slightly, suggesting exchange between the monomer and tetramer on an intermediate timescale (ca. 10^{-1} sec) or additional non-specific interactions.

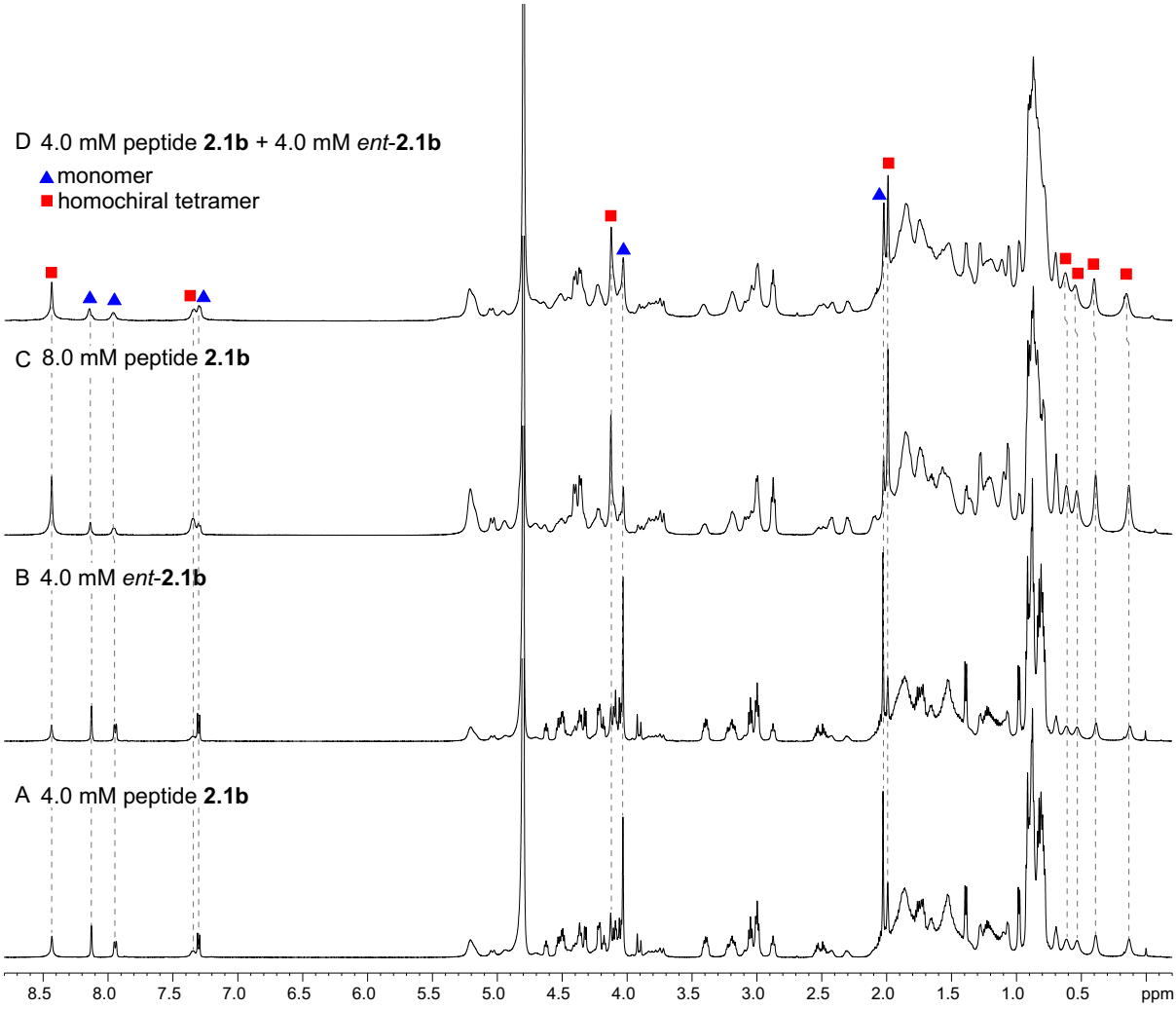

Figure 2.8. ^{1}H NMR spectra of (A) 4.0 mM peptide **2.1b**, (B) 4.0 mM peptide *ent*-**2.1b**, (C) 8.0 mM peptide **2.1b**, and (D) 4.0 mM peptide **2.1b** and 4.0 mM peptide *ent*-**2.1b** in D_2O at 600 MHz and 298 K with 0.06 mM DSA.[25] (Spectra were referenced against an external DSA standard.) Dashed lines mark key resonances associated with the monomer and homochiral tetramer. These resonances are labeled as follows: blue triangle, monomer; red square, homochiral tetramer.

When peptides **2.1b** and *ent*-**2.1b** are mixed (4.0 mM of each), no new peaks form, and only peaks associated with the monomer and homochiral tetramer are observed (Figure 2.8D). As with the 8.0 mM spectrum of peptide **2.1b**, there is slight broadening of the spectrum of the mixture of peptides **2.1b** and *ent*-**2.1b**, suggesting exchange on an intermediate timescale or additional non-specific interactions.

The DOSY spectrum of 1.0 mM peptide **2.1b** in D_2O shows a monomer with a diffusion coefficient of 19.5 ± 0.7 x 10^{-11} m^2/s (Figure S2.7). This value is similar to that which we have previously reported for peptide **2.1b** at 1.0 mM and 298 K.[20] At 4.0 mM, an additional set of smaller resonances associated with the homochiral tetramer appears (Figure S2.8); the monomer shows a diffusion coefficient of 17.7 ± 0.6 x 10^{-11} m^2/s, and the tetramer shows a diffusion coefficient of 13.0 ± 0.4 x 10^{-11} m^2/s. The decrease in diffusion coefficient of the monomer, as well as the somewhat higher than expected diffusion coefficient of the tetramer — typically about 0.6X that of the monomer,[26] ca. 12 x 10^{-11} m^2/s — suggest intermediate exchange between the monomer and the tetramer on the 75-ms time scale of the DOSY experiment.

When the concentration of peptide **2.1b** is doubled to 8.0 mM, the resonances associated with the homochiral tetramer predominate (Figure S2.9); the monomer shows a diffusion coefficient of 15.9 ± 0.7 x 10^{-11} m^2/s, and the tetramer shows a diffusion coefficient of 12.5 ± 0.4 x 10^{-11} m^2/s. The further decrease in diffusion coefficient of the monomer is consistent with intermediate exchange. The DOSY spectrum of the mixture of peptides **2.1b** and *ent*-**2.1b** (4.0 mM of each) shows diffusion coefficients of the monomer and tetramer of 14.4 ± 1.1 x 10^{-11} m^2/s and 10.7 ± 0.8 x 10^{-11} m^2/s, respectively (Figure S2.10). The low value of the monomer is consistent with intermediate exchange between the monomer and the tetramer. The value of the tetramer is somewhat lower than expected, suggesting additional transient non-specific interactions among the tetramers.[26,27] The absence of any additional new peaks in the spectrum of the mixture, not present in the spectra of the enantiomerically pure peptides,

provides good evidence that mixing peptides **2.1b** and *ent*-**2.1b** does not result in any detectable heterochiral assembly.

^{1}H,^{15}N HSQC studies corroborate the presence of only monomer and homochiral tetramer in the mixture of peptides **2.1b** and *ent*-**2.1b**. To identify and confirm the monomer and homochiral tetramer by ^{1}H,^{15}N HSQC, we prepared an isotopologue of peptide **2.1b** containing an ^{15}N label on Gly_{33} — peptide **2.2b** — and studied its mixture with peptide *ent*-**2.1b**. We studied increasing concentrations of enantiomerically pure peptide **2.2b** (1.0 mM, 4.0 mM, and 8.0 mM), and compared the crosspeaks to those found in the mixture of peptides **2.2b** and *ent*-**2.1b** (8.0 mM total).

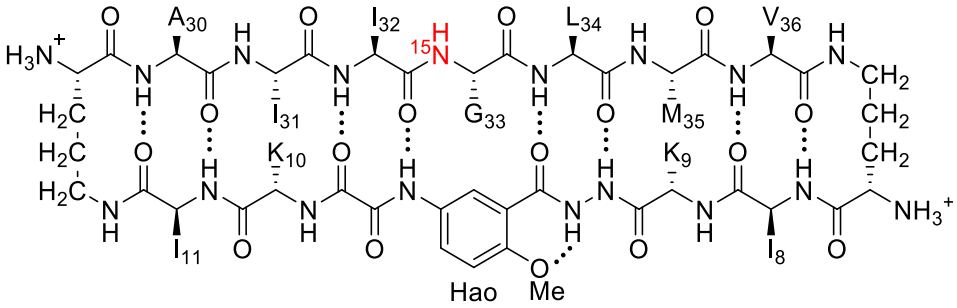

peptide **2.2b**

The ^{1}H,^{15}N HSQC spectrum of 1.0 mM peptide **2.2b** in 9:1 H_2O:D_2O solution shows only a crosspeak associated with the monomer, at 8.35 ppm in the ^{1}H dimension and 112.2 ppm in the ^{15}N dimension (Figure 2.9A). At 4.0 mM peptide **2.2b**, the monomer is still present and a crosspeak associated with the homochiral tetramer appears 115.8 ppm in the ^{15}N dimension and 9.31 ppm in the ^{1}H dimension (Figure 2.9B).[20] When the concentration of peptide **2.2b** is doubled to 8.0 mM, the relative intensity of the tetramer crosspeak increases (Figure 2.9C). When peptide **2.2b** is mixed with peptide *ent*-**2.1b** (4.0 mM each),

crosspeaks associated with the monomer and homochiral tetramer are still present and no new crosspeaks are observed (Figure 2.9D). The lack of new crosspeaks further establishes that enantiomeric β-sheet peptides prefer to self-assemble in a homochiral fashion.

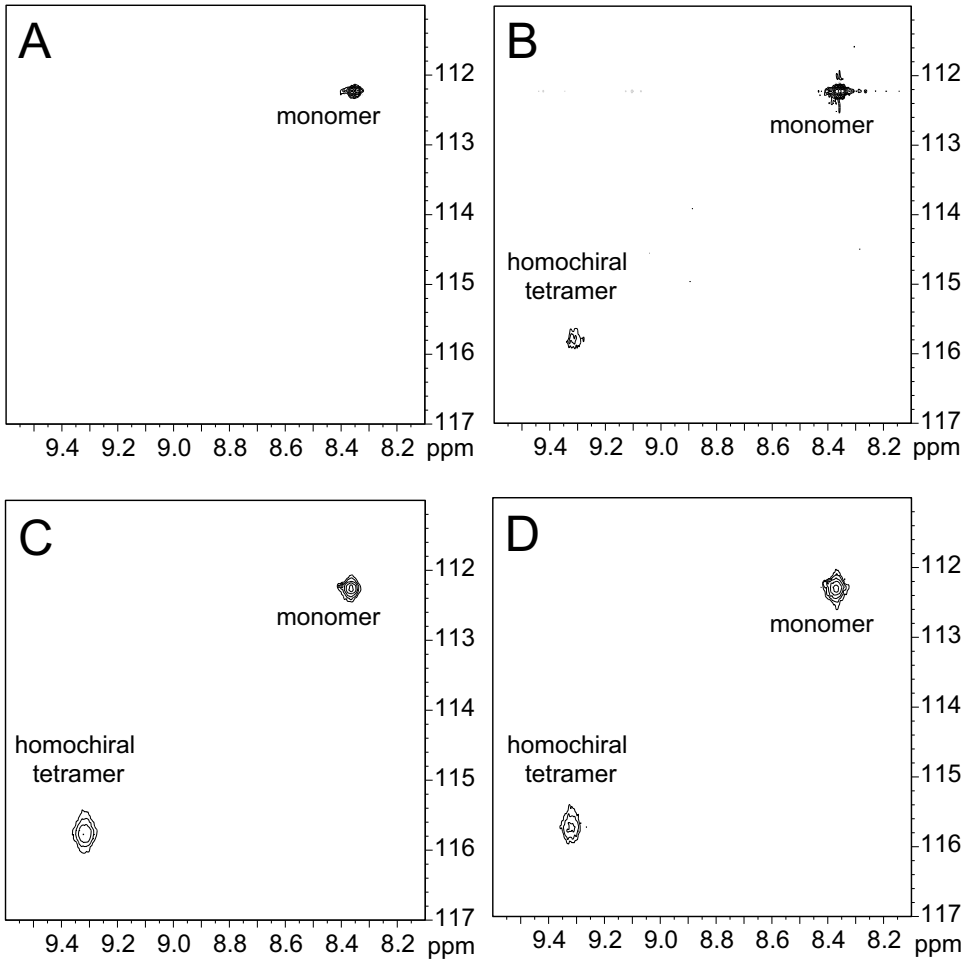

Figure 2.9. $^{1}H,^{15}N$ HSQC spectra of (A) 1.0 mM peptide **2.2b**, (B) 4.0 mM peptide **2.2b**, (C) 8.0 mM peptide **2.2b**, and (D) 4.0 mM peptide **2.2b** and 4.0 mM peptide *ent*-**2.1b** in 9:1 H_2O:D_2O at 500 MHz and 298 K.

CONCLUSION

The solution-phase NMR studies of Aβ-derived peptides **2.1a** and **2.1b** and the corresponding enantiomers and isotopologues provide further evidence that enantiomeric β-sheet peptides prefer to self-assemble in a homochiral fashion. These studies recapitulate our laboratory's findings that small β-sheet peptides

strongly prefer to form homochiral dimers in chloroform solution,[18] as well as Gellman's findings in homo- and heterochiral β-hairpin systems.[19] How then, do we reconcile these findings with the findings of other researchers where heterochiral assembly is preferred?

In the studies of Schneider, Nilsson, Raskatov, and Tycko described in the introduction, heterochiral assembly occurs in the solid or gel state.[5–17] Heterochiral assembly in the solid state is driven heavily by the packing of molecules, which in addition to edge-to-edge hydrogen bonding, drives the formation of fibrils and crystal lattices. These packing interactions involve not just the side chains within individual β-sheets, but also the packing of β-sheets together. Heterochiral packing is generally preferred over homochiral packing in the crystal state, which leads to denser solids and a preference for racemic crystal formation — a phenomenon known as "Wallach's rule".[31–33] Thus, it appears that packing in the solid state may drive the formation of heterochiral mixtures of β-sheet peptides, and in some cases the formation of rippled β-sheets. In the solution phase, where crystal packing forces are absent, rippled β-sheet formation is strongly disfavored. Thus, no evidence of heterochiral pairing to form rippled β-sheets is observed with peptides **2.1a** and **2.1b** and the corresponding enantiomers.

REFERENCES AND NOTES

[1] Pauling, L.; Corey, R, B. *Proc. Natl. Acad. Sci. U. S. A.* 1951, *37*, 251–256.

[2] Pauling, L.; Corey, R, B. *Proc. Natl. Acad. Sci. U. S. A.* 1951, *37*, 729–740.

[3] Pauling, L.; Corey, R, B. *Proc. Natl. Acad. Sci. U. S. A.* 1953, *39*, 253–256.

[4] Lotz, B. *ChemBioChem* 2022, e202100658.

[5] Raskatov, J. A.; Schneider, J. P.; Nilsson, B. L. *Acc. Chem. Res.* 2021, *54*, 2488 2501.

[6] Foley, A. R.; Raskatov, J. A. *Curr. Opin. Chem. Biol.* 2021, *64*, 1–9.

[7] Nagy, K. J.; Giano, M. C.; Jin, A.; Pochan, D. J.; Schneider, J. P. *J. Am. Chem. Soc.* 2011, *133*, 14975–14977.

[8] Nagy-Smith, K.; Beltramo, P. J.; Moore, E.; Tycko, R.; Furst, E. M.; Schneider, J. P. *ACS Cent. Sci.* 2017, *3*, 586–597.

[9] Swanekamp, R. J.; Dimaio, J. T. M.; Bowerman, C. J.; Nilsson, B. L. *J. Am. Chem. Soc.* 2012, *134*, 5556–5559.

[10] Swanekamp, R. J.; Welch, J. J.; Nilsson, B. L. *Chem. Commun.* 2014, *50*, 10133–10136.

[11] Urban, J. M.; Ho, J.; Piester, G.; Fu, R.; Nilsson, B. L. *Molecules* 2019, *24*, 1983.

[12] Dutta, S.; Foley, A. R.; Warner, C. J. A.; Zhang, X.; Rolandi, M.; Abrams, B.; Raskatov, J. A. *Angew. Chemie. Int. Ed.* 2017, *56*, 11506–11510.

[13] Raskatov, J. A. *Chem. Eur. J.* 2017, *23*, 16920–16923.

[14] Raskatov, J. A.; Foley, A. R.; Louis, J. M.; Yau, W. M.; Tycko, R. *J. Am. Chem. Soc.* 2021, *143*, 13299–13313.

[15] Kuhn, A. J.; Ehlke, B.; Johnstone, T. C.; Oliver, S. R. J.; Raskatov, J. A. *Chem. Sci.* 2022, *13*, 671–680.

[16] Raskatov, J. A. *ChemBioChem* 2020, *21*, 2945–2949.

[17] Raskatov, J. A. *Biopolymers* 2021, *112,* e23391.

[18] Chung, D. M.; Nowick, J. S. *J. Am. Chem. Soc.* 2004, *126*, 3062–3063.

[19] Liu, X.; Gellman, S. H. *ChemBioChem* 2021, *22*, 2772–2776.

[20] Truex, N. L.; Wang, Y.; Nowick, J. S. J. Am. Chem. Soc. 2016, 138, 13882–13890.

[21] Truex, N. L.; Nowick, J. S. *J. Am. Chem. Soc.* 2016, *138*, 13891–13900.

[22] Nowick, J. S.; Brower, J. O. *J. Am. Chem. Soc.* 2003, *125*, 876–877.

[23] Nowick, J. S.; Chung, D. M.; Maitra, K.; Maitra, S.; Stigers, K. D.; Sun, Y. *J. Am. Chem. Soc.* 2000, *122*, 7654–7661.

[24] The EXSY experiments were performed with a mixing time of 500 ms. Exchange occurs too slowly to be detected at 298 K but is observed at 328 K, suggesting that exchange occurs on the time scale of seconds at 328 K and tens of seconds at 298 K.

[25] Nowick, J. S.; Khakshoor, O.; Hashemzadeh, M.; Brower, J. O. *Org. Lett.* 2003, *5*, 3511–3513.

[26] Khakshoor, O.; Demeler, B.; Nowick, J. S. *J. Am. Chem. Soc.* 2007, *129*, 5558–5569.

[27] Alternatively, the formation of hexamers in rapid equilibrium with the tetramers cannot be precluded. We have previously observed that β-sheet peptides that form a tetramer comprising two β-sheet dimers in solution can form a hexamer comprising

three β-sheet dimers in the crystal state. Khakshoor, O.; Lin, A. J.; Korman, T. P.; Sawaya, M. R.; Tsai, S. C.; Eisenberg, D.; Nowick, J. S. *J. Am. Chem. Soc.* 2010, *132*, 11622–11628.

[28] Nowick, J. S. *Org. Biomol. Chem.* 2006, *4*, 3869-3885.

[29] Wüthrich, K. *NMR of Proteins and Nucleic Acids*; Wiley: New York, 1986; pp 125-129.

[30] d_8-Phenylalanine was purchased from Cambridge Isotope Laboratories and was reported to be 98% isotopic purity. The ^{1}H NMR spectrum of the d_8-phenylalanine shows a disproportionate amount of ^{1}H isotopic impurity at the α-position. See Figure S11 for spectral data.

[31] Brock, C. P.; Schweizer, W. B.; Dunitz, J. D. *J. Am. Chem. Soc.* 1991, *113*, 9811–9820.

[32] Friščić, T.; Fábián, L.; Burley, J. C.; Reid, D. G.; Duer, M. J.; Jones, W. *Chem. Commun.* 2008, 1644–1646.

[33] Navare, P. S.; MacDonald, J. C. *Cryst. Growth Des.* 2011, *11*, 2422–2428.

Table of Contents

Supplementary information 138

Figure S2.1 140

Figure S2.2 141

Figure S2.3 142

Figure S2.4 143

Supplementary Table 2.1 144

Figure S2.5 144

Figure S2.6 145

Supplementary Table 2.2 146

Figure S2.7 146

Figure S2.8 147

Figure S2.9 148

Figure S2.10 149

Figure S2.11 150

Synthesis of peptides 151

Peptide synthesis procedure. 151

Synthesis of Fmoc-protected amino acids 155

Fmoc-protection procedure. 155

NMR spectroscopy of peptides 156

Sample preparation, data collection, and data processing 156

References 159

Characterization Data 160

NMR spectroscopic studies of β-hairpin peptides 160

^{1}H NMR, TOCSY, and NOESY spectra of 8.0 mM peptide **2.1a** 160

^{1}H NMR, TOCSY, and NOESY spectra of peptides **2.1a** and *ent*-**2.1a** (16 mM) 166

^{1}H NMR, TOCSY, and NOESY spectra of peptides **2.3a** and *ent*-**2.1a** (16 mM) 173

^{1}H NMR, TOCSY, and NOESY spectra of 4.0 mM peptide **2.1b** 179

^{1}H NMR, TOCSY, and NOESY spectra of peptides **2.1b** and *ent*-**2.1b** (8 mM) 185

Analytical HPLC trace and MALDI mass spectrum of peptides 191

Analytical HPLC trace and MALDI mass spectrum of peptide **2.1a** 191

Analytical HPLC trace and MALDI mass spectrum of peptide *ent*-**2.1a** 193
Analytical HPLC trace and MALDI mass spectrum of peptide **2.2a** 195
Analytical HPLC trace and MALDI mass spectrum of peptide **2.3a** 197
Analytical HPLC trace and MALDI mass spectrum of peptide **2.1b** 199
Analytical HPLC trace and MALDI mass spectrum of peptide *ent*-**2.1b** 201
Analytical HPLC trace and MALDI mass spectrum of peptide **2.2b** 203

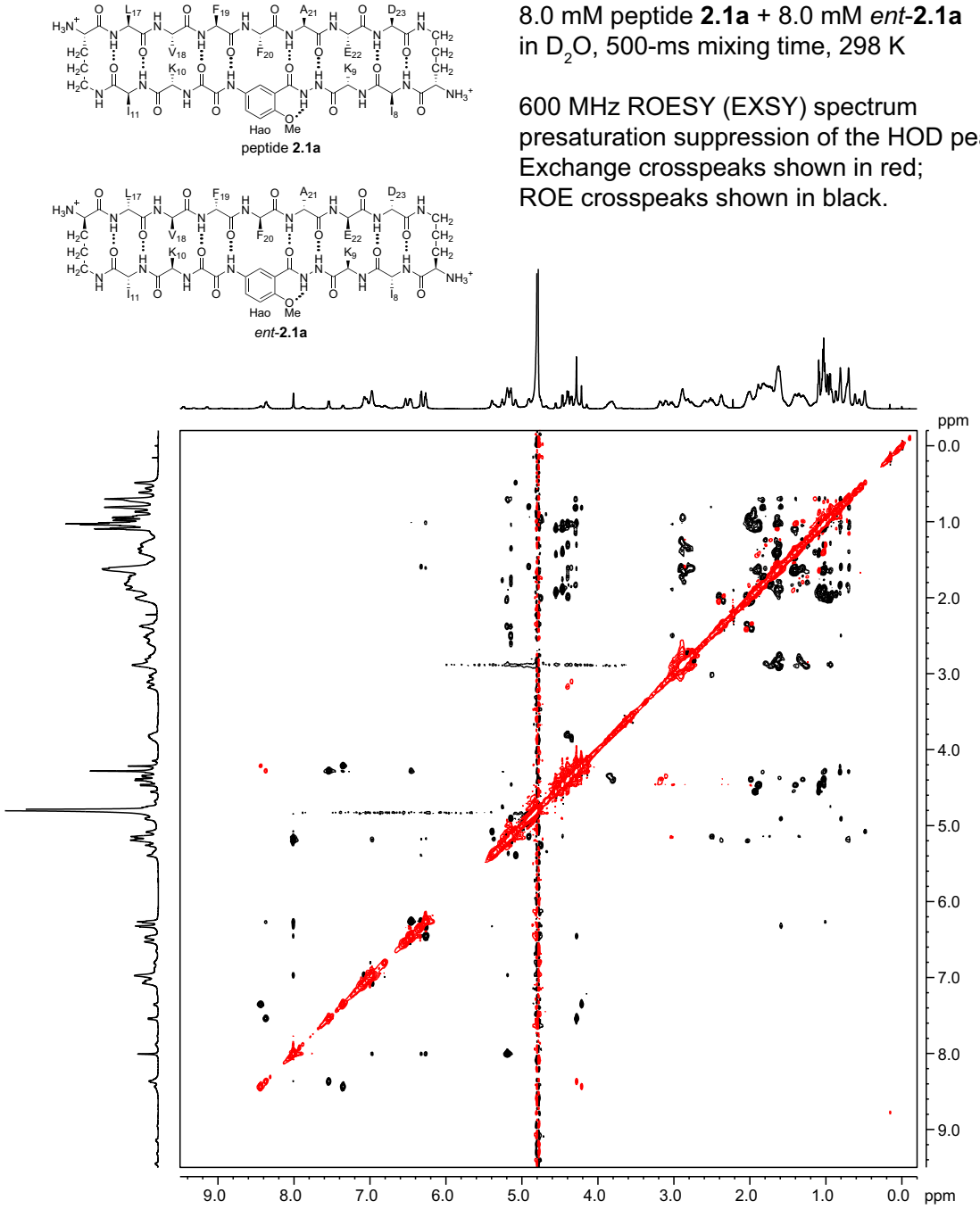

Figure S2.1. 2D ROESY (EXSY) spectrum of 8.0 mM peptide **2.1a** and 8.0 mM peptide *ent*-**2.1a** in D_2O at 600 MHz and 298 K, with 0.06 mM DSA[1]. Residual HOD was suppressed by presaturation of the water peak. A mixing time of 500-ms was used to acquire the spectrum. The two phases of the spectrum are colored with black (ROE crosspeaks) and red (exchange crosspeaks).

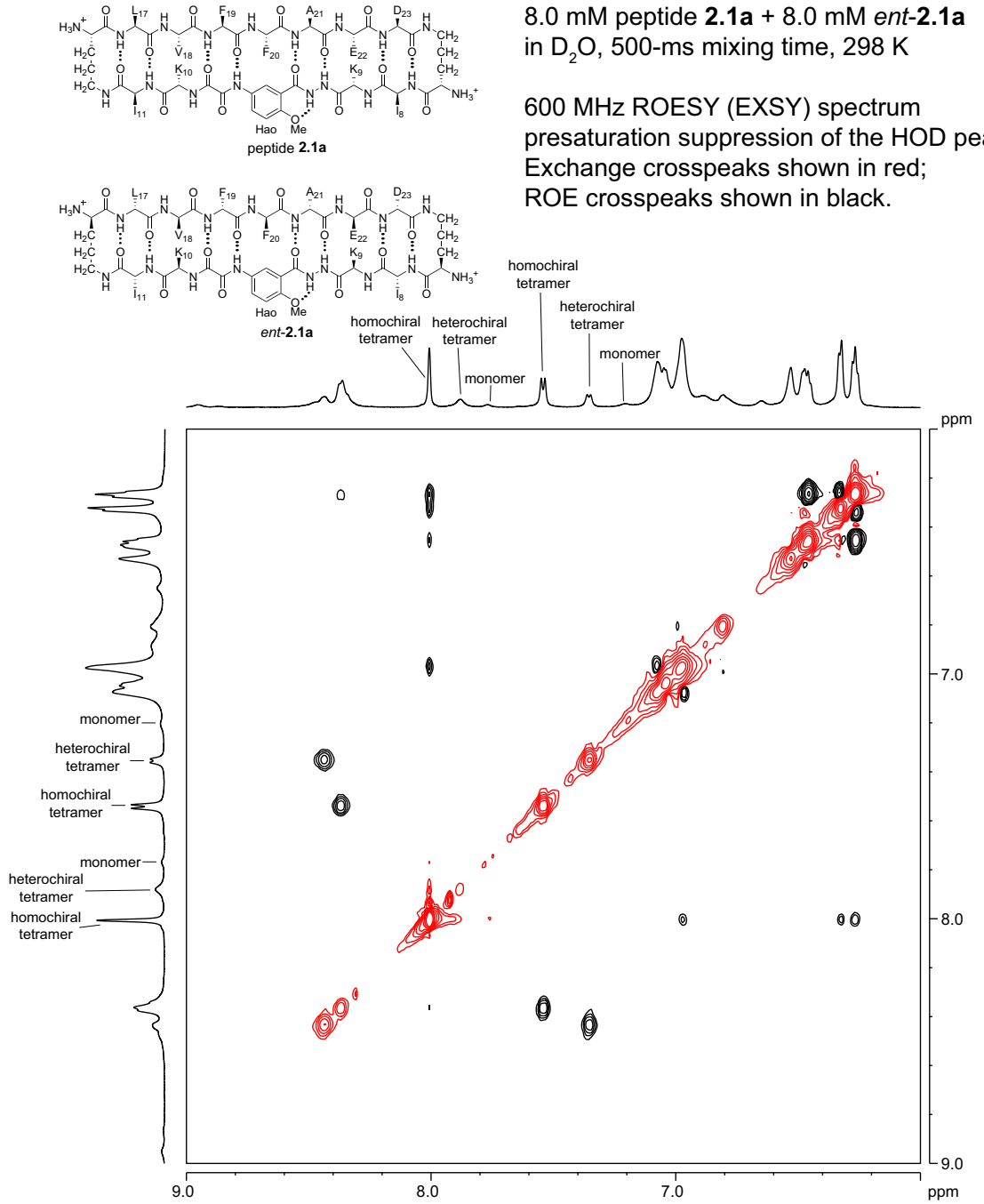

Figure S2.2. Expansion of Figure S2.1. No crosspeaks associated with exchange are observed at 298 K.

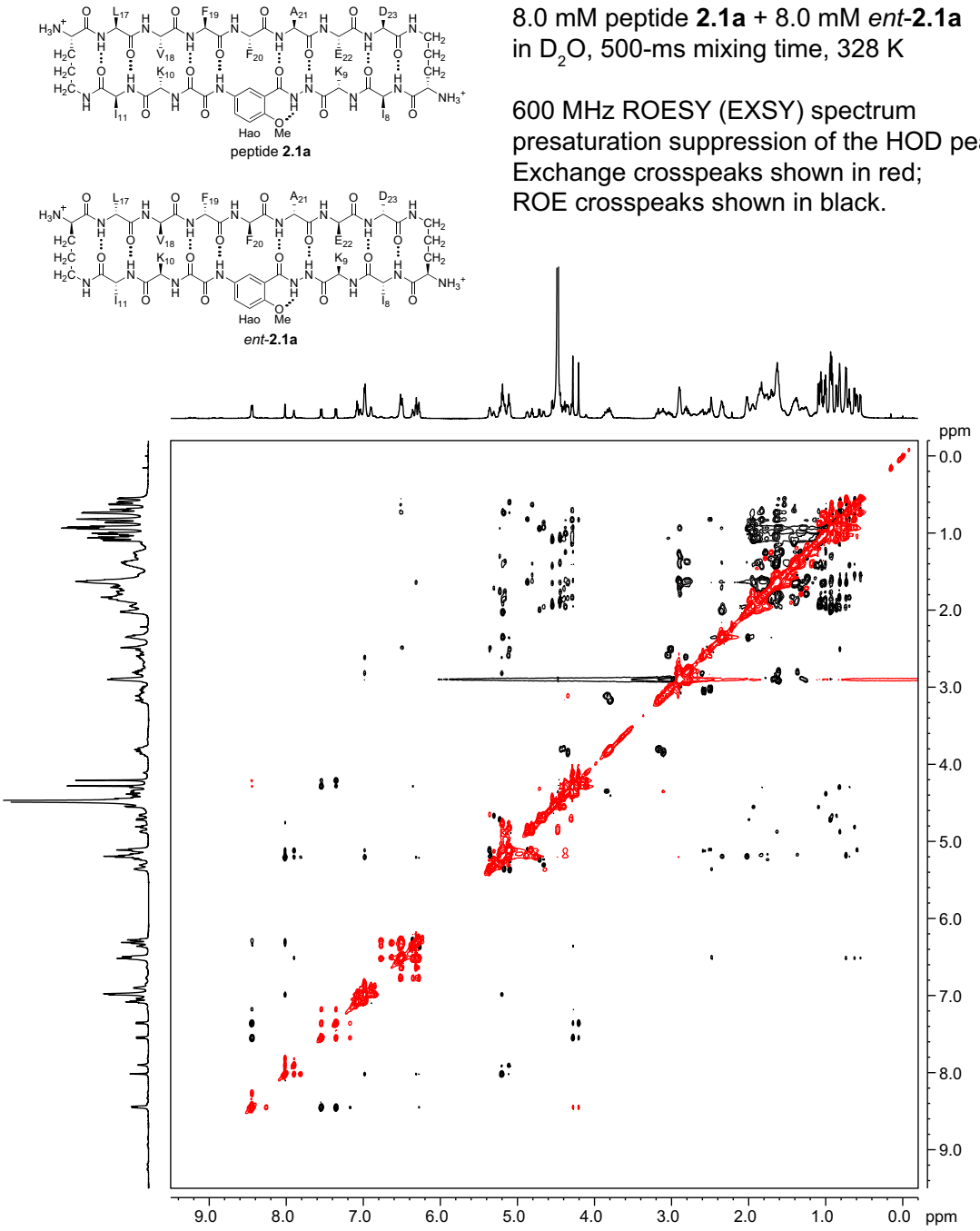

Figure S2.3. 2D ROESY (EXSY) spectrum of 8.0 mM peptide **2.1a** and 8.0 mM peptide *ent*-**2.1a** in D_2O at 600 MHz and 328 K, with 0.06 mM DSA[1]. Residual HOD was suppressed by presaturation of the water peak. A mixing time of 500-ms was used to acquire the spectrum. The two phases of the spectrum are colored with black (ROE crosspeaks) and red (exchange crosspeaks).

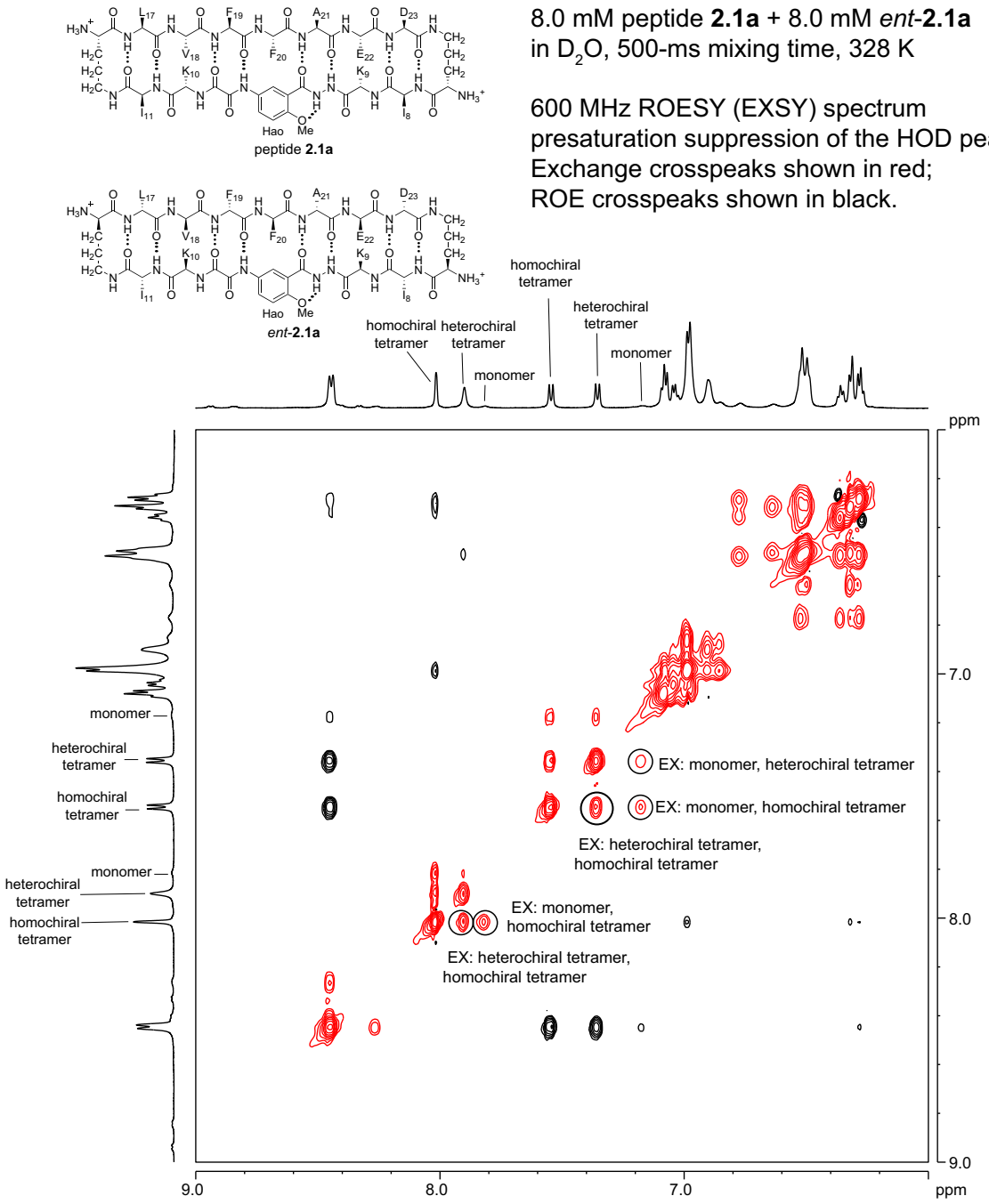

Figure S2.4. Expansion of Figure S2.3. Exchange (EX) between different species is shown with labeled representative crosspeaks.

Table S2.1. Diffusion coefficients (*D*) of peptides 2.1a and *ent*-2.1a in D_2O at 298 K

	MW Monomer (Da)	MW Tetramer (Da)	Concentration (mM)	D ($x10^{-11}$ m^2/s)	Oligomer State
Peptide **2.1a**	1767	7068	8.0	11.6 ± 0.9	homochiral tetramer
Peptides **2.1a** + *ent*-**2.1a**	1767	7068	8.0 + 8.0	10.7 ± 0.7 10.2 ± 0.7	homochiral tetramer heterochiral tetramer

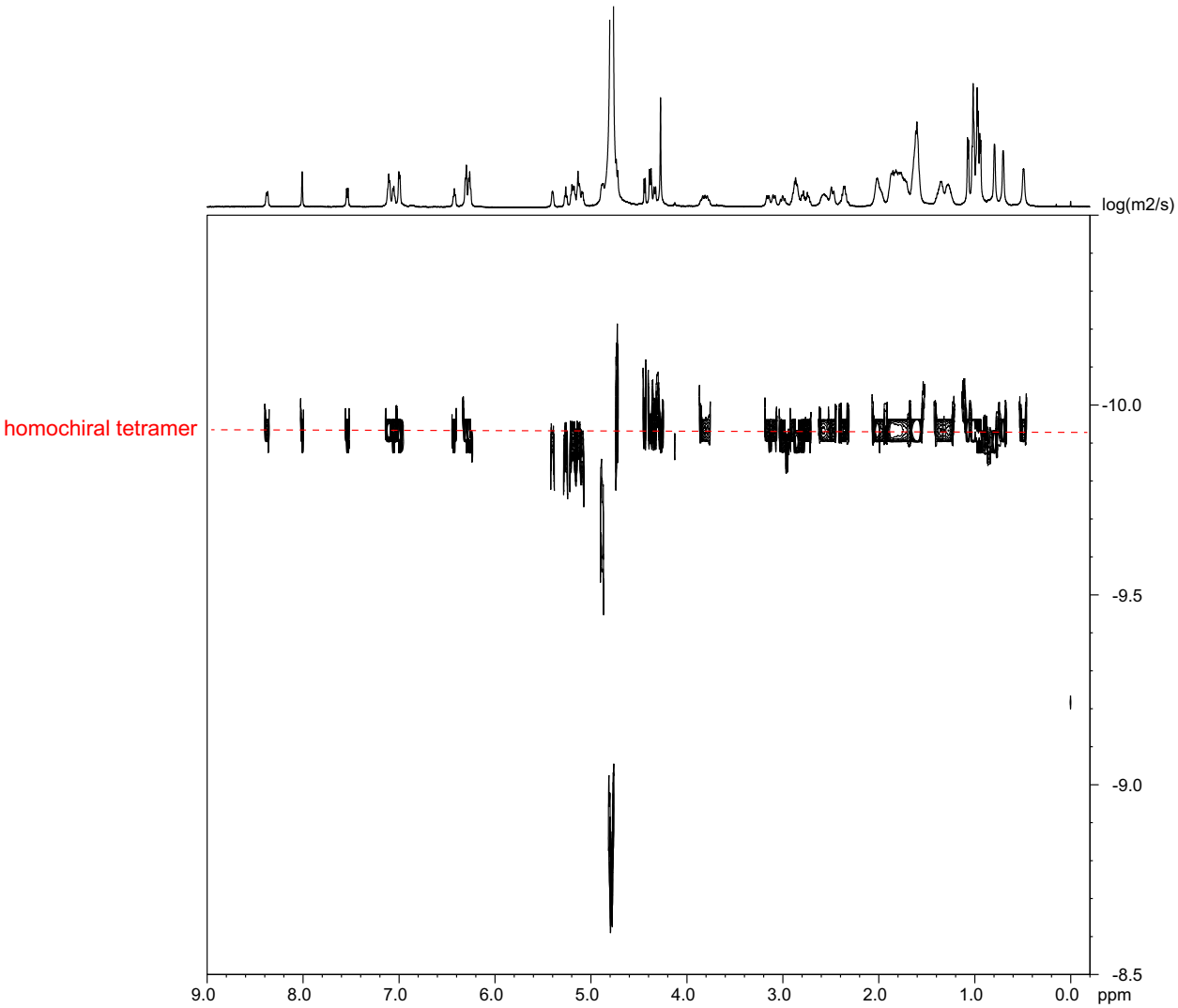

Figure S2.5. DOSY NMR spectrum of 8.0 mM peptide **2.1a** in D_2O at 600 MHz and 298 K with 0.06 mM DSA[1]. The homochiral tetramer (red) shows a diffusion coefficient of 11.6 ± 0.9 x 10^{-11} m^2/s. The HOD peak is calibrated to 19.0 x 10^{-10} m^2/s.[2]

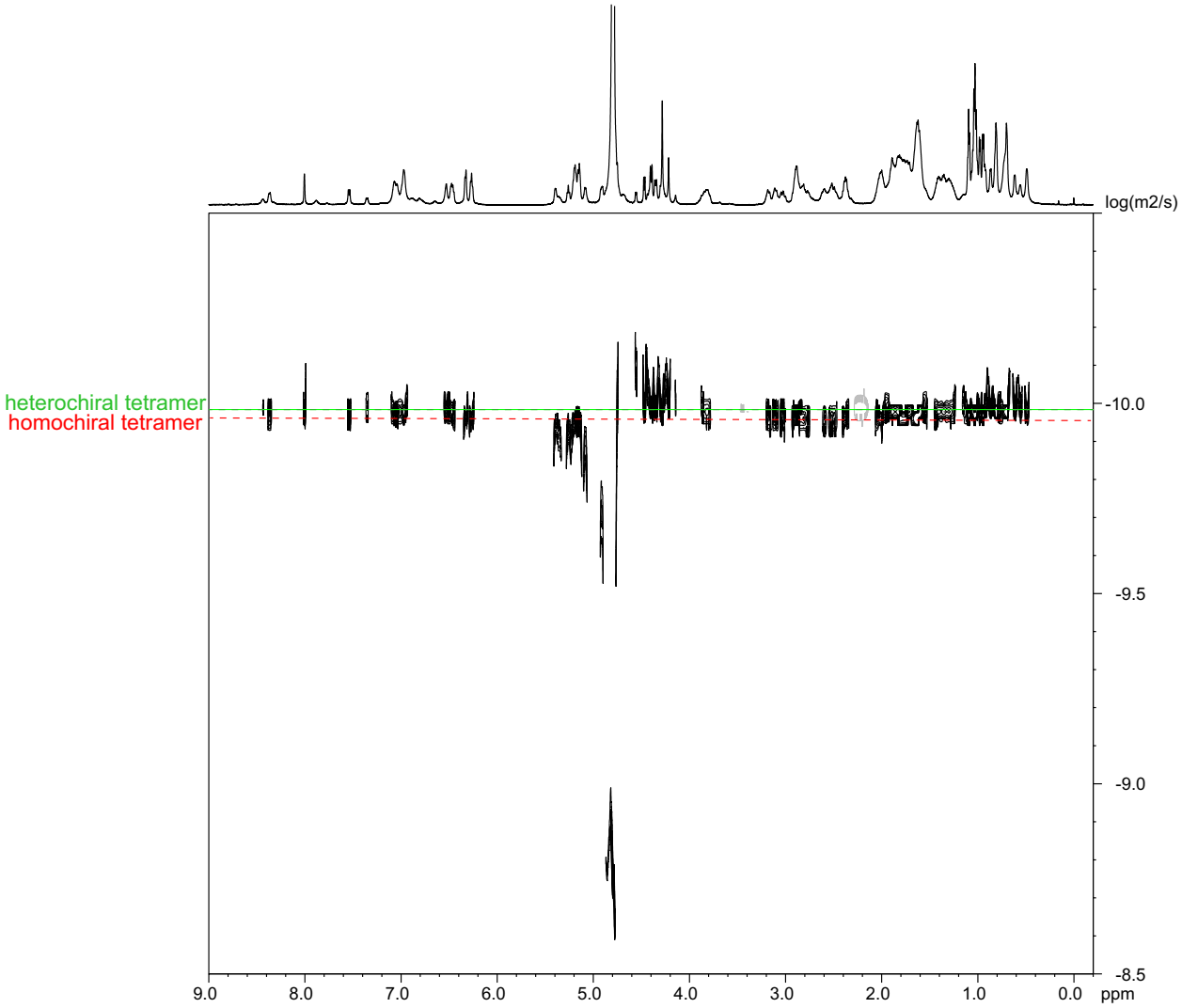

Figure S2.6. DOSY NMR spectrum of 8.0 mM peptide **2.1a** and 8.0 mM peptide *ent*-**2.1a** in D_2O at 600 MHz and 298 K with 0.06 mM DSA[1]. The heterochiral tetramer (green) shows a diffusion coefficient of 10.2 ± 0.7 x 10^{-11} m^2/s. The homochiral tetramer (red) shows a diffusion coefficient of 10.7 ± 0.7 x 10^{-11} m^2/s. The HOD peak is calibrated to 19.0 x 10^{-10} m^2/s.[2]

Table S2.2. Diffusion coefficients (*D*) of peptides 2.1b and *ent*-2.1b in D_2O at 298 K

	MW Monomer (Da)	MW Tetramer (Da)	Concentration (mM)	D ($x10^{-11}$ m^2/s)	Oligomer State
Peptide **2.1b**	1643	6572	1.0	19.5 ± 0.7	monomer
			4.0	17.7 ± 0.6 13.0 ± 0.4	monomer homochiral tetramer
			8.0	15.9 ± 0.7 12.5 ± 0.4	monomer homochiral tetramer
Peptides **2.1b** + *ent*-**2.1b**	1643	6572	4.0 + 4.0	14.4 ± 1.1 10.7 ± 0.8	monomer homochiral tetramer

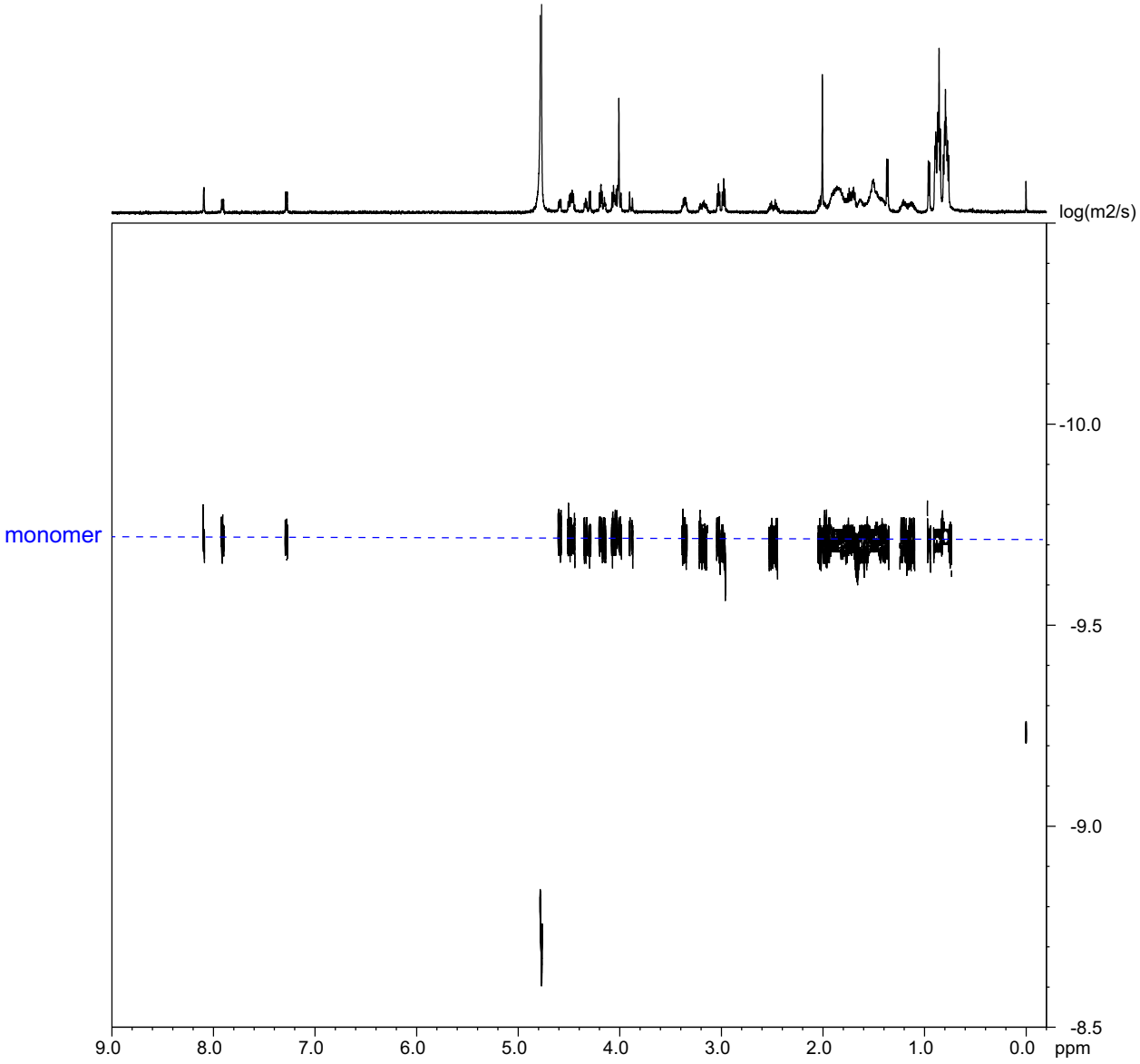

Figure S2.7. DOSY NMR spectrum of 1.0 mM peptide **2.1b** in D_2O at 600 MHz and 298 K with 0.06 mM DSA[1]. The monomer (blue) shows a diffusion coefficient of 19.5 ± 0.7 x 10^{-11} m^2/s. The HOD peak is calibrated to 19.0 x 10^{-10} m^2/s.[2]

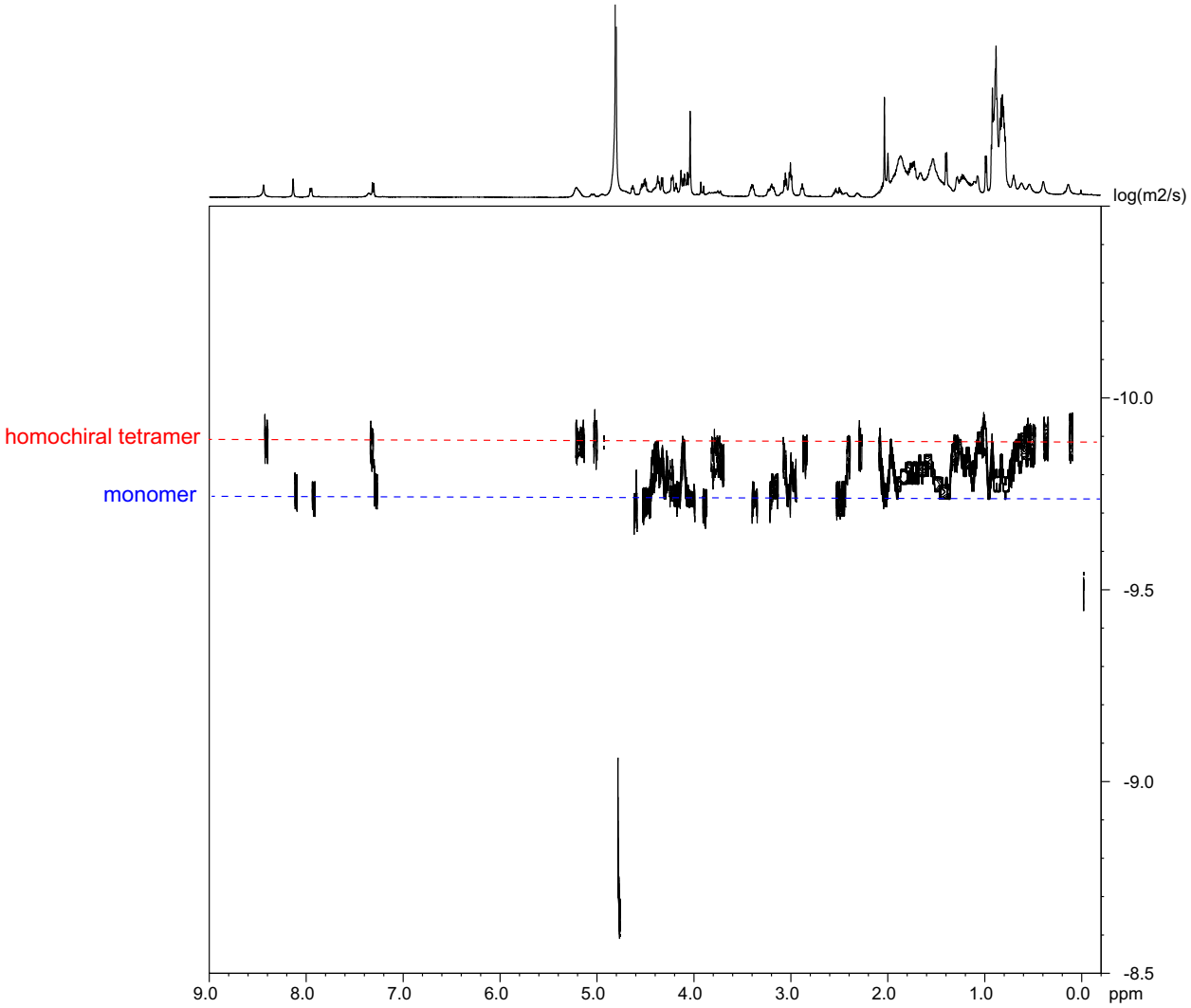

Figure S2.8. DOSY NMR spectrum of 4.0 mM peptide **2.1b** in D_2O at 600 MHz and 298 K with 0.06 mM DSA[1]. The homochiral tetramer (red) shows a diffusion coefficient of 13.0 ± 0.4 x 10^{-11} m^2/s. The monomer (blue) shows a diffusion coefficient of 17.7 ± 0.6 x 10^{-11} m^2/s. The HOD peak is calibrated to 19.0 x 10^{-10} m^2/s.[2]

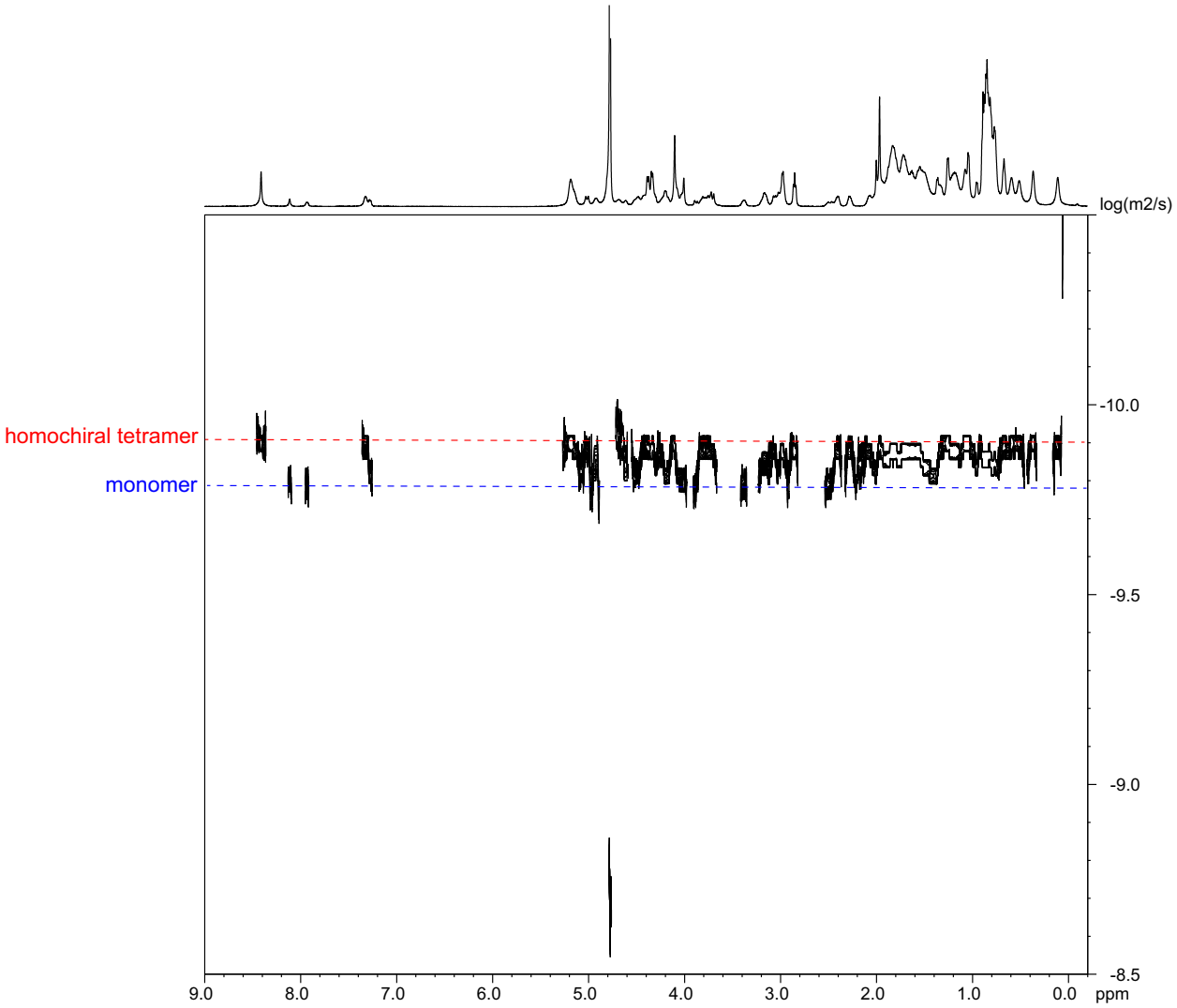

Figure S2.9. DOSY NMR spectrum of 8.0 mM peptide **2.1b** in D_2O at 600 MHz and 298 K with 0.06 mM DSA[1]. The homochiral tetramer (red) shows a diffusion coefficient of 12.5 ± 0.4 x 10^{-11} m^2/s. The monomer (blue) shows a diffusion coefficient of 15.9 ± 0.7 x 10^{-11} m^2/s. The HOD peak is calibrated to 19.0 x 10^{-10} m^2/s.[2]

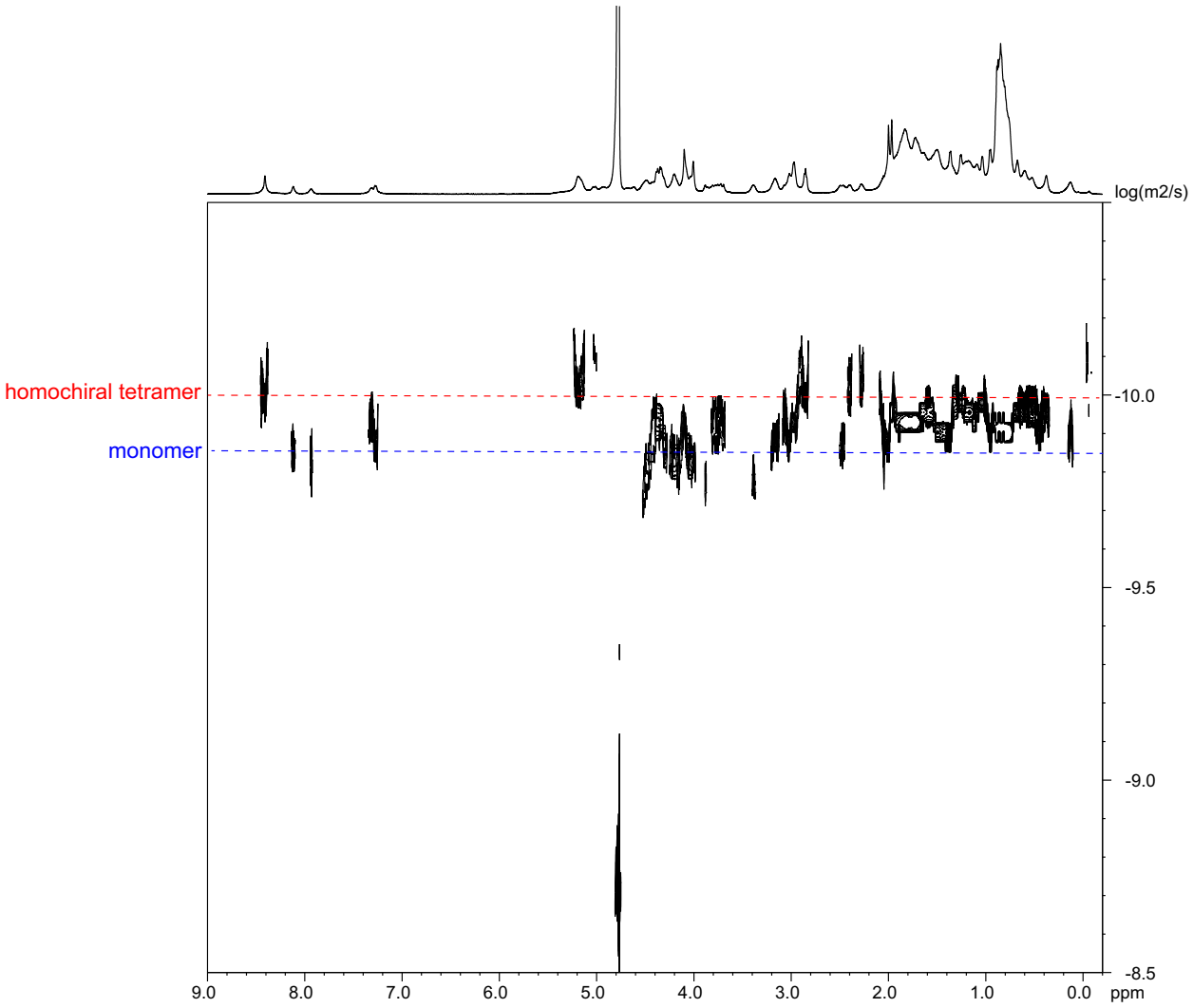

Figure S2.10. DOSY NMR spectrum of 4.0 mM peptide **2.1b** and 4.0 mM peptide *ent*-**2.1b** in D_2O at 600 MHz and 298 K with 0.06 mM DSA[1]. The homochiral tetramer (red) shows a diffusion coefficient of 10.7 ± 0.8 x 10^{-11} m^2/s. The monomer (blue) shows a diffusion coefficient of 14.4 ± 1.1 x 10^{-11} m^2/s. The HOD peak is calibrated to 19.0 x 10^{-10} m^2/s.[2]

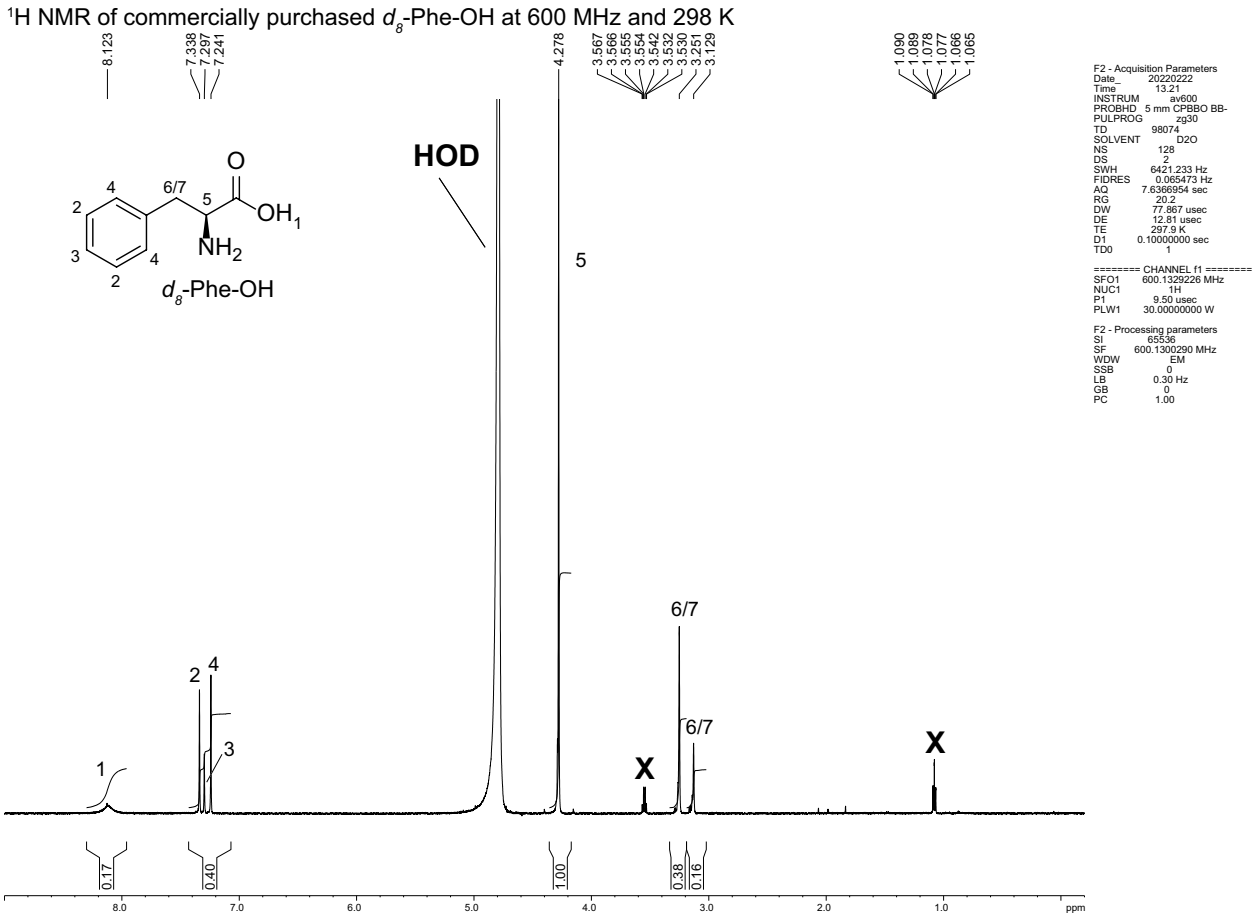

Figure S2.11. ¹H NMR spectrum of deuterated L-phenylalanine (d_8-Phe-OH) used to synthesize peptide **2.3a**. The d_8-Phe-OH was purchased from Cambridge Isotope Laboratories with a reported isotopic purity of 98%. The spectrum was recorded in D_2O with DCl at 600 MHz and 298 K. Incomplete deuterium labeling at the α-position is disproportionately large. Thus, the relative integration of the α-proton is 2.5X that of the aromatic protons and 2X that of the β-protons. If the ¹H isotopic impurity was uniformly distributed, the integration of the α-proton would be 0.2X that of the aromatic protons and 0.5X that of the β-protons.

Synthesis of Peptides

Peptide synthesis procedure. Macrocyclic peptides **2.1a**, **2.1b,** and homologues were synthesized by manual solid-phase peptide synthesis of the corresponding linear peptide on 2-chlorotrityl resin, followed by solution-phase cyclization, deprotection, and purification. A step-by-step procedure is detailed below.

a. Loading the resin. 2-Chlorotrityl chloride resin (300 mg, 1.07 mmol/g) was added to a Bio-RAD Poly-Prep chromatography column (10 mL). Dry CH_2Cl_2 (8 mL) was used to suspend and swell the resin for 30 min with gentle rocking. After the solution was drained from the resin, a separate solution of N^{α}-Boc-N^{δ}-Fmoc-L-ornithine (Boc-Orn(Fmoc)-OH, 0.7 equiv, 100 mg) in 6% (v/v) 2,4,6-collidine in dry CH_2Cl_2 (8 mL) was added and the suspension was gently rocked for 6–14 h. The solution was then drained and a mixture of CH_2Cl_2/MeOH/*N*,*N*-diisopropylethylamine (DIPEA) (17:2:1, 8 mL) was added immediately. The resin was gently rocked for 1 h, to cap the unreacted 2-chlorotrityl chloride resin sites. The resin was then washed three times with dry CH_2Cl_2 and dried by passing nitrogen through the vessel. This procedure typically yields 0.15–0.20 mmol of loaded resin, as assessed by spectrophotometric analysis.

b. Manual peptide coupling. The loaded resin was suspended in dry DMF and then transferred to a solid-phase peptide synthesis vessel. Each residue was manually coupled using Fmoc-protected amino acid building blocks. The coupling cycle consisted of *i*. Fmoc-deprotection with of 20% (v/v) piperidine in DMF (5 mL) for 5–10 min at room temperature, *ii*. washing with dry DMF (4 x 5 mL), *iii*. coupling of the amino acid (4 equiv) with HCTU (4 equiv) in 20% (v/v) 2,4,6-collidine in dry DMF (5 mL) for 20–30 min, and *iv.* washing with dry DMF (4 x 5 mL). [NOTE: The unnatural amino acid Fmoc-Hao-OH (2.0 equiv) was coupled twice with 2.0 equiv of HCTU per coupling, for 1 h each

to achieve complete coupling.[4]] *v.* After the last amino acid was coupled, and its Fmoc protecting group deprotected, the resin was transferred from the solid-phase peptide synthesis vessel to a new BioRad Poly-Prep chromatography column. The resin was washed with CH_2Cl_2 (3 x 5 mL) and dried by passing nitrogen through the column.

c. *Cleavage of the linear peptide from chlorotrityl resin*. The linear peptide was cleaved from the resin by rocking the resin in a solution of 20% (v/v) 1,1,1,3,3,3-hexafluoroispropanol (HFIP) in CH_2Cl_2 (8 mL) for 1 h. The suspension was filtered, and the filtrate was collected in a 250-mL round-bottomed flask. The resin was washed with additional cleavage solution (8 mL) for 30 min and filtered into the same 250 mL round bottom-bottomed flask. The combined filtrates were concentrated by rotary evaporation and further dried by vacuum pump to afford the crude protected linear peptide, which was cyclized without further purification.

d. *Cyclization of the linear peptide*. The crude protected linear peptide was dissolved in dry DMF (125 mL). PyBOP (6 equiv) were dissolved in 8 mL of dry DMF in a test tube to which 300 μL of 4-methylmorpholine was added and the solution mixed until homogenous. The solution was then added to the round-bottom flask containing the dissolved peptide and the mixture was stirred under nitrogen at room temperature for 48 h. The reaction mixture was concentrated by rotary evaporation and further dried by vacuum pump to afford the crude protected cyclized peptide, which was immediately subjected to global deprotection.

e. Global deprotection of the cyclic peptide. For the preparation of peptides **2.1a,** *ent*-**2.1a**, **2.2a,** and **2.3a**, the protected cyclic peptides were dissolved in TFA:triisopropylsilane (TIPS):H_2O (18:1:1, 10 mL) in a 1000-mL round-bottomed flask equipped with a stir bar. The solution was stirred for 1 h under nitrogen. For the

preparation of peptides **2.1b,** *ent*-**2.1b**, and **2.2b** containing a methionine amino acid, the protected cyclic peptides were dissolved in TFA:triisopropylsilane (TIPS):H_2O (18:1:1, 10 mL) with 350 mgs of ammonium iodide (NH_4I) and ca. 5 mL of dimethyl sulfide (DMS) in a 1000-mL round-bottomed flask equipped with a stir bar. The solution was stirred for 1 h under nitrogen.

During the 1 h deprotection, two 50-mL conical tubes containing 40 mL of dry Et_2O each were chilled on ice. After the 1 h deprotection, the peptide solution was split between the two conical tubes of Et_2O. The tubes were then centrifuged at 600x*g* for 10 min, decanted, and washed with fresh Et_2O. This process of decanting and washing was repeated for two more times. The pelleted peptides were dried under nitrogen for 15–20 min. The deprotected cyclic peptide was then purified by reverse-phase HPLC (RP-HPLC).

f. Reverse-phase HPLC purification. The peptide was dissolved in 20% CH_3CN in H_2O (5 mL) and pre-purified on a Biotage Isolera One flash chromatography instrument equipped with a Biotage® Sfär Bio C18 D - Duo 300 Å 20 µm 25 g column. The solution of crude cyclic peptide was injected at 20% CH_3CN and eluted with a gradient of 20–50% CH_3CN. Fractions containing the desired peptide was concentrated by rotary evaporation, diluted in 20% CH_3CN, injected on a Rainin Dynamax instrument, and eluted over a gradient of 20–50% CH_3CN over 90 min. The collected fractions were analyzed by analytical HPLC and MALDI-TOF, and the pure fractions were concentrated by rotary evaporation and lyophilized. This synthesis typically yielded 40 mgs of peptides **2.1a** and **2.1b** isolated as the TFA salt.

Peptides *ent*-**2.1a**, *ent*-**2.1b**, **2.2a**, **2.2b**, and **2.3a** were synthesized in the same way as peptides **2.1a**.and **2.1b**. Commercially available D-amino acids were used to

synthesize peptides *ent*-**2.1a** and *ent*-**2.1b**. Fmoc-protected ^{15}N L-phenylalanine replaced Phe_{20} in the preparation of labeled peptide **2.2a**. Fmoc-protected ^{15}N glycine replaced Gly_{33} in the preparation of labeled peptide **2.2b**. Fmoc-protected deuterated L-phenylalanine, ^{15}N L-phenylalanine, and deuterated L-alanine replaced Phe_{19}, Phe_{20}, and Ala_{21} in the preparation of labeled peptide **2.3a**. The syntheses typically yielded 20–40 mgs of each peptide as the TFA salt.

Fmoc-Protection of ^{15}N-Labeled and Deuterated Amino Acid[3]

Fmoc-protected ^{15}N-labeled phenylalanine and Fmoc-protected ^{15}N-labeled glycine were prepared as previously reported.[3] Fmoc-protected deuterated L-phenylalanine and deuterated L-alanine were prepared in a similar fashion, as described below:

Fmoc-d_4-Ala-OH: A 100-mL one-neck round-bottom flask equipped with a magnetic stirring bar was charged with deuterated alanine (0.40 g, 4.3 mmol) and a solution of 1:1 CH_3CN/H_2O (25 mL). Et_3N (610 µL, 4.3 mmol) and Fmoc-OSu (1.32 g, 3.9 mmol) were added, then the reaction mixture was stirred for 10 minutes, and additional Et_3N was added until a clear solution formed (pH ca. 8.9). The mixture was stirred for 1 h. After the 1 h stir, the mixture was poured into a solution of 1.0 M HCl (200 mL) in a 400-mL beaker while stirring vigorously. The Fmoc-d_4-Ala-OH precipitated from the solution and the solid was isolated by filtering the mixture through a sintered glass filter funnel with a medium frit. The funnel was covered with a piece of filter paper and the solid was dried by aspirating air through the funnel. The solid was suspended in ca. 100 mL of EtOAc to form a turbid solution. The solution was stirred vigorously for 10 min, dried over $MgSO_4$, filtered, and then concentrated under vacuum to give a white solid. The isolated solid was ground into a fine powder to give ca. 1.13 g (83%) of Fmoc-d_4-

Ala-OH. A sample was re-dissolved in acetone, concentrated by rotary evaporation, dried under vacuum overnight, and evaluated by NMR spectroscopy. ^{1}H NMR (600 MHz, $CDCl_3$): δ 7.76 (d, J = 7.4 Hz, 2H), 7.59 (t, J = 6.3 Hz, 1.56H), 7.55 (bs, 0.44H), 7.40 (t, J = 7.4 Hz, 2H), 7.31 (t, J = 7.5 Hz, 2H), 6.25–5.46 (bs, 1H), 4.51 (m, 0.51H), 4.42 (m, 1.52H), 4.23 (appar t, J = 6.8 Hz, 1H). ^{13}C NMR (125 MHz, $CDCl_3$) δ 177.4, 156.0, 143.9, 143.8, 141.5, 127.9, 127.2, 125.2, 125.2, 124.9 (minor rotamer), 120.1, 67.7 (minor rotamer), 67.3, 49.1, 47.2, 17.7.

Fmoc-d_8-Phe-OH: A 100-mL one-neck round-bottom flask equipped with a magnetic stirring bar was charged with deuterated phenylalanine (0.49 g, 2.8 mmol) and a solution of 1:1 CH_3CN/H_2O (25 mL). Et_3N (390 μL, 2.8 mmol) and Fmoc-OSu (0.83 g, 2.6 mmol) were added, then the reaction mixture was stirred for 10 minutes, and additional Et_3N was added until a clear solution formed (pH ca. 8.7). The mixture was stirred for 1 h. After the 1 h stir, the mixture was poured into a solution of 1.0 M HCl (200 mL) in a 400-mL beaker while stirring vigorously. The Fmoc-d_8-Phe-OH precipitated from the solution and the solid was isolated by filtering the mixture through a sintered glass filter funnel with a medium frit. The funnel was covered with a piece of filter paper and the solid was dried by aspirating air through the funnel. The solid was suspended in ca. 100 mL of EtOAc to form a turbid solution. The solution was stirred vigorously for 10 min, dried over $MgSO_4$, filtered, and then concentrated under vacuum to give a white solid. The isolated solid was ground into a fine powder to give ca. 0.86 g (77%) of Fmoc-d_8-Phe-OH. A sample was re-dissolved in acetone, concentrated by rotary evaporation, dried under vacuum overnight, and evaluated by NMR spectroscopy. ^{1}H NMR (600 MHz, DMSO-d_6): δ 12.71 (bs, 1H), 7.88 (d, J = 7.5 Hz, 2H), 7.73 (s, 1H), 7.64 (dd, J = 12.1 Hz, J = 7.4 Hz, 1.78H), 7.50 (dd, J = 13.1 Hz, J = 7.6 Hz, 0.28H), 7.41 (td, J = 7.4 Hz, J = 4.3 Hz, 2H), 7.30 (dt, J = 17.9 Hz, J = 7.5 Hz, 2H), 4.18 (m,

3H). ^{13}C NMR (125 MHz, DMSO-d_6) δ 173.4, 155.9, 143.8, 140.7, 140.7, 137.7, 128.7, 127.8, 127.6, 127.0, 125.9, 125.3, 125.2, 120.1, 65.6, 55.1, 46.6, 35.6.

NMR Spectroscopy of Unlabeled Peptides

Sample Preparation. NMR spectroscopic studies of peptides **2.1a**, *ent*-**2.1a**, **2.1b**, and *ent*-**2.1b** were performed in D_2O. The solutions were prepared by dissolving a weighed portion of the peptide in the appropriate volume of solvent. The molecular weights of the peptides were calculated as the TFA salts with all amino groups assumed to be protonated (**2.1a**, M.W. 2224.19; **2.1b**, M.W. 2100.20). 4,4-Dimethyl-4-silapentane-1-ammonium trifluoroacetate (DSA) was added as an internal standard for referencing chemical shifts.[1] The solutions were allowed to stand for at least 24–60 h to allow complete hydrogen to deuterium exchange of the amide NH protons.

TOCSY, NOESY, and ROESY Data Collection. NMR spectra were recorded on a Bruker 600 MHz spectrometer with a Bruker CBBFO helium-cooled cryoprobe. Presaturation water suppression was applied as needed. TOCSY spectra were recorded with 2048 points in the *f*2 dimension and either 512 or 256 increments in the *f*1 dimension with NS = 8 and a 150-ms spin-lock mixing time. NOESY spectra were recorded with 2048 points in the *f*2 dimension and 512 increments in the *f*1 dimension with NS = 16 and a 200-ms mixing time. EXSY (ROESY) spectra were recorded with 2048 points in the *f*2 dimension and 256 increments in the *f*1 dimension with NS = 16 and a 500-ms mixing time.

TOCSY, NOESY, and ROESY Data Processing. NMR spectra were processed with Bruker TopSpin software. Automatic baseline correction was applied in both dimensions after phasing the spectra. 2D TOCSY, NOESY, and ROESY spectra were

Fourier transformed to a final matrix size of 1024 x 1024 real points using a Qsine weighting function and forward linear prediction in the *f*1 dimension.

Diffusion-Ordered Spectroscopy (DOSY) Experiments. DOSY experiments were performed on a Bruker 600 MHz spectrometer equipped with a Bruker CBBFO helium-cooled cryoprobe, with a diffusion delay (Δ) of 75-ms and a diffusion gradient length (δ) of 2.5-ms. Sixteen sets of FIDs were recorded with the gradient strength incremented from 5%–95% using a linear ramp. The combined FIDs were Fourier transformed in Bruker's TopSpin software to give a pseudo-2D spectrum. After phasing and performing baseline correction, each pseudo-2D spectrum was processed with logarithmic scaling on the Y-axis. The Y-axis was calibrated to the diffusion coefficient of the residual HOD peak in D_2O (1.9×10^{-9} m^2/s at 298 K).[2] The diffusion coefficients of the peptides were read and converted from logarithmic values to linear values.

NMR Spectroscopy of ^{15}N-Labeled Peptides

Sample Preparation. NMR spectroscopic studies of peptides **2.2a**, **2.3a**, and **2.2b** were performed in 9:1 H_2O/D_2O. The solutions were prepared by dissolving a weighed portion of the peptide in the appropriate volume of solvent. The molecular weights of the peptides were calculated as the TFA salts with all amino groups assumed to be protonated (**2.2a**, M.W. 2225.18; **2.3a**, M.W. 2236.25; **2.2b** M.W. 2101.19). 4,4-Dimethyl-4-silapentane-1-ammonium trifluoroacetate (DSA) was added as an internal standard for referencing chemical shifts.[1]

^{1}H,^{15}N HSQC, and ^{1}H,^{15}N NOESY-HSQC (^{15}N-edited NOESY) Data Collection. NMR spectra were recorded on a Bruker AVANCE 500 MHz spectrometer with Bruker TCI

helium-cooled cryoprobe. Gradient water suppression was applied as needed. ^{1}H,^{15}N HSQC spectra were generally recorded with 2048 points in the *f*2 dimension and 512 increments in the *f*1 dimension with NS = 16, but the spectrum of 8.0 mM peptide **2.1a** was taken with 1024 in the *f*1 and with NS = 8. ^{1}H,^{15}N NOESY-HSQC spectra were recorded as follows: Peptide **2.2a**, 250-ms mixing time, 2048 points in the *f*3 dimension (^{1}H), 1 increment in the *f*2 dimension (^{15}N), and 512 increments in the *f*1 dimension (^{1}H). Mixture of peptides **2.2a** and *ent*-**2.1a**, 250-ms mixing time, 4096 points in the *f*3 dimension (^{1}H), 1 increment in the *f*2 dimension (^{15}N), and 1024 increments in the *f*1 dimension (^{1}H). Peptide **2.3a**, 250-ms mixing time, 2048 points in the *f*3 dimension (^{1}H), 1 increment in the *f*2 dimension (^{15}N), and 512 increments in the *f*1 dimension (^{1}H). Mixture of peptides **2.3a** and *ent*-**2.1a**, 250-ms mixing time, 2048 points in the *f*3 dimension (^{1}H), 1 increment in the *f*2 dimension (^{15}N), and 512 increments in the *f*1 dimension (^{1}H).

^{1}H,^{15}N HSQC, and ^{1}H,^{15}N NOESY-HSQC (^{15}N-edited NOESY) Data Processing. NMR spectra were Fourier transformed in Bruker TopSpin software. Automatic baseline correction was applied in both dimensions after phasing the spectra. The ^{1}H,^{15}N HSQC spectra were processed to a final matrix size of 2048 x 512 real points with GB = 0.1 in both *f* dimensions using a Qsine weighting function, and forward linear prediction in the *f*1 dimension. The ^{1}H,^{15}N NOESY-HSQC spectra were processed to a final matrix size of 4096 x 2048 real points (*f*3, *f*1) with GB = 0.05 in both dimensions, using a Qsine weighting function and forward linear prediction in the *f*1 dimension.

References

[1] Nowick, J. S.; Khakshoor, O.; Hashemzadeh, M.; Brower, J. O. *Org. Lett*. **2003**, *5*, 3511–3513.

[2] Longsworth, L. G. *J. Phys. Chem*. **1960**, *64*, 1914–1917.

[3] The general information and instrumentations follow closely to those that our laboratory has previously published. The procedures in this section are adapted from and in some cases taken verbatim from: Truex, N. L.; Wang, Y.; Nowick, J. S. *J. Am. Chem. Soc.* **2016**, *138*, 13882–13890.

[4] (a) Nowick, J. S.; Chung, D. M.; Maitra, K.; Maitra, S.; Stigers, K. D.; Sun, Y. *J. Am. Chem. Soc.* **2000**, *122*, 7654–7661. (b) Cheng, P.–N.; Nowick, J. S. *J. Org. Chem*. **2011**, *76*, 3166–3173.

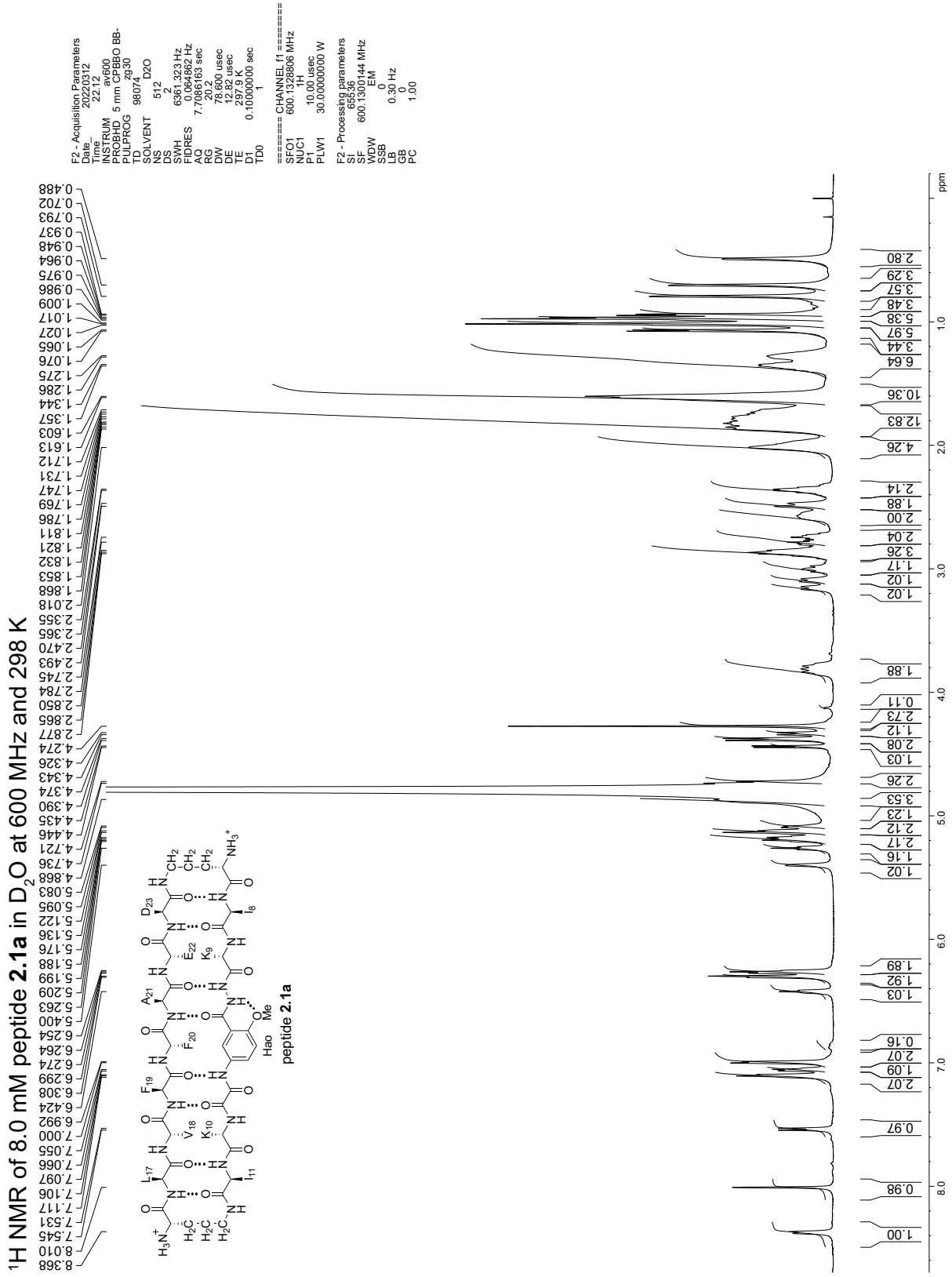
1H NMR of 8.0 mM peptide 2.1a in D2O at 600 MHz and 298 K
peptide 2.1a
F2 - Acquisition Parameters
Date_ 20220312
Time 22.12
INSTRUM av600
PROBHD 5 mm CPBBO BB-
PULPROG zg30
TD 98074
SOLVENT D2O
NS 512
DS 2
SWH 6361.323 Hz
FIDRES 0.064862 Hz
AQ 7.7069163 sec
RG 203
DW 78.600 usec
DE 12.82 usec
TE 297.9 K
D1 0.10000000 sec
TD0 1
======== CHANNEL f1 ========
SFO1 600.1328806 MHz
NUC1 1H
P1 10.00 usec
PLW1 30.00000000 W
F2 - Processing parameters
SI 65536
SF 600.1300144 MHz
WDW EM
SSB 0
LB 0.30 Hz
GB 0
PC 1.00
ppm

^{1}H NMR of 8.0 mM peptide **2.1a** in D_2O at 600 MHz and 298 K

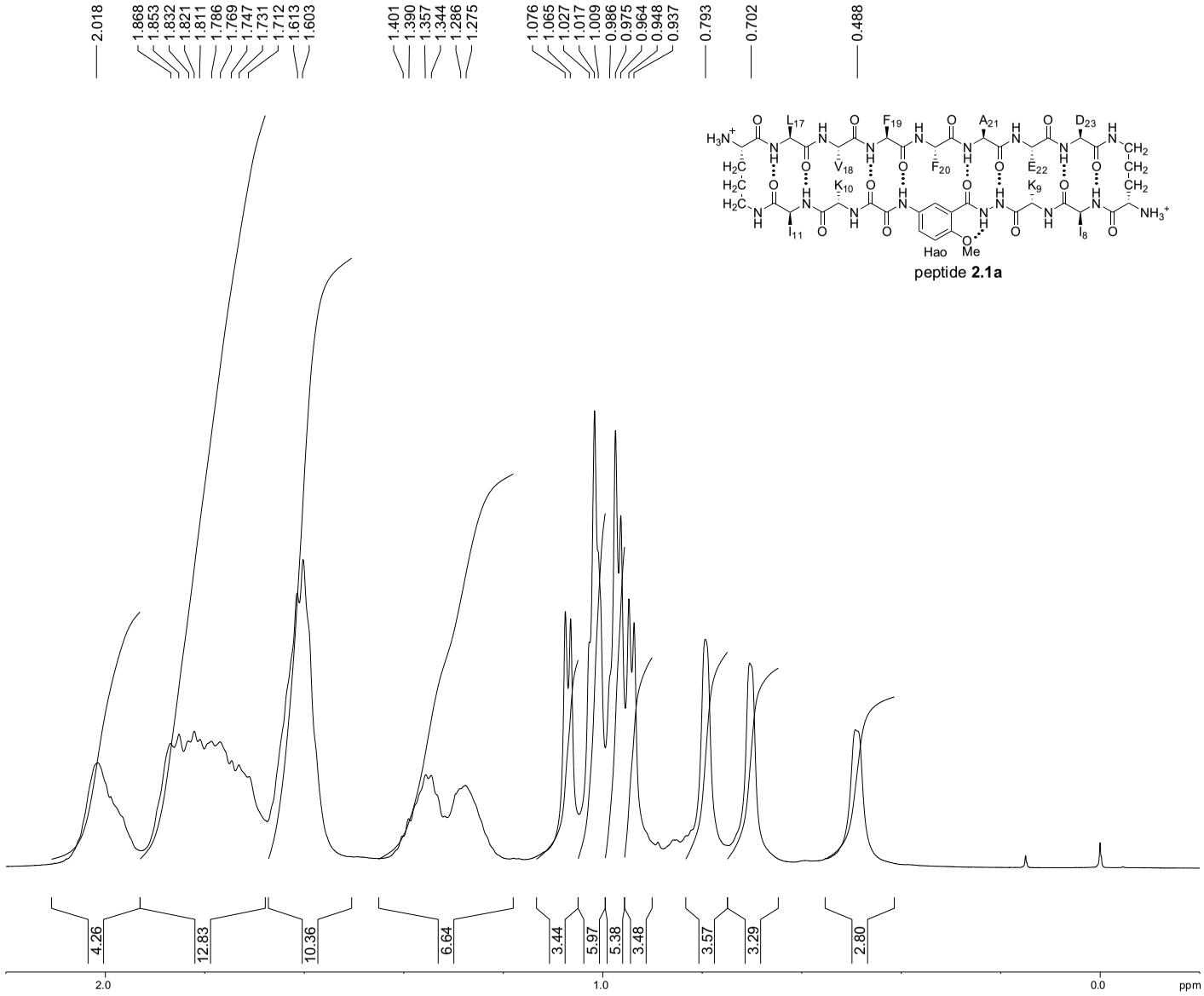

peptide **2.1a**

F2 - Acquisition Parameters
Date_ 20220312
Time 22.12
INSTRUM av600
PROBHD 5 mm CPBBO BB-
PULPROG zg30
TD 98074
SOLVENT D2O
NS 512
DS 2
SWH 6361.323 Hz
FIDRES 0.064862 Hz
AQ 7.7086163 sec
RG 20.2
DW 78.600 usec
DE 12.82 usec
TE 297.9 K
D1 0.10000000 sec
TD0 1

======== CHANNEL f1 ========
SFO1 600.1328806 MHz
NUC1 1H
P1 10.00 usec
PLW1 30.00000000 W

F2 - Processing parameters
SI 65536
SF 600.1300144 MHz
WDW EM
SSB 0
LB 0.30 Hz
GB 0
PC 1.00

^{1}H NMR of 8.0 mM peptide **2.1a** in D_2O at 600 MHz and 298 K

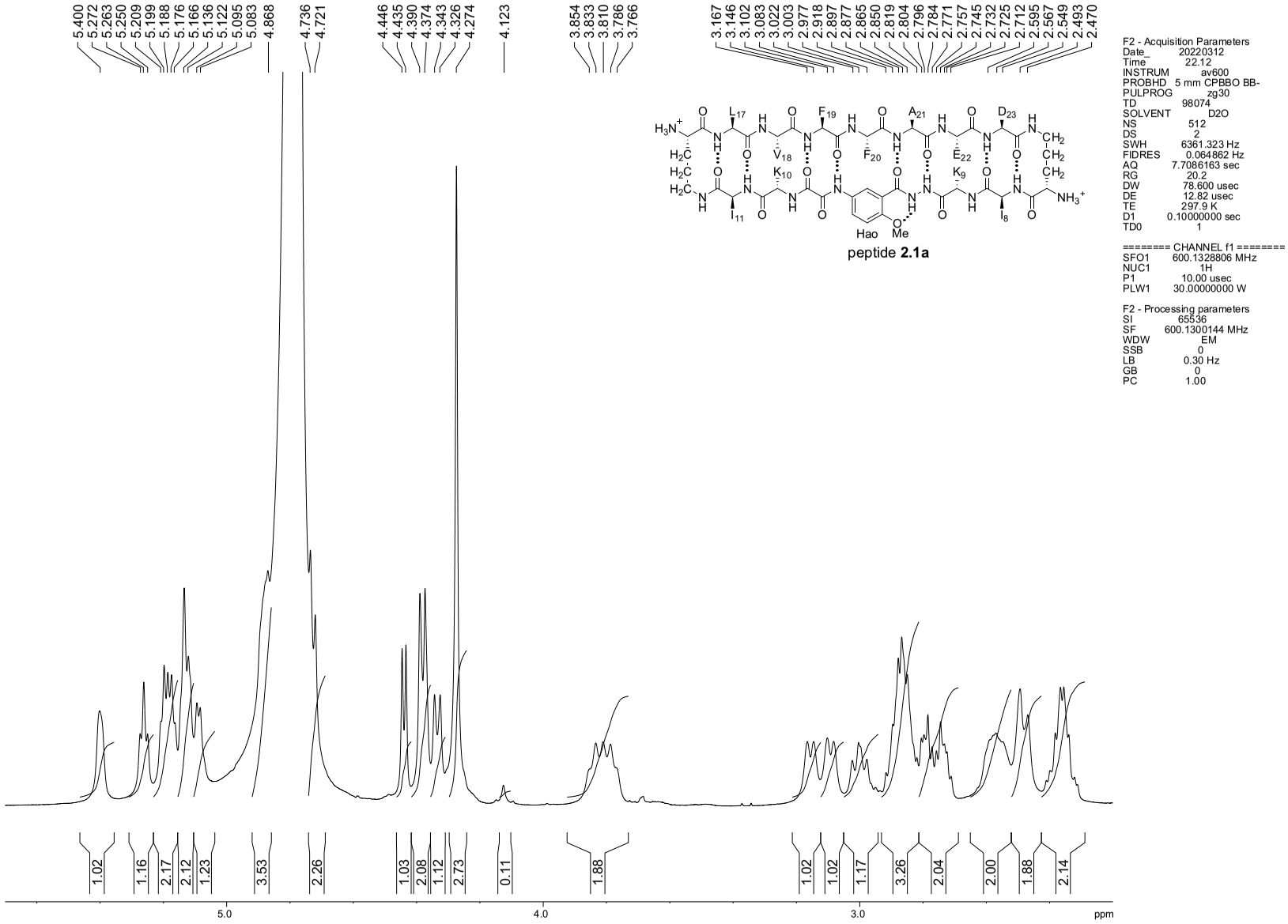

peptide **2.1a**

F2 - Acquisition Parameters
Date_ 20220312
Time 22.12
INSTRUM av600
PROBHD 5 mm CPBBO BB-
PULPROG zg30
TD 98074
SOLVENT D2O
NS 512
DS 2
SWH 6361.323 Hz
FIDRES 0.064862 Hz
AQ 7.7086163 sec
RG 20.2
DW 78.600 usec
DE 12.82 usec
TE 297.9 K
D1 0.10000000 sec
TD0 1

======== CHANNEL f1 ========
SFO1 600.1328806 MHz
NUC1 1H
P1 10.00 usec
PLW1 30.00000000 W

F2 - Processing parameters
SI 65536
SF 600.1300144 MHz
WDW EM
SSB 0
LB 0.30 Hz
GB 0
PC 1.00

^{1}H NMR of 8.0 mM peptide **2.1a** in D_2O at 600 MHz and 298 K

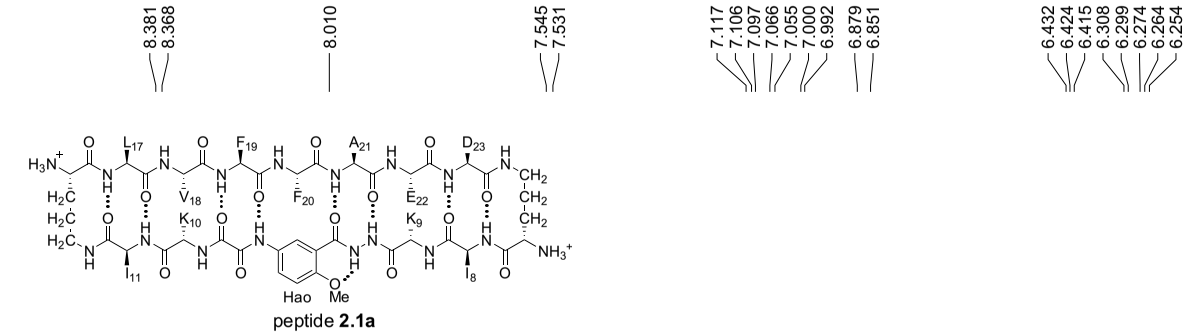

peptide **2.1a**

```
F2 - Acquisition Parameters
Date_          20220312
Time             22.12
INSTRUM          av600
PROBHD   5 mm CPBBO BB-
PULPROG          zg30
TD              98074
SOLVENT           D2O
NS                512
DS                  2
SWH          6361.323 Hz
FIDRES       0.064862 Hz
AQ           7.7086163 sec
RG                20.2
DW             78.600 usec
DE             12.82 usec
TE             297.9 K
D1          0.10000000 sec
TD0                 1

======== CHANNEL f1 ========
SFO1       600.1328806 MHz
NUC1               1H
P1             10.00 usec
PLW1       30.00000000 W

F2 - Processing parameters
SI                65536
SF         600.1300144 MHz
WDW                EM
SSB                 0
LB              0.30 Hz
GB                  0
PC                1.00
```

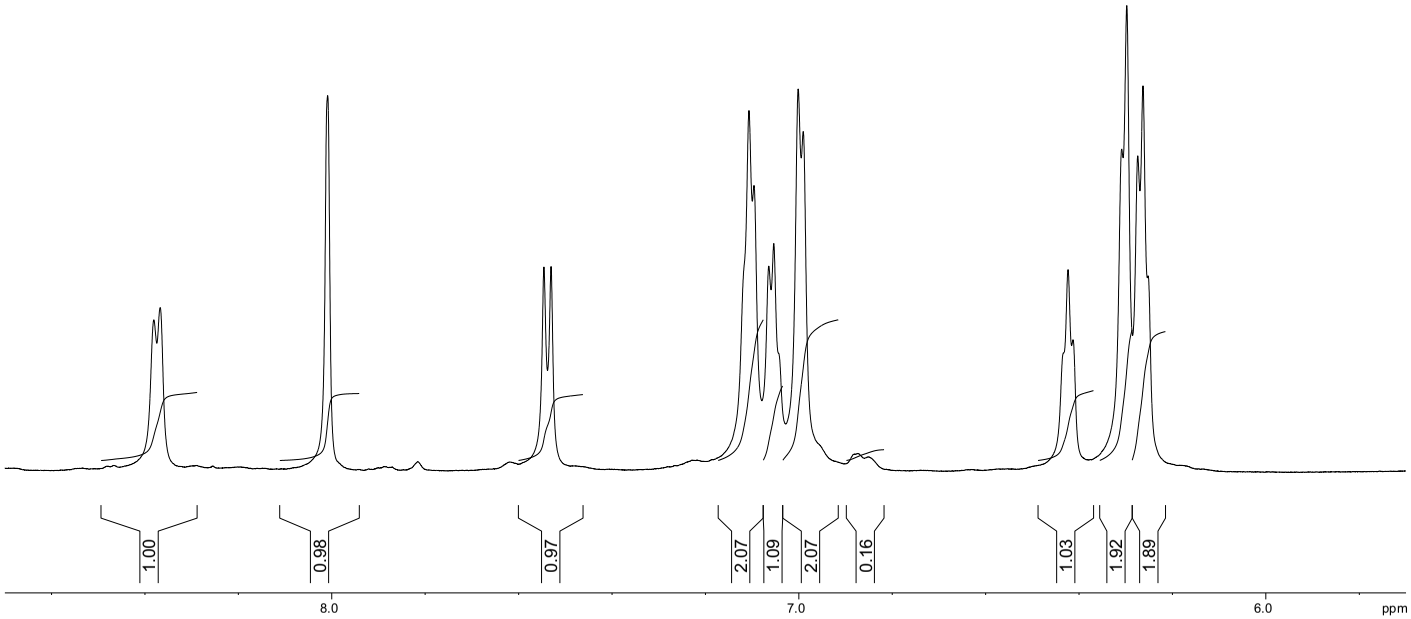

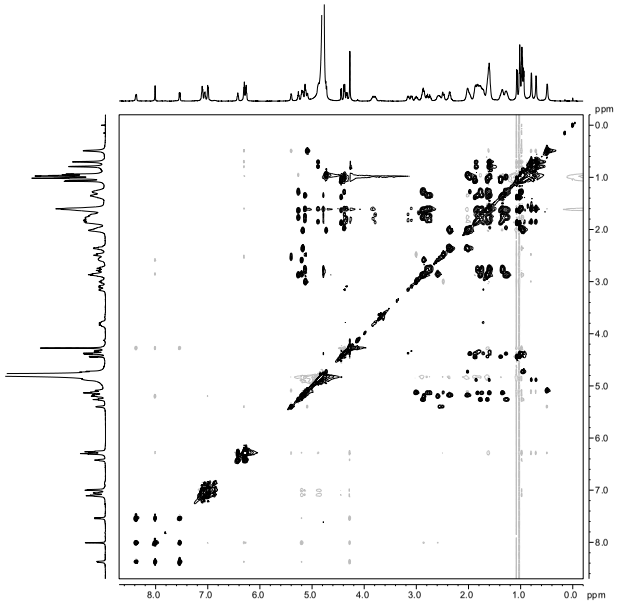

8.0 mM peptide **2.1a**
in D_2O, 150-ms mixing time, 298 K
600 MHz TOCSY spectrum
presaturation suppression of the HOD peak

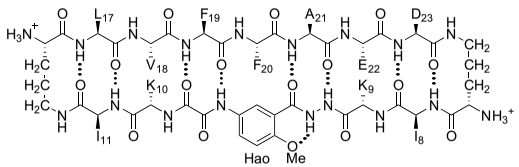

peptide **2.1a**

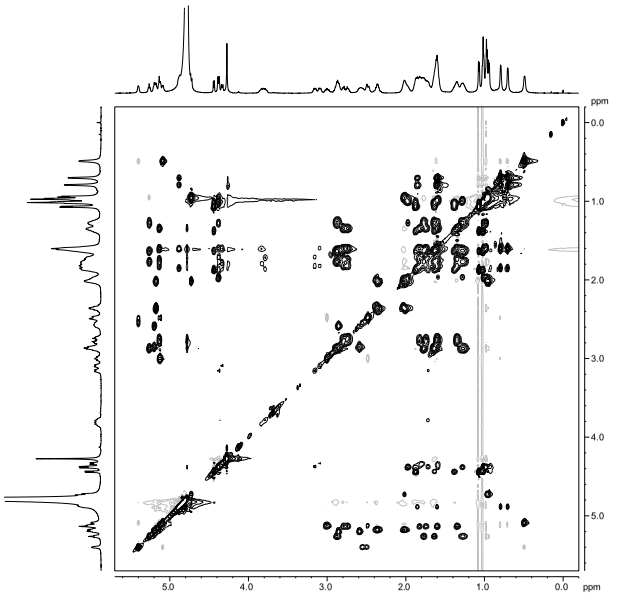

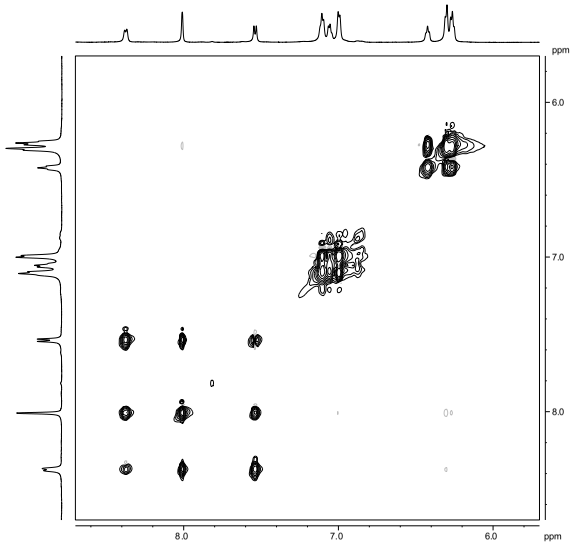

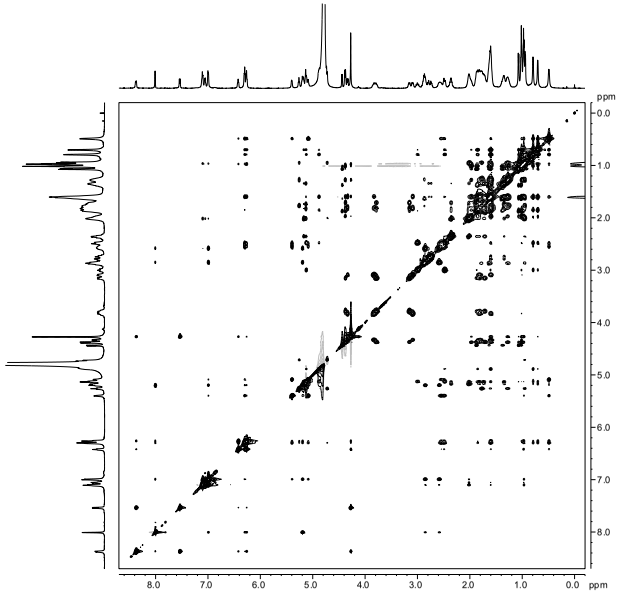

8.0 mM peptide **2.1a**
in D_2O, 200-ms mixing time, 298 K
600 MHz NOESY spectrum
presaturation suppression of the HOD peak

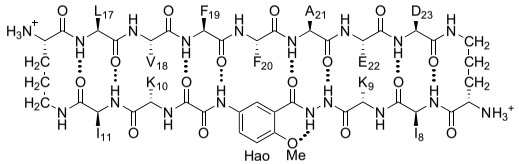

peptide **2.1a**

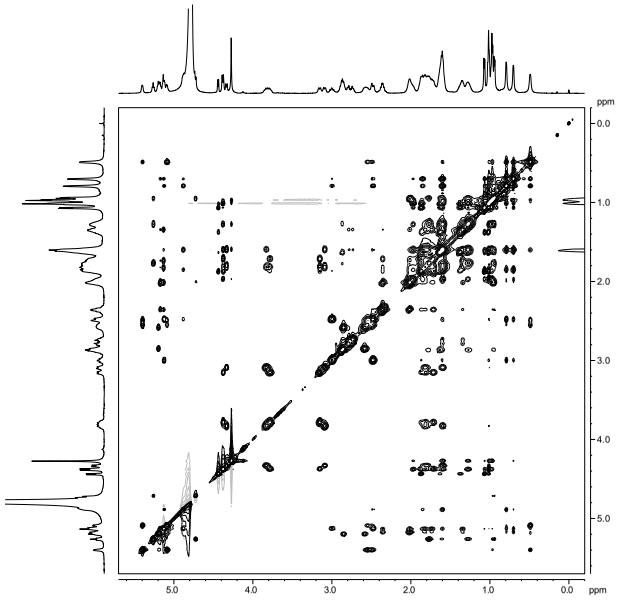

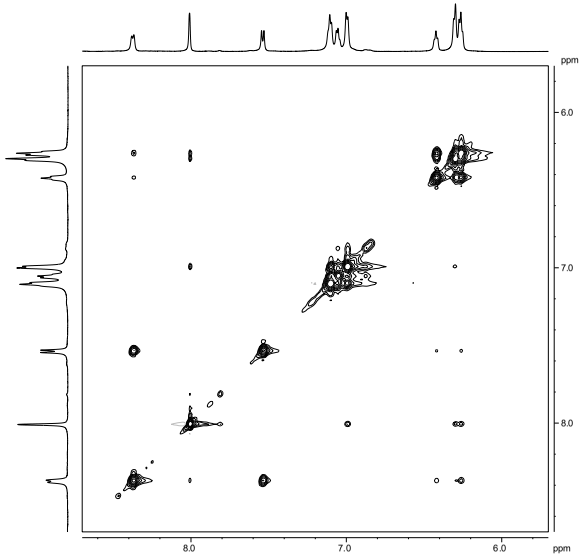

^{1}H NMR of 8.0 mM peptide **2.1a** + 8.0 mM peptide *ent*-**2.1a** in D_2O at 600 MHz and 298 K

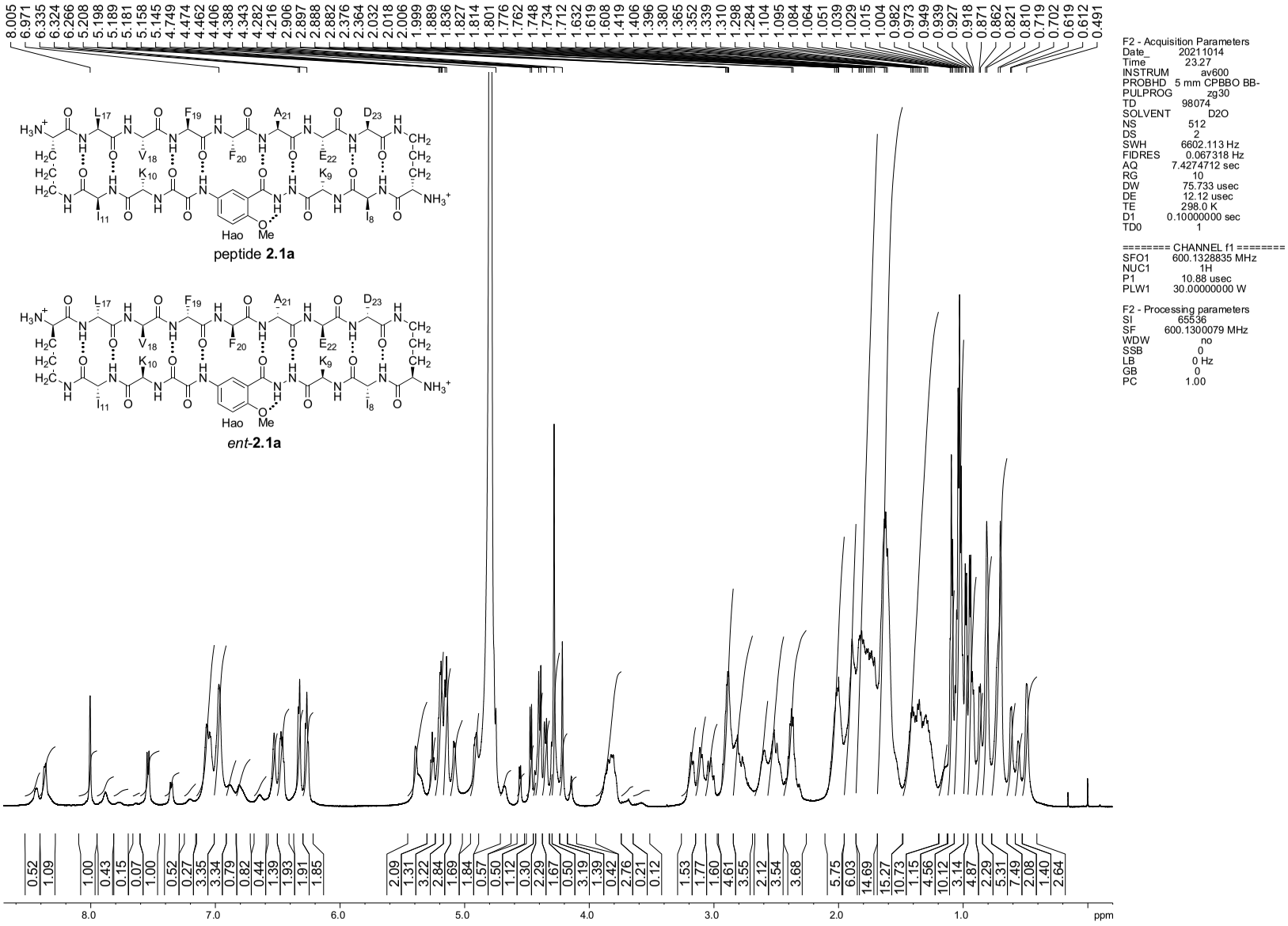

^{1}H NMR of 8.0 mM peptide **2.1a** + 8.0 mM peptide *ent*-**2.1a** in D_2O at 600 MHz and 298 K

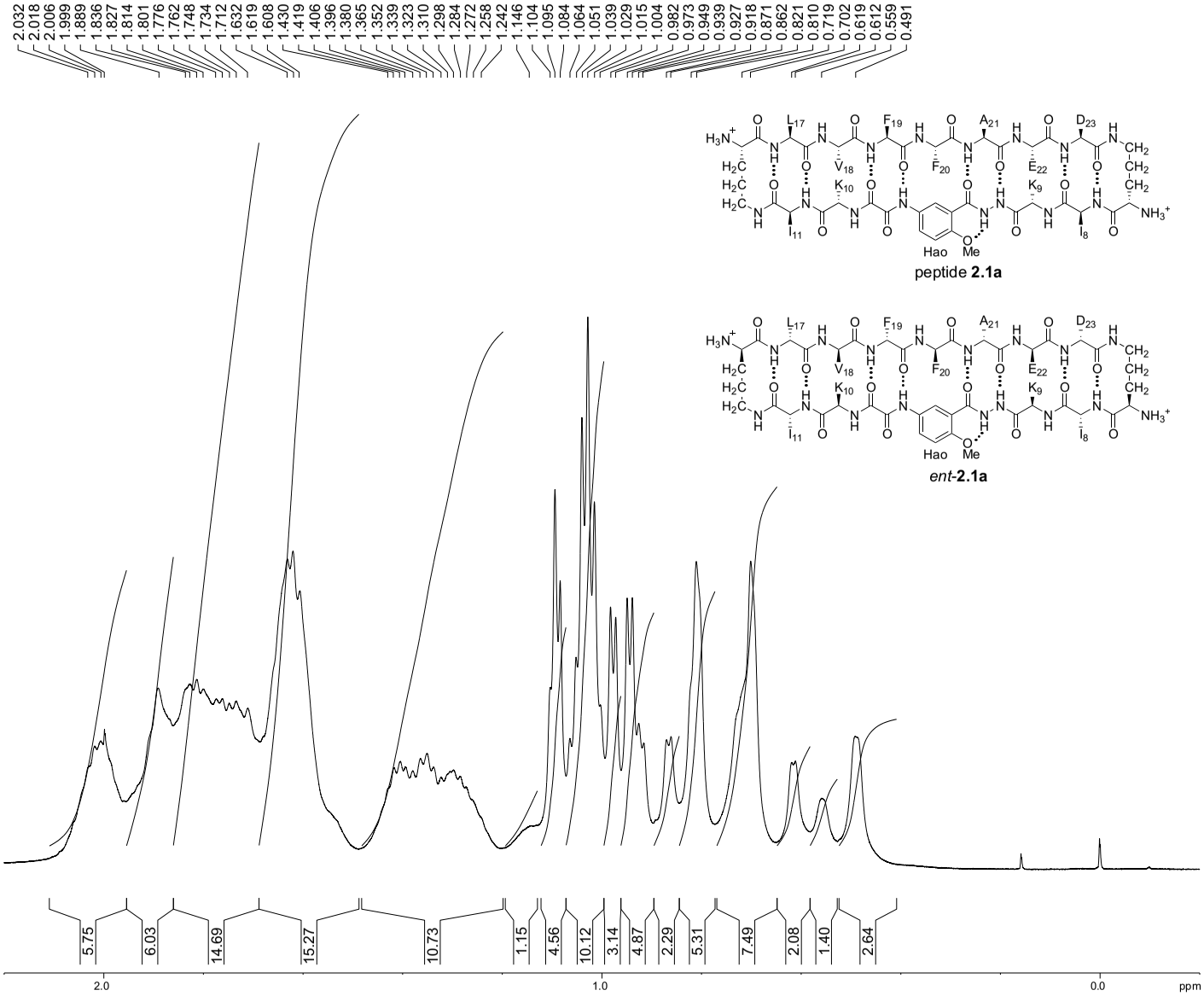

F2 - Acquisition Parameters
Date_ 20211014
Time 23.27
INSTRUM av600
PROBHD 5 mm CPBBO BB-
PULPROG zg30
TD 98074
SOLVENT D2O
NS 512
DS 2
SWH 6602.113 Hz
FIDRES 0.067318 Hz
AQ 7.4274712 sec
RG 10
DW 75.733 usec
DE 12.12 usec
TE 298.0 K
D1 0.10000000 sec
TD0 1

======== CHANNEL f1 ========
SFO1 600.1328835 MHz
NUC1 1H
P1 10.88 usec
PLW1 30.00000000 W

F2 - Processing parameters
SI 65536
SF 600.1300079 MHz
WDW no
SSB 0
LB 0 Hz
GB 0
PC 1.00

^{1}H NMR of 8.0 mM peptide **2.1a** + 8.0 mM peptide *ent*-**2.1a** in D_2O at 600 MHz and 298 K

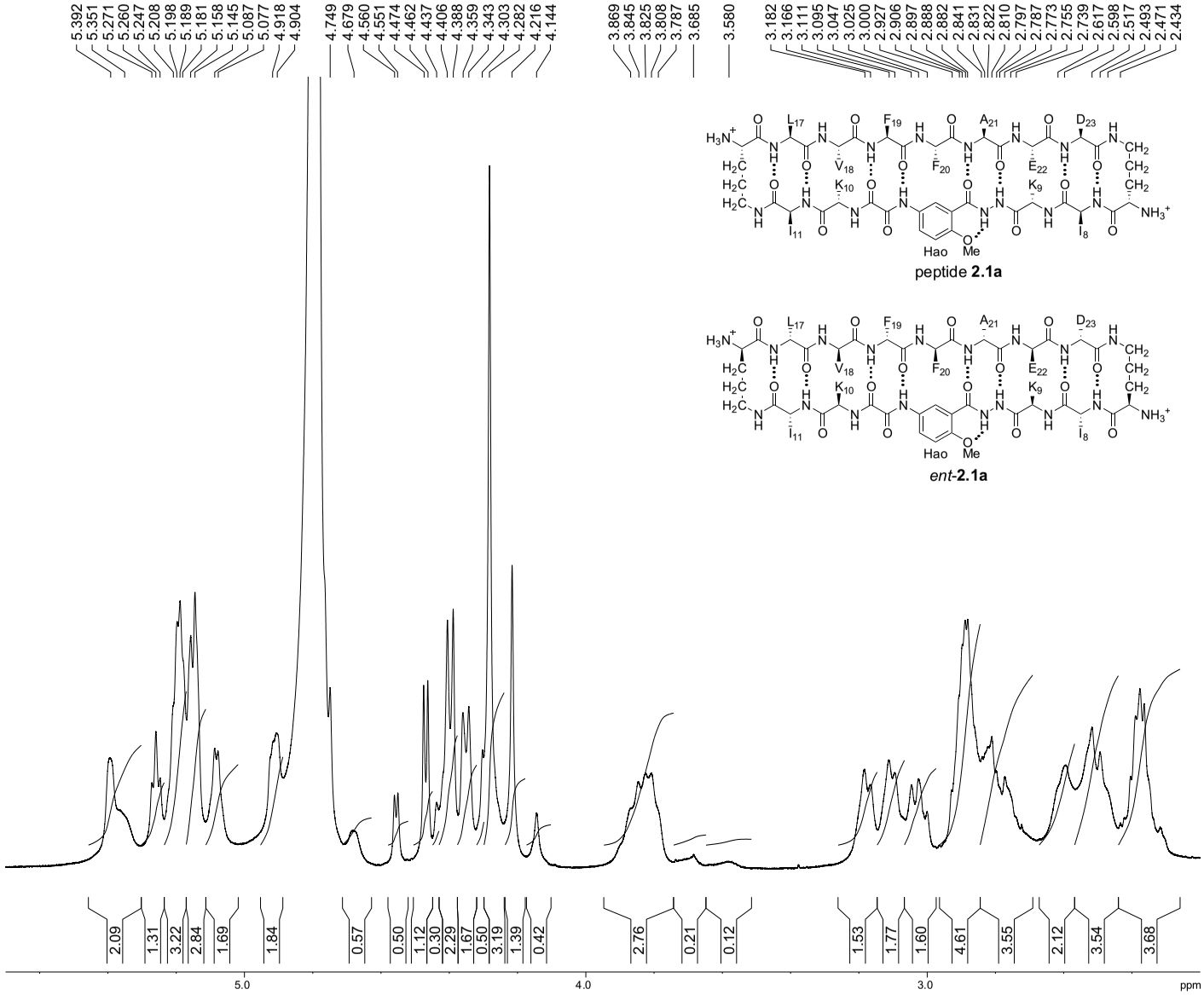

F2 - Acquisition Parameters
Date_ 20211014
Time 23.27
INSTRUM av600
PROBHD 5 mm CPBBO BB-
PULPROG zg30
TD 98074
SOLVENT D2O
NS 512
DS 2
SWH 6602.113 Hz
FIDRES 0.067318 Hz
AQ 7.4274712 sec
RG 10
DW 75.733 usec
DE 12.12 usec
TE 298.0 K
D1 0.10000000 sec
TD0 1

======== CHANNEL f1 ========
SFO1 600.1328835 MHz
NUC1 1H
P1 10.88 usec
PLW1 30.00000000 W

F2 - Processing parameters
SI 65536
SF 600.1300079 MHz
WDW no
SSB 0
LB 0 Hz
GB 0
PC 1.00

^{1}H NMR of 8.0 mM peptide **2.1a** + 8.0 mM peptide *ent*-**2.1a** in D_2O at 600 MHz and 298 K

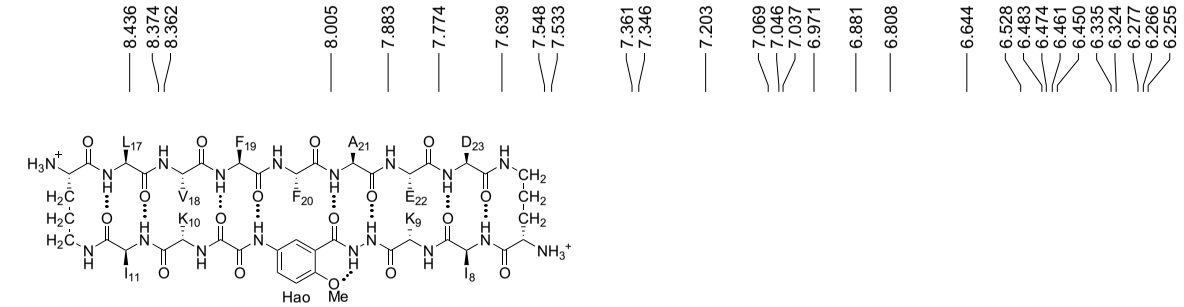

peptide **2.1a**

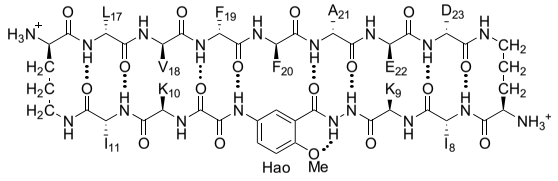

ent-**2.1a**

F2 - Acquisition Parameters
Date_ 20211014
Time 23.27
INSTRUM av600
PROBHD 5 mm CPBBO BB-
PULPROG zg30
TD 98074
SOLVENT D2O
NS 512
DS 2
SWH 6602.113 Hz
FIDRES 0.067318 Hz
AQ 7.4274712 sec
RG 10
DW 75.733 usec
DE 12.12 usec
TE 298.0 K
D1 0.10000000 sec
TD0 1

======== CHANNEL f1 ========
SFO1 600.1328835 MHz
NUC1 1H
P1 10.88 usec
PLW1 30.00000000 W

F2 - Processing parameters
SI 65536
SF 600.1300079 MHz
WDW no
SSB 0
LB 0 Hz
GB 0
PC 1.00

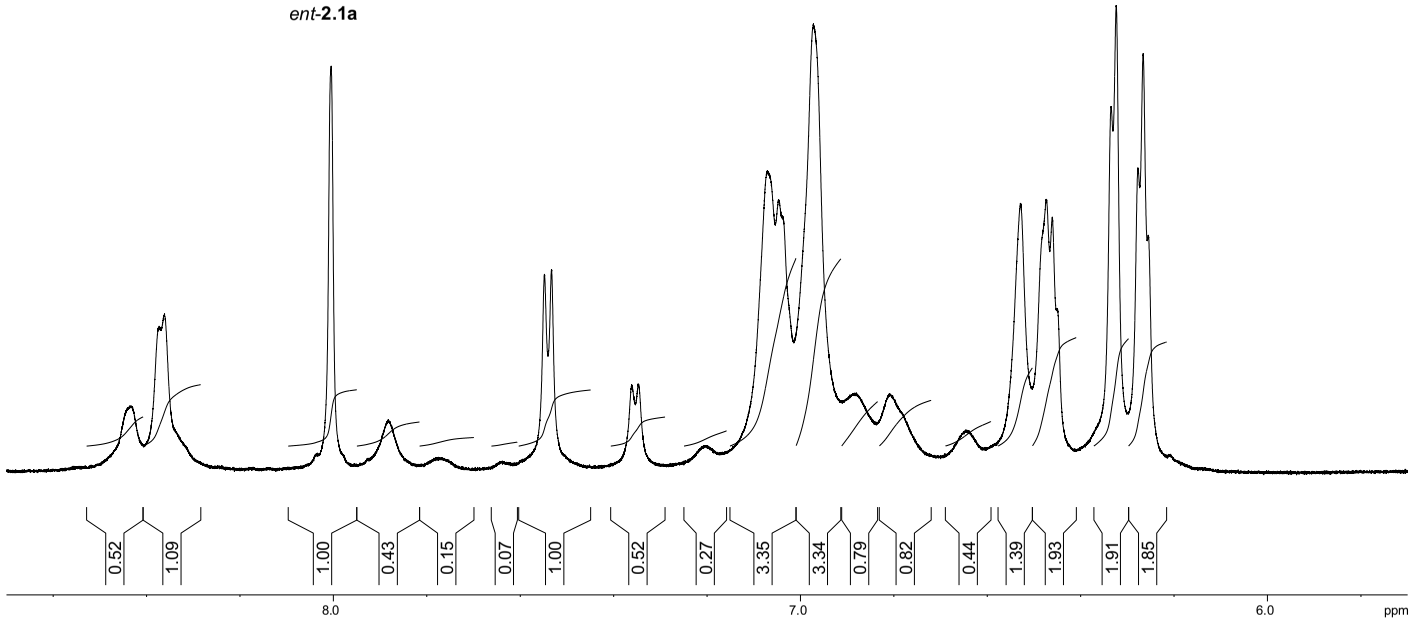

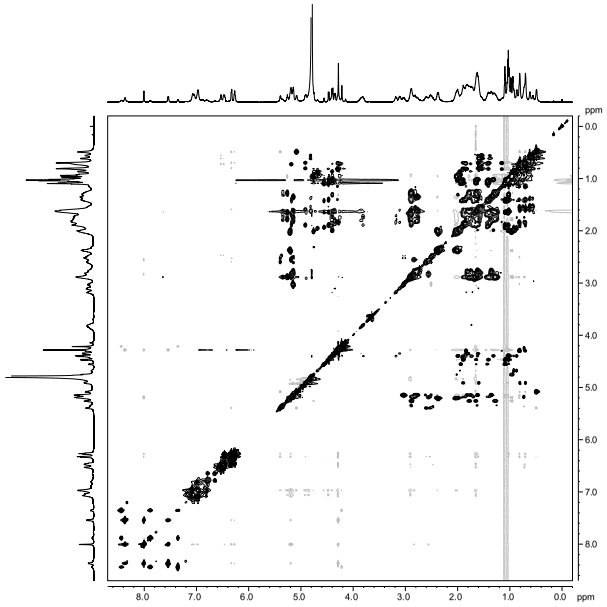

8.0 mM peptide **2.1a** + 8.0 mM *ent*-**2.1a**
in D_2O, 150-ms mixing time, 298 K
600 MHz TOCSY spectrum
presaturation suppression of the HOD peak

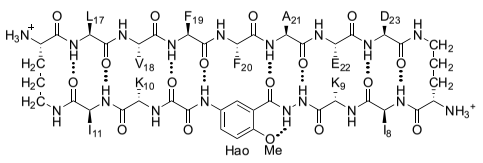

peptide **2.1a**

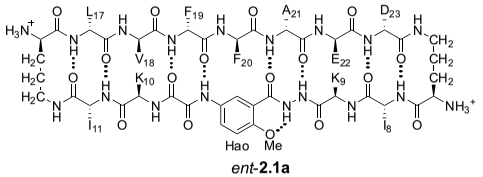

ent-**2.1a**

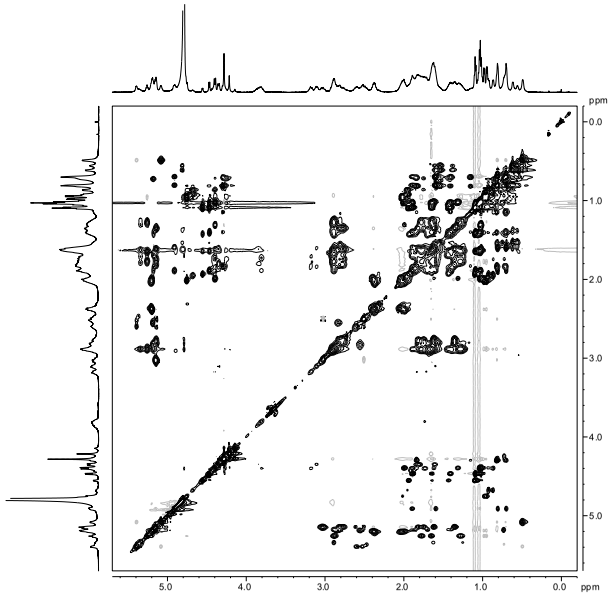

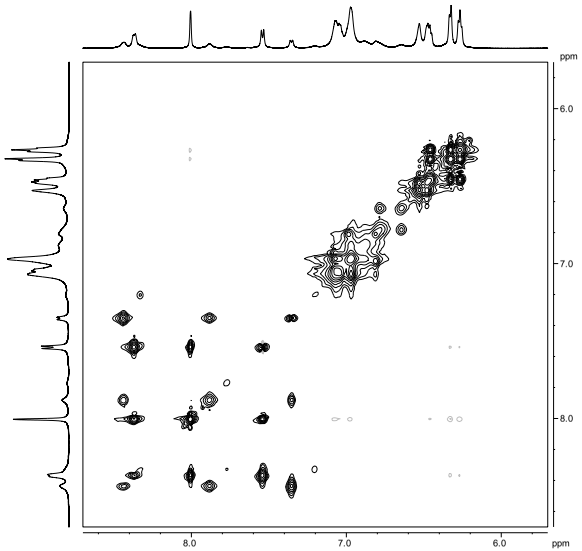

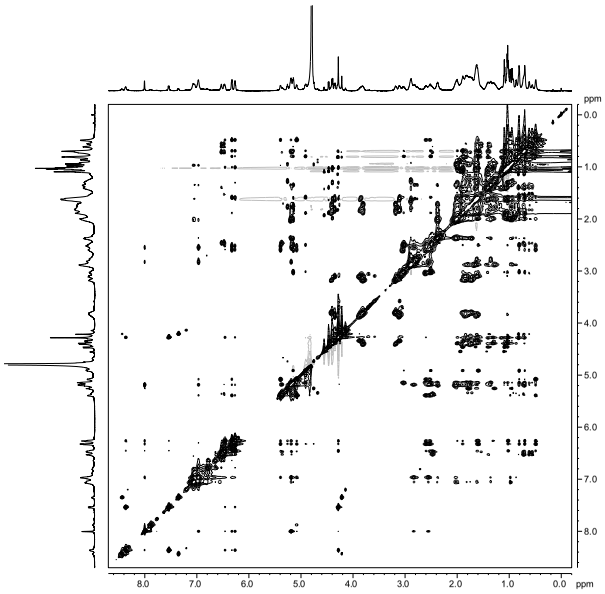

8.0 mM peptide **2.1a** + 8.0 mM *ent*-**2.1a**
in D_2O, 200-ms mixing time, 298 K
600 MHz NOESY spectrum
presaturation suppression of the HOD peak

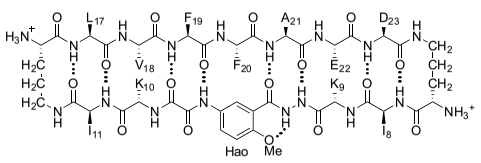

peptide **2.1a**

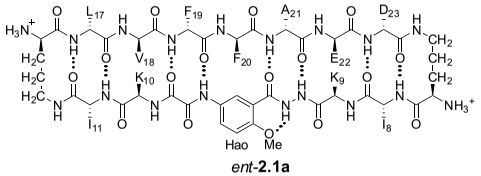

ent-**2.1a**

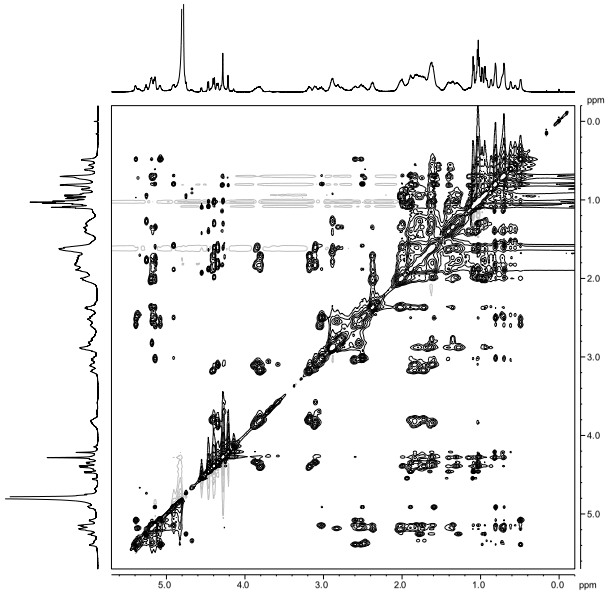

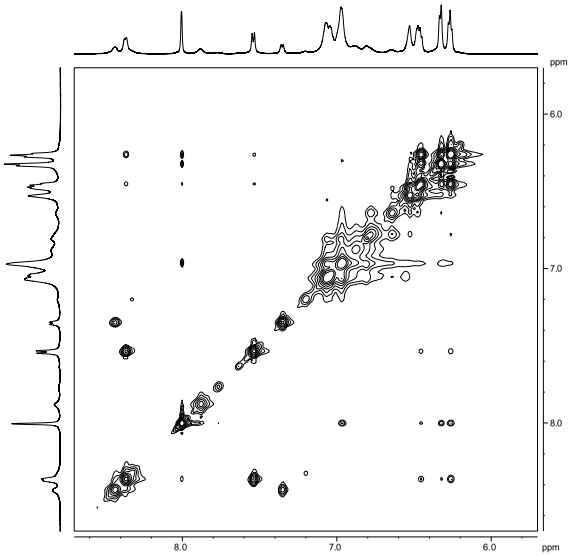

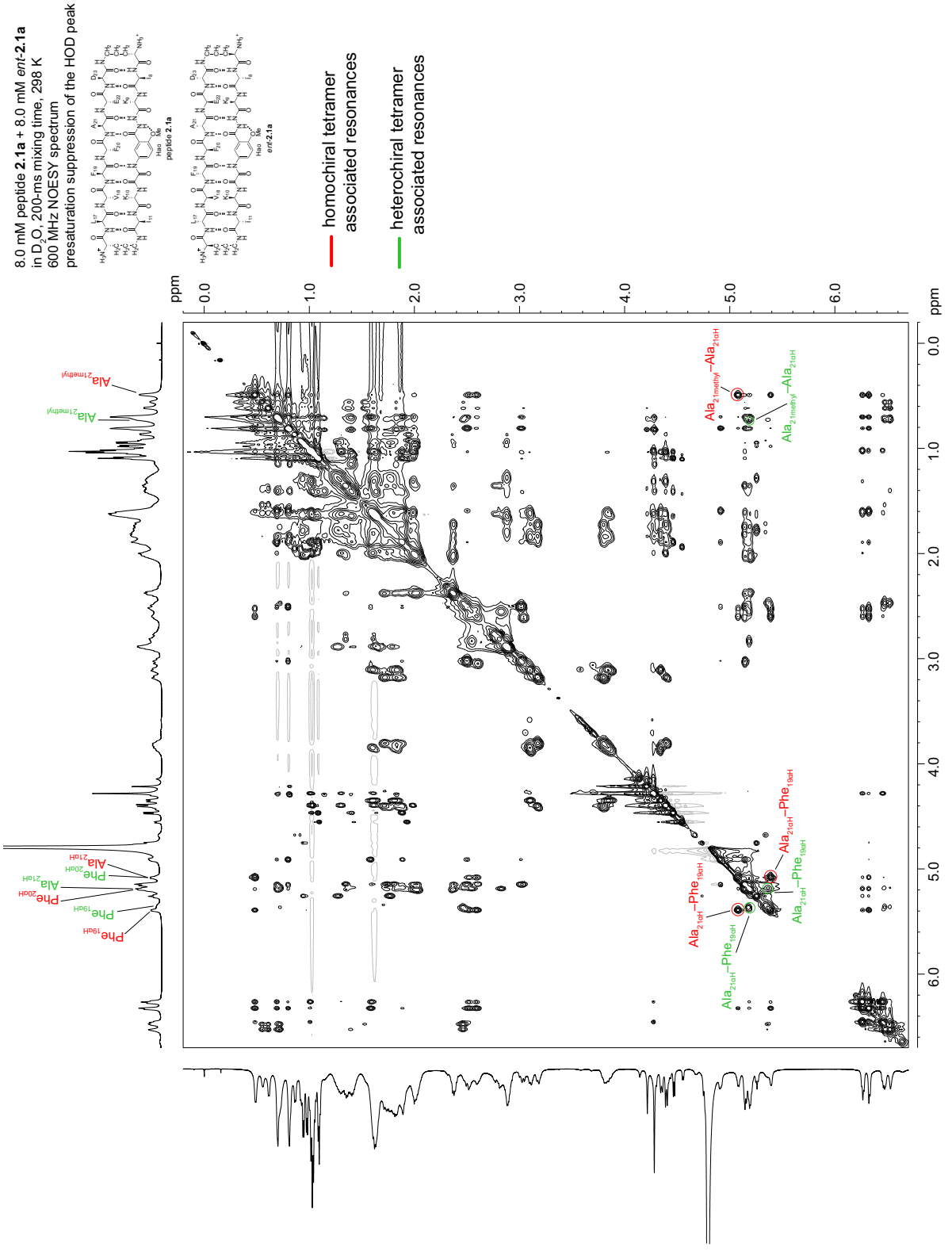
8.0 mM peptide 2.1a + 8.0 mM ent-2.1a
in D2O, 200-ms mixing time, 298 K
600 MHz NOESY spectrum
presaturation suppression of the HOD peak
peptide 2.1a
ent-2.1a
homochiral tetramer associated resonances
heterochiral tetramer associated resonances
ppm
Phe19αH
Phe19βH
Ala2αH
Phe20αH
Phe20βH
Ala2βH
Ala2αH
Ala2βH
Ala2αH–Phe19αH
Ala2αH–Phe19βH
Ala2βH–Phe19αH
Ala2βH–Phe19βH
Ala2αH–Ala2αH
Ala2αH–Ala2βH
Ala2βH–Ala2αH

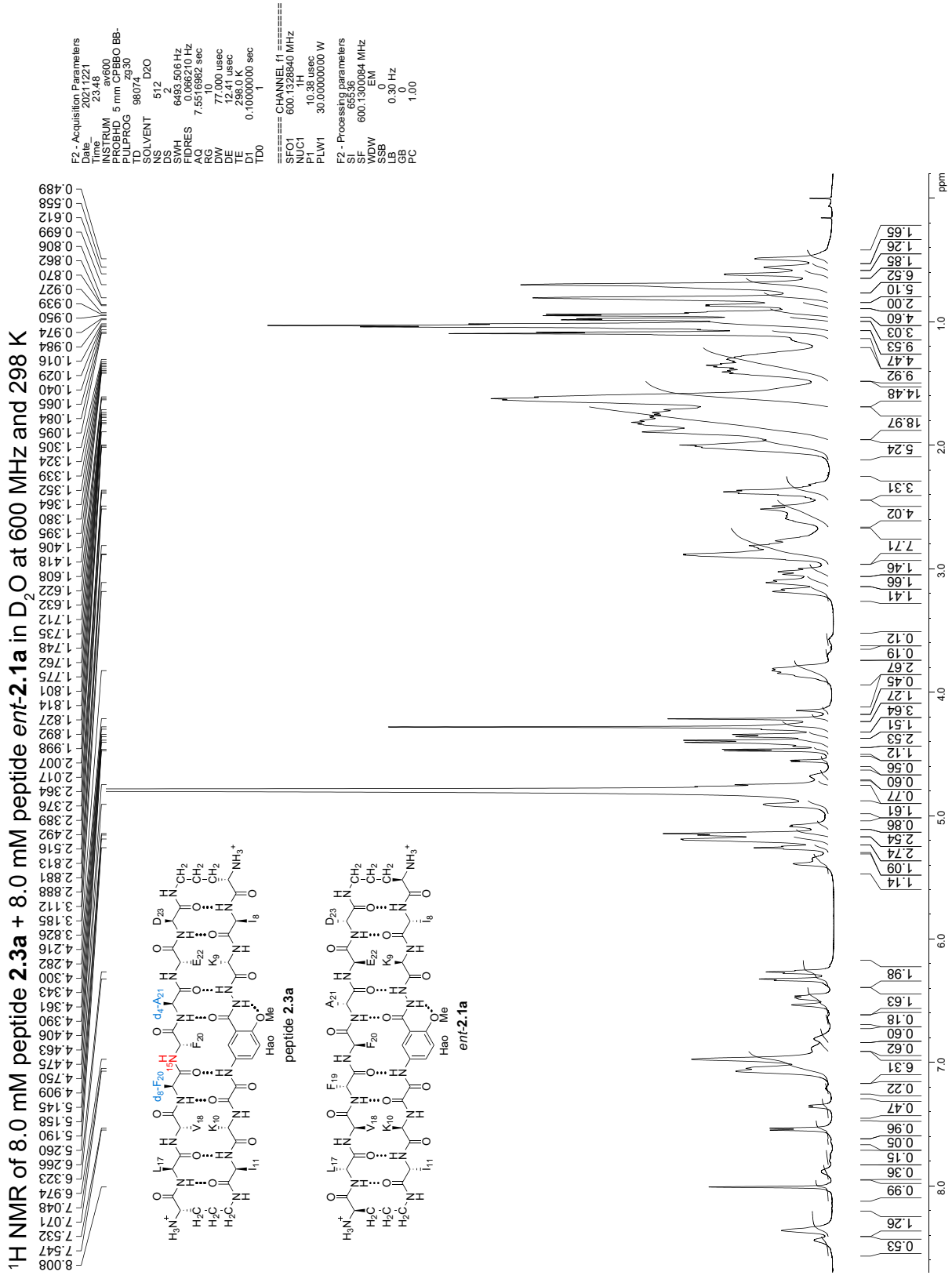

^{1}H NMR of 8.0 mM peptide **2.3a** + 8.0 mM peptide *ent*-**2.1a** in D_2O at 600 MHz and 298 K

^{1}H NMR of 8.0 mM peptide **2.3a** + 8.0 mM peptide *ent*-**2.1a** in D_2O at 600 MHz and 298 K

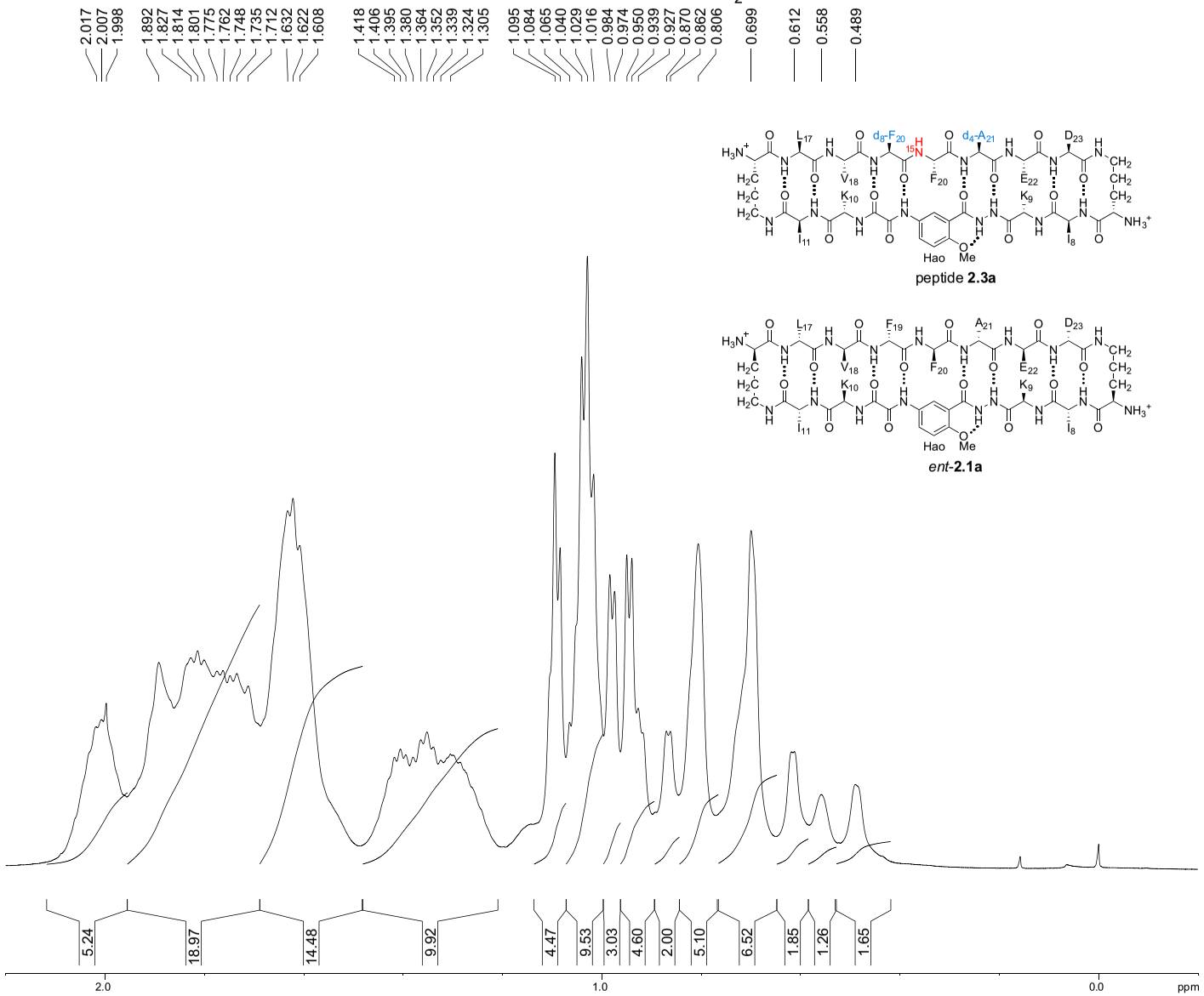

F2 - Acquisition Parameters
Date_ 20211221
Time 23.48
INSTRUM av600
PROBHD 5 mm CPBBO BB-
PULPROG zg30
TD 98074
SOLVENT D2O
NS 512
DS 2
SWH 6493.506 Hz
FIDRES 0.066210 Hz
AQ 7.5516982 sec
RG 10
DW 77.000 usec
DE 12.41 usec
TE 298.0 K
D1 0.10000000 sec
TD0 1

======== CHANNEL f1 ========
SFO1 600.1328840 MHz
NUC1 1H
P1 10.38 usec
PLW1 30.00000000 W

F2 - Processing parameters
SI 65536
SF 600.1300084 MHz
WDW EM
SSB 0
LB 0.30 Hz
GB 0
PC 1.00

^{1}H NMR of 8.0 mM peptide **2.3a** + 8.0 mM peptide *ent*-**2.1a** in D_2O at 600 MHz and 298 K

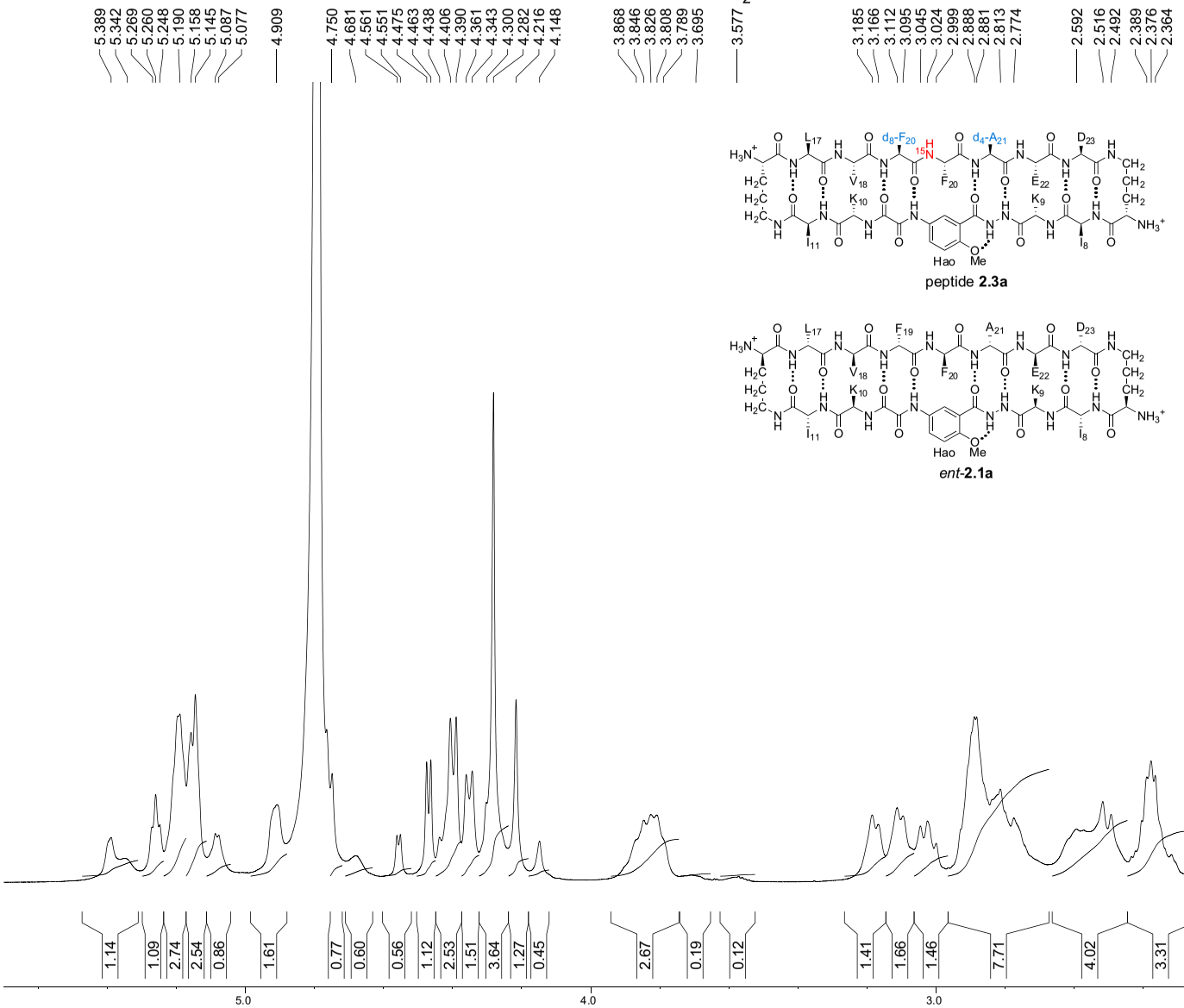

peptide **2.3a**

ent-**2.1a**

F2 - Acquisition Parameters
Date_ 20211221
Time 23.48
INSTRUM av600
PROBHD 5 mm CPBBO BB-
PULPROG zg30
TD 98074
SOLVENT D2O
NS 512
DS 2
SWH 6493.506 Hz
FIDRES 0.066210 Hz
AQ 7.5516982 sec
RG 10
DW 77.000 usec
DE 12.41 usec
TE 298.0 K
D1 0.10000000 sec
TD0 1

======== CHANNEL f1 ========
SFO1 600.1328840 MHz
NUC1 1H
P1 10.38 usec
PLW1 30.00000000 W

F2 - Processing parameters
SI 65536
SF 600.1300084 MHz
WDW EM
SSB 0
LB 0.30 Hz
GB 0
PC 1.00

^{1}H NMR of 8.0 mM peptide **2.3a** + 8.0 mM peptide *ent*-**2.1a** in D_2O at 600 MHz and 298 K

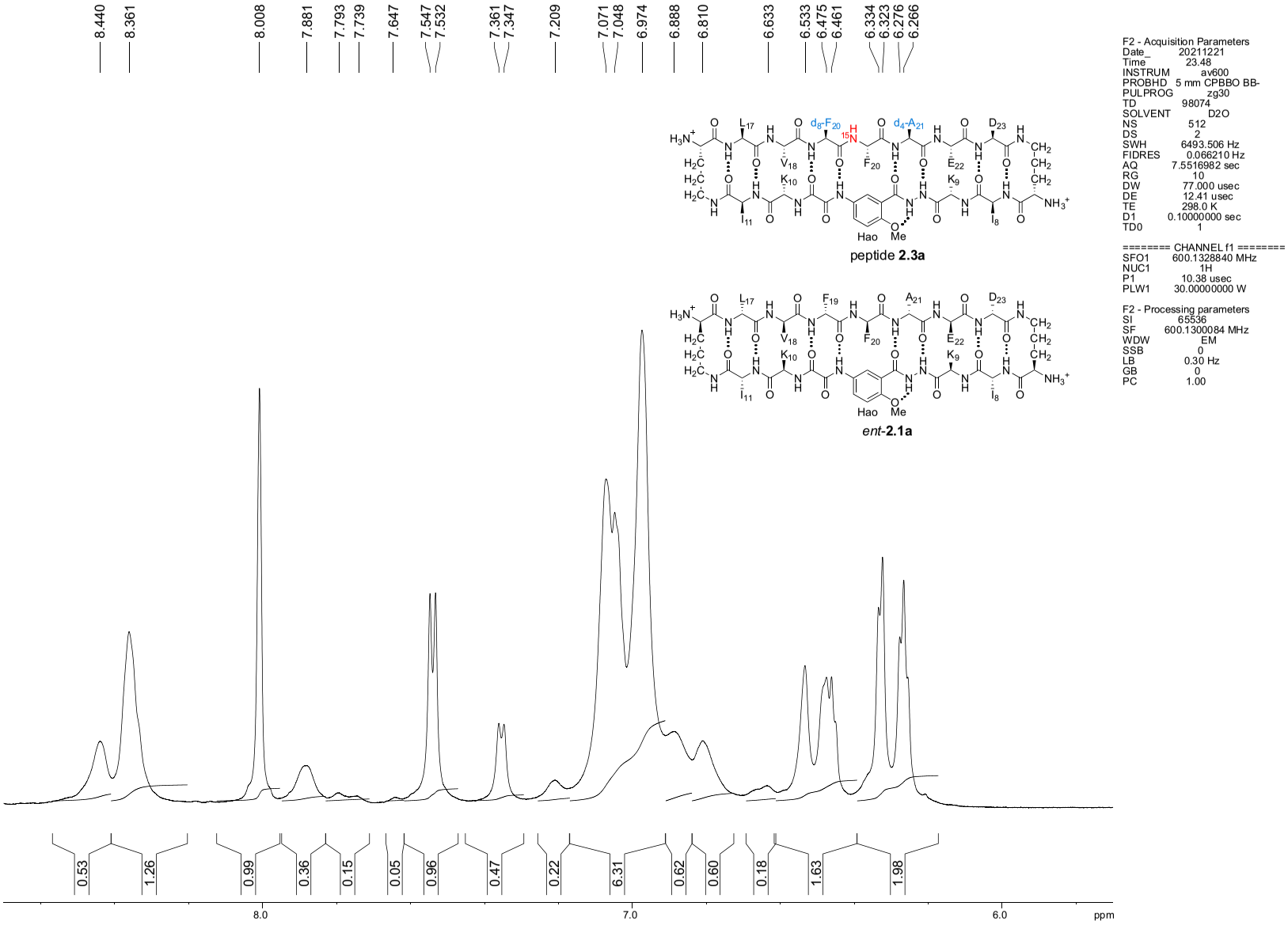

F2 - Acquisition Parameters
Date_ 20211221
Time 23.48
INSTRUM av600
PROBHD 5 mm CPBBO BB-
PULPROG zg30
TD 98074
SOLVENT D2O
NS 512
DS 2
SWH 6493.506 Hz
FIDRES 0.066210 Hz
AQ 7.5516982 sec
RG 10
DW 77.000 usec
DE 12.41 usec
TE 298.0 K
D1 0.10000000 sec
TD0 1

======== CHANNEL f1 ========
SFO1 600.1328840 MHz
NUC1 1H
P1 10.38 usec
PLW1 30.00000000 W

F2 - Processing parameters
SI 65536
SF 600.1300084 MHz
WDW EM
SSB 0
LB 0.30 Hz
GB 0
PC 1.00

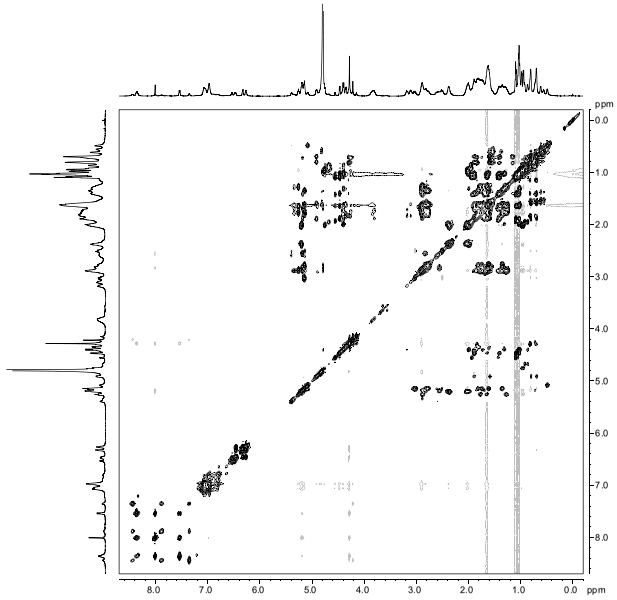

8.0 mM peptide **2.3a** + 8.0 mM *ent*-**2.1a**
in D_2O, 150-ms mixing time, 298 K
600 MHz TOCSY spectrum
presaturation suppression of the HOD peak

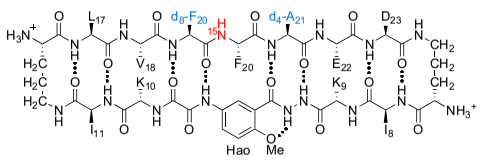

peptide **2.3a**

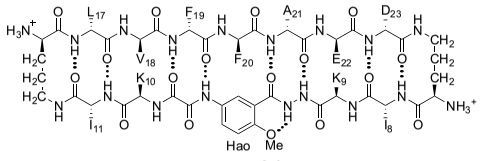

ent-**2.1a**

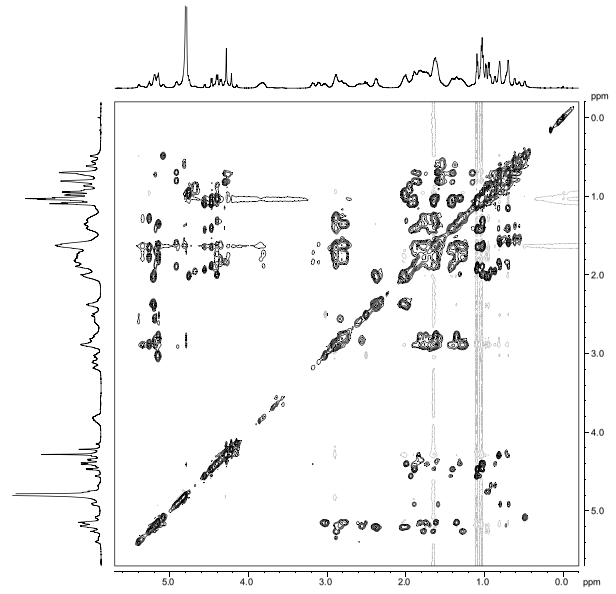

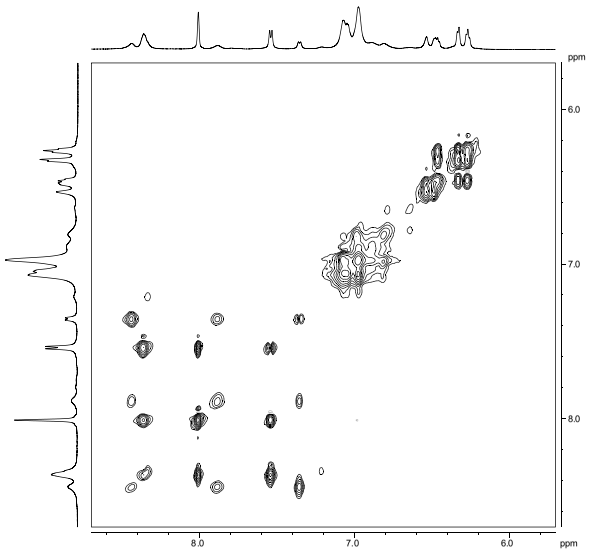

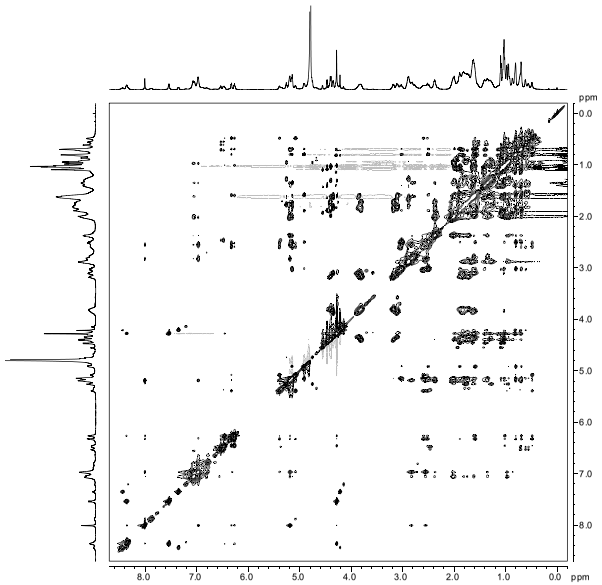

8.0 mM peptide **2.3a** + 8.0 mM *ent*-**2.1a**
in D_2O, 200-ms mixing time, 298 K
600 MHz NOESY spectrum
presaturation suppression of the HOD peak

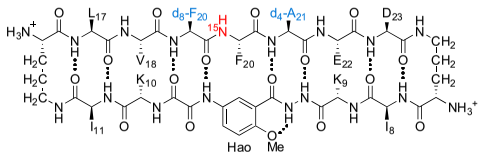

peptide **2.3a**

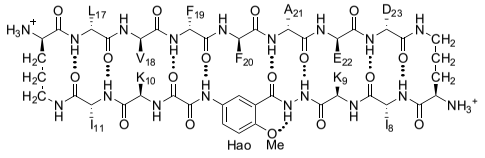

ent-**2.1a**

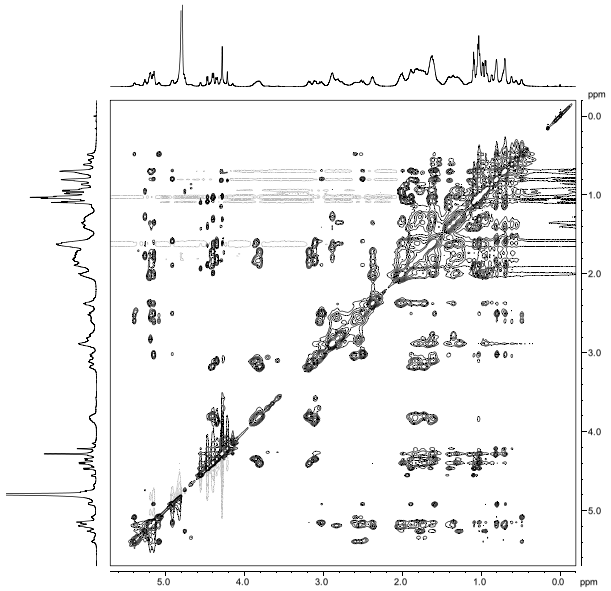

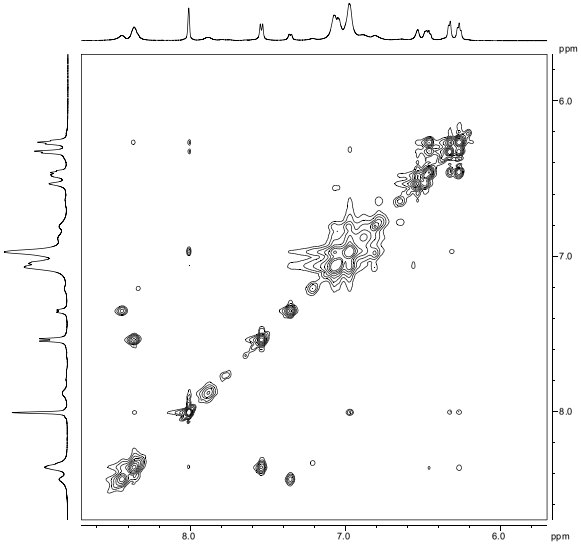

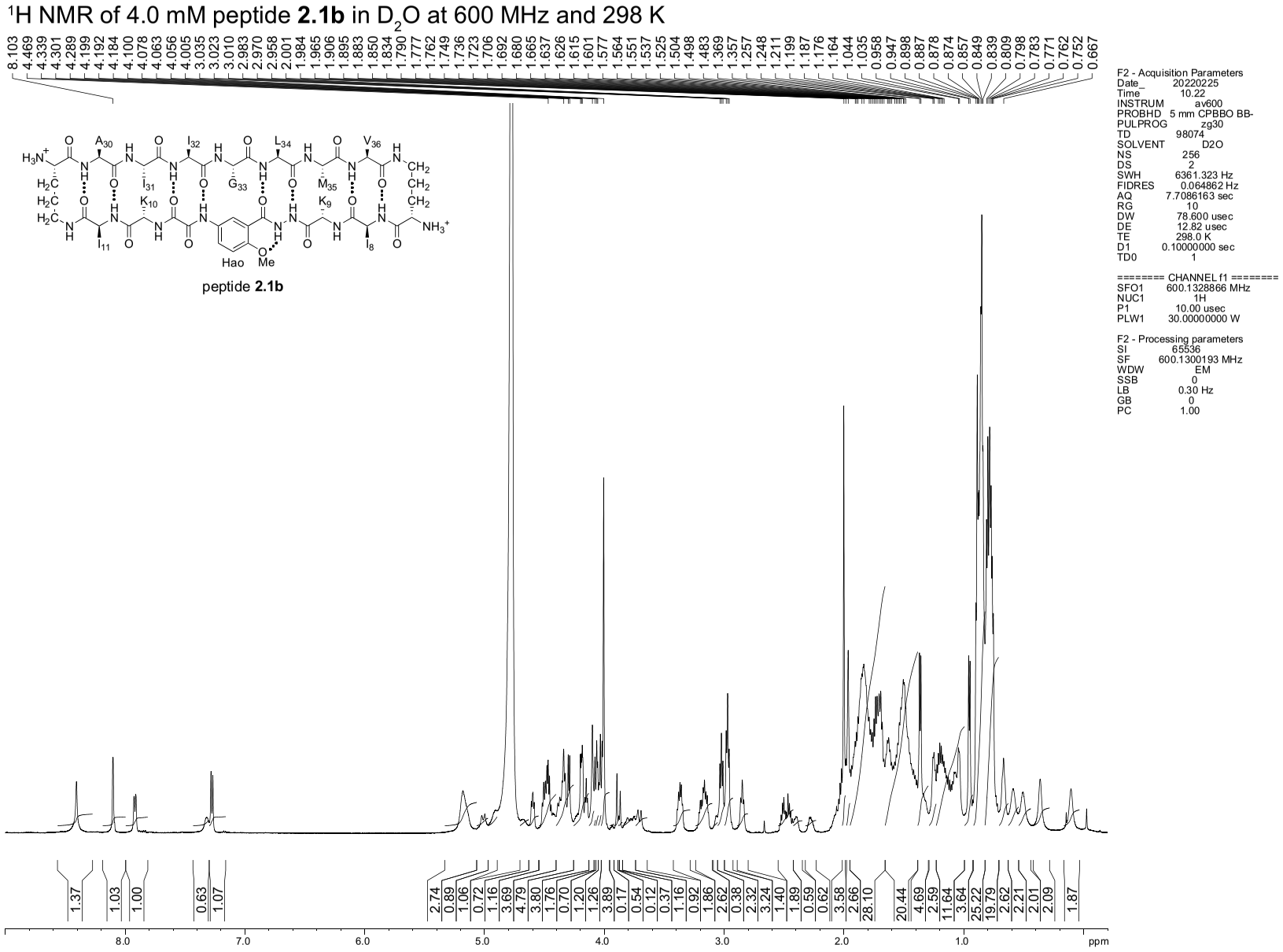
^{1}H NMR of 4.0 mM peptide **2.1b** in D_2O at 600 MHz and 298 K
peptide **2.1b**
F2 - Acquisition Parameters
Date_ 20220225
Time 10.22
INSTRUM av600
PROBHD 5 mm CPBBO BB-
PULPROG zg30
TD 98074
SOLVENT D2O
NS 256
DS 2
SWH 6361.323 Hz
FIDRES 0.064862 Hz
AQ 7.7086163 sec
RG 1.0
DW 78.600 usec
DE 12.82 usec
TE 298.0 K
D1 0.10000000 sec
TD0 1
======== CHANNEL f1 ========
SFO1 600.1328866 MHz
NUC1 1H
P1 10.00 usec
PLW1 30.00000000 W
F2 - Processing parameters
SI 65536
SF 600.1300193 MHz
WDW EM
SSB 0
LB 0.30 Hz
GB 0
PC 1.00
ppm

^{1}H NMR of 4.0 mM peptide **2.1b** in D_2O at 600 MHz and 298 K

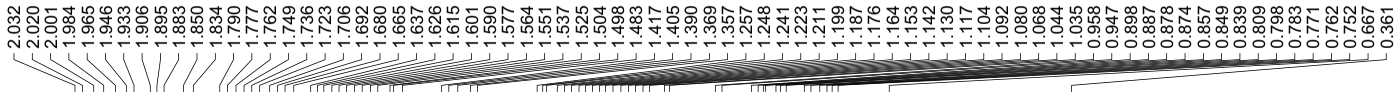

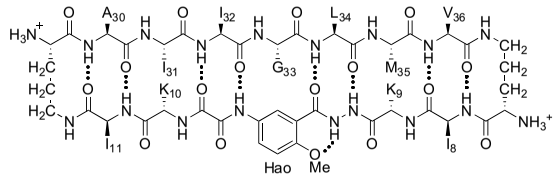

peptide **2.1b**

F2 - Acquisition Parameters
Date_ 20220225
Time 10.22
INSTRUM av600
PROBHD 5 mm CPBBO BB-
PULPROG zg30
TD 98074
SOLVENT D2O
NS 256
DS 2
SWH 6361.323 Hz
FIDRES 0.064862 Hz
AQ 7.7086163 sec
RG 1.0
DW 78.600 usec
DE 12.82 usec
TE 298.0 K
D1 0.10000000 sec
TD0 1

======== CHANNEL f1 ========
SFO1 600.1328866 MHz
NUC1 1H
P1 10.00 usec
PLW1 30.00000000 W

F2 - Processing parameters
SI 65536
SF 600.1300193 MHz
WDW EM
SSB 0
LB 0.30 Hz
GB 0
PC 1.00

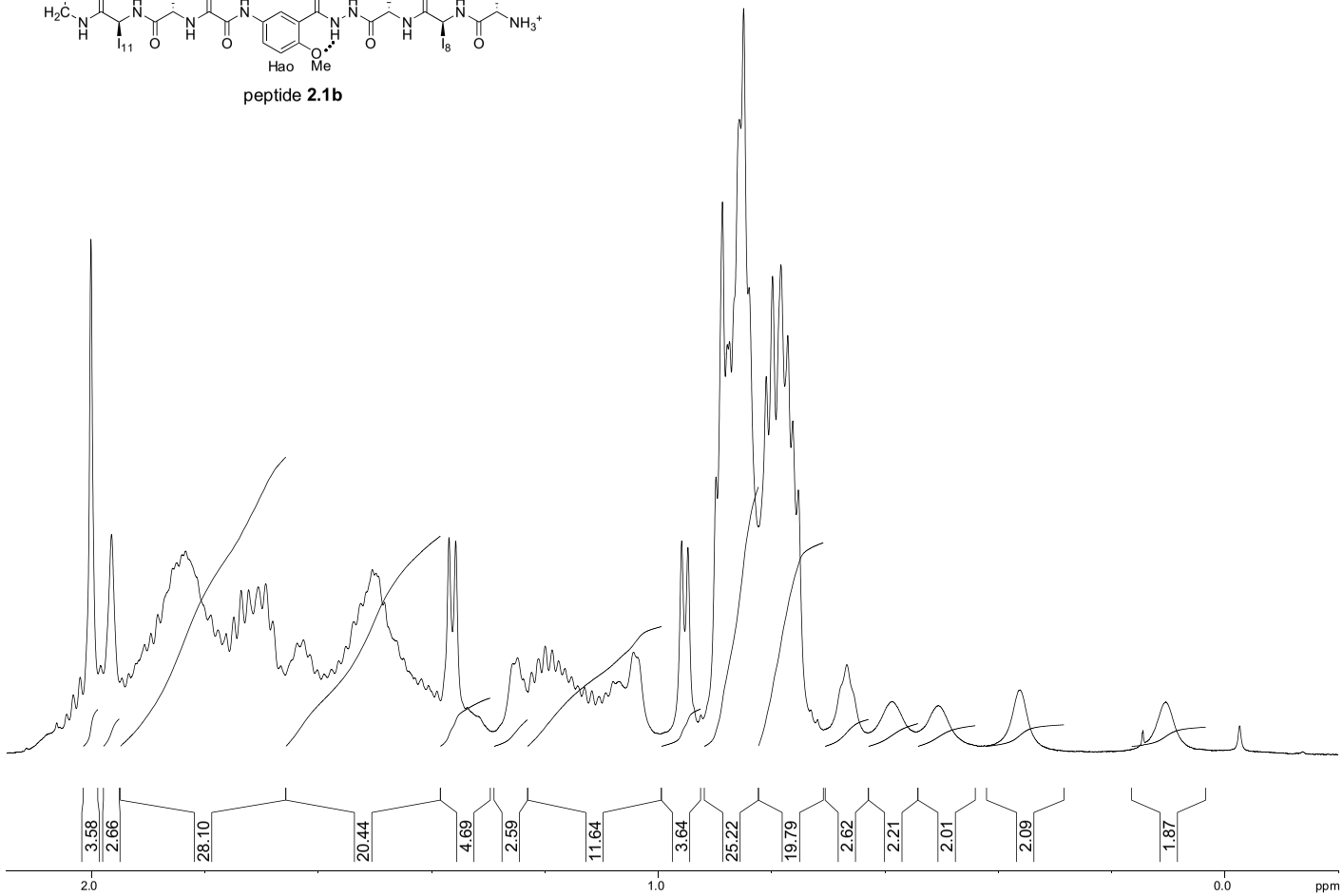

^{1}H NMR of 4.0 mM peptide **2.1b** in D_2O at 600 MHz and 298 K

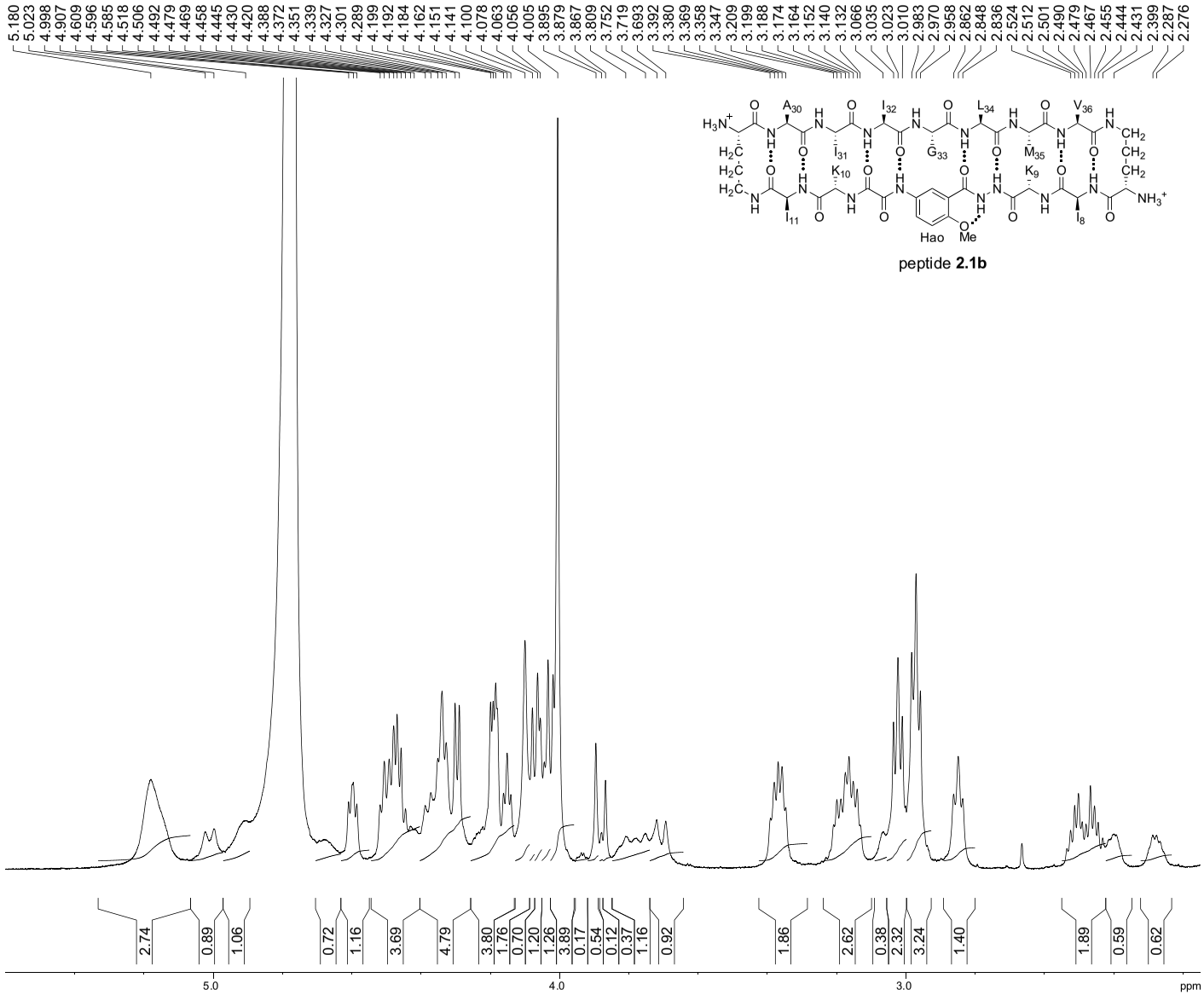

peptide **2.1b**

F2 - Acquisition Parameters
Date_ 20220225
Time 10.22
INSTRUM av600
PROBHD 5 mm CPBBO BB-
PULPROG zg30
TD 98074
SOLVENT D2O
NS 256
DS 2
SWH 6361.323 Hz
FIDRES 0.064862 Hz
AQ 7.7086163 sec
RG 10
DW 78.600 usec
DE 12.82 usec
TE 298.0 K
D1 0.10000000 sec
TD0 1

======== CHANNEL f1 ========
SFO1 600.1328866 MHz
NUC1 1H
P1 10.00 usec
PLW1 30.00000000 W

F2 - Processing parameters
SI 65536
SF 600.1300193 MHz
WDW EM
SSB 0
LB 0.30 Hz
GB 0
PC 1.00

^{1}H NMR of 4.0 mM peptide **2.1b** in D_2O at 600 MHz and 298 K

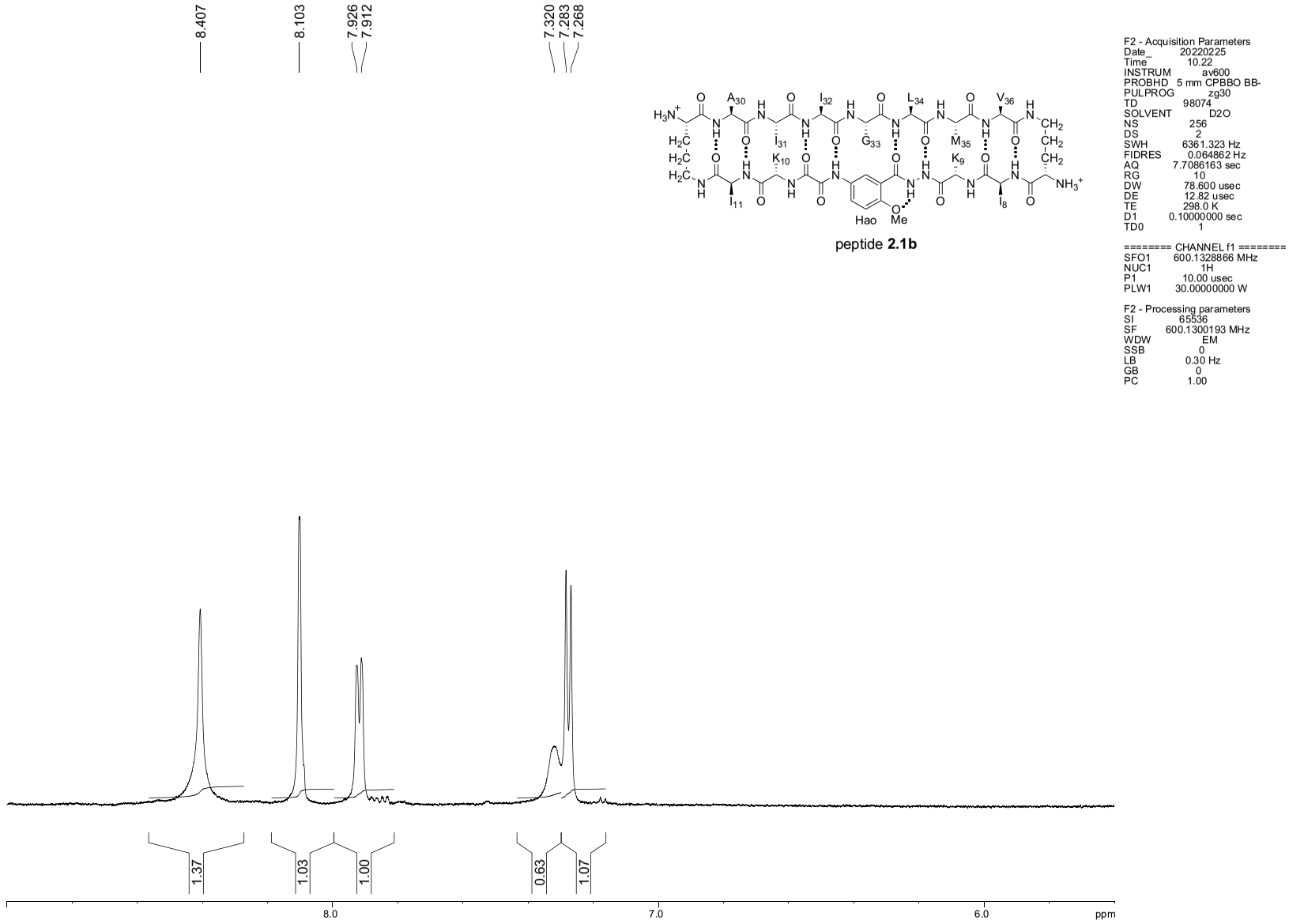

peptide **2.1b**

F2 - Acquisition Parameters
Date_ 20220225
Time 10.22
INSTRUM av600
PROBHD 5 mm CPBBO BB-
PULPROG zg30
TD 98074
SOLVENT D2O
NS 256
DS 2
SWH 6361.323 Hz
FIDRES 0.064862 Hz
AQ 7.7086163 sec
RG 1.0
DW 78.600 usec
DE 12.82 usec
TE 298.0 K
D1 0.10000000 sec
TD0 1

======== CHANNEL f1 ========
SFO1 600.1328866 MHz
NUC1 1H
P1 10.00 usec
PLW1 30.00000000 W

F2 - Processing parameters
SI 65536
SF 600.1300193 MHz
WDW EM
SSB 0
LB 0.30 Hz
GB 0
PC 1.00

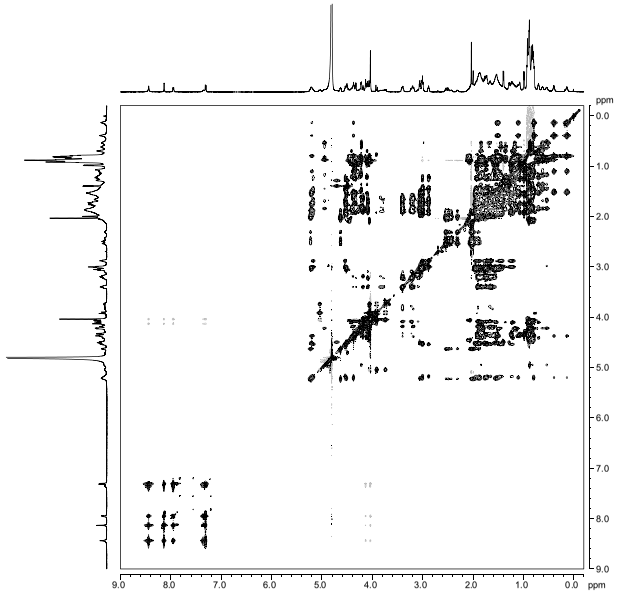

4.0 mM peptide **2.1b**
in D_2O, 150-ms mixing time, 298 K
600 MHz TOCSY spectrum
presaturation suppression of the HOD peak

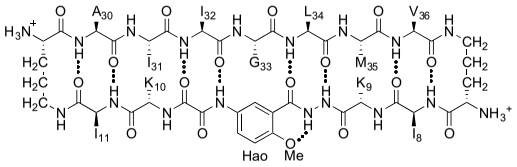

peptide **2.1b**

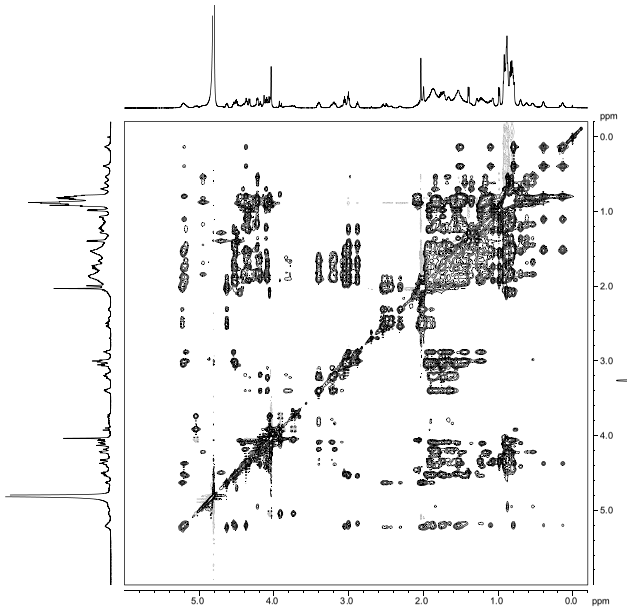

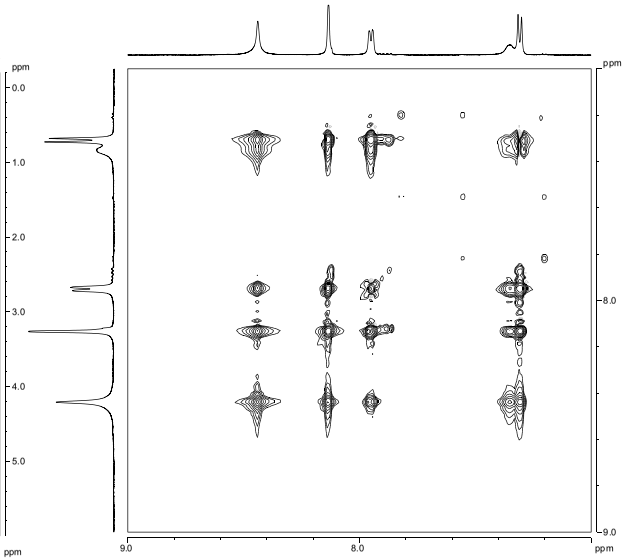

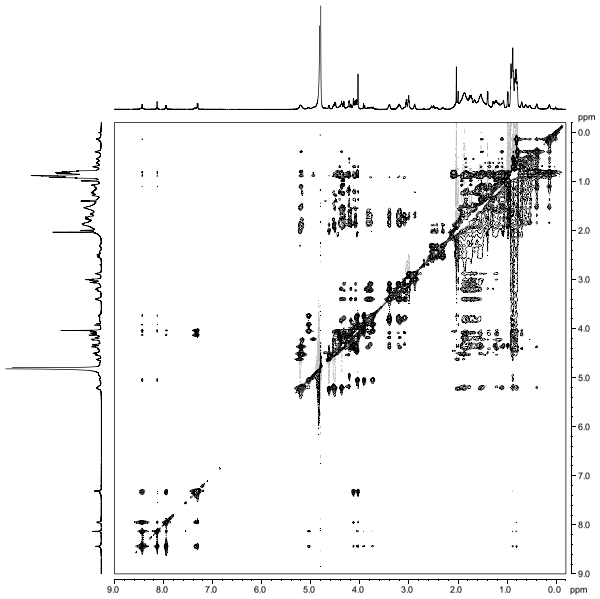

4.0 mM peptide **2.1b**
in D_2O, 200-ms mixing time, 298 K
600 MHz NOESY spectrum
presaturation suppression of the HOD peak

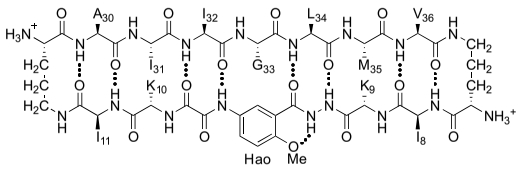

peptide **2.1b**

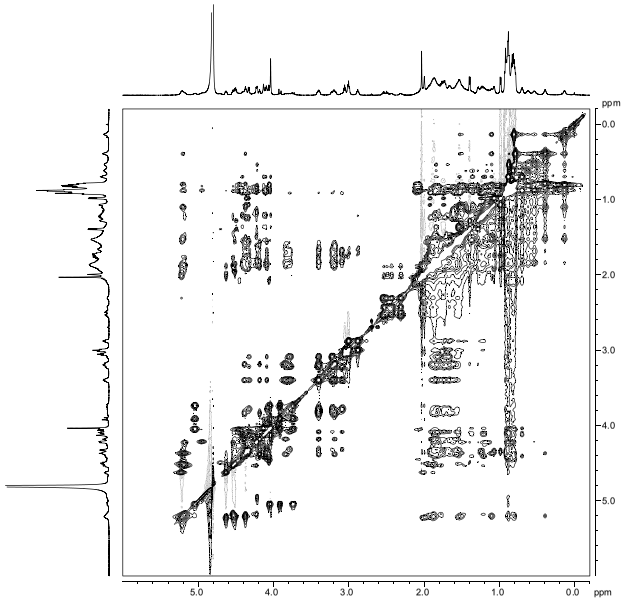

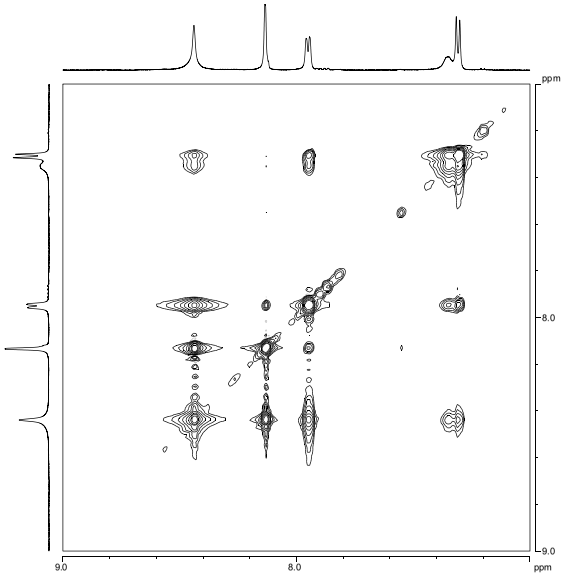

^{1}H NMR of 4.0 mM peptide **2.1b** + 4.0 mM peptide *ent*-**2.1b** in D_2O at 600 MHz and 298 K

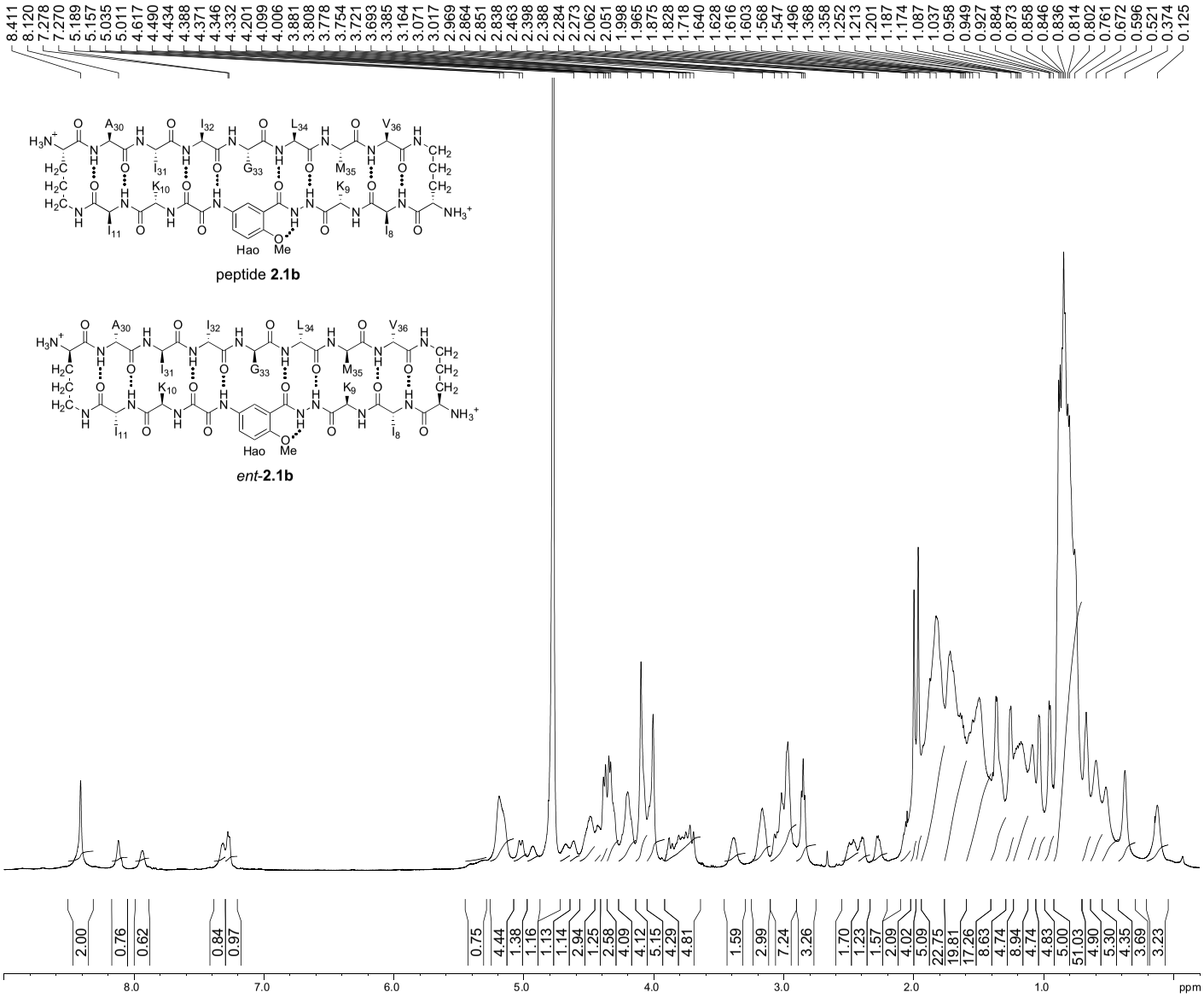

^{1}H NMR of 4.0 mM peptide **2.1b** + 4.0 mM peptide *ent*-**2.1b** in D_2O at 600 MHz and 298 K

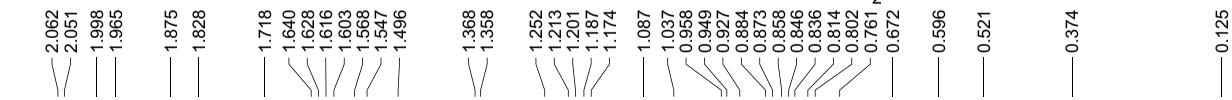

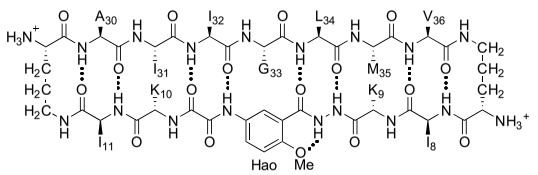

peptide **2.1b**

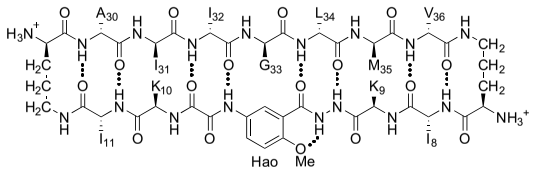

ent-**2.1b**

F2 - Acquisition Parameters
Date_ 20220206
Time 23.06
INSTRUM av600
PROBHD 5 mm CPBBO BB-
PULPROG zg30
TD 98074
SOLVENT D2O
NS 512
DS 2
SWH 6487.889 Hz
FIDRES 0.066153 Hz
AQ 7.5582361 sec
RG 10
DW 77.067 usec
DE 13.04 usec
TE 298.0 K
D1 0.10000000 sec
TD0 1

======== CHANNEL f1 ========
SFO1 600.1327096 MHz
NUC1 1H
P1 10.06 usec
PLW1 30.00000000 W

F2 - Processing parameters
SI 65536
SF 600.1300183 MHz
WDW EM
SSB 0
LB 0.30 Hz
GB 0
PC 1.00

^{1}H NMR of 4.0 mM peptide **2.1b** + 4.0 mM peptide *ent*-**2.1b** in D_2O at 600 MHz and 298 K

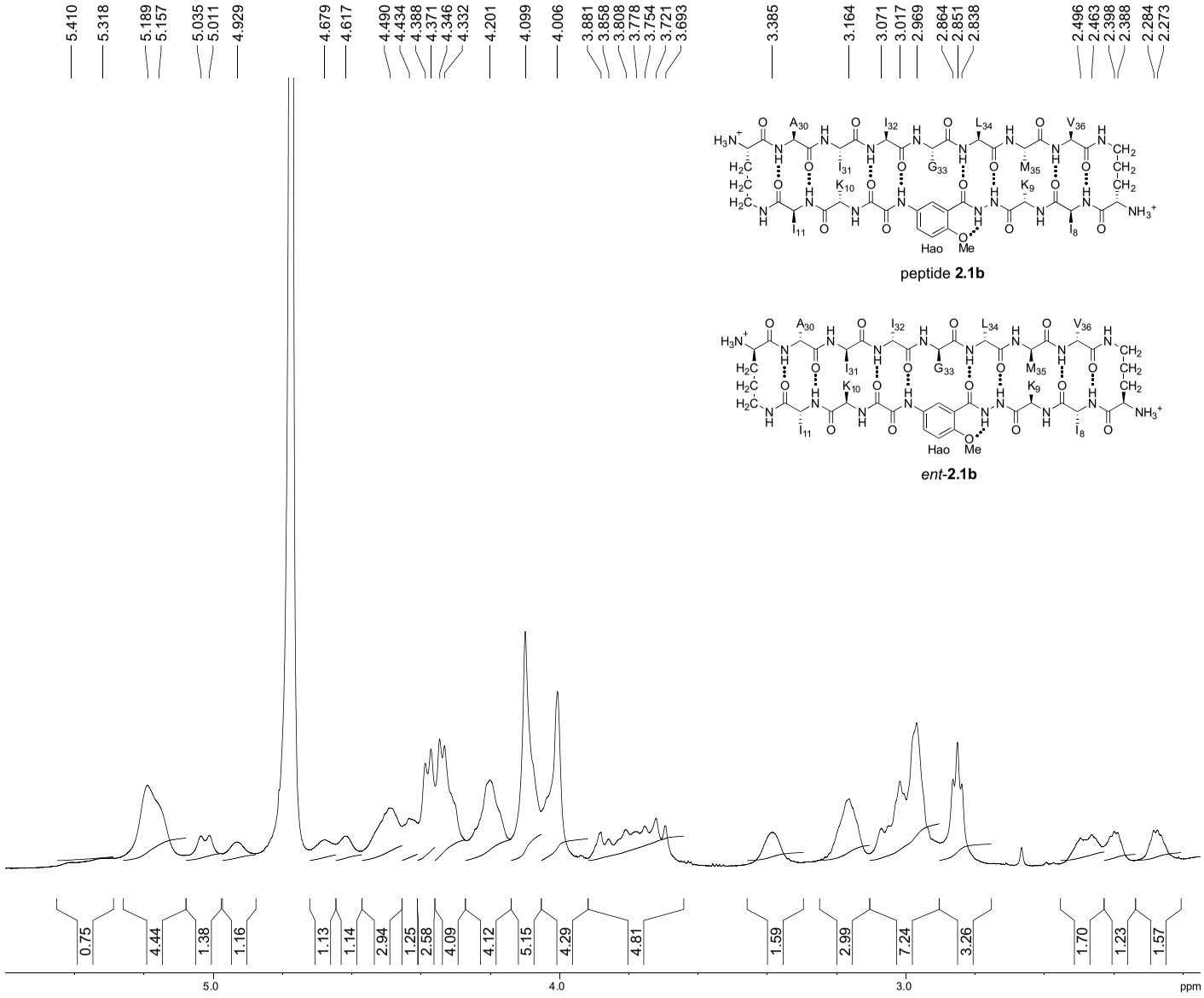

F2 - Acquisition Parameters
Date_ 20220206
Time 23.06
INSTRUM av600
PROBHD 5 mm CPBBO BB-
PULPROG zg30
TD 98074
SOLVENT D2O
NS 512
DS 2
SWH 6487.889 Hz
FIDRES 0.066153 Hz
AQ 7.5582361 sec
RG 10
DW 77.067 usec
DE 13.04 usec
TE 298.0 K
D1 0.10000000 sec
TD0 1

======== CHANNEL f1 ========
SFO1 600.1327096 MHz
NUC1 1H
P1 10.06 usec
PLW1 30.00000000 W

F2 - Processing parameters
SI 65536
SF 600.1300183 MHz
WDW EM
SSB 0
LB 0.30 Hz
GB 0
PC 1.00

^{1}H NMR of 4.0 mM peptide **2.1b** + 4.0 mM peptide *ent*-**2.1b** in D_2O at 600 MHz and 298 K

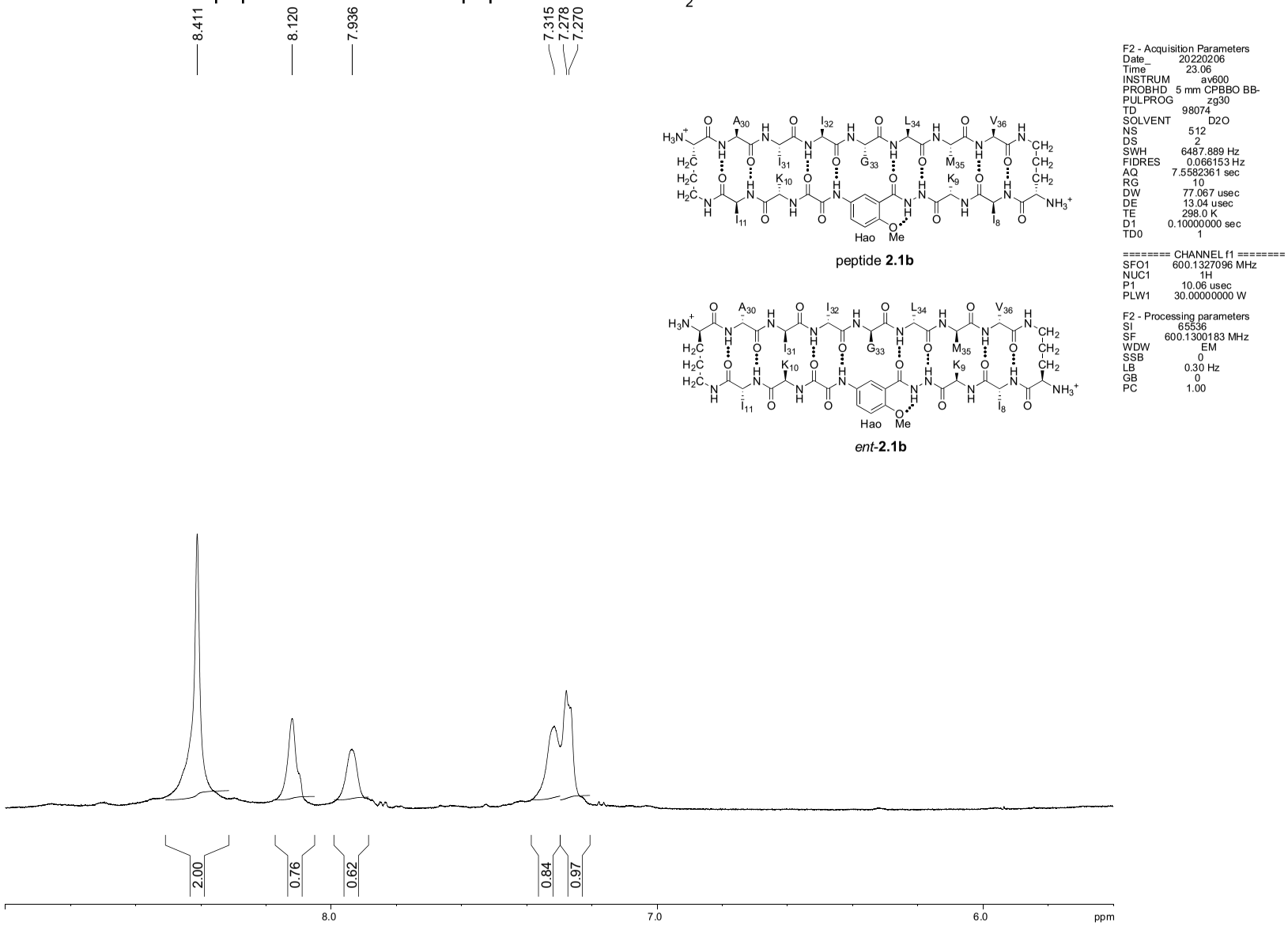

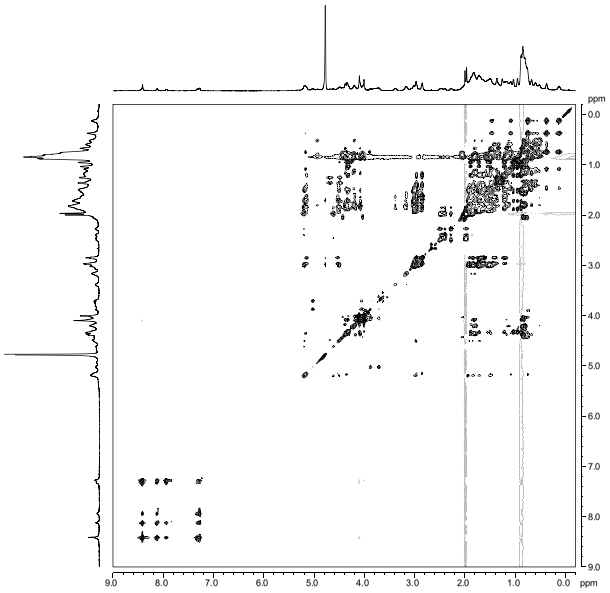

4.0 mM peptide **2.1b** + 4.0 mM *ent*-**2.1b**
in D_2O, 150-ms mixing time, 298 K
600 MHz TOCSY spectrum
presaturation suppression of the HOD peak

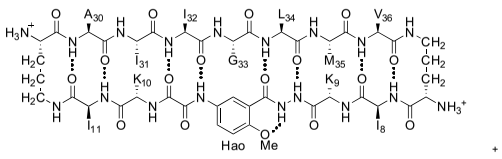

peptide **2.1b**

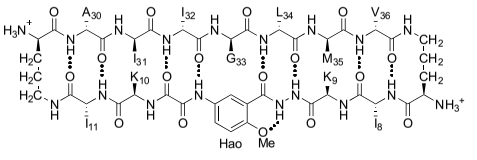

ent-**2.1b**

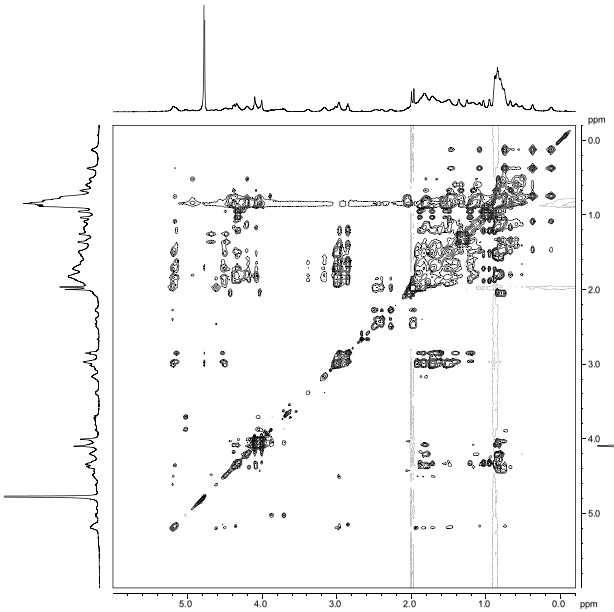

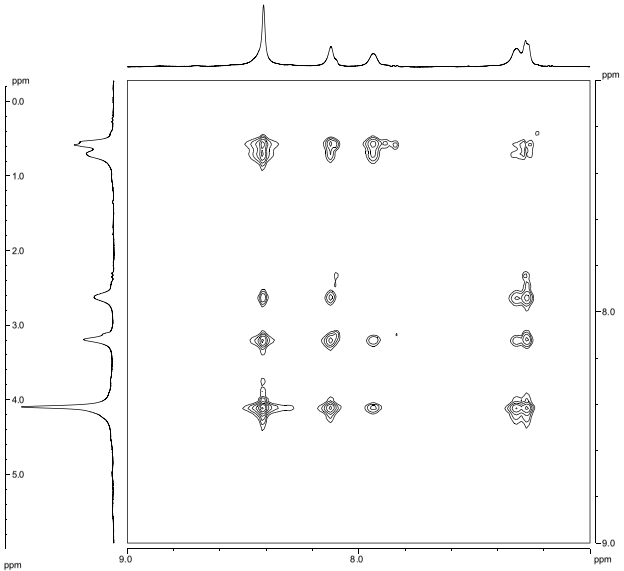

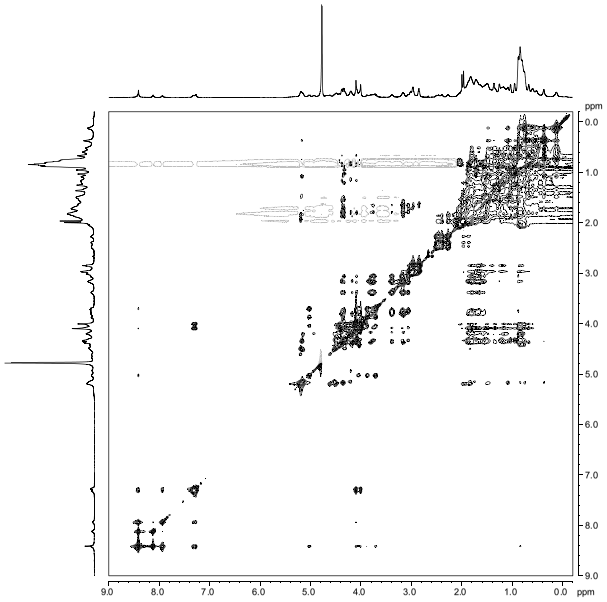

4.0 mM peptide **2.1b** + 4.0 mM *ent*-**2.1b**
in D_2O, 200-ms mixing time, 298 K
600 MHz NOESY spectrum
presaturation suppression of the HOD peak

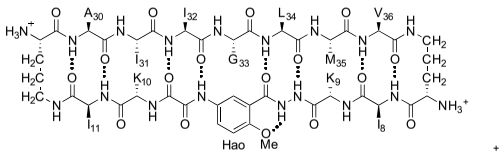

peptide **2.1b**

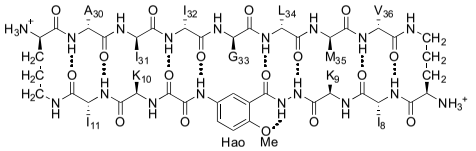

ent-**2.1b**

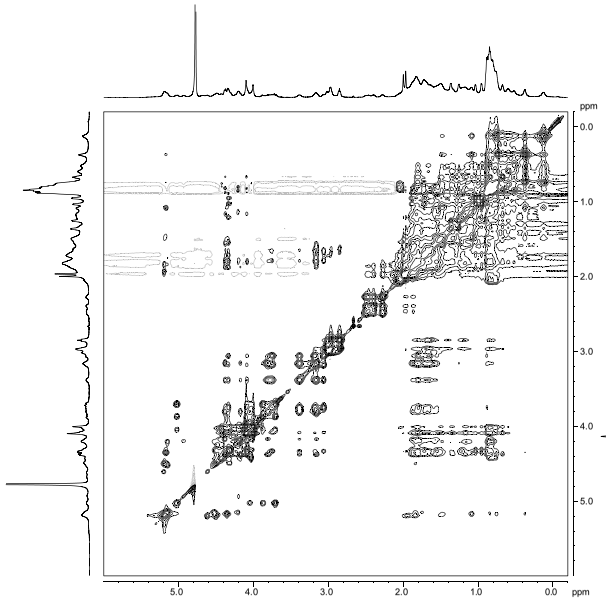

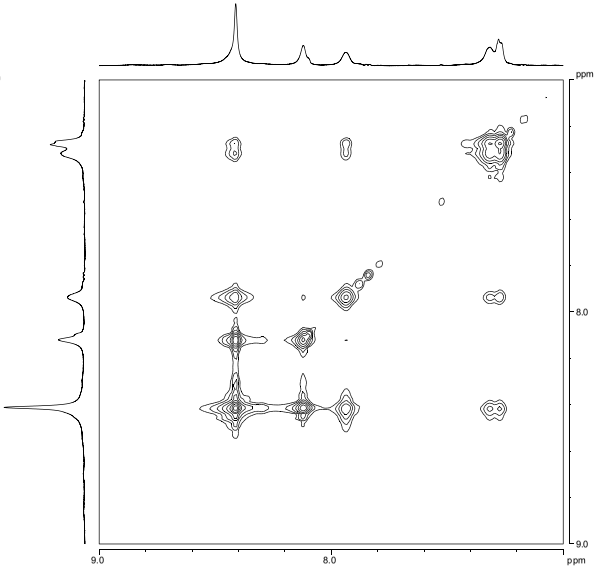

Characterization of peptide ***2.1a***

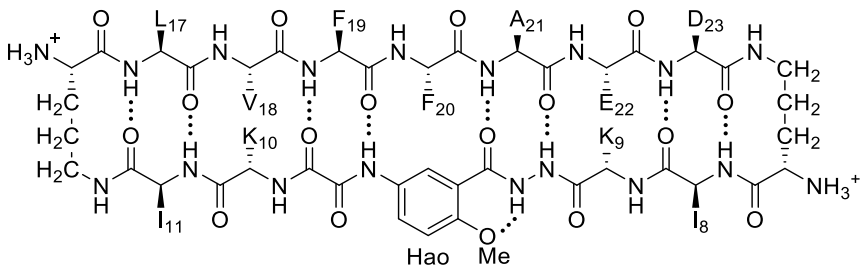

peptide **2.1a**

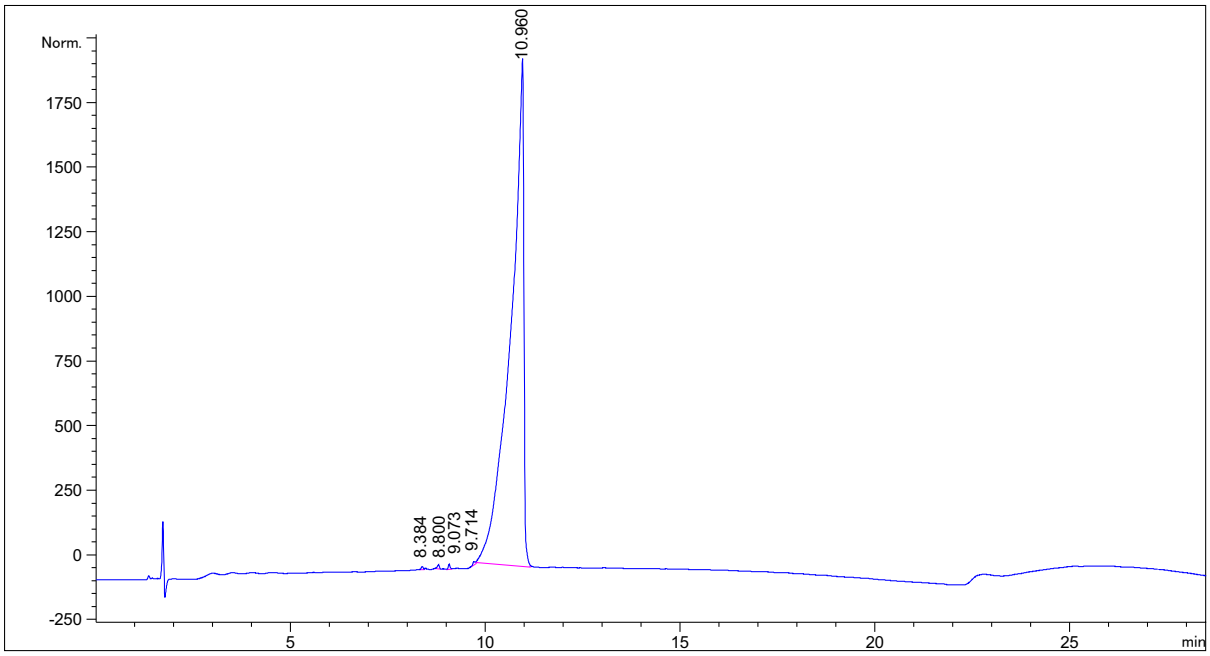

Signal 1: MWD1 A, Sig=214,4 Ref=off

Peak #	RetTime [min]	Type	Width [min]	Area [mAU*s]	Height [mAU]	Area %
1	8.384	MM	0.0569	40.10479	11.75607	0.0964
2	8.800	MM	0.0592	49.23368	13.86946	0.1183
3	9.073	MM	0.0552	59.23932	17.88090	0.1423
4	9.714	MM	0.0729	53.46276	12.22763	0.1285
5	10.960	MM	0.3892	4.14158e4	1773.62488	99.5145

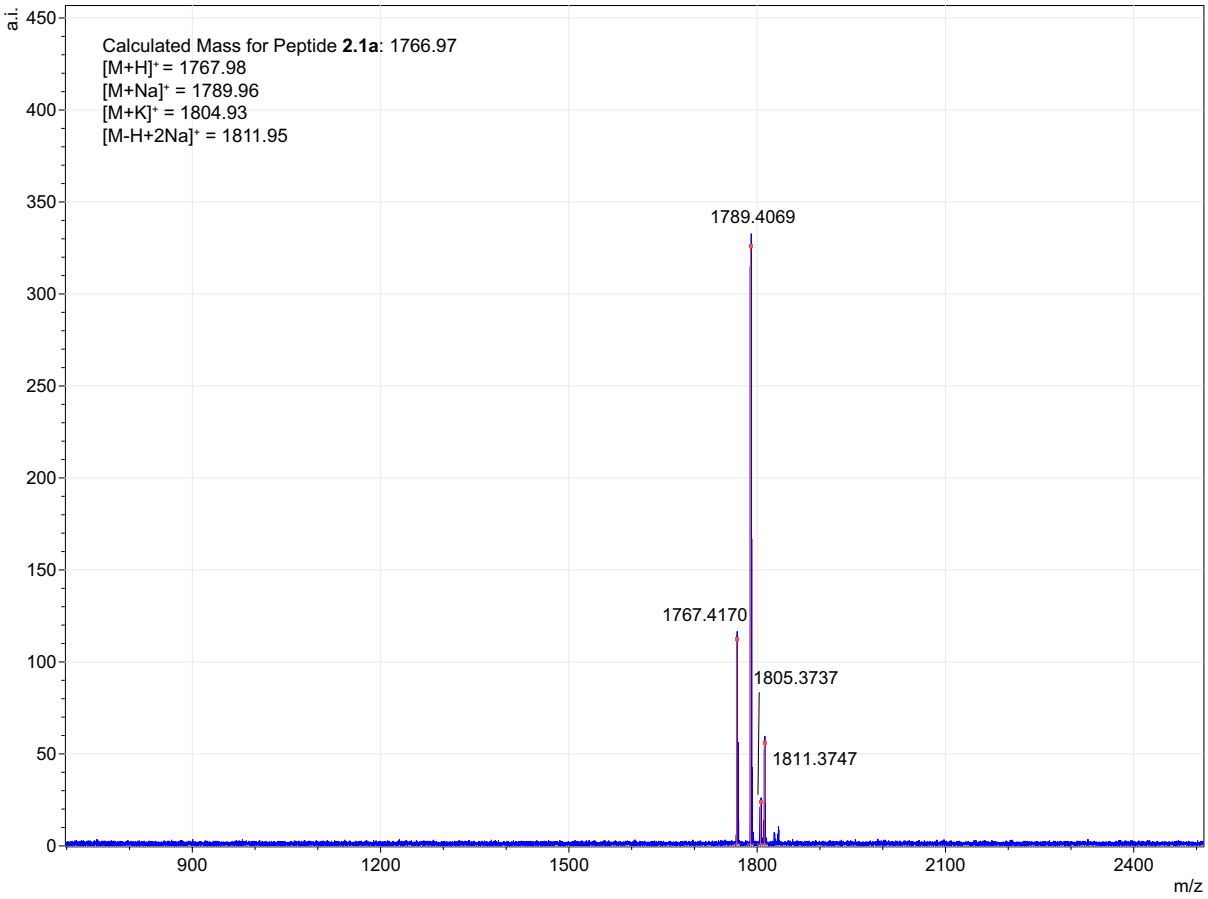
Calculated Mass for Peptide **2.1a**: 1766.97
[M+H]+ = 1767.98
[M+Na]+ = 1789.96
[M+K]+ = 1804.93
[M-H+2Na]+ = 1811.95
1789.4069
1767.4170
1805.3737
1811.3747
a.i.
m/z

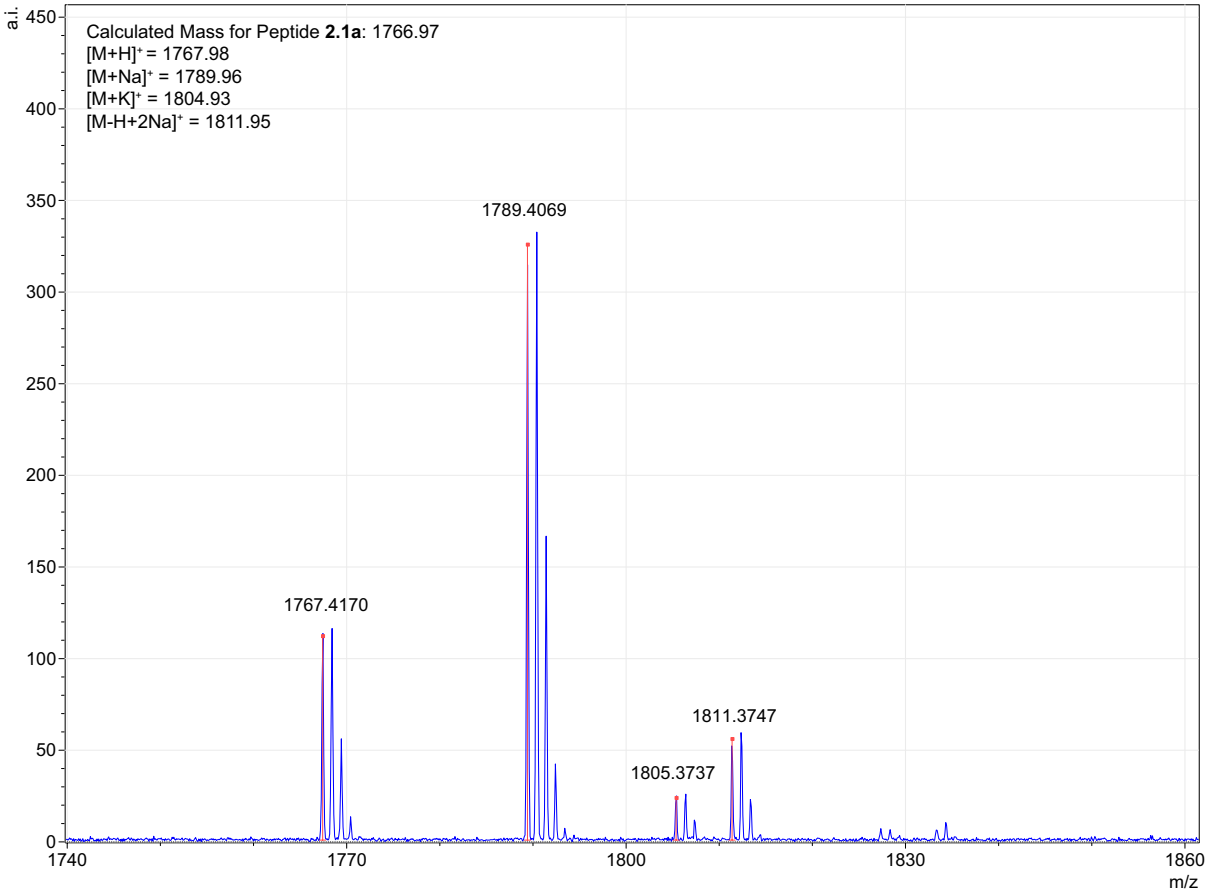
Calculated Mass for Peptide **2.1a**: 1766.97
[M+H]+ = 1767.98
[M+Na]+ = 1789.96
[M+K]+ = 1804.93
[M-H+2Na]+ = 1811.95
1789.4069
1767.4170
1811.3747
1805.3737
a.i.
m/z

Characterization of peptide ent-***2.1a***

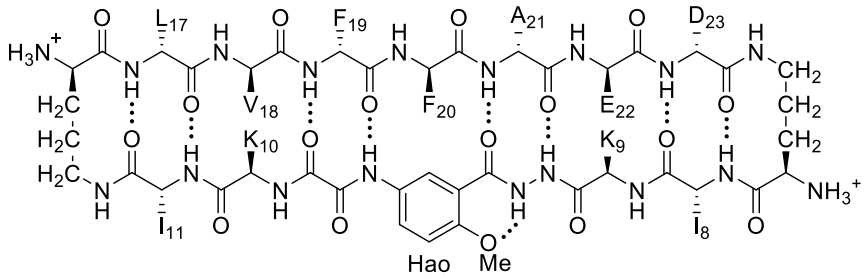

***ent*-2.1a**

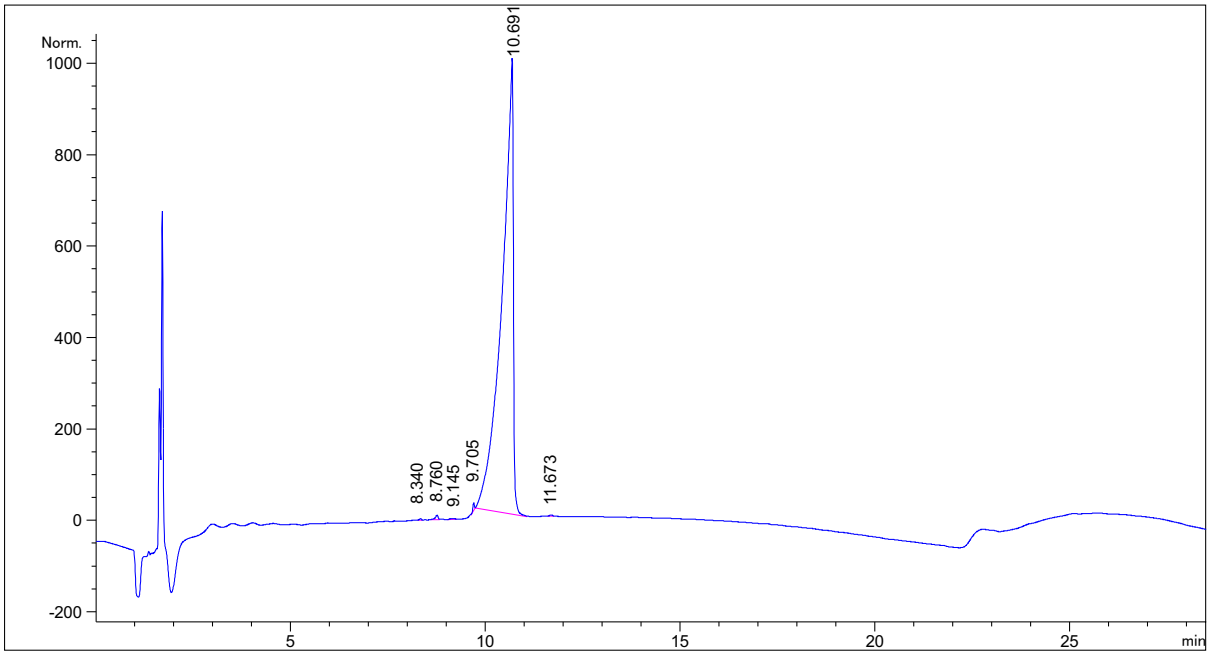

Signal 1: MWD1 A, Sig=214,4 Ref=off

Peak #	RetTime [min]	Type	Width [min]	Area [mAU*s]	Height [mAU]	Area %
1	8.340	MM	0.0577	11.30358	3.26538	0.0616
2	8.760	MM	0.0800	41.89858	8.72646	0.2282
3	9.145	MM	0.1498	17.51583	1.94829	0.0954
4	9.705	MM	0.0430	39.48652	15.31090	0.2150
5	10.691	MM	0.3378	1.82403e4	899.93854	99.3321
6	11.673	MM	0.0801	12.43770	2.58835	0.0677

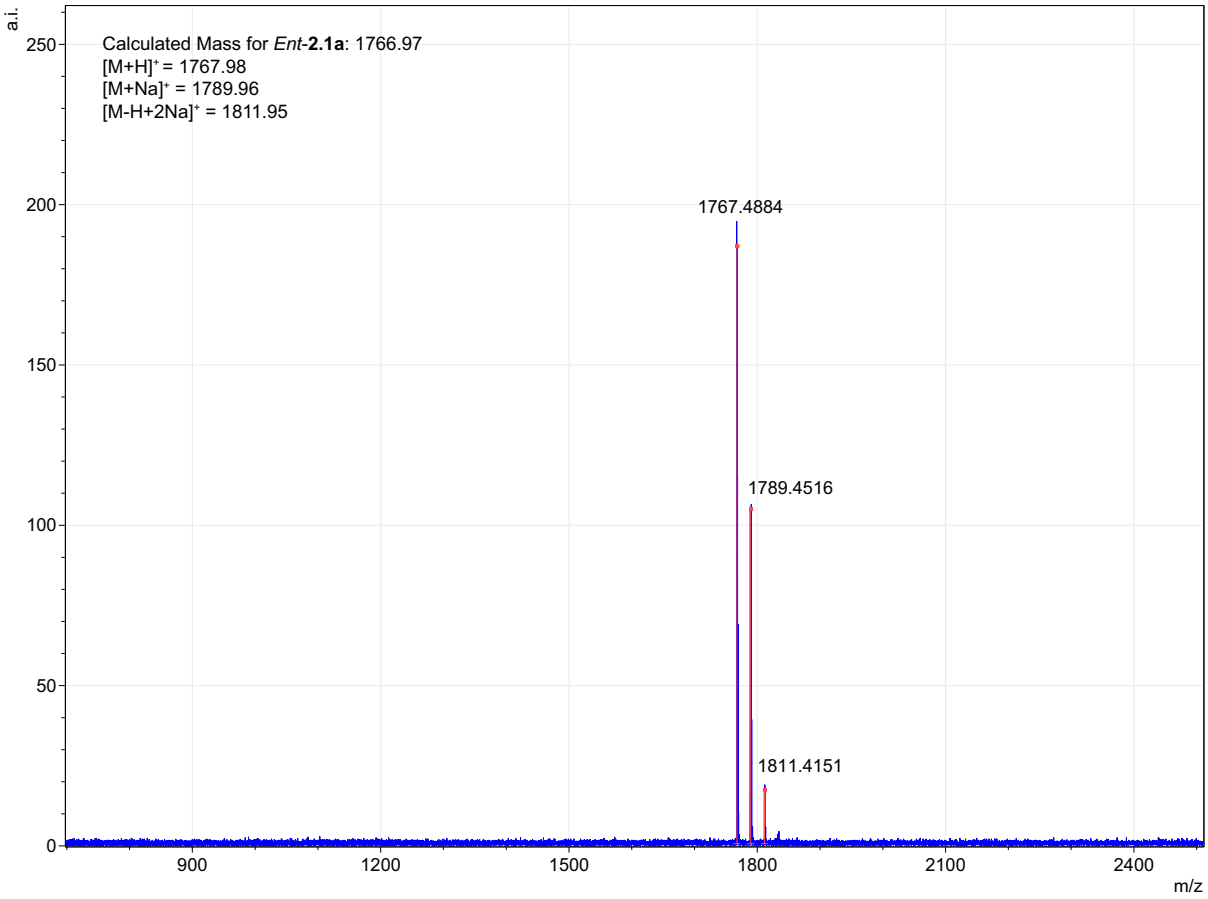
a.i.
Calculated Mass for *Ent*-**2.1a**: 1766.97
[M+H]+ = 1767.98
[M+Na]+ = 1789.96
[M-H+2Na]+ = 1811.95
1767.4884
1789.4516
1811.4151
250
200
150
100
50
0
900
1200
1500
1800
2100
2400
m/z

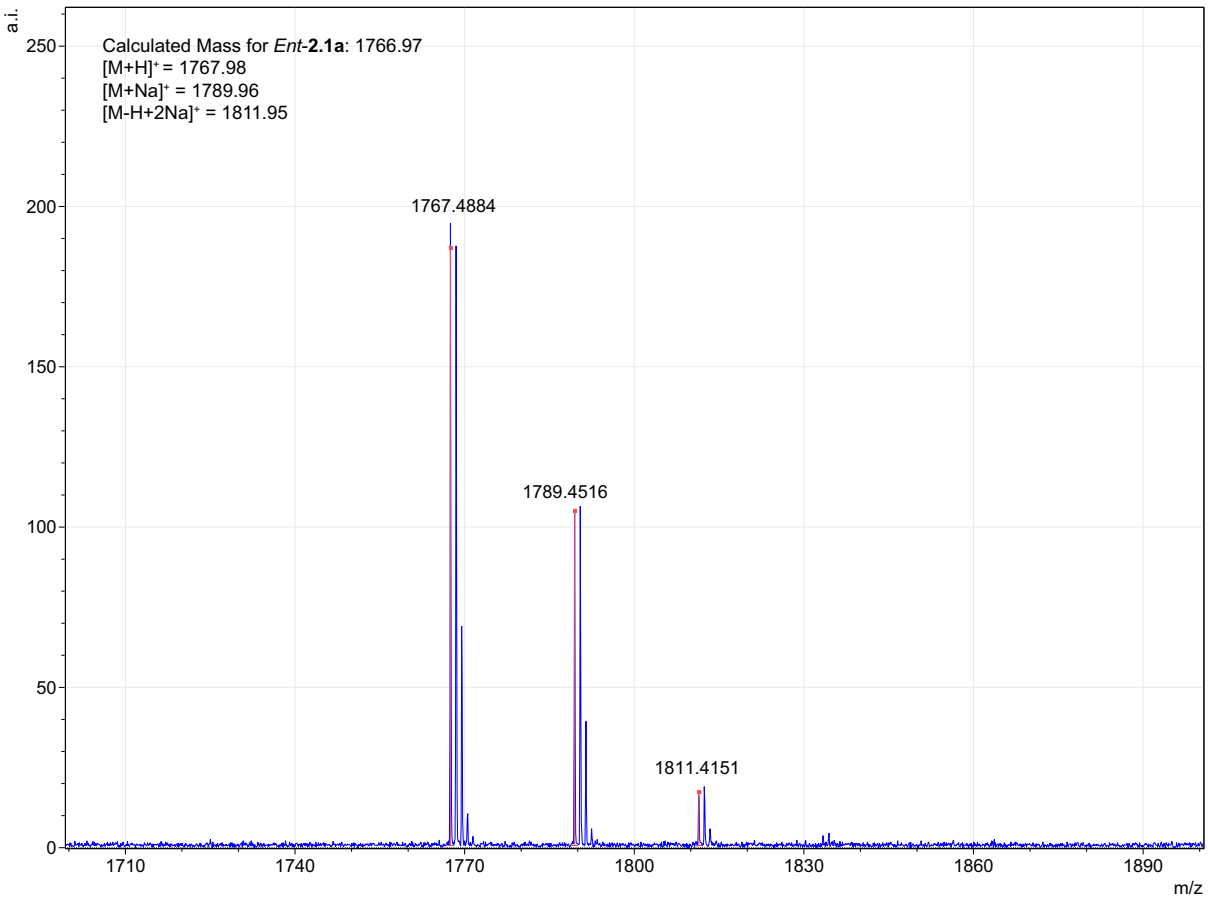
a.i.
Calculated Mass for *Ent*-**2.1a**: 1766.97
[M+H]+ = 1767.98
[M+Na]+ = 1789.96
[M-H+2Na]+ = 1811.95
1767.4884
1789.4516
1811.4151
250
200
150
100
50
0
1710
1740
1770
1800
1830
1860
1890
m/z

Characterization of peptide ***2.2a***

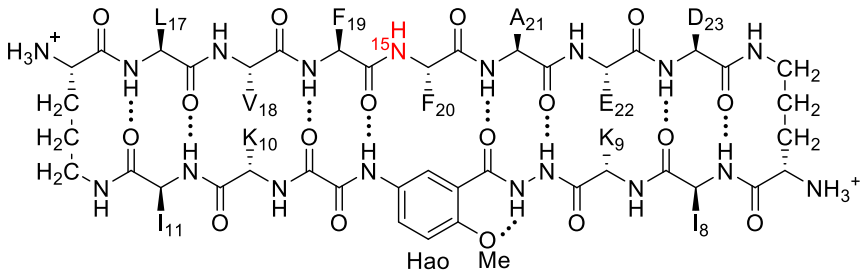

peptide **2.2a**

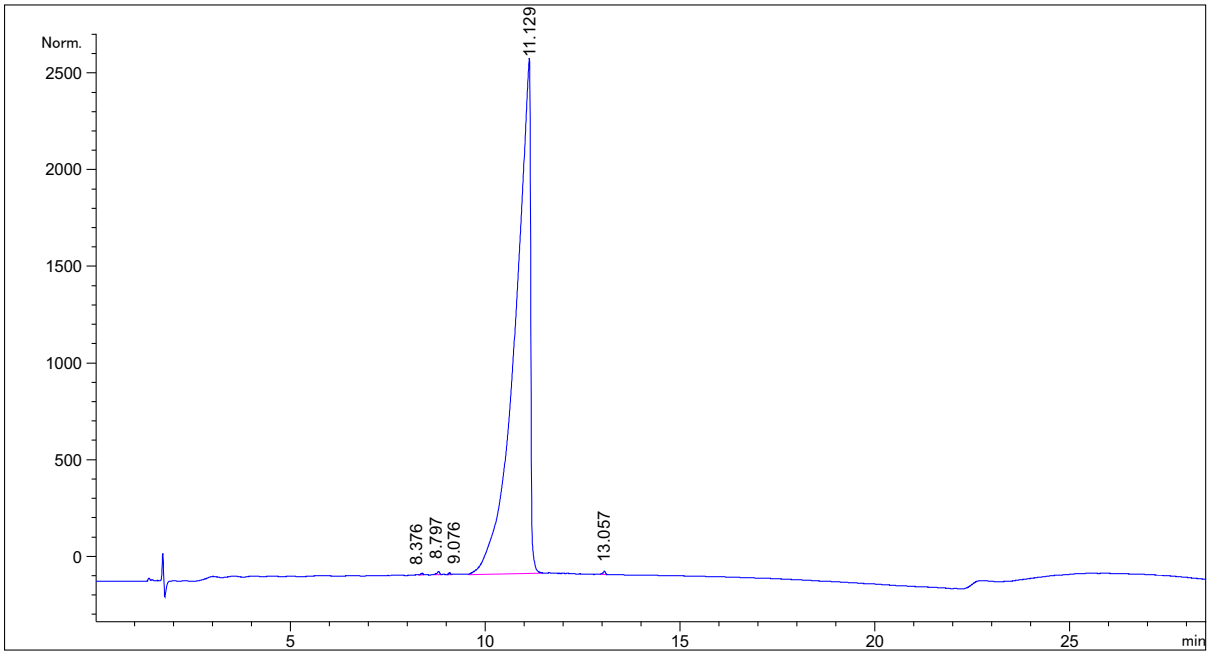

Signal 1: MWD1 A, Sig=214,4 Ref=off

Peak #	RetTime [min]	Type	Width [min]	Area [mAU*s]	Height [mAU]	Area %
1	8.376	MM	0.0707	34.15193	8.05459	0.0514
2	8.797	MM	0.0726	60.69348	13.94270	0.0914
3	9.076	MM	0.0597	32.12604	8.97329	0.0484
4	11.129	MM	0.4589	6.62052e4	2404.37671	99.7111
5	13.057	MM	0.0704	64.87210	15.35158	0.0977

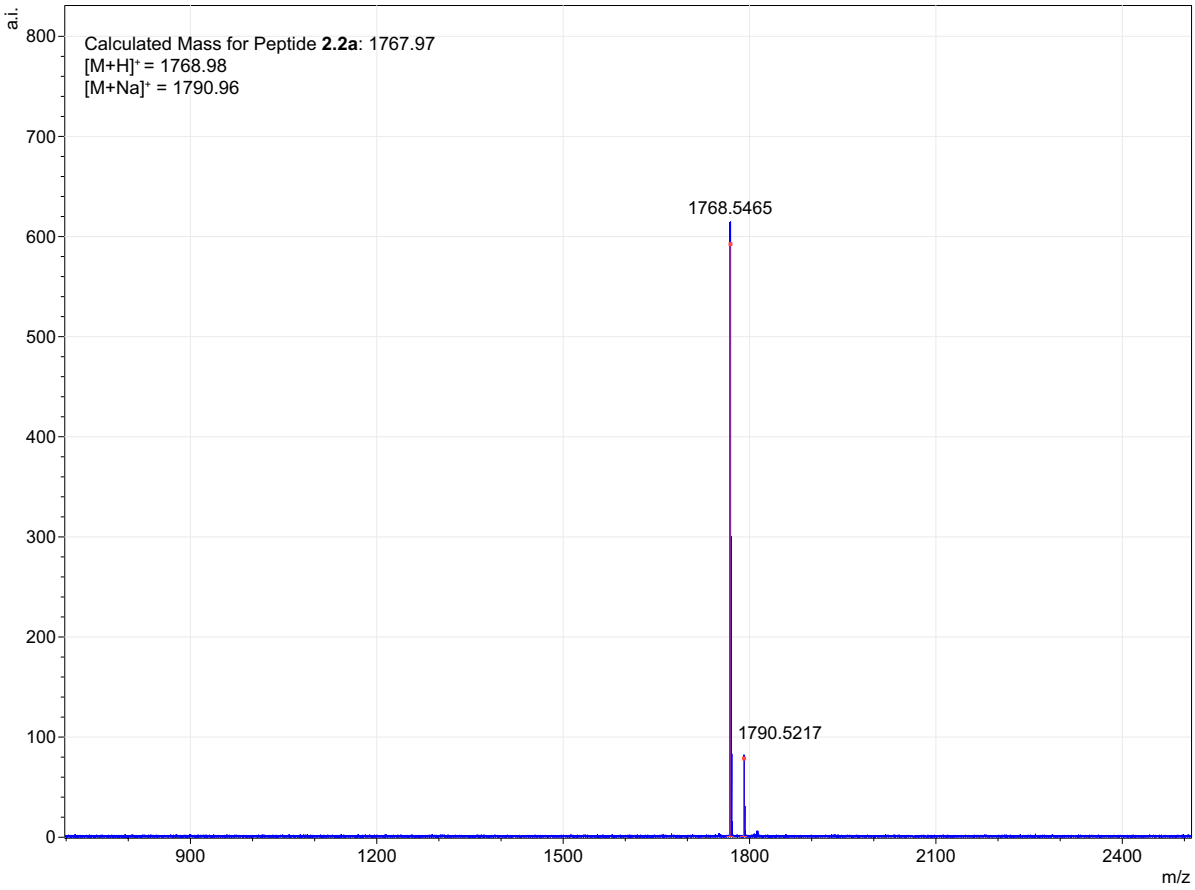
Calculated Mass for Peptide **2.2a**: 1767.97
[M+H]+ = 1768.98
[M+Na]+ = 1790.96
1768.5465
1790.5217
a.i.
m/z

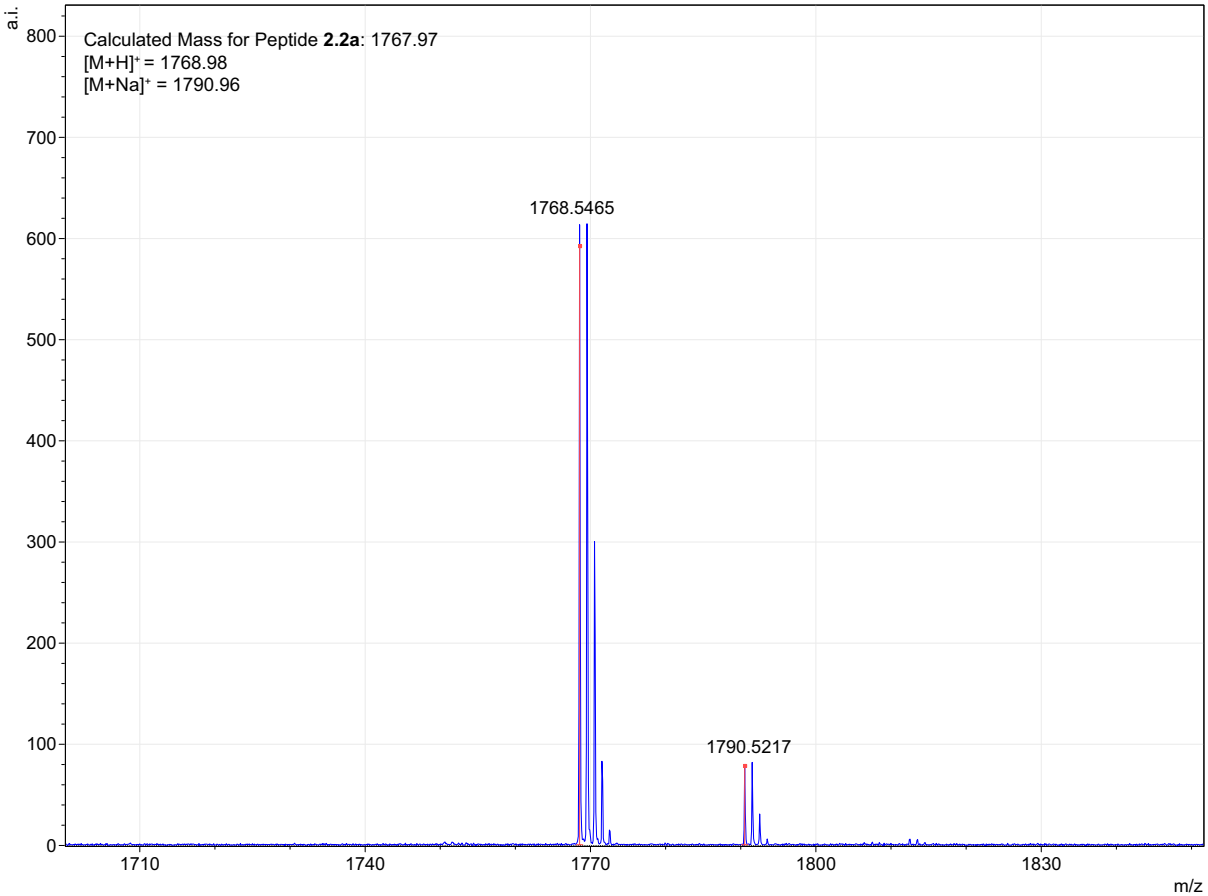
Calculated Mass for Peptide **2.2a**: 1767.97
[M+H]+ = 1768.98
[M+Na]+ = 1790.96
1768.5465
1790.5217
a.i.
m/z

*Characterization of peptide **2.3a***

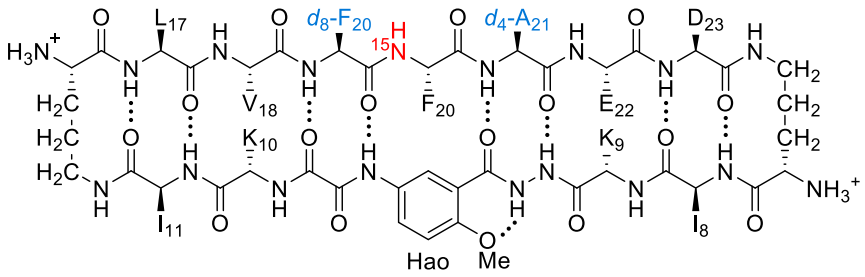

peptide **2.3a**

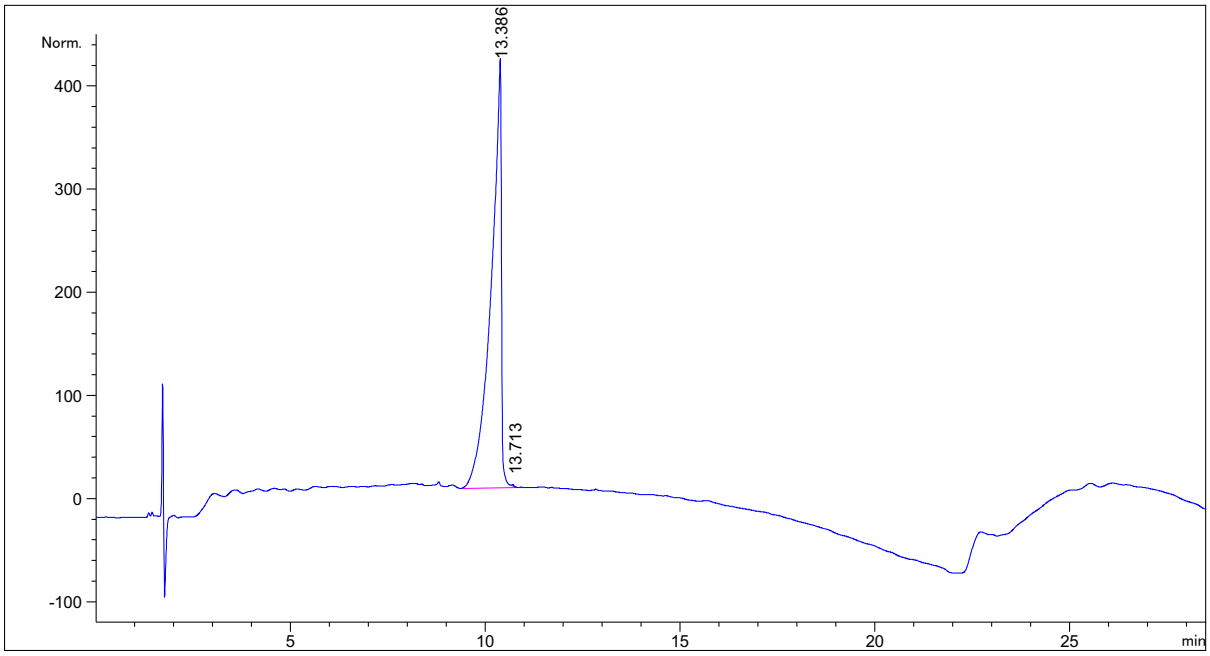

Signal 1: MWD1 A, Sig=214,4 Ref=off

Peak #	RetTime [min]	Type	Width [min]	Area [mAU*s]	Height [mAU]	Area %
1	10.386	MM R	0.3037	6846.85889	375.73801	99.9235
2	10.713	MM T	0.0610	5.23864	1.43016	0.0765

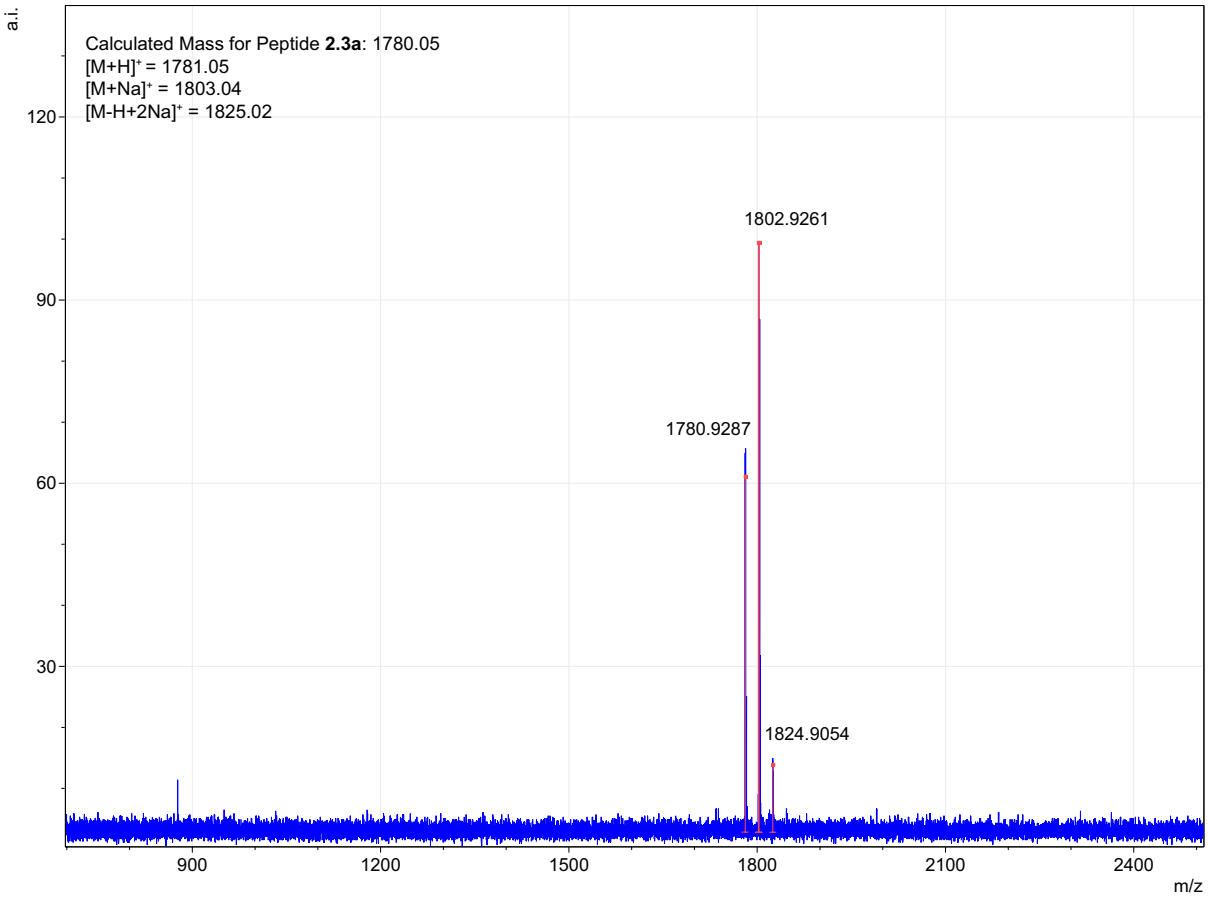
a.i.
Calculated Mass for Peptide **2.3a**: 1780.05
[M+H]+ = 1781.05
[M+Na]+ = 1803.04
[M-H+2Na]+ = 1825.02
120
90
60
30
1802.9261
1780.9287
1824.9054
900
1200
1500
1800
2100
2400
m/z

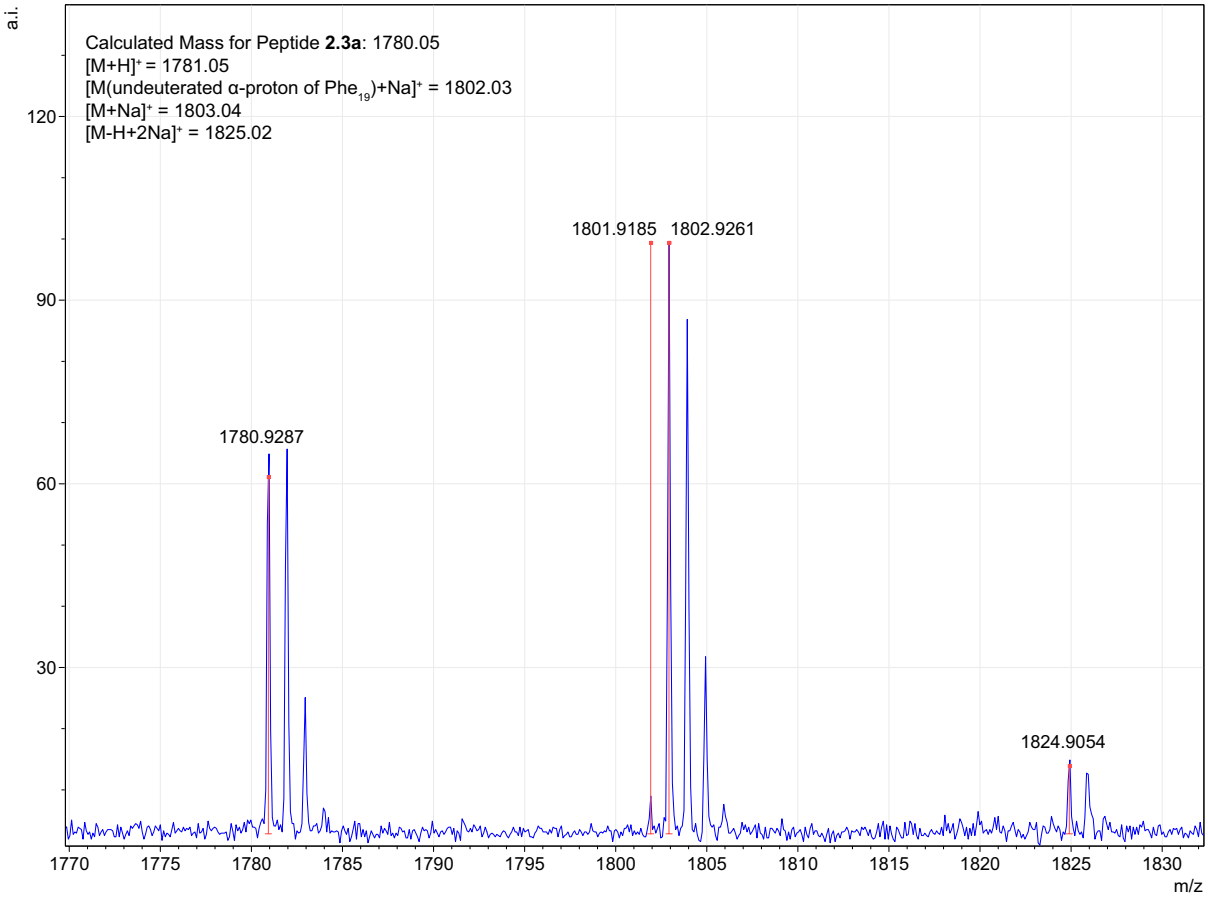
a.i.
Calculated Mass for Peptide **2.3a**: 1780.05
[M+H]+ = 1781.05
[M(undeuterated α-proton of Phe19)+Na]+ = 1802.03
[M+Na]+ = 1803.04
[M-H+2Na]+ = 1825.02
120
90
60
30
1801.9185
1802.9261
1780.9287
1824.9054
1770
1775
1780
1785
1790
1795
1800
1805
1810
1815
1820
1825
1830
m/z

Characterization of peptide ***2.1b***

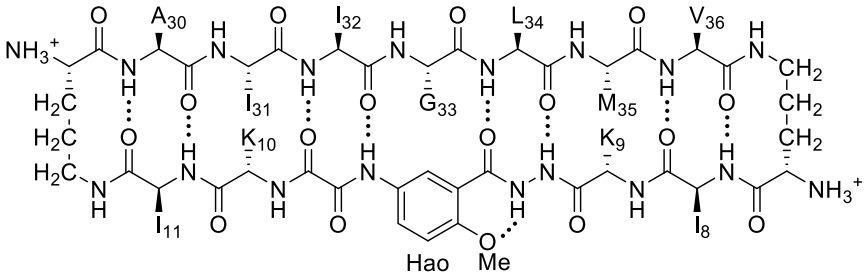

peptide **2.1b**

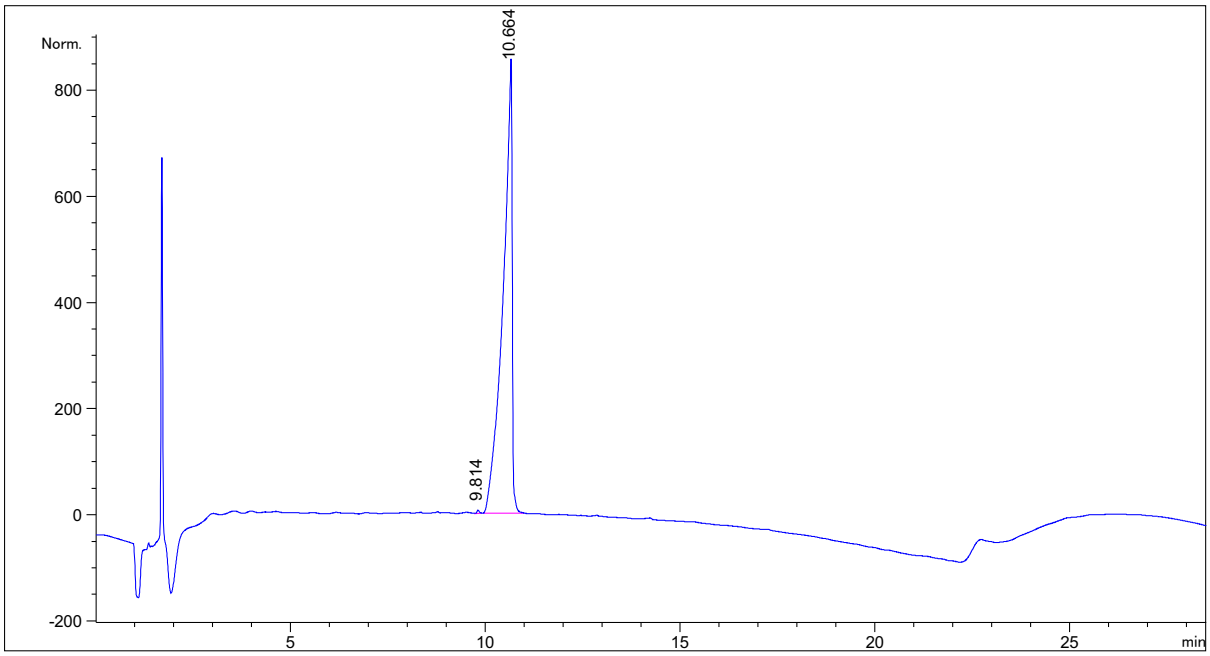

Signal 1: MWD1 A, Sig=214,4 Ref=off

Peak #	RetTime [min]	Type	Width [min]	Area [mAU*s]	Height [mAU]	Area %
1	9.814	MM	0.0699	23.07438	5.50104	0.1828
2	10.664	MM	0.2712	1.26018e4	774.44647	99.8172

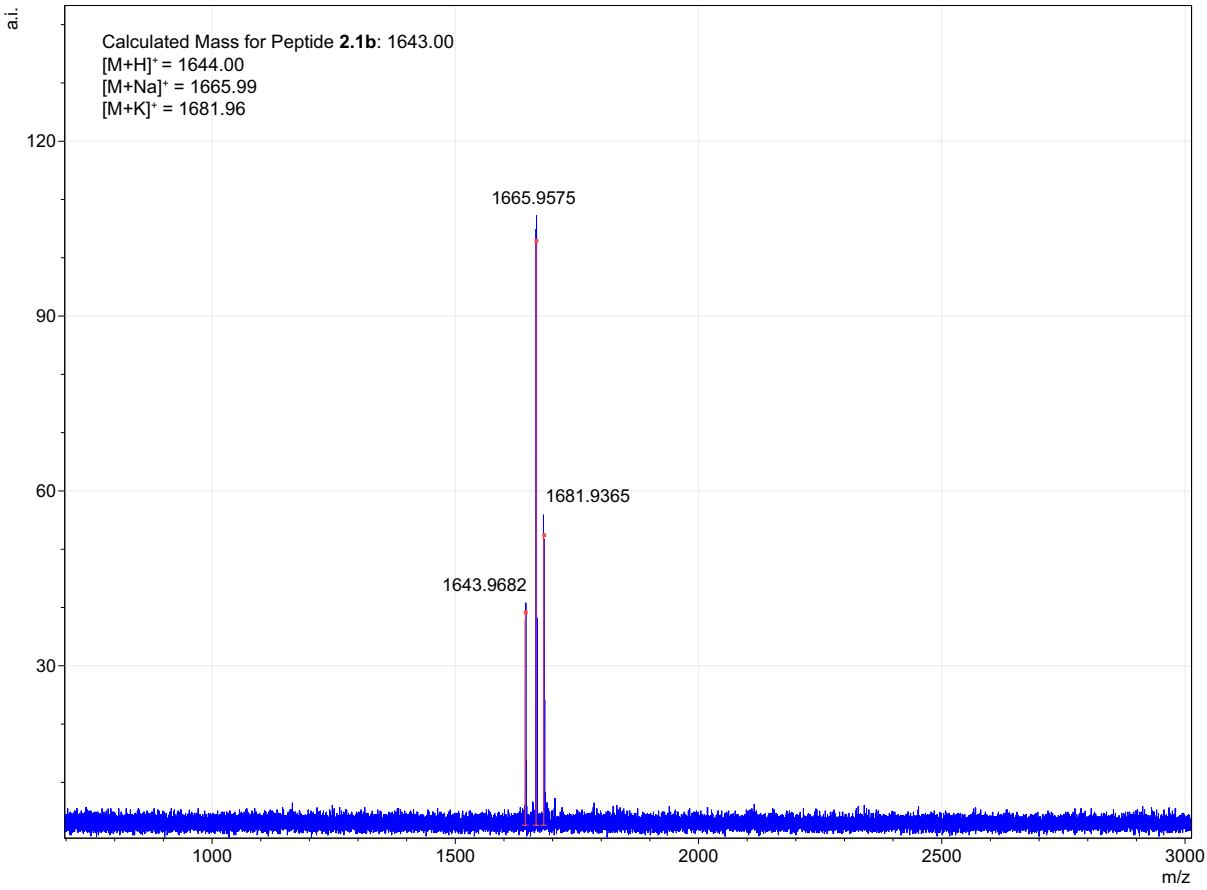
a.i.
Calculated Mass for Peptide **2.1b**: 1643.00
[M+H]+ = 1644.00
[M+Na]+ = 1665.99
[M+K]+ = 1681.96
120
90
60
30
1665.9575
1681.9365
1643.9682
1000
1500
2000
2500
3000
m/z

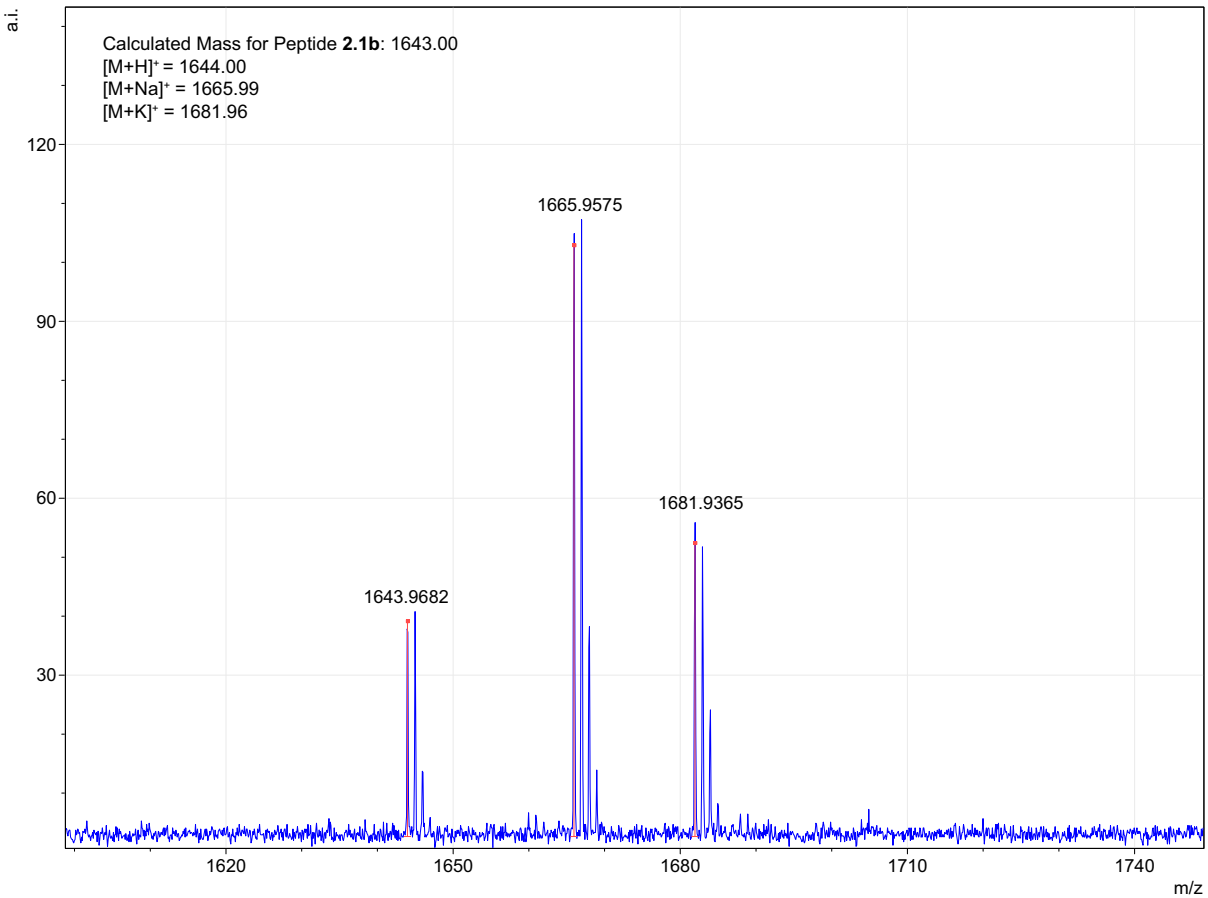
a.i.
Calculated Mass for Peptide **2.1b**: 1643.00
[M+H]+ = 1644.00
[M+Na]+ = 1665.99
[M+K]+ = 1681.96
120
90
60
30
1665.9575
1681.9365
1643.9682
1620
1650
1680
1710
1740
m/z

Characterization of peptide ent-***2.1b***

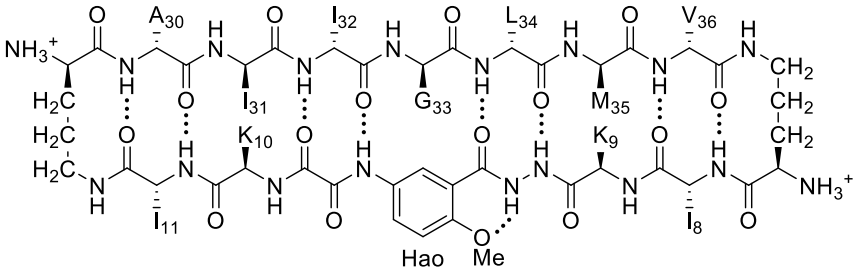

***ent*-2.1b**

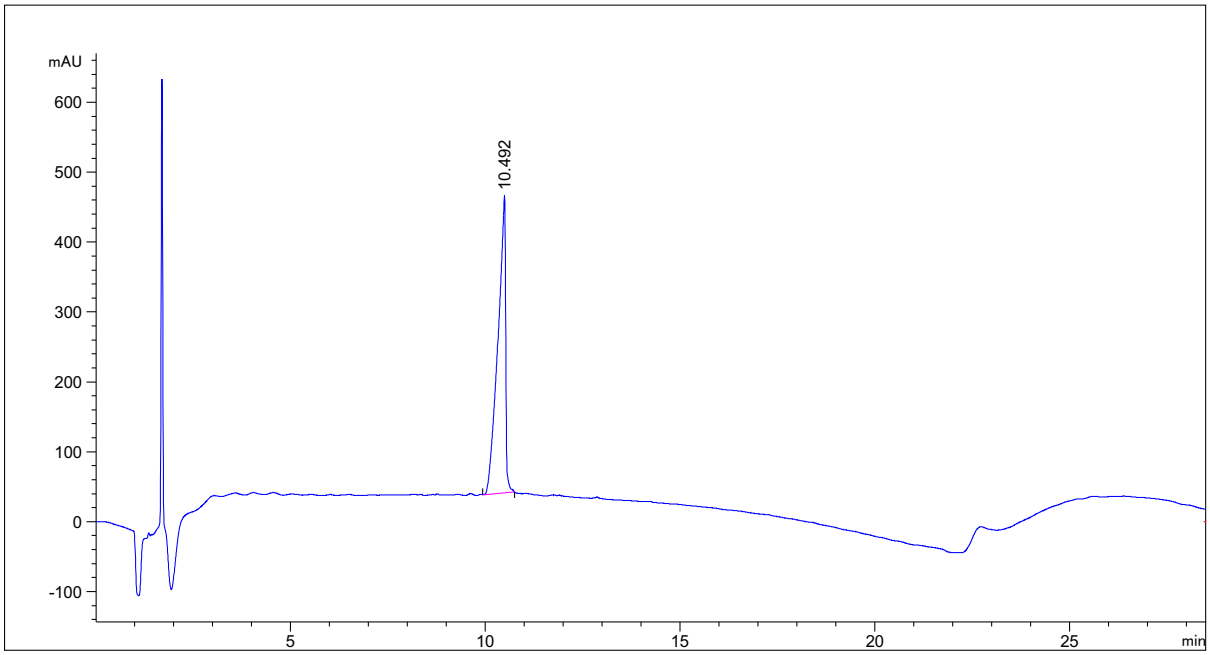

Signal 1: MWD1 A, Sig=214,4 Ref=off

Peak #	RetTime [min]	Type	Width [min]	Area [mAU*s]	Height [mAU]	Area %
1	10.492	MM	0.2310	5919.69141	427.04166	100.0000

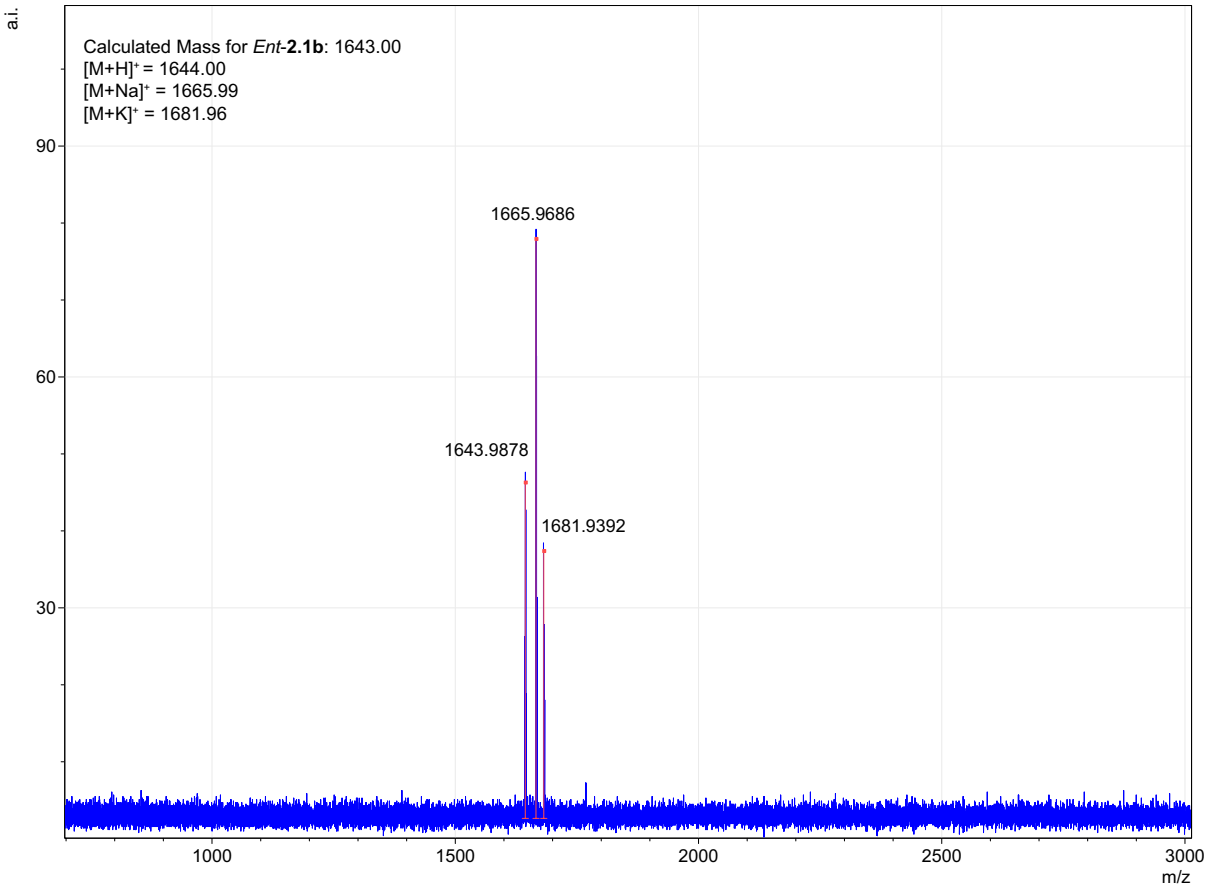
a.i.
Calculated Mass for *Ent*-**2.1b**: 1643.00
[M+H]+ = 1644.00
[M+Na]+ = 1665.99
[M+K]+ = 1681.96
90
60
30
1665.9686
1643.9878
1681.9392
1000
1500
2000
2500
3000
m/z

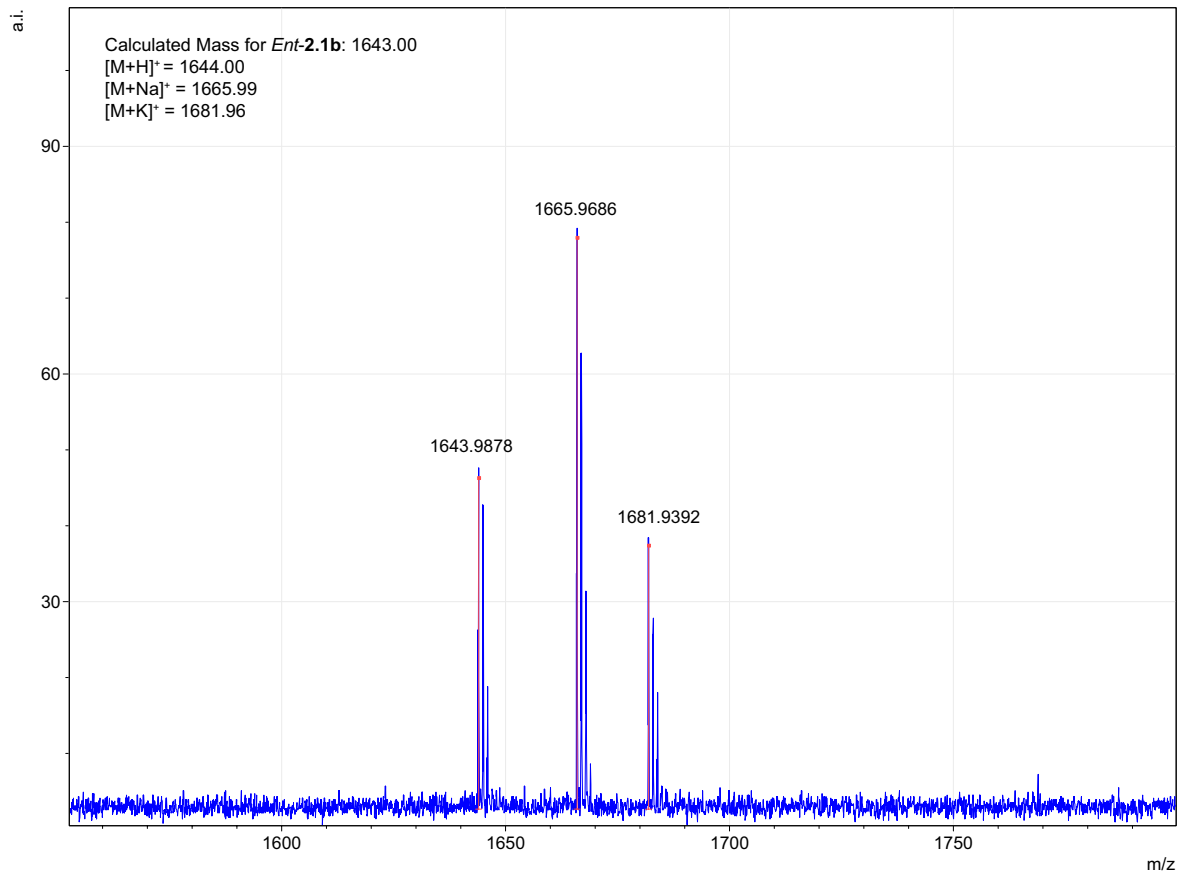
a.i.
Calculated Mass for *Ent*-**2.1b**: 1643.00
[M+H]+ = 1644.00
[M+Na]+ = 1665.99
[M+K]+ = 1681.96
90
60
30
1665.9686
1643.9878
1681.9392
1600
1650
1700
1750
m/z

Characterization of peptide ***2.2b***

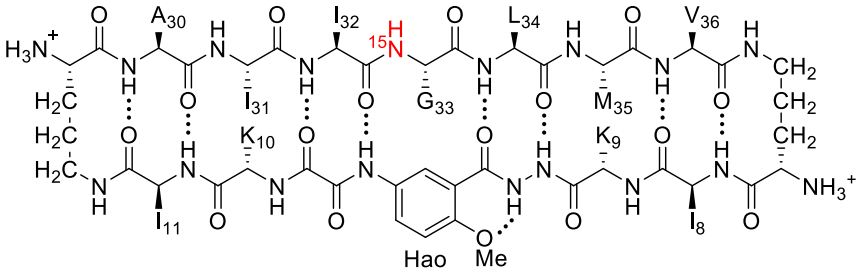

peptide **2.2b**

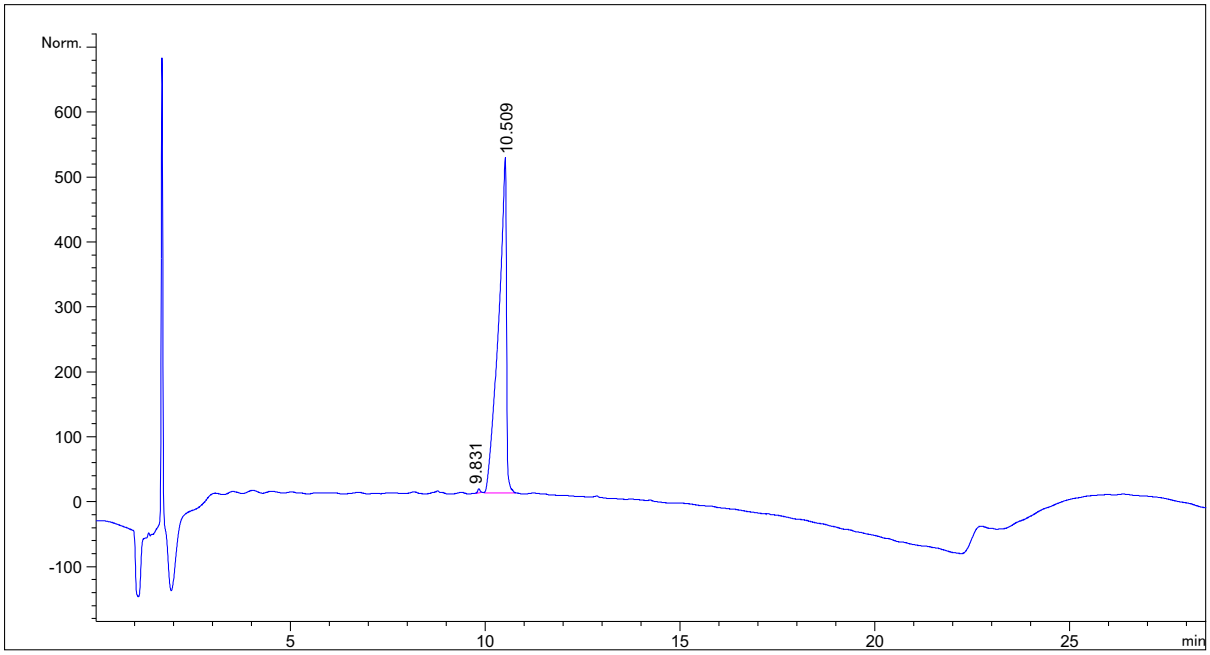

Signal 1: MWD1 A, Sig=214,4 Ref=off

Peak #	RetTime [min]	Type	Width [min]	Area [mAU*s]	Height [mAU]	Area %
1	9.831	MM	0.0704	25.07612	5.94035	0.3799
2	10.509	MM	0.2349	6576.07031	466.65961	99.6201

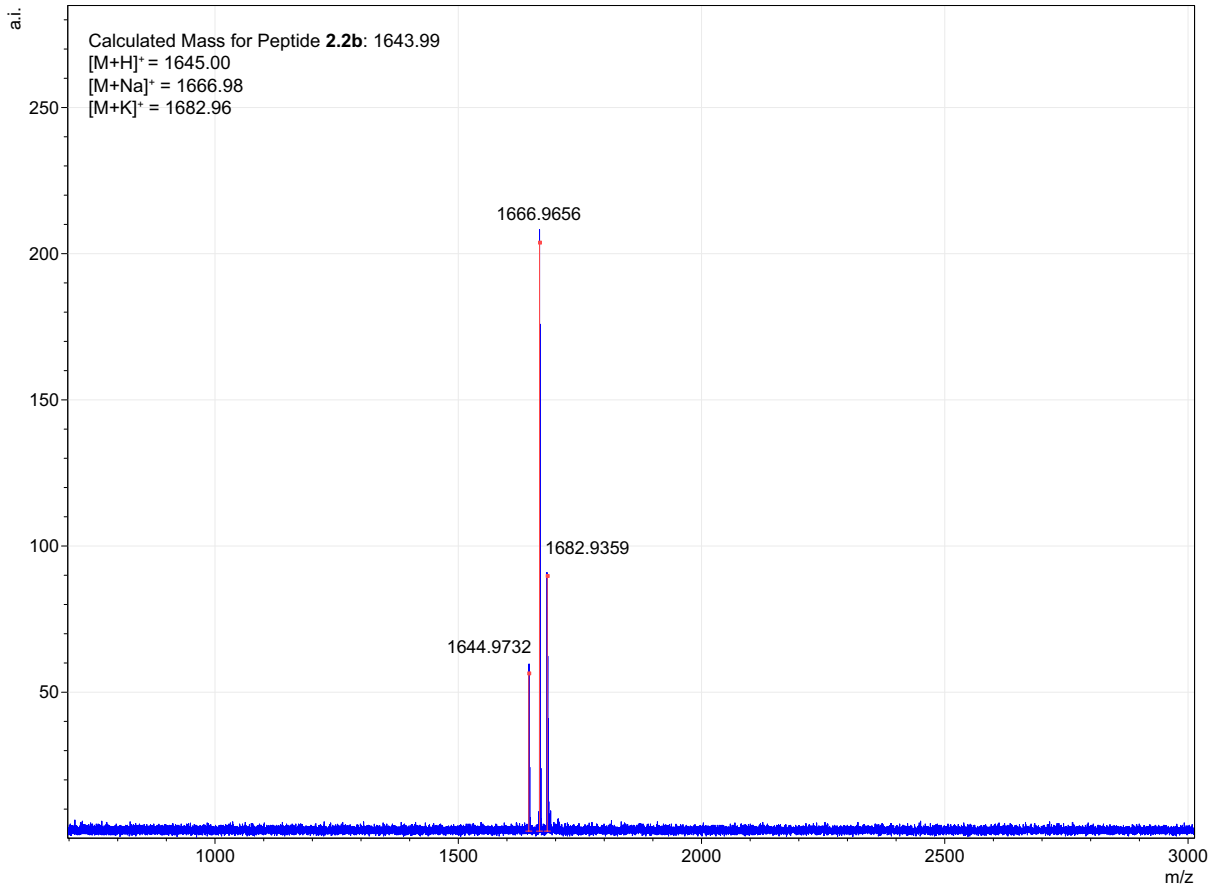
a.i.
Calculated Mass for Peptide **2.2b**: 1643.99
[M+H]+ = 1645.00
[M+Na]+ = 1666.98
[M+K]+ = 1682.96
1666.9656
1682.9359
1644.9732
250
200
150
100
50
1000
1500
2000
2500
3000
m/z

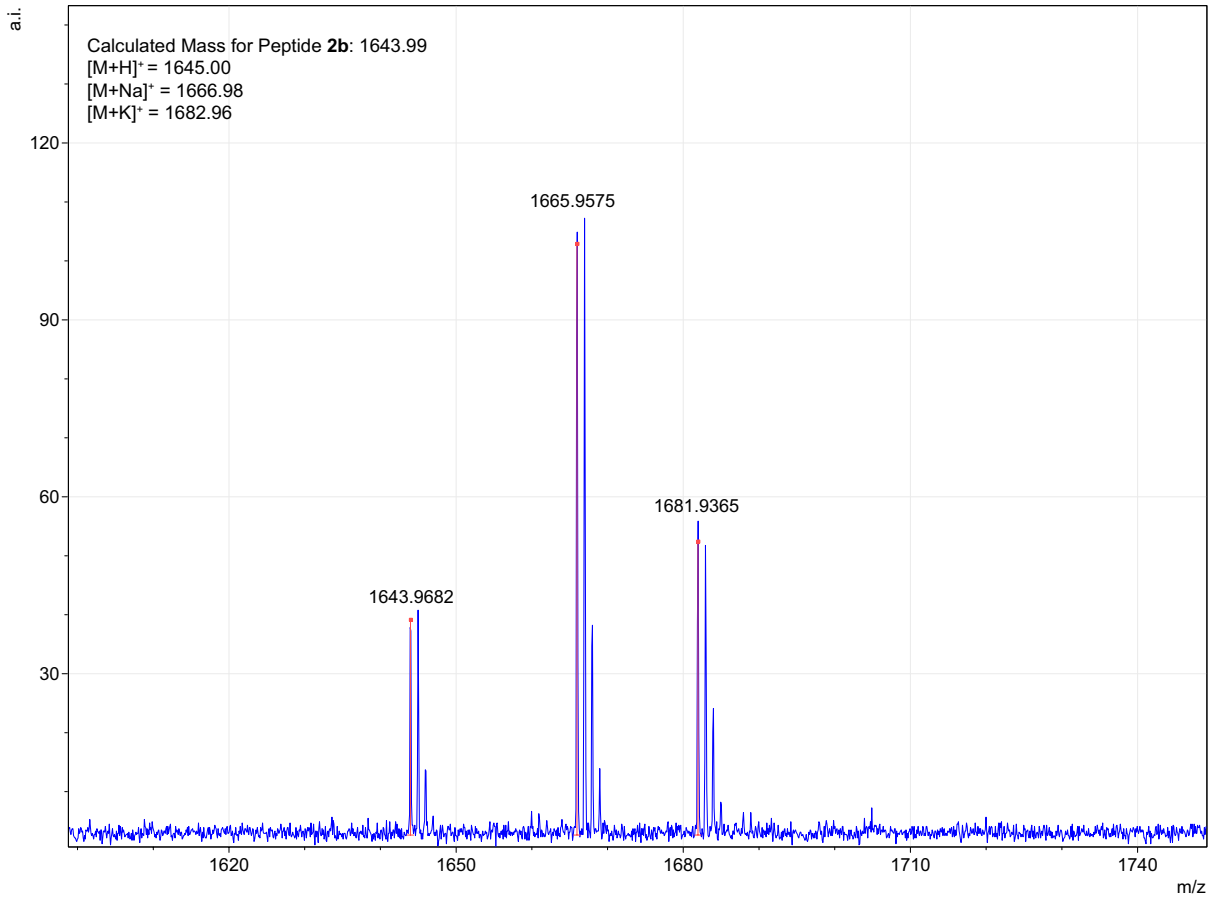
a.i.
Calculated Mass for Peptide **2b**: 1643.99
[M+H]+ = 1645.00
[M+Na]+ = 1666.98
[M+K]+ = 1682.96
1665.9575
1681.9365
1643.9682
120
90
60
30
1620
1650
1680
1710
1740
m/z

CHAPTER 3

Synthesis and Stereochemical Determination of Novo29, a New Peptide Antibiotic

Preface to Chapter 3

Chapter 3 describes a collaborative project that I had the fortune of working on with my colleague, Maj Krumberger. This chapter introduces a recently reported peptide antibiotic, Novo29, and details our efforts toward determining its stereochemistry through chemical synthesis, NMR spectroscopy, and functional assay correlation. Together, we designed and executed the syntheses of Fmoc-(*2R,3R*)-hydroxyasparagine-OH and Fmoc-(*2R,3S*)-hydroxyasparagine-OH amino acids, which enabled us to synthesize and evaluate Novo29 and *epi*-Novo29 compared to the natural product.

The work presented in Chapter 3 builds upon my prior experience in noncanonical amino acid synthesis, but also provides a direct application toward investigating a potential drug candidate. To delineate contributions, I will primarily focus on the chemical synthesis of the Fmoc-(*2R,3S*)-hydroxyasparagine-OH amino acid, followed by its incorporation into *epi*-Novo29. This chapter will also present my work on the downstream characterizations of natural and synthetic Novo29 homologues by ^{1}H NMR, 2D TOCSY and NOESY studies, minimum inhibitory concentration (MIC)

assays, and contributions on obtaining the X-ray crystallographic structure of the *epi*-Novo29.

I am very thankful that I had the opportunity to work on the synthesis and stereochemical determination of Novo29. The work began as a secondary passion project, but in less than 7 months, we were able to successfully synthesize and determine the stereochemistry of Novo29. I would like to thank Maj Krumberger for his contributions on the chemical synthesis, Adam Kreutzer for his expertise on solving the crystal structure, Chelsea Jones for her guidance on performing MIC experiments, and Novobiotic Pharmaceuticals for providing us with knowledge on the discovery of Novo29.

The introduction of Chapter 3 dives directly into Novo29, a new peptide antibiotic that was discovered by Novobiotic Pharmaceuticals, and why we should be interested in antibiotics with new mechanisms of action. The introduction also briefly highlights two related peptides, teixobactin and hypeptin, both of which share structural and binding similarities to Novo29. The results and discussion describe the syntheses of (*2R,3R*)- and (*2R,3S*)-hydroxyasparagine, with my contributions involved in the latter. Both amino acids were used to synthesize the Novo29 sequence, and the stereochemistry was determined by comparing to the natural product using NMR spectroscopy and functional assay correlations. Chapter 3 finishes with an X-ray crystallographic structure of the *epi*-Novo29, and future directions on how the structure can be used as a guide for modelling the natural product.

INTRODUCTION

New antibiotics are desperately needed to fight the growing threat of antibiotic-resistant pathogens. The discovery and introduction of antibiotics as medicines in the 20th century ushered in a wave of effective strategies to fight against infectious pathogens – targeting different parts of bacteria through unique mechanisms of action.[1] However, overuse of these early antibiotics has since led to the rapid increase in antibiotic resistance beginning in the latter half of the 20th century. In 2019, CDC reported that antibiotic-resistant bacteria are responsible for over 2.8 million infections, and 35,000 deaths annually in the US. Gram-positive bacteria cause more than 54 % of these illnesses and 60 % of these deaths.[2] As new resistance mechanisms continue to emerge – and the discovery of novel antibiotics continue to dwindle – efforts to find new antibiotics with unique mechanisms of action are desperately needed in order to stay one step ahead against the threat of antibiotic resistant pathogens.[3,4]

In 2015, Lewis and co-workers reported the discovery of teixobactin as a novel antibiotic that kills Gram-positive pathogens without detectable resistance.[5] Teixobactin is an 11-residue depsipeptide containing a macrolactone ring and a linear tail and produced from *E. terrae.* Hypeptin, an 8-residue depsipeptide with similar structural features as teixobactin and isolated from the Gram negative *Lysobacter* sp. K5869 is also active against broad spectrum Gram-positive bacteria.[6,7] Both teixobactin and hypeptin bind to the prenyl-pyrophosphate-saccharide regions of lipid II as their mechanism of action. This region is highly conserved in bacteria, thus making it an

attractive target for drug discovery. However, challenges with gel formation of teixobactin at high concentrations has prevented its introduction into the clinic.[8,9]

Novo29, a new antibiotic from a soil bacterium closely related to *E. terrae* was recently reported.[10,11] Novo29 is active against Gram-positive bacteria and is an eight-residue depsipeptide comprising a macrolactone ring and a linear tail. Although the amino acid sequence of Novo29 has been reported, the unnatural amino acid hydroxyasparagine at position 5 precludes unambiguous stereochemical assignment by Marfey analysis, and NMR spectroscopic analysis of Novo29 did not permit the determination of this residue.

Novo29 is an exciting potential drug candidate because it does not display a propensity to gel at high concentrations, but shares similarities to teixobactin and hypeptin. Novo29 contains a macrolactone ring and linear tail, which resemble structural features of teixobactin and hypeptin. Furthermore, Novo29 and teixobactin were isolated from Gram-negative bacteria with 99% sequence homology to each other. In this current study, we aim to establish the stereochemistry of the hydroxyasparagine residue at position 5 through chemical synthesis and confirm the structure of Novo29 through spectroscopic and functional correlation. We also report the X-ray crystallographic structure of a synthetic epimer of Novo29, which may provide insights into how the natural Novo29 may bind bacterial cell wall precursors.

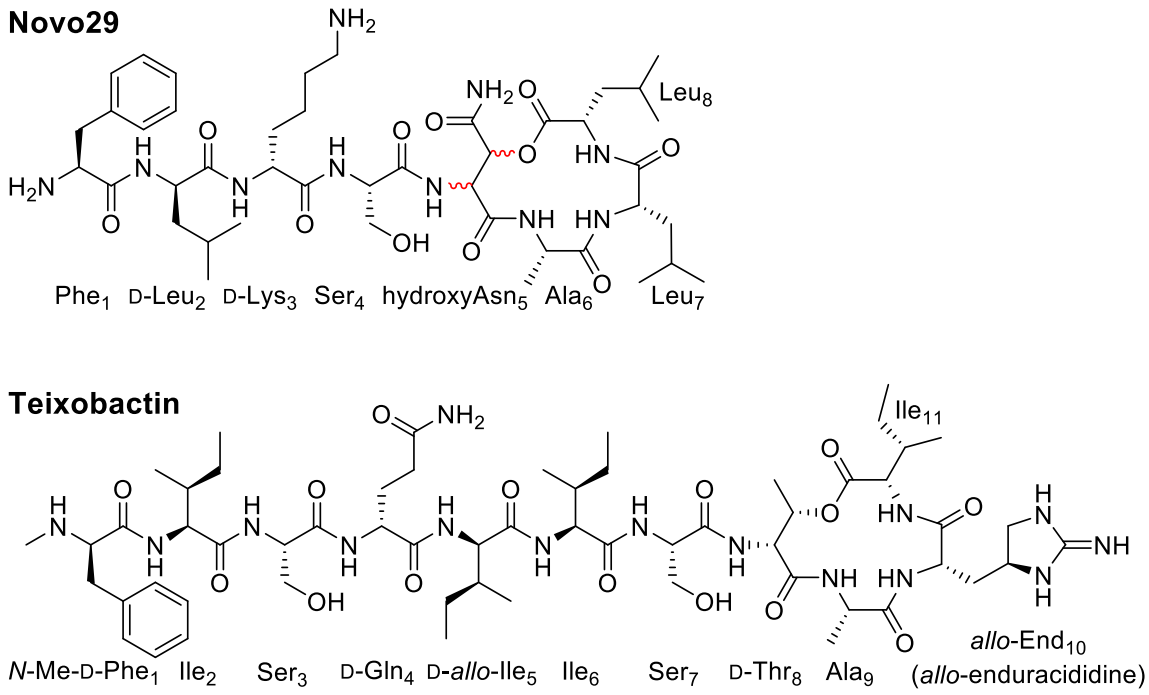

Figure 3.1. Structure of Novo29 and teixobactin. The unassigned stereochemistry of hydroxyasparagine at position 5 of Novo29 is denoted by the red-colored bonds.

RESULTS AND DISCUSSION

We hypothesized the stereochemistry of residue 5 to be (*2R,3R)*-hydroxyasparagine, based on the similarity in structure and connectivity of D-threonine$_8$ in teixobactin. Together with my colleague, Maj Krumberger, we developed and carried out the syntheses of the desired (*2R,3R*)-hydroxyasparagine amino acid, as well as the (*2R,3S*)-hydroxyasparagine amino acid as a control. Both these amino acids would have an Fmoc protecting group at the α-amine and a trityl protecting group on the amide side chain, allowing for facile incorporation into solid-phase peptide synthesis (SPPS). Thus far, we have successfully isolated Fmoc-(*2R,3R*)-hydroxyaspragine-OH and Fmoc-(*2R,3S*)-hydroxyasparagine-OH, and are working toward the trityl protection at the amide position. We have found that leaving both the

hydroxyl and amide group unprotected do not generate significant undesired side products during SPPS. To improve our yields, we will aim for Fmoc- and trityl protected versions of both amino acids.

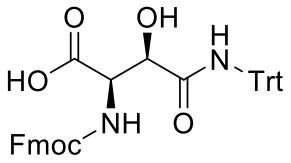

Fmoc-(*2R,3R*)-hydroxyasparagine-OH

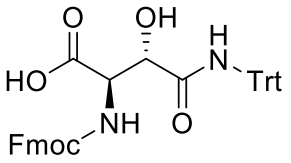

Fmoc-(*2R,3S*)-hydroxyasparagine-OH

To delineate contributions, I will only describe the synthesis of the Fmoc-(*2R,3S*)-hydroxyasparagine-OH, for which I had major contributions in developing. I will also be showing results that I obtained from NMR spectroscopic studies, functional assays, and X-ray crystallographic studies on both the (*2R,3R*)-hydroxyasparagine and (*2R,3S*)-hydroxyasparagine containing peptides. The synthesis of Fmoc-(*2R,3S*)-hydroxyasparagine-OH borrows from precedence in reported literature, but begins with either dimethyl or diisopropyl tartrate.

We developed a synthesis that would allow us to access all four possible diastereomers of suitably protected hydroxyasparagine from just two starting materials. The synthesis can begin with either (-)-diethyl-D-tartrate to afford the (*2R,3S*) or the (*2S,3S*) stereochemistry, or begin with the (+)-diethyl-L-tartrate to afford the (*2S,3R*) or (*2R,3R*) stereochemistry. Scheme 3.1 depicts the synthesis of the Fmoc-(*2R,3S*)-hydroxyasparagine-OH.

Diethyl-D-tartrate is first oxidized with thionyl chloride to afford the cyclic sulfite **3.1**, which is then opened by treatment with sodium azide overnight at room temperature. Ring opening of the cyclic sulfite with sodium azide can be achieved in

good yield without requiring oxidation of the sulfite to the sulfate, and leads to the formation of only one product with an inversion of stereochemistry at the newly installed azide.[12,13] Subsequent reduction of the azide with H_2 and Pd/C affords amino alcohol **3.2**.

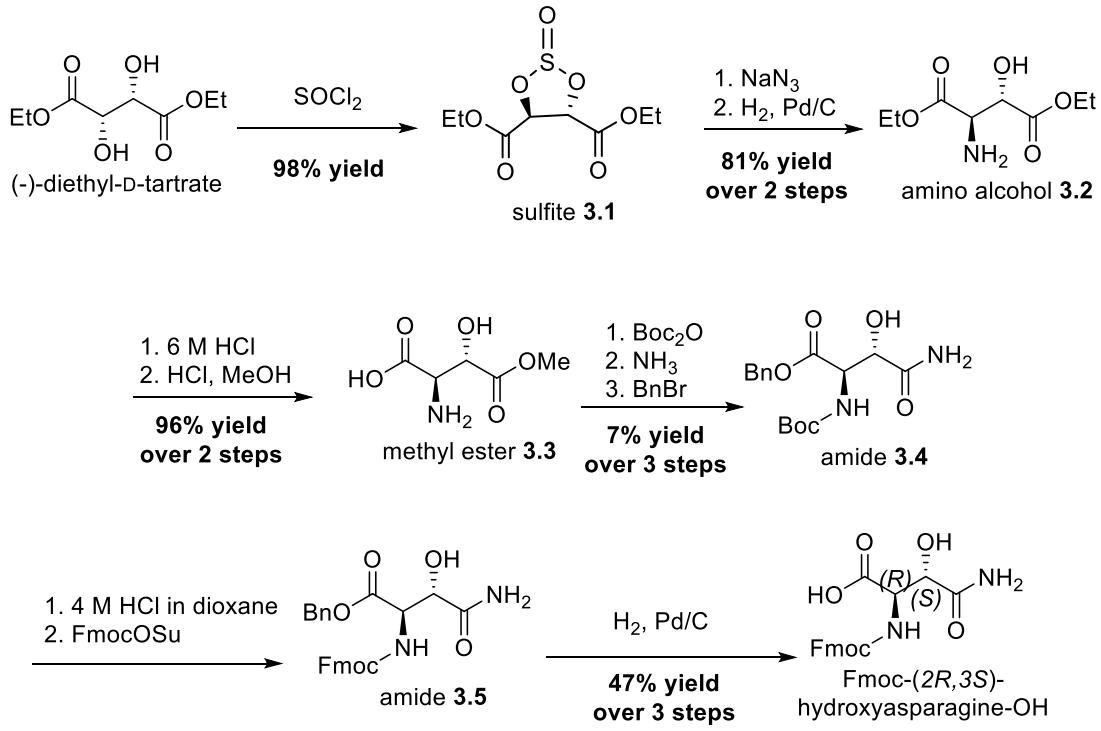

Scheme 3.1. Synthesis of Fmoc-(*2R,3S*)-hydroxyasparagine-OH.

Differentiation of the two diethyl esters at the 1- and 4-positions can be achieved by way of hydrolysis with 6 M HCl at 100 °C overnight, followed by methyl esterification with MeOH and concentrated HCl at 40 °C for 3 hours to yield methyl ester **3.3**. The carboxylic acid at the 4-position is regioselectivity esterified because the ammonium group at the 2-position deactivates the carboxylic acid at the 1-position.[14] We have also found that extended reaction times of greater than 3 hours lead to the undesired di-esterification.

Methyl ester **3.3** is converted to amide **3.4** by Boc-protection of the amino group at the 2-position, ammonolysis of the methyl ester at the 4-position with NH_3 in MeOH, and benzyl ester protection of the carboxylic acid at the 1-position. Replacement of the Boc-protecting group with an Fmoc-protecting group is achieved by first cleaving the Boc protecting group with 4 M HCl in dioxane, followed by Fmoc protection with Fmoc-OSu to yield amide **3.5**. Lastly, cleavage of the benzyl ester at the 1-position with H_2 Pd/C will furnish the penultimate product, Fmoc-(*2R,3S*)-hydroxyasparagine-OH. I have successfully incorporated Fmoc-(*2R,3S*)-hydroxyasparagine-OH into SPPS, and demonstrated that I can isolate the corresponding peptide. To maximize yield and purity in the peptide synthesis, future directions will aim to protect the side chain amide of the hydroxyasparagine with trityl alcohol and catalytic sulfuric acid based on established procedures.[14]

The following work post-synthesis represent my individual results obtained from using Fmoc-(*2R,3S*)-hydroxyasparagine-OH to synthesize and evaluate a synthetic homologue of Novo29. To determine the stereochemistry of the natural product, I compared the (*2R,3R*)-hydroxyasparagine containing peptide provided by Maj Krumberger and the (*2R,3S*)-hydroxyasparagine containing peptide that I synthesized to the authentic Novo29. Scheme 3.2 illustrates the workflow for the peptide synthesis of (*2R,3S*)-hydroxyasparagine containing Novo29 peptide.

The synthesis begins with loading Fmoc-Leu-OH (residue 7) onto 2-chlorotrityl resin, followed by elongation of residues 6 through 1 to the linear sequence. The Fmoc-(*2R,3S*)-hydroxyasparagine-OH residue was introduced without protecting groups on the hydroxy group at the β-position nor the amide side chain. Esterification at the β-

hydroxy group of the (*2R,3S*)-hydroxyasparagine with Fmoc-Leu-OH was achieved using DIC and DMAP. Fmoc deprotection of Leu_8 and cleavage of the linear sequence from the resin with 20% hexafluoroisopropanol (HFIP) in CH_2Cl_2 affords the linear peptide with a free carboxyl *C*-terminus. Cyclization between the free amino group of Leu_8 and the free carboxylic acid was performed with HATU and HOAt. Global deprotection with trifluoracetic acid (TFA) and reverse-phase purification yielded the (*2R,3S*)-hydroxyasparagine containing Novo29 peptide.

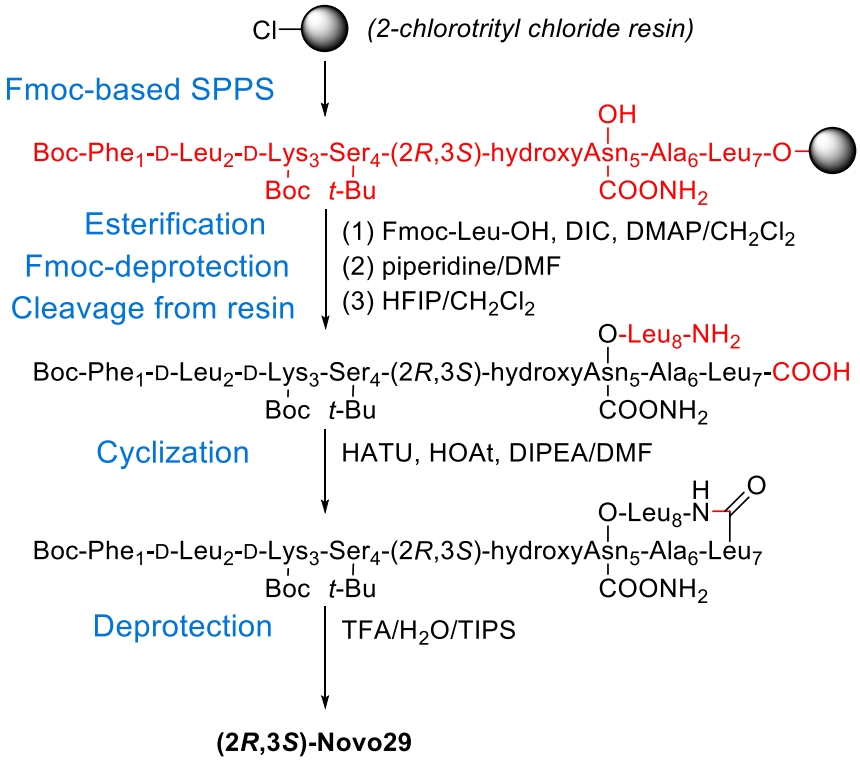

Scheme 3.2. Synthesis of Novo29 derivative containing (*2R,3S*)-hydroxyasparagine at position 5.

^{1}H NMR spectroscopic studies reveal the hydroasparagine at position 5 of natural Novo29 has (*2R,3R*) stereochemistry. ^{1}H NMR, TOCSY, and NOESY spectra were acquired for natural Novo29, and synthetic peptides at 2.0 mM concentration in DMSO-

d_6. Figure 3.2 illustrates the ^{1}H NMR overlay of the three peptides; the α-and β-proton resonances at the 2- and 3-positions of the hydroxyasparagine residue match identically for natural Novo29 and the synthetic peptide containing (*2R,3R*)-hydroxyasparagine, but are mismatched for the epimer containing the (*2R,3S*)-hydroxyasparagine.

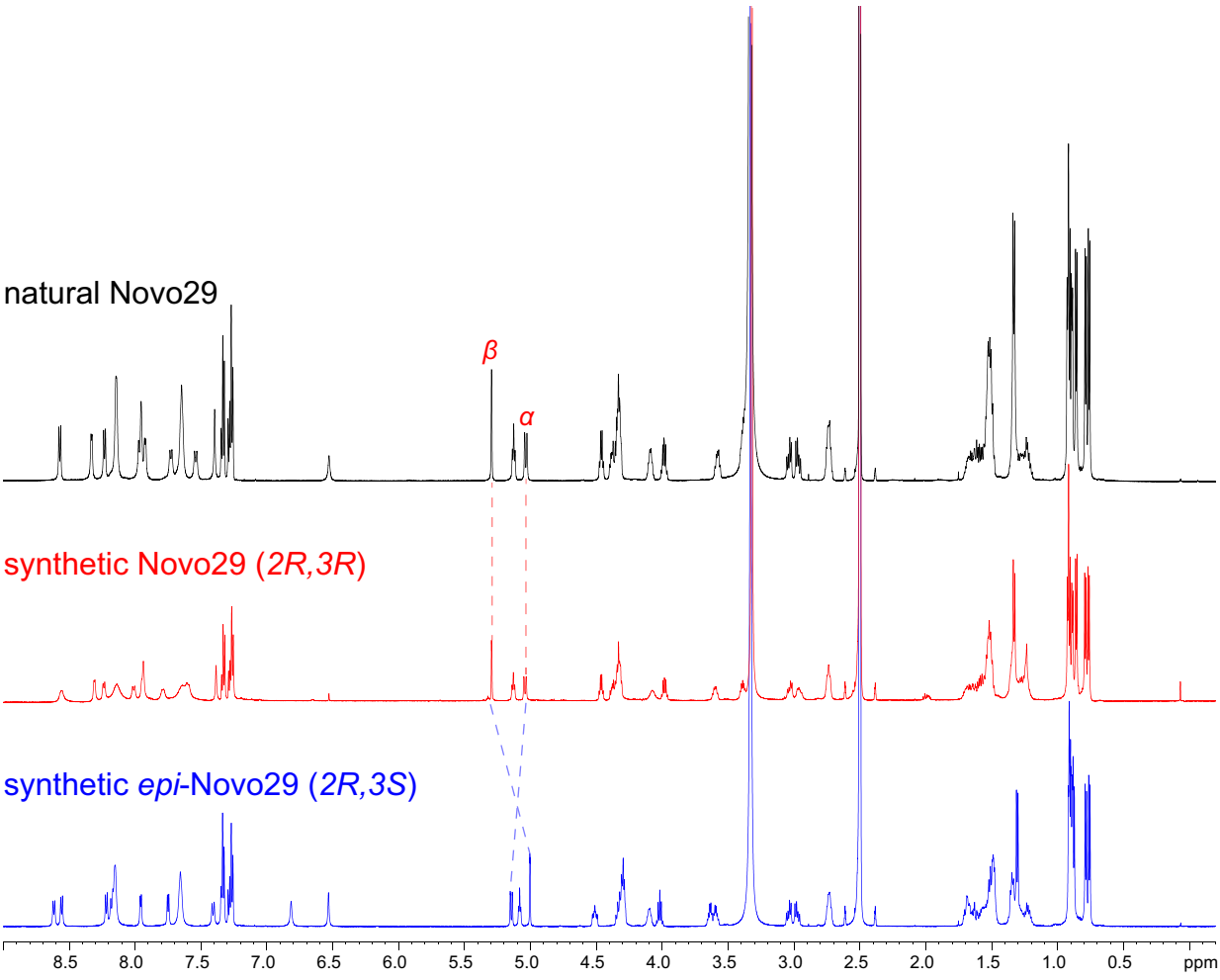

Figure 3.2. ^{1}H NMR overlay of Natural Novo29 (black), synthetic Novo29 (red), and *epi*-Novo29 (blue). The α- and β-protons of the hydroxyasparagine residue are labeled. Dashed lines trace the chemical shifts of the two protons in each of the peptides. The samples were prepared as 2.0 mM solutions in DMSO-d_6.

The ^{1}H NMR spectrum of the natural Novo29 largely resembles that of the synthetic (*2R,3R*) Novo29; both spectra exhibit similar chemical shifts at 5.5 ppm and

below, and slight differences in resonances greater than 6.0 ppm. The α-proton resonance of the hydroxyasparagine residue in natural Novo29 has a chemical shift at 5.04 ppm and appears as a doublet; the β-proton resonance has a chemical shift at 5.29 and appears as a broad singlet (Figure S3.1). The α-proton resonance of the hydroxyasparagine residue in the synthetic (*2R,3R*) Novo29 is identical in chemical shift and appearance to that of natural Novo29; the β-proton resonance also has a chemical shift of 5.29 ppm but appears as a doublet. The subtle differences in splitting pattern suggest slight variations in shimming. Unlike the synthetic (*2R,3R*) Novo29, the hydroxyasparagine residue in the synthetic (*2R,3S*) Novo29 (*epi*-Novo29) has an α-proton resonance with a chemical shift of 5.15 ppm and a β-proton resonance with a chemical shift of 5.00 ppm — both of which differ substantially to that of the natural Novo29. The downfield chemical shift region greater than 6.0 ppm suggests differing pH of samples resulting from the natural Novo29 being dissolved as an HCl salt vs. the TFA salts of the synthetic peptides. Overall, the striking similarities in the proton chemical shifts of the hydroxyasparagine residue between the natural Novo29 and the synthetic peptides provide strong evidence in favor of the hypothesized (*2R,3R*) stereochemistry.

To further corroborate the (*2R,3R*) stereochemistry of the hydroxyasparagine residue at position 5, I investigated the antibiotic activity of Novo29 and synthetic peptides against Gram-positive bacteria using a minimum inhibitory concentration (MIC) assay (Table 3.1). The natural Novo29 peptide was used as the positive control, and *E.coli* was used as the negative control. Table 3.1 shows that Novo29 and synthetic Novo29 exhibit very comparable activity against *B. subtilis* and *S. epidermidis*, while the *epi*-Novo29 appears to be inactive (> 32 μg/mL).

Table 3.1. MIC values of natural Novo29 and synthetic peptides in µg/mL.

	Bacillus subtilis ATCC 6051	*Staphylococcus epidermidis* ATCC 14990	*Escherichia coli* ATCC 10798
Natural Novo29	0.125	0.5	8
Synthetic Novo29 (*2R,3R*)	0.125	0.25	8
Synthetic *epi*-Novo29 (*2R,3S*)	>32	>32	>32

I next turned to X-ray crystallography to gain insight into the structure of Novo29. Both synthetic Novo29 and *epi*-Novo29 were screened in 96-well plate format using crystallization kits from Hampton Research (PEG/Ion, Index, and Crystal Screen). Within 24 hours, rectangular rods grew from a screening condition of 2.8 M sodium acetate at pH 7.0 for the *epi*-Novo29; no conditions facilitated crystal growth for the synthetic Novo29. It has been reported that Novo29 is susceptible to hydrolysis in phosphate buffer[15]; the rate of hydrolysis for the active *2R,3R* stereochemistry in the synthetic Novo29 might not permit stable crystal growth. Based on the screening condition, e*pi*-Novo29 was further optimized in a 24-well plate format, and a condition of 2.8 M sodium acetate trihydrate at pH 6.6 yielded long, rectangular crystals suitable for diffraction. These crystals of *epi*-Novo29 degrade 72 –96 hours after crystal formation at room temperature.

We elucidated the X-ray crystallographic structure of *epi*-Novo29 at 1.13 Å resolution (PDB 8CUG). The X-ray crystallographic structure was determined by soaking a single crystal in a mixture of potassium iodide (KI) and well solution to incorporate iodide heavy atoms into the lattice. Diffraction data was then collected using an in-house X-ray diffractometer and single-wavelength anomalous diffraction

(SAD) phasing was used to determine the phases. Higher-resolution diffraction data was subsequently collected on a synchrotron X-ray source. Phases for the higher-resolution structure were determined by molecular replacement using the KI-soaked structure (PDB 8CUF) as a search model.

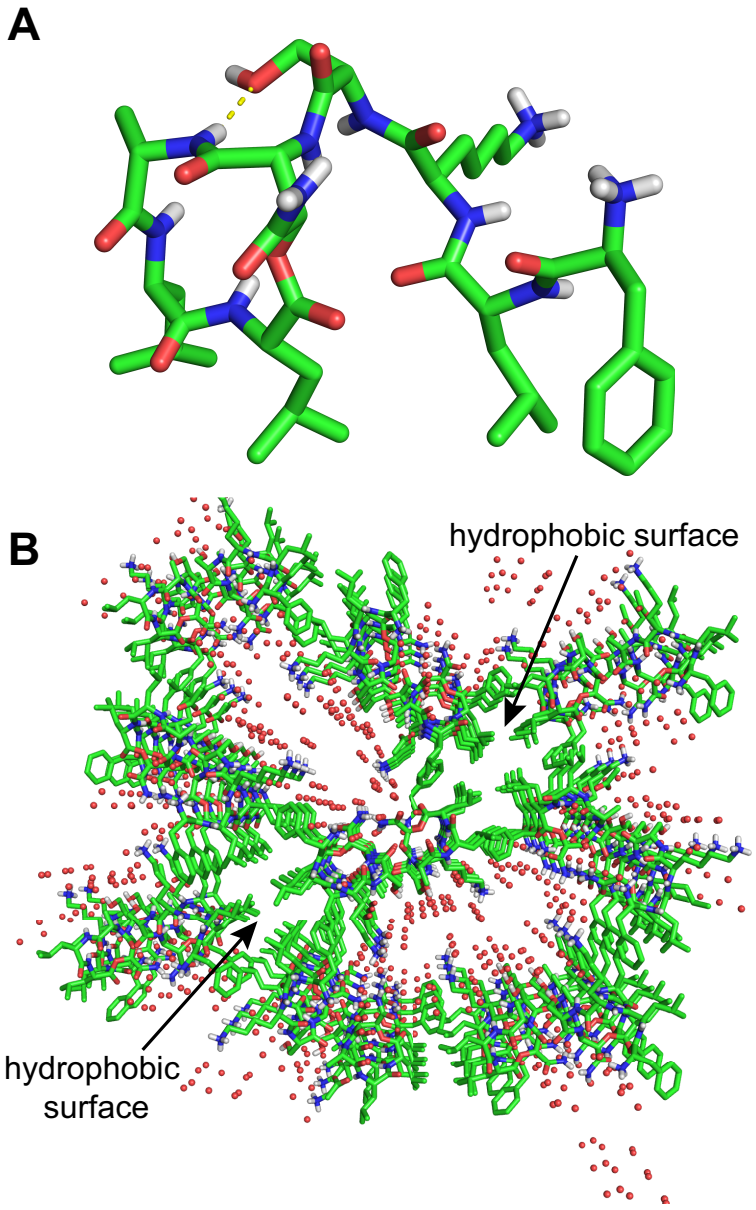

Figure 3.3. (A) X-ray crystallographic structure of *epi*-Novo29 solved to 1.13 Å; a hydrogen bond is shown between the hydroxyl group sidechain of Ser_7 and the NH amide backbone of Ala_9. (B) Extended network composed of symmetry mates of *epi*-Novo29 depicting hydrophobic surfaces devoid of water molecules (red spheres).

In the X-ray crystallographic structure, *epi*-Novo29 adopts an amphiphilic conformation, with the side chains of Phe_1, D-Leu_2, Leu_7, and Leu_8 creating a hydrophobic surface and the side chains of D-Lys_2, Ser_4, and (*2R,3S*)-hydroxyasparagine creating a hydrophilic surface (Figure 3.3A). An intramolecular hydrogen bond between the amide NH group of Ala_6 and the side chain OH group of Ser_4 helps enforce this conformation. This amphiphilic structure is reminiscent of the amphiphilic structure our laboratory has previously observed for teixobactin derivatives, in which the side chains of *N*-methyl- D-Phe_1, Ile_2, D-*allo*-Ile_5, and Ile_6 create a hydrophobic surface and the side chains of Ser_3, d-Gln_4, Ser_7 create a hydrophilic surface.[11,16] In the lattice, *epi*-Novo29 packs so that the hydrophobic surfaces come together, with four sets of *epi*-Novo29 molecules forming a hydrophobic core (Figure 3.3B). Our X-ray crystallographic structures of teixobactin derivatives, as well as NMR studies by other researchers, indicate that the hydrophobic surface of teixobactin interacts with the bacterial cell membranes and are a key feature of its mechanism of action.[17] The X-ray crystallographic structure of *epi*-Novo29 suggests that Novo29 may interact with bacterial cell membranes in a similar fashion.

FUTURE DIRECTIONS:

Together with my colleague, Maj Krumberger, we have successfully determined the stereochemistry of Novo29, a new antibiotic that was recently reported. Our syntheses of (*2R,3R*)-hydroxyasparagine and (*2R,3S*)-hydroxyasparagine amino acids enabled us to access Novo29 and *epi*-Novo29. My work on the *epi*-Novo29 served as an important control, and further corroborated our initial hypothesis of the (*2R,3R*) stereochemistry of

the hydroxyasparagine amino acid at position 5. Furthermore, *epi*-Novo29 crystalized in screening conditions and after optimizations, yielded a crystal that diffracted with 1.13 Å to provide a high-resolution X-ray crystal structure. Using the X-ray crystallographic structure of *epi*-Novo29 as a guide, I can envision that a molecular model of Novo29 can be generated by inversion of the hydroxyl group at position 3 from *R*- to *S*-stereochemistry. The newly generated model may provide insights for how the packing of the hydrophobic surfaces interact with lipid membrane bacteria.

REFERENCES AND NOTES

[1] Hutchings, M.; Truman, A.; Wilkinson, B. *Curr. Opin. Microbiol.* **2019**, *51*, 72–80.

[2] Antibiotic resistance threats in the United States, **2019**. U.S. Department of Health and Human Services Centers for Disease Control and Prevention. https://www.cdc.gov/drugresistance/pdf/threats-report/2019-ar-threats-report-508.pdf.

[3] Zinner, S. H. *Expert Rev. Anti. Infect. Ther.* **2005**, *3*, 907–913.

[4] Miethke, M.; Pieroni, M.; Weber, T.; Brönstrup, M.; Hammann, P.; Halby, L.; Arimondo, P. B.; Glaser, P.; Aigle, B.; Bode, H. B.; et al. *Nat. Rev. Chem.* **2021**, *5*, 726–749.

[5] Ling, L. L.; Schneider, T.; Peoples, A. J.; Spoering, A. L.; Engels, I.; Conlon, B. P.; Mueller, A.; Schäberle, T. F.; Hughes, D. E.; Epstein, S.; et al. *Nature* **2015**, *517*, 455–459.

[6] Shoji, J.; Hinoo, H.; Hattori, T.; Hirooka, K.; Kimura, Y.; Yoshida, T. *J. Antibiot. (Tokyo).* **1989**, *42*, 1460–1464.

[7] Wirtz, D. A.; Ludwig, K. C.; Arts, M.; Marx, C. E.; Krannich, S.; Barac, P.; Kehraus, S.; Josten, M.; Henrichfreise, B.; Müller, A.; et al. *Angew. Chemie - Int. Ed.* **2021**, *60*, 13579–13586.

[8] Chen, K. H.; Le, S. P.; Han, X.; Frias, J. M.; Nowick, J. S. *Chem. Commun.* **2017**, *53*, 11357–11359.

[9] Yang, H.; Wierzbicki, M.; Du Bois, D. R.; Nowick, J. S. *J. Am. Chem. Soc.* **2018**, *140*, 14028–14032.

[10] Hughes et al., Depsipeptides and Uses Thereof, U.S. Patent 11,203,616, Dec 21, 2021.

[11] Novobiotic Pharmaceuticals. https://www.novobiotic.com/the-science.

[12] Gao, Y.; Sharpless, K. B. *J. Am. Chem. Soc.* **1988**, *110*, 7538–7539.

[13] Chavan, S. P.; Harale, K. R.; Pawar, K. P. *Tetrahedron Lett.* **2013**, *54*, 4851–4853.

[14] Guzmán-Martínez, A.; VanNieuwenhze, M. S. *Synlett* **2007**, *10*, 1513–1516.

[15] Dr. Dallas Hughes and Dr. Losee Ling, NovoBiotic Pharmaceuticals, personal communications.

[16] Yang, H; Pishenko, A. V.; Li, X.; Nowick, J. S. *J. Org. Chem.* **2020**, *85*, 1331-133.

[17] Shukla, R.; Medeiros-Silva, J.; Parmar, A.; Vermeulen, B. J. A.; Das, S.; Paioni, A. L.; Jekhmane, S.; Lorent, J.; Bonvin, A. M. J. J.; Baldus, M.; et al. *Nat. Commun.* **2020**, *11*, 1–10.

Supporting information for:

Synthesis and Stereochemical Determination of Novo29, a New Peptide Antibiotic

Table of Contents

Supplementary information 222
Figure S3.1 223
Supplementary Table 3.1 224
Chemical synthesis 225
Synthesis of *epi*-Novo29 232
Peptide synthesis procedure. 232
NMR spectroscopy of peptides 235
Sample preparation, data collection, and data processing 235
MIC assay 236
Preparation and setup. 236
X-ray crystallography 237
Crystallization, data collection, processing, and structure determination. 237
References 239
Characterization Data 240
Analytical HPLC trace and MALDI mass spectrum of peptides 240
Analytical HPLC trace and Xevo mass spectrum of natural Novo29 240
Analytical HPLC trace and Xevo mass spectrum of synthetic Novo29 242
Analytical HPLC trace and Xevo mass spectrum of synthetic *epi*-Novo29 244
NMR spectra of isolated compounds 246
^{1}H NMR and spectrum of sulfite **3.1** 246
^{1}H NMR spectrum of amino alcohol **3.2** 247
^{1}H NMR spectrum of methyl ester **3.3** 248
^{1}H NMR spectrum of amide **3.4** 249
NMR spectroscopic studies of peptides 250
^{1}H NMR, TOCSY, and NOESY spectra of natural Novo29 250

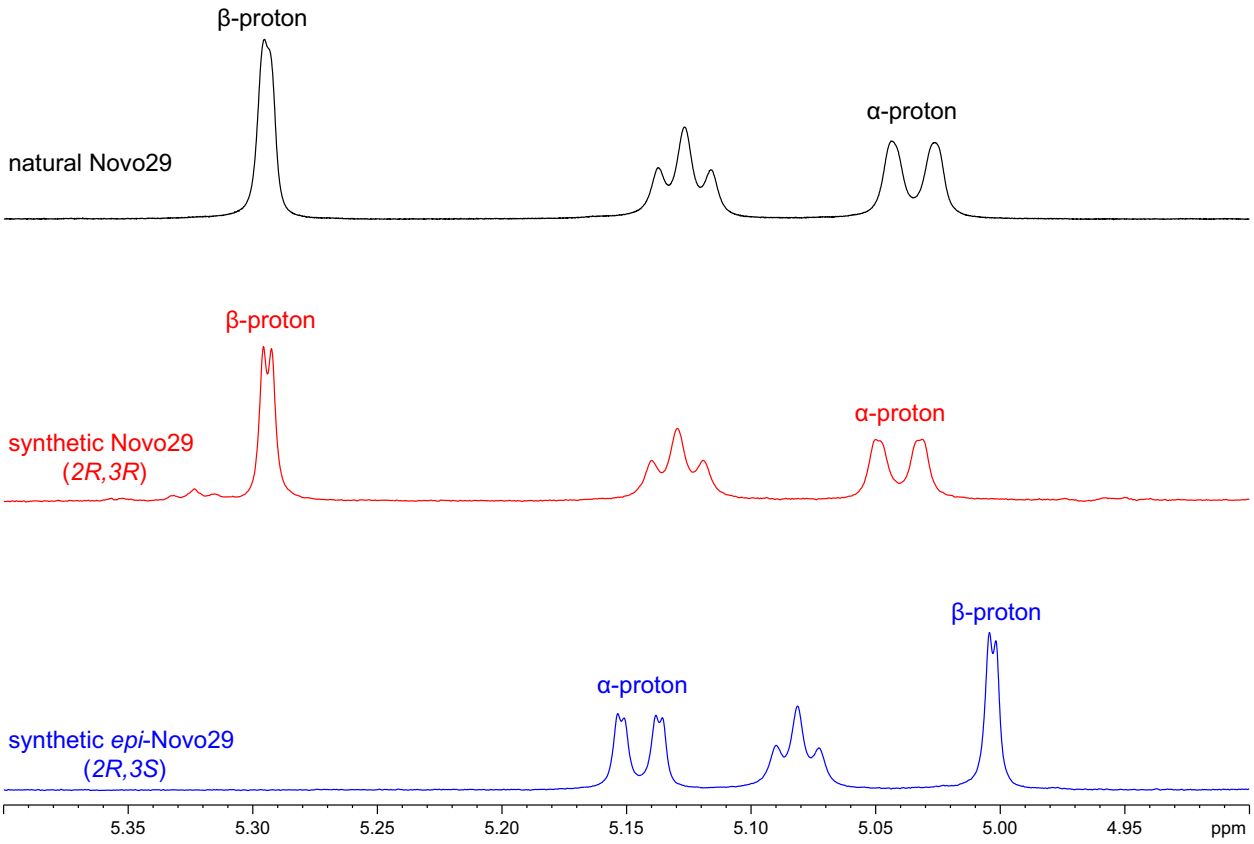

Figure S3.1. Zoom in 1D overlay of natural Novo29 (black), synthetic Novo29 (red), and *epi*-Novo29 (blue) comparing the α- and β-proton chemical shifts of the corresponding hydroxyasparagine. The chemical shifts between natural Novo29 and synthetic Novo29 containing the *2R,3R*-hydroxyasparagine match identically, but differ substantially from that of the *epi*-Novo29.

Table S3.1. Crystallographic properties, crystallization conditions, and data collection and model refinement statistics for *epi*-Novo29.

peptide	*epi*-Novo29 (synchrotron)
PDB ID	8CUG
space group	$P2_12_12_1$
a, *b*, *c* (Å)	12.105, 31.898, 37.101
α, β, λ (°)	90, 90, 90
peptides per asymmetric unit	2
crystallization conditions	2.8 M sodium acetate trihydrate pH 6.6
wavelength (Å)	1.00
resolution (Å)	24.19–1.13 (24.19–1.131)
total reflections	58890 (1401)
unique reflections	5590 (398)
multiplicity	10.5 (3.5)
completeness (%)	96.44 (69.54)
mean I/σ	22.28 (4.20)
Wilson B factor	8.32
R_{merge}	0.07324 (0.3204)
$R_{measure}$	0.07694 (0.3701)
$CC_{1/2}$	0.998 (0.938)
CC^*	0.999 (0.984)
R_{work}	0.1308 (0.2378)
R_{free}	0.1450 (0.2242)
number of non-hydrogen atoms	174
RMS_{bonds}	0.012
RMS_{angles}	1.63
Ramachandran favored (%)	100
outliers (%)	0
clashscore	3.77
average B-factor	13.49
ligands/ions	1
water molecules	42

Chemical synthesis

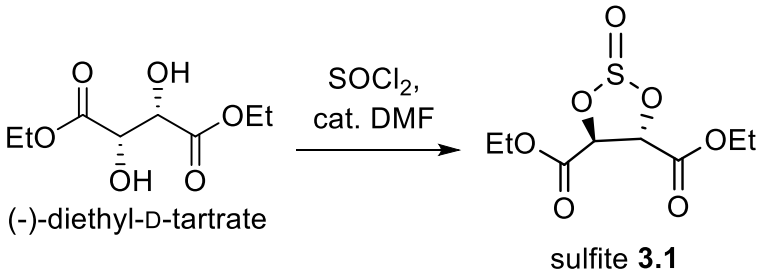

Sulfite 3.1. A 500-mL, single-necked, round-bottom flask equipped with a magnetic stirring bar and a condenser fitted with a nitrogen inlet adapter was charged with a solution of diethyl-D-tartrate (8.56 mL, 50.0 mmol, 1.0 equiv) in 250 mL of CH_2Cl_2 (the reaction was run at ca. 0.2 M concentration of the diethyl-D-tartrate). To the solution, $SOCl_2$ (7.25 mL, 100.0 mmol, 2.0 equiv) was added dropwise, followed by 0.25 mL cat. anhydrous DMF. The reaction mixture heated and stirred for 2 h at reflux. After 2 h, the solution was cooled to room temperature, and concentrated to dryness by rotary evaporation to afford sulfite **3.1** as a yellow oil (12.4 g, 98 % yield). ^{1}H NMR (400 MHz, $CDCl_3$): δ 5.72 (d, *J* = 3.9 Hz, 1 H), 5.25 (d, *J* = 3.5 Hz, 1 H), 4.28–4.38 (m, 4 H), 1.34 (t, *J* = 7.0 Hz, 6 H).

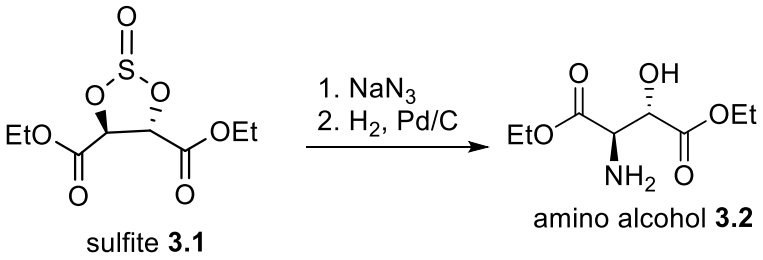

Amino alcohol 3.2. A 250-mL, single-necked, round-bottom flask equipped with a magnetic stirring bar, a nitrogen inlet adapter, was charged with a solution of sulfite **3.1**

(12.4 g, 49.2 mmol, 1.0 equiv) in 100 mL of anhydrous DMF (the reaction was run at 0.5 M concentration of the sulfite **3.1**). NaN_3 (3.99 g, 61.5 mmol, 1.25 equiv) was added to the solution, and the suspension was stirred for 21 h. The suspension was transferred to a separatory funnel and the round bottom flask was rinsed with 300 mL H_2O. The layers were separated and the aqueous layer was extracted with EtOAc (3 x 200 mL). The combined organic layer was dried over Na_2SO_4, filtered, and dried using rotary evaporation.

A 500-mL, three-necked, round-bottom flask equipped with a magnetic stirring bar, a nitrogen inlet adapter, an inlet adapter fitted with a hydrogen balloon, and a rubber septum was charged with a solution of the crude azido alcohol from the previous step (3.42 g, 14.84 mmol, 1.0 equiv) in 74 mL of anhydrous CH_3OH. (The reaction was run at 0.2 M concentration of the azido alcohol). The flask was evacuated and back filled with nitrogen, and 10 % Pd/C (50% wet with H_2O, 1.71 g) was added. A balloon containing H_2 gas was fitted to an inlet adapter and the system was evacuated and back filled with H_2 gas. The resulting suspension was stirred for 6 h, filtered through Celite, and washed with 150 mL of additional CH_3OH. The resulting solution was concentrated by rotary evaporation to and purified by column chromatography on silica gel (elution with 5:95 CH_3OH:CH_2Cl_2) to afford amino alcohol **3.2** as an oil (2.48 g, 81 % yield over two steps). ^1H NMR (400 MHz, $CDCl_3$): δ 4.50 (d, *J* = 5.9 Hz, 1 H), 4.15–4.30 (m, 4 H), 3.90 (d, *J* = 3.2 Hz, 1 H), 1.28 (q, *J* = 7.2 Hz, 1 H),

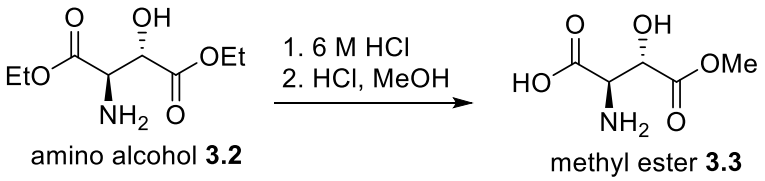

amino alcohol **3.2** methyl ester **3.3**

Methyl ester 3.3. A 250-mL, single-necked, round-bottom flask equipped with a magnetic stirring bar and a condenser fitted with a nitrogen inlet adapter was charged with a solution of amino alcohol **3.2** (2.48 g, 12.08 mmol, 1.0 equiv) in 60 mL of 6 M HCl (the reaction was run at ca. 0.2 M concentration of the amino alcohol **3.2**). The mixture was heated in an oil bath and stirred for 3.5 h at 100 °C, cooled to room temperature, and concentrated to dryness by rotary evaporation to get rid of ethanol byproduct. The solid was then redissolved in 60 mL of 6 M HCl and heated at reflux for 18 h overnight. The mixture was cooled to room temperature and concentrated to dryness by rotary evaporation to afford a beige solid. The crude intermediate was used in the next step without purification.

A 250-mL, single-necked, round-bottom flask equipped with a magnetic stirring bar and a condenser fitted with a nitrogen inlet adapter was charged with a solution of the crude amino alcohol diacid HCl salt (2.16g, 11.60 mmol, 1.0 equiv) in 60 mL of CH_3OH (the reaction was run at ca. 0.2 M concentration of the crude intermediate). The mixture was cooled to 0 °C using an ice bath. A solution of neat HCl (12 M, 1.9 mL) was then added dropwise to the flask over a few minutes. The flask was then heated in an oil bath to reflux at 65 °C for 3 hours. [NOTE: We have observed that longer reflux times leads to the increasing formation of the dimethyl ester]. The mixture was cooled to room temperature and concentrated to dryness by rotary evaporation to afford methyl ester **3.3** as a beige foam (2.30 g, 96 % yield over two steps). The crude intermediate was pure by NMR, and

used in the next step without transformation. ^{1}H NMR (400 MHz, D_2O): δ 4.81 (d, *J* = 2.7 Hz, 1 H), 4.60 (d, *J* = 2.8, 1 H), 3.87 (s, 3 H).

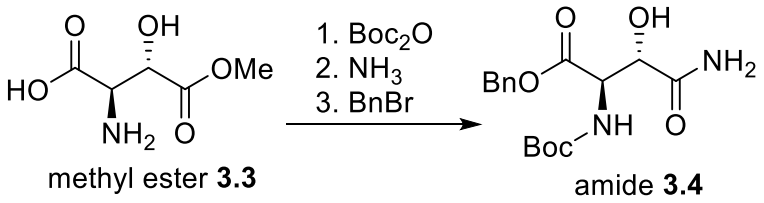

methyl ester **3.3** amide **3.4**

Amide 3.4. A 250-mL, single-necked, round-bottom flask equipped with a magnetic stirring bar and fitted with a nitrogen inlet adapter was charged with a solution of methyl ester **3.3** (8.60 g, 43.1 mmol, 1.0 equiv) in 140 mL of 10 % w/v Na_2CO_3. The solution was cooled to 0 °C using an ice bath. While on ice, a separate solution of Boc_2O (7.51 g, 34.62 mmol, 3.0 equiv) dissolved in 140 mL dioxane (to give a final concentration of 0.15 M for the methyl ester **3.3**) was slowly added over 2–3 minutes. The mixture was brought to room temperature, stirred for 19.5 h, and concentrated to dryness using rotary evaporation. The resulting residue was dissolved in 500 mL EtOAc and transferred to a separatory funnel. The mixture was washed with 1 M HCl (3 x 500 mL). The organic layer was dried over Na2SO_4 and concentrated to a yellow oil. The crude product was purified by column chromatography on silica gel (elution with 10:90 CH_3OH:$CHCl_3$) to afford the Boc-protected intermediate as an oil (1.65 g, 14.5 % yield, 1.0 equiv).

A 125-mL, single-necked, high-pressure flask equipped with a magnetic stirring bar was charged with a solution of the preceding Boc-protected intermediate (1.65 g, 6.27 mmol, 1.0 equiv) in ca. 20 mL CH_3OH (the reaction was run at ca. 0.3 M concentration of the intermediate). A flow of NH_3 gas was applied through a syringe directly into the solution and bubbled for 20–30 min to ensure saturation of the NH_3. The vessel was then capped,

and the solution was stirred for 72 h. The solution was worked up by concentration to dryness using rotary evaporation to afford the amide intermediate as a beige solid (1.46 g, 3.64 mmol, 1.0 equiv).

A 100-mL, single-necked, round-bottom flask equipped with a magnetic stirring bar and fitted with a nitrogen inlet adapter was charged with a solution of the amide intermediate (1.46 g, 6.12 mmol, 1.0 equiv) in ca. 31 mL of anhydrous DMF (the reaction was run at ca. 0.2 M concentration of the intermediate). The solution was cooled to 0 °C using an ice bath, and $NaHCO_3$ (1.29 g, 15.3 mmol, 2.5 equiv) followed by benzyl bromide (2.90 mL, 24.6 mmol, 4.0 equiv, dropwise) was added. The mixture was stirred for 2 h at 0 °C, brought to room temperature, and stirred for an additional 24 h under N_2. The resulting solution was cooled again to 0 °C using an ice bath 75 mL of H_2O was added to quench the reaction. The solution was transferred to a separatory funnel and extracted with EtOAC (3 x 50 mL). The combined organic layer was washed with 50 mL brine, dried with Na_2SO_4, and concentrated to using rotary evaporation. The crude product was then purified by column chromatography on silica gel (elution with 5:95 CH_3OH:CH_3Cl) to afford amide **3.4** as white solid (1.00 g, 47.2 % yield). ^{1}H NMR (400 MHz, $CDCl_3$): δ 7.31–7.40 (m, 5 H), 6.81 (br s, 1 H), 5.81 (br d, *J* = 4.2, 1 H), 5.60 (br s, 1 H), 5.52 (br d, *J* = 5.2, 1 H), 5.17–5.30 (m, 2 H), 4.71 (br d, *J* = 4.6, 1 H), 4.6 (br d, *J* = 4.6, 1 H), 1.44 (s, 9 H),

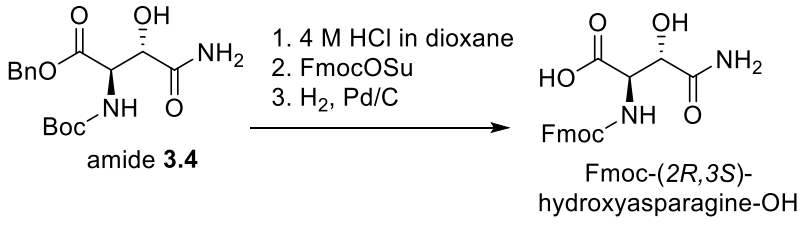

Fmoc-(*2R,3S*)-hydroxyasparagine-OH. A 250-mL, single-necked, round-bottom flask equipped with a magnetic stirring bar and fitted with a nitrogen inlet adapter was charged with a solution of the amide **3.4** (1.00 g, 2.96 mmol, 1.0 equiv) in ca. 30 mL of 4 N HCl in dioxane (the reaction was run at ca. 0.1 M concentration of the amide **3.4**). The solution was stirred for 2 h and concentrated to dryness by rotary evaporation. The crude intermediate was dissolved in 52 mL of 1:1 dioxane:water (0.06 M). The solution was cooled to 0 °C using an ice bath, and $NaHCO_3$ was added until the solution reached a pH of 6.8. Fmoc-OSu (1.20 g, 3.55 mmol, 1.2 equiv) was then subsequently added, and mixture was stirred for 1 h on ice, brought to room temperature, and stirred for an additional 18–20 h under N_2. The resulting suspension was diluted with 120 mL EtOAC and 180 mL of sat'd $NaHCO_3$ and stirred for ca. 5 min. The solution was transferred to a separatory funnel and the organic layer was collected; the aqueous layer was then extracted with EtOAC (2 x 80 mL). The combined organic layer was then dried with Na_2SO_4 and concentrated to by rotary evaporation to a white solid.

A 250-mL, three-necked, round-bottom flask equipped with a magnetic stirring bar, a nitrogen inlet adapter, an inlet adapter fitted with a hydrogen balloon, and a rubber septum was charged with a solution of the Fmoc-protected intermediate from the previous step in ca. 55 mL of anhydrous CH_3OH (the reaction was run at 0.05 M concentration of the Fmoc-protected intermediate assuming 100 % conversion). The flask was evacuated and back filled with nitrogen, and ca. 10 % Pd/C (50% wet with H_2O, 214 mg) was added. A balloon containing H_2 gas was fitted to an inlet adapter and the system was evacuated and back filled with H_2 gas. The resulting suspension was stirred for 24 h, filtered through Celite, and washed with additional CH_3OH. The resulting solution was concentrated by

rotary evaporation to afford Fmoc-(*2R,3S*)-hydroxyasparagine-OH as an off-white solid (512 mg, 47 % yield over three steps). The ^{1}H NMR of the Fmoc-(*2R,3S*)-hydroxyasparagine is not available. However low-resolution ESI data is provided as follows: *m/z*: $[M - H]^-$ calcd for $C_{19}H_{17}N_2O_6H^-$ 369.1092, found 369.5.

Synthesis of epi-Novo29 [1]

Peptide synthesis procedure. *Epi*-Novo29 were synthesized by manual solid-phase peptide synthesis of the corresponding linear peptide on 2-chlorotrityl resin, followed by on-resin esterification, solution-phase cyclization, deprotection, and purification. A step-by-step procedure is detailed below.

a. Loading the resin. 2-Chlorotrityl chloride resin (300 mg, 1.07 mmol/g) was added to a Bio-Rad Poly-Prep chromatography column (10 mL). Dry CH_2Cl_2 (8 mL) was used to suspend and swell the resin for 30 min with gentle rocking. After the solution was drained from the resin, a separate solution of Fmoc-Leu-OH (75 mg, 0.7 equiv, 0.21 mmol) in 6% (v/v) 2,4,6-collidine in dry CH_2Cl_2 (8 mL) was added and the suspension was gently rocked for 5–6 h. The solution was then drained, and a mixture of CH_2Cl_2/ CH_3OH /*N*,*N*-diisopropylethylamine (DIPEA) (17:2:1, 8 mL) was added immediately. The resin was gently rocked for 1 h, to cap the unreacted 2-chlorotrityl chloride resin sites. The resin was then washed three times with dry CH_2Cl_2 and dried by passing nitrogen through the vessel. This procedure typically yields 0.15–0.20 mmol of loaded resin, as assessed by spectrophotometric analysis.

b. Manual peptide coupling. The loaded resin was suspended in dry DMF and then transferred to a solid-phase peptide synthesis vessel. Residues 6 through 1 were manually coupled using Fmoc-protected amino acid building blocks. The coupling cycle consisted of *i*. Fmoc-deprotection with of 20% (v/v) piperidine in DMF (5 mL) for 5–10 min at room temperature, *ii*. washing with dry DMF (4 x 5 mL), *iii*. coupling of the amino acid (4 equiv) with HCTU (4 equiv) in 20% (v/v) 2,4,6-collidine in dry DMF (5 mL) for 20–30 min, and *iv.* washing with dry DMF (4 x 5 mL). The last amino acid coupling of the linear sequence is

Boc-Phe-OH, which intentionally protects the *N*-terminus from being reactive during the esterification step and cyclization steps. The resin was then transferred to a clean Bio-Rad PolyPrep chromatography column.

c. *Esterification.* In a test tube, Fmoc-Leu-OH (10 equiv) and diisopropylcarbodiimide (10 equiv) were dissolved in dry CH_2Cl_2 (5 mL). The resulting solution was filtered through a 0.20-μm nylon filter, and 4-dimethylaminopyridine (1 equiv) was added to the filtrate. The resulting solution was transferred to the resin and gently agitated for 1 h. The solution was then drained, and the resin was washed with dry CH_2Cl_2 (3 x 5 mL) and DMF (3 x 5 mL).

d. *Fmoc deprotection of* Leu_8. The Fmoc protecting group on Leu_8 was removed by adding 20% (v/v) piperidine in DMF for 30 min. The solution was drained, and the resin was washed with dry DMF (3 x 5 mL) and CH_2Cl_2 (3 x 5 mL).

e. *Cleavage of the linear peptide from chlorotrityl resin*. The linear peptide was cleaved from the resin by rocking the resin in a solution of 20% (v/v) 1,1,1,3,3,3-hexafluoroispropanol (HFIP) in CH_2Cl_2 (8 mL) for 1 h. The suspension was filtered, and the filtrate was collected in a 250-mL round-bottomed flask. The resin was washed with additional cleavage solution (8 mL) for 30 min and filtered into the same 250 mL round bottom-bottomed flask. The combined filtrates were concentrated by rotary evaporation and further dried by vacuum pump to afford the crude protected linear peptide, which was cyclized without further purification.

d. *Cyclization of the linear peptide*. The crude protected linear peptide was dissolved in dry DMF (125 mL). HOAt (6 equiv) and HATU (6 equiv) were dissolved in 8 mL of dry DMF in a test tube to which 300 μL of diisopropylethylamine was added and the solution

mixed until homogenous. The solution was then added to the round-bottom flask containing the dissolved peptide and the mixture was stirred under nitrogen at room temperature for 16–20 h. The reaction mixture was concentrated by rotary evaporation and further dried by vacuum pump to afford the crude protected cyclized peptide, which was immediately subjected to global deprotection.

e. Global deprotection of the cyclic peptide. The protected cyclic peptides were dissolved in TFA:triisopropylsilane (TIPS):H_2O (18:1:1, 10 mL) in a 1000-mL round-bottomed flask equipped with a stir bar. The solution was stirred for 1 h under nitrogen. During the 1 h deprotection, two 50-mL conical tubes containing 40 mL of dry Et_2O each were chilled on ice. After the 1 h deprotection, the peptide solution was split between the two conical tubes of Et_2O. The tubes were then centrifuged at 600x*g* for 10 min, decanted, and washed with fresh Et_2O. This process of decanting and washing was repeated for two more times. The pelleted peptides were dried under nitrogen for 15–20 min. The deprotected cyclic peptide was then purified by reverse-phase HPLC (RP-HPLC).

f. Reverse-phase HPLC purification. The peptide was dissolved in 20% CH_3CN in H_2O (5 mL) and pre-purified on a Biotage Isolera One flash chromatography instrument equipped with a Biotage® Sfär Bio C18 D - Duo 300 Å 20 µm 25 g column. The solution of crude cyclic peptide was injected at 20% CH_3CN and eluted with a gradient of 20–50% CH_3CN. Fractions containing the desired peptide was concentrated by rotary evaporation, diluted in 20% CH_3CN, injected on a Rainin Dynamax instrument, and eluted over a gradient of 20–40% CH_3CN over 90 min. The collected fractions were analyzed by analytical HPLC and MALDI-TOF, and the pure fractions were concentrated by rotary

evaporation and lyophilized. This synthesis typically yielded 5 mgs of peptide as the TFA salt.

NMR spectroscopic studies of natural Novo29, synthetic Novo29, and epi-Novo29[2]

Sample Preparation. NMR spectroscopic studies of natural Novo29 and synthetic peptides were performed in DMSO-d_6. The solutions were prepared by dissolving a weighed portion of the peptide in the appropriate volume of solvent. The molecular weights of the peptides were calculated as the TFA salts with all amino groups assumed to be protonated (synthetic Novo29, M.W. 1131.14; *epi*-Novo29, M.W. 1131.14). The natural Novo29 hydrochloride salt provided by Novobiotic Pharmaceuticals (M.W. 976.00) was incorrectly weighed as the TFA salt, resulting in a concentration of ca. 1.7 mM instead of 2.0 mM.

TOCSY and NOESY Data Collection. NMR spectra were recorded on a Bruker 600 MHz spectrometer with a Bruker CBBFO helium-cooled cryoprobe. TOCSY spectra were recorded with 2048 points in the *f*2 dimension and either 512 increments in the *f*1 dimension with NS = 8 and a 150-ms spin-lock mixing time. NOESY spectra were recorded with 2048 points in the *f*2 dimension and 512 increments in the *f*1 dimension with NS = 8 and a 200-ms mixing time.

TOCSY and NOESY Data Processing. NMR spectra were processed with Bruker TopSpin software. Automatic baseline correction was applied in both dimensions after phasing the spectra. 2D TOCSY and NOESY spectra were Fourier transformed to a final matrix size of 1024 x 1024 real points using a Qsine weighting function and forward linear prediction in the *f*1 dimension.

MIC assay [3]

Preparation and tray setup. Bacillus subtilis (ATCC 6051), *Staphylococcus epidermidis* (ATCC 14990), and *Escherichia coli* (ATCC 10798) were cultured from glycerol stocks in Mueller-Hinton broth overnight in a shaking incubator at 37 °C. An aliquot of the 1 mg/mL or 20 mg/mL antibiotic stock solution was diluted with culture media to make a 64 μg/mL solution. A 200-μL aliquot of the 64 μg/mL solution was transferred to a 96-well plate. Two-fold serial dilutions were made with media across a 96-well plate to achieve a final volume of 100 μL in each well. These solutions had the following concentrations: 64, 32, 16, 8, 4, 2, 1, 0.5, 0.25, 0.125, and 0.0625 μg/mL. The overnight cultures of each bacterium were diluted with either Mueller-Hinton broth (*Bacillus subtilis*, *Staphylococcus epidermidis*, and *Escherichia coli*) to an OD600 of 0.075 as measured for 200 μL in a 96-well plate. The diluted mixture was further diluted to 1×10^6 CFU/mL with the appropriate media. A 100-μL aliquot of the 1×10^6 CFU/mL bacterial solution was added to each well in 96-well plates, resulting in final bacteria concentrations of 5×10^5 CFU/mL in each well. As 100 μL of bacteria were added to each well, natural Novo29 and synthetic peptides were also diluted to the following concentrations: 32, 16, 8, 4, 2, 1, 0.5, 0.25, 0.125, 0.0625, and 0.03125 μg/mL. The plate was covered with a lid and incubated at 37 °C for 16 h. The optical density measurements were recorded at 600 nm and were measured using a 96-well UV/vis plate reader (MultiSkan GO, Thermo Scientific). The MIC values were taken as the lowest concentration that had no bacteria growth. Each MIC assay was run in triplicate in three independent runs to ensure reproducibility.

X-ray crystallography of epi-Novo29[4]

Crystallization of epi-Novo29. The hanging-drop vapor-diffusion method was used to determine initial crystallization conditions for *epi*-Novo29. Each peptide was screened in 96-well plate format using three crystallization kits (Crystal Screen, Index, and PEG/ION) from Hampton Research. A TTP LabTech Mosquito nanondisperse was used to make three 150 nL hanging drops for each well condition. The three hanging drops differed in the ratio of peptide to well solution for each condition in the 96-well plate. A 10 mg/mL solution of *epi*-Novo29 peptide in deionized water was combined with a well solution in ratios of 1:1, 1:2, and 2:1 peptide:well solution at appropriate volumes to create the three 150 nL hanging drops. Crystals of *epi*-Novo29 grew in well conditions of 2.8 M sodium acetate at pH 7.0.

Crystallization conditions for *epi*-Novo29 were optimized using a 4 x 6 matrix Hampton 24-well plate. For the *epi*-Novo29, the pH of the buffer was varied in each row (6.5, 6.6, 6.8, and 7.0). The concentration of sodium acetate in each column was varied in increments of 0.2 M (2.2, 2.4, 2.6, 2.8, 3.0, 3.2). Three hanging-drops were prepared on borosilicate glass slides by combing a 10 mg/mL solution of *epi*-Novo29 in deionized water with the well solution in the following amounts: 1 µL:1 µL, 2 µL:1 µL, and 1 µL:2 µL. Slides were inverted and pressed firmly against the silicone grease surrounding each well. Crystals were harvested with a nylon loop attached to a copper or steel pin, and flash frozen in liquid nitrogen prior to data collection. A single crystal was soaked in a mixture of potassium iodide (KI) and well solution to incorporate iodide heavy atoms into the lattice. A higher resolution data set was subsequently collected from crystals grown in similar

conditions and collected on a synchrotron X-ray source. The final optimized crystallization condition for *epi*-Novo29 is summarized in Supplementary Table 3.1.

Data collection, data processing, and structure determination. Diffraction data for the *epi*-Novo29 peptide were collected at the Advanced Light Source at Lawrence Berkeley National Laboratory with a synchrotron source at 1.0-Å wavelength beamline 5.0.2 up to a resolution of 1.13 Å. The dataset was indexed and integrated with XDS and scaled and merged with pointless and aimless. The crystallographic phase determination was done with Phaser. The structure was refined using phenix.refine, with manipulation of the model performed using Coot. Data collection and refinement statistics are shown below in Supplementary Table 3.1.

References

[1] The procedure for peptide synthesis follow closely to those that our laboratory has previously published. The procedures in this section are adapted from and in some cases taken verbatim from: Yang, H.; Du Bois, D. R.; Ziller, J. W.; Nowick, J. S. *Chem. Commun*. **2017**, *53*, 2772-2775.

[2] General procedures for NMR spectroscopy were either adapted from or taken verbatim from: Li, X.; Rios, S. E.; Nowick, J. S. *Chem. Sci.* **2022** *ASAP*. DOI: 10.1039/d2sc02080g.

[3] General procedures for minimum inhibitory concentration assays were either adapted from or taken verbatim from: Morris, M. A.; Malek, M.; Hashemian, M. H.; Nguyen, B. T.; Manuse S.; Lewis, K.; Nowick, J. S. *ACS Chem. Biol.* **2020**, *15*, 1222-1231

[4] General procedures for peptide synthesis and X-ray crystallography were either adapted from or taken verbatim from: Li, X.; Sabol, A. L.; Wierzbicki, M.; Salveson, P. J.; Nowick, J. S. *Angew. Chem. Int. Ed.* **2021**, *60*, 22776-22782 and Samdin, T. D.; Wierzbicki, M.; Kreutzer, A. G.; Howitz, W. J.; Valenzuela, M.; Smith, A.; Sahrai, V.; Truex, N. L.; Klun, M.; Nowick, J. S. *J. Am. Chem. Soc.* **2020**, *142*, 11593–11601.

Characterization of natural Novo29

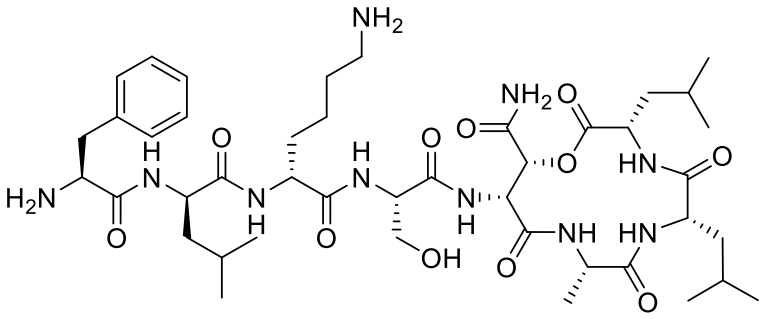

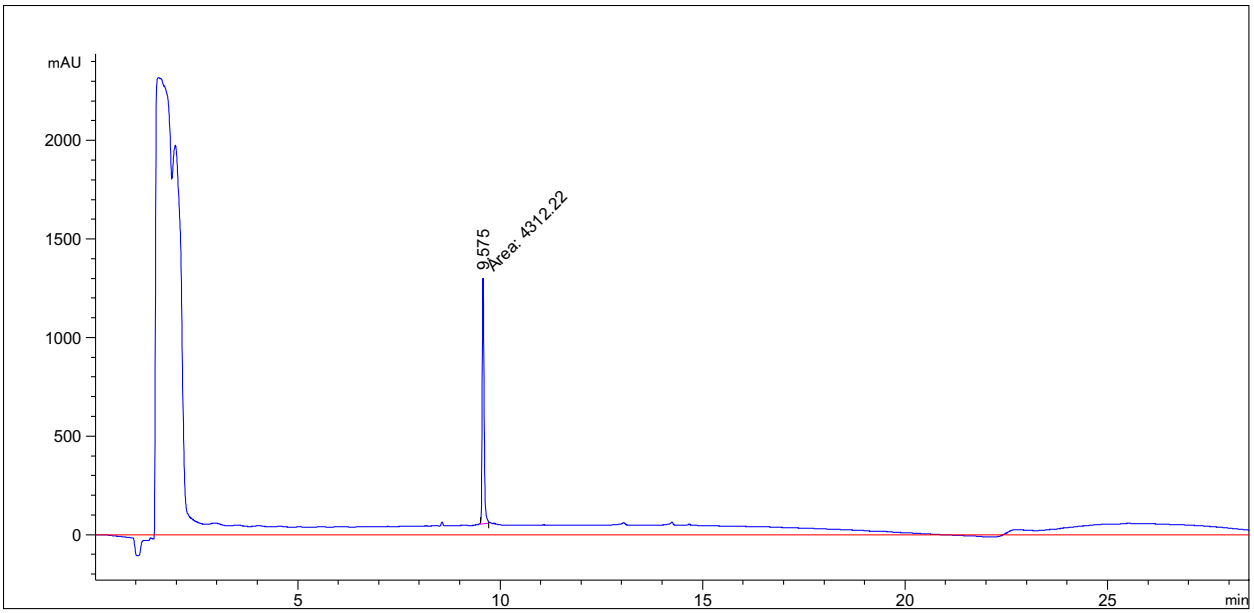

Signal 1: MWD1 A, Sig=214,4 Ref=off

Peak #	RetTime [min]	Type	Width [min]	Area [mAU*s]	Height [mAU]	Area %
1	9.575	MM	0.0569	4312.21582	1262.37280	100.0000

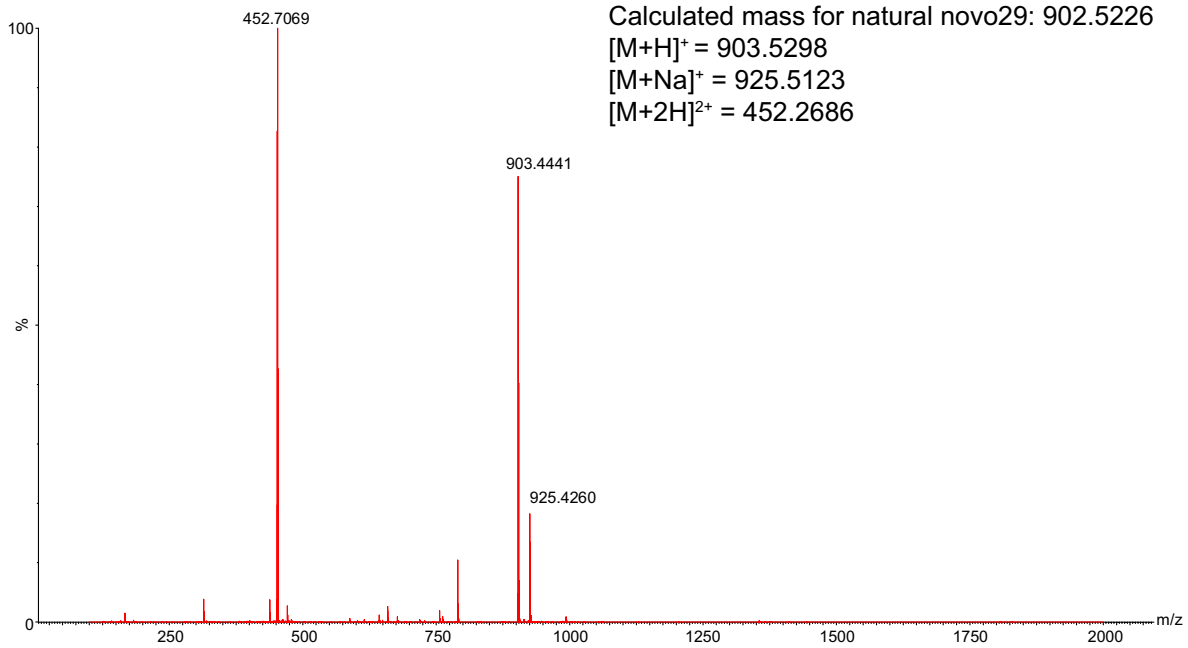
Calculated mass for natural novo29: 902.5226
[M+H]+ = 903.5298
[M+Na]+ = 925.5123
[M+2H]2+ = 452.2686
452.7069
903.4441
925.4260
100
%
0
250
500
750
1000
1250
1500
1750
2000
m/z

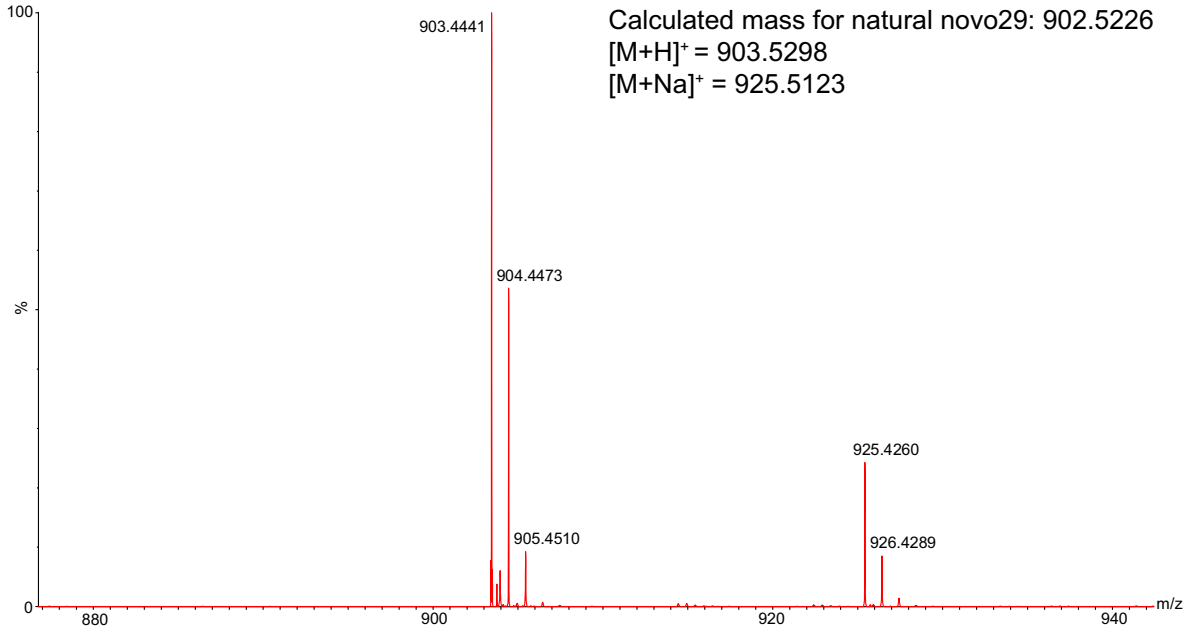
Calculated mass for natural novo29: 902.5226
[M+H]+ = 903.5298
[M+Na]+ = 925.5123
903.4441
904.4473
925.4260
905.4510
926.4289
100
%
0
880
900
920
940
m/z

Characterization of synthetic Novo29

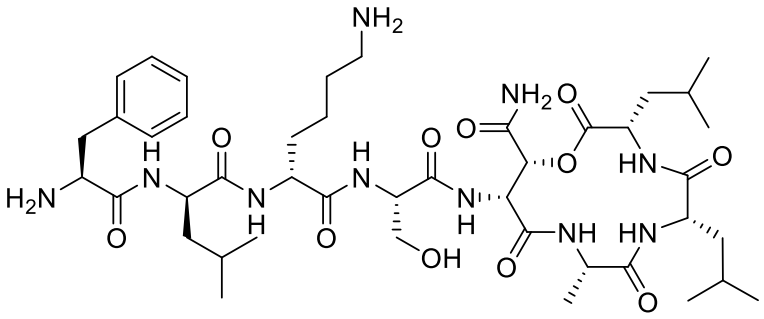

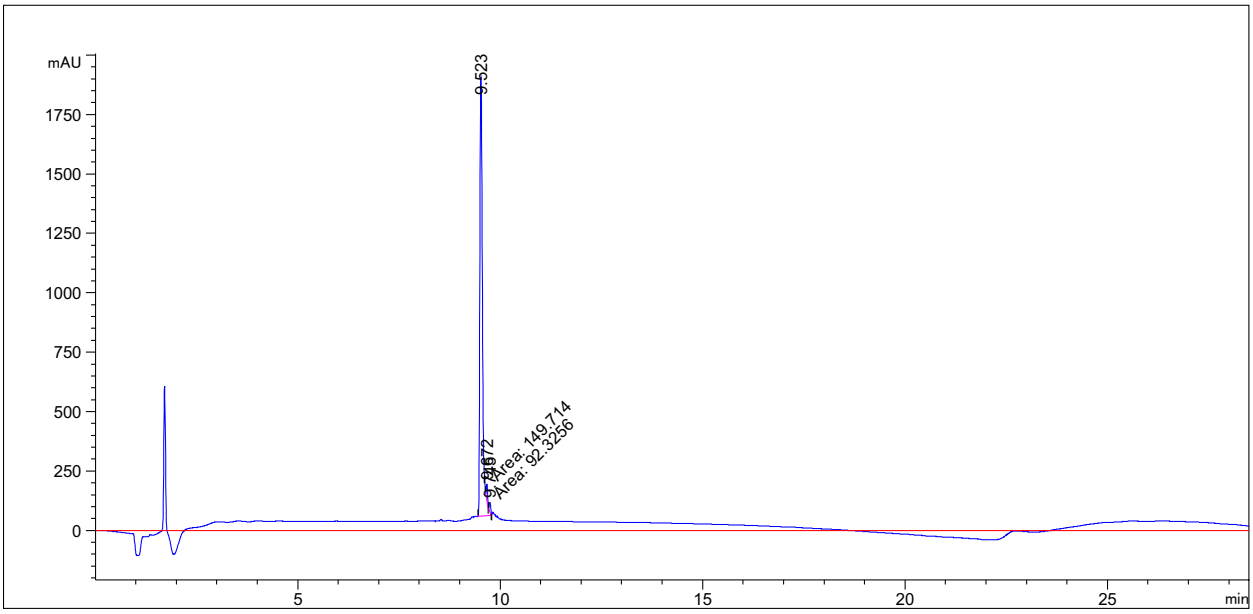

Signal 1: MWD1 A, Sig=214,4 Ref=off

Peak #	RetTime [min]	Type	Width [min]	Area [mAU*s]	Height [mAU]	Area %
1	9.523	MM R	0.0728	8129.04150	1861.80823	97.1086
2	9.672	MM T	0.0363	149.71405	68.68908	1.7885
3	9.745	MM T	0.0403	92.32558	38.15857	1.1029

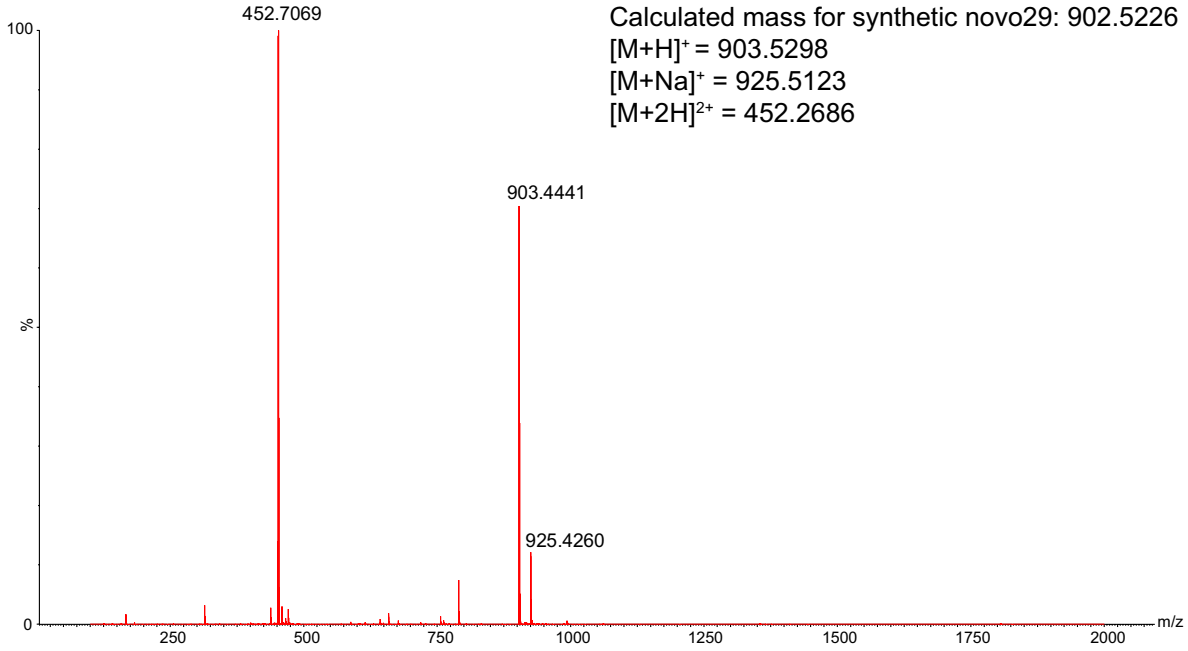

Calculated mass for synthetic novo29: 902.5226
$[M+H]^+$ = 903.5298
$[M+Na]^+$ = 925.5123
$[M+2H]^{2+}$ = 452.2686

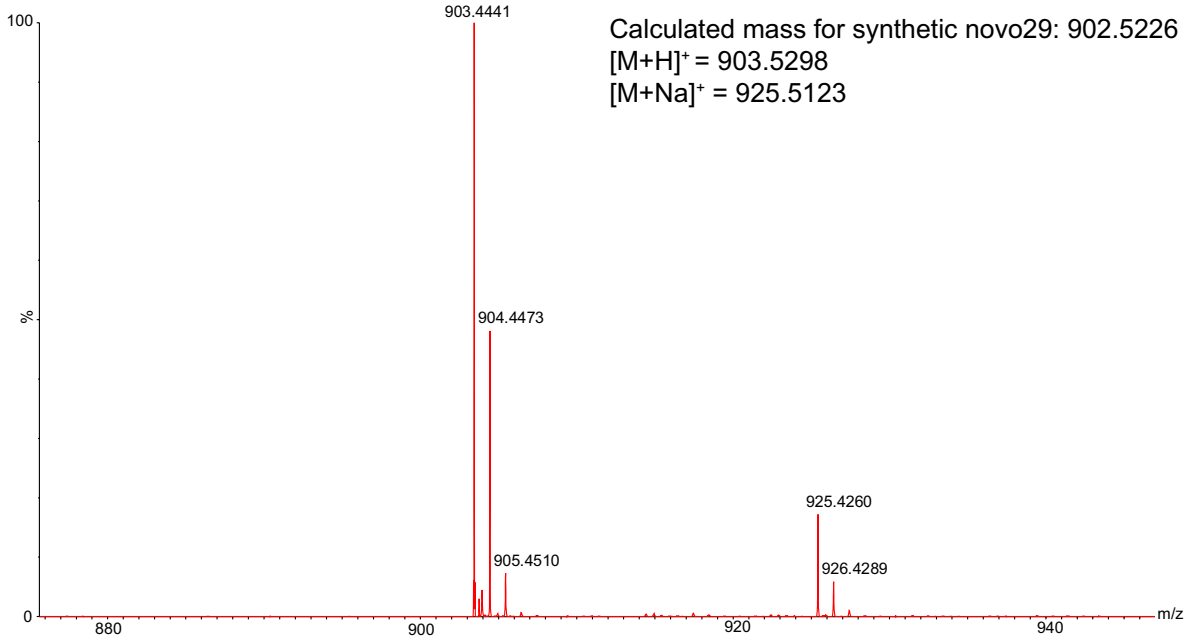

Calculated mass for synthetic novo29: 902.5226
$[M+H]^+$ = 903.5298
$[M+Na]^+$ = 925.5123

Characterization of synthetic epi-Novo29

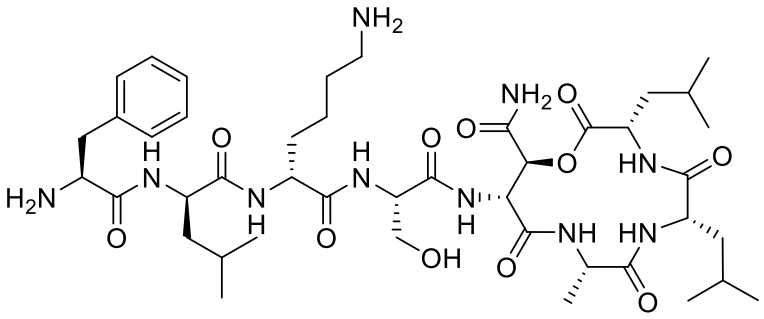

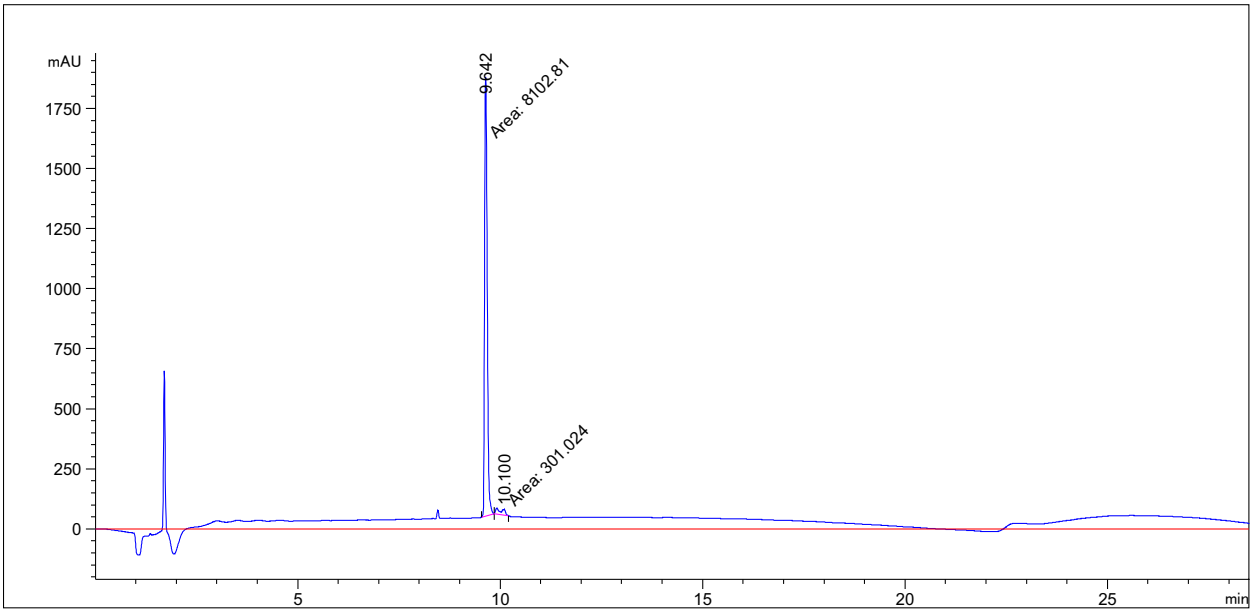

Signal 1: MWD1 A, Sig=214,4 Ref=off

Peak #	RetTime [min]	Type	Width [min]	Area [mAU*s]	Height [mAU]	Area %
1	9.642	MM	0.0735	8102.80859	1836.76953	96.4180
2	10.100	MM	0.2067	301.02429	24.26878	3.5820

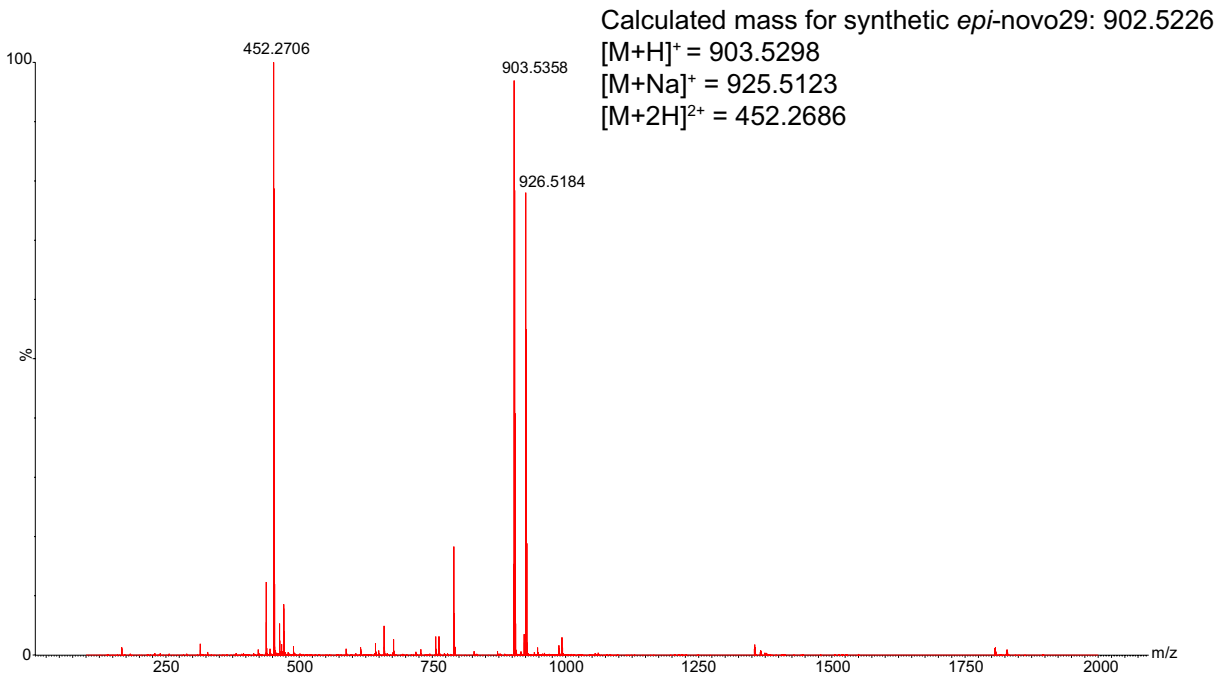
Calculated mass for synthetic *epi*-novo29: 902.5226
[M+H]+ = 903.5298
[M+Na]+ = 925.5123
[M+2H]2+ = 452.2686
452.2706
903.5358
926.5184
100
%
0
250
500
750
1000
1250
1500
1750
2000
m/z

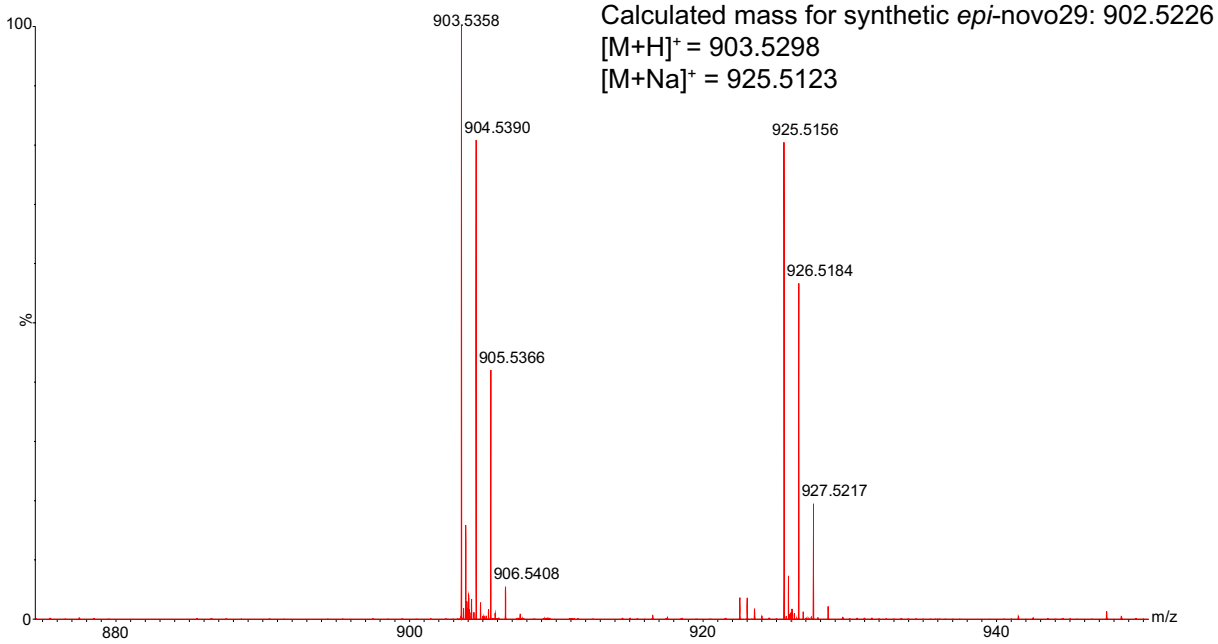
Calculated mass for synthetic *epi*-novo29: 902.5226
[M+H]+ = 903.5298
[M+Na]+ = 925.5123
903.5358
904.5390
925.5156
926.5184
905.5366
927.5217
906.5408
100
%
0
880
900
920
940
m/z

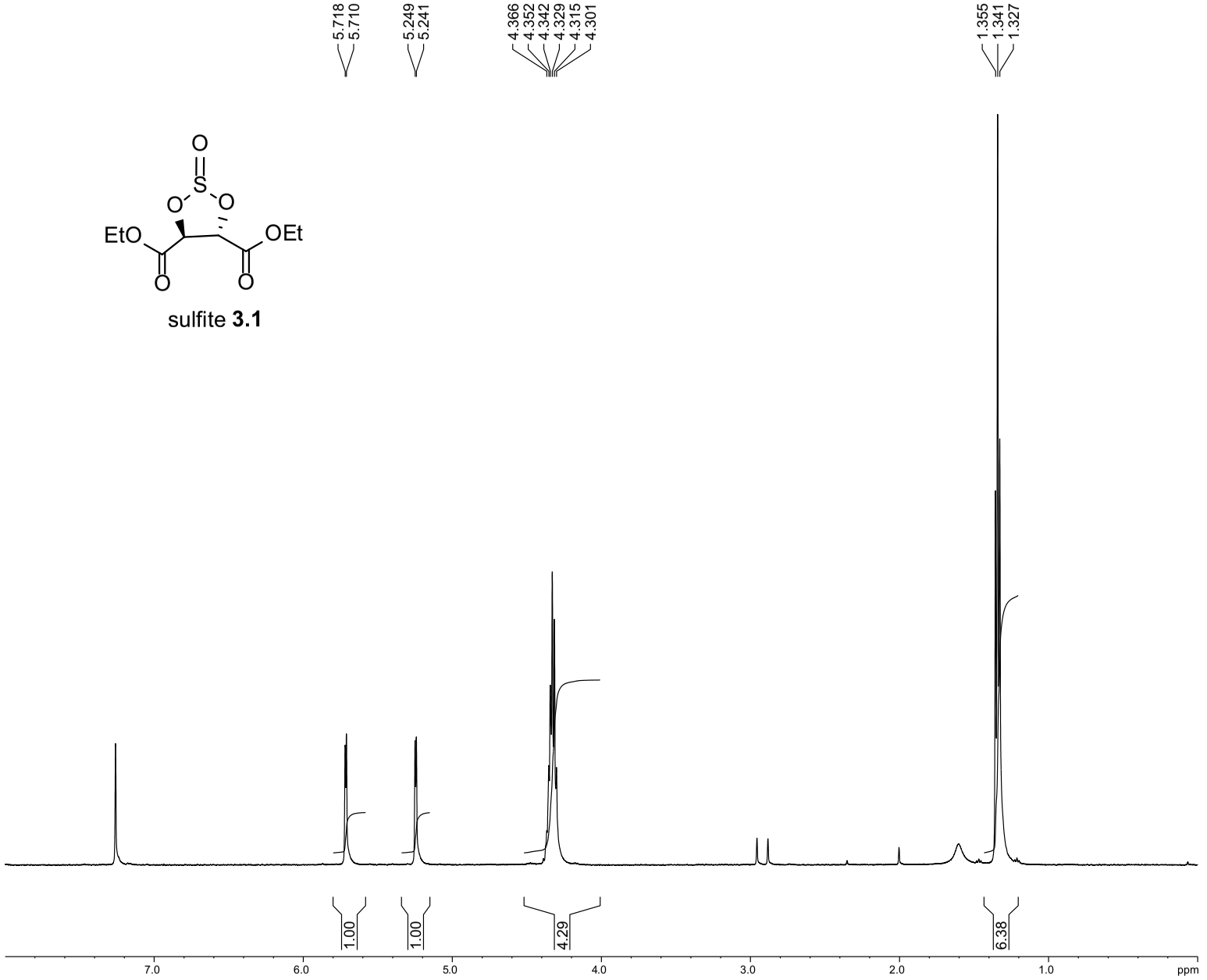
5.718
5.710
5.249
5.241
4.366
4.352
4.342
4.329
4.315
4.301
1.355
1.341
1.327
O
S
O
O
EtO
OEt
O
O
1.00
1.00
4.29
6.38
7.0
6.0
5.0
4.0
3.0
2.0
1.0
ppm

sulfite **3.1**

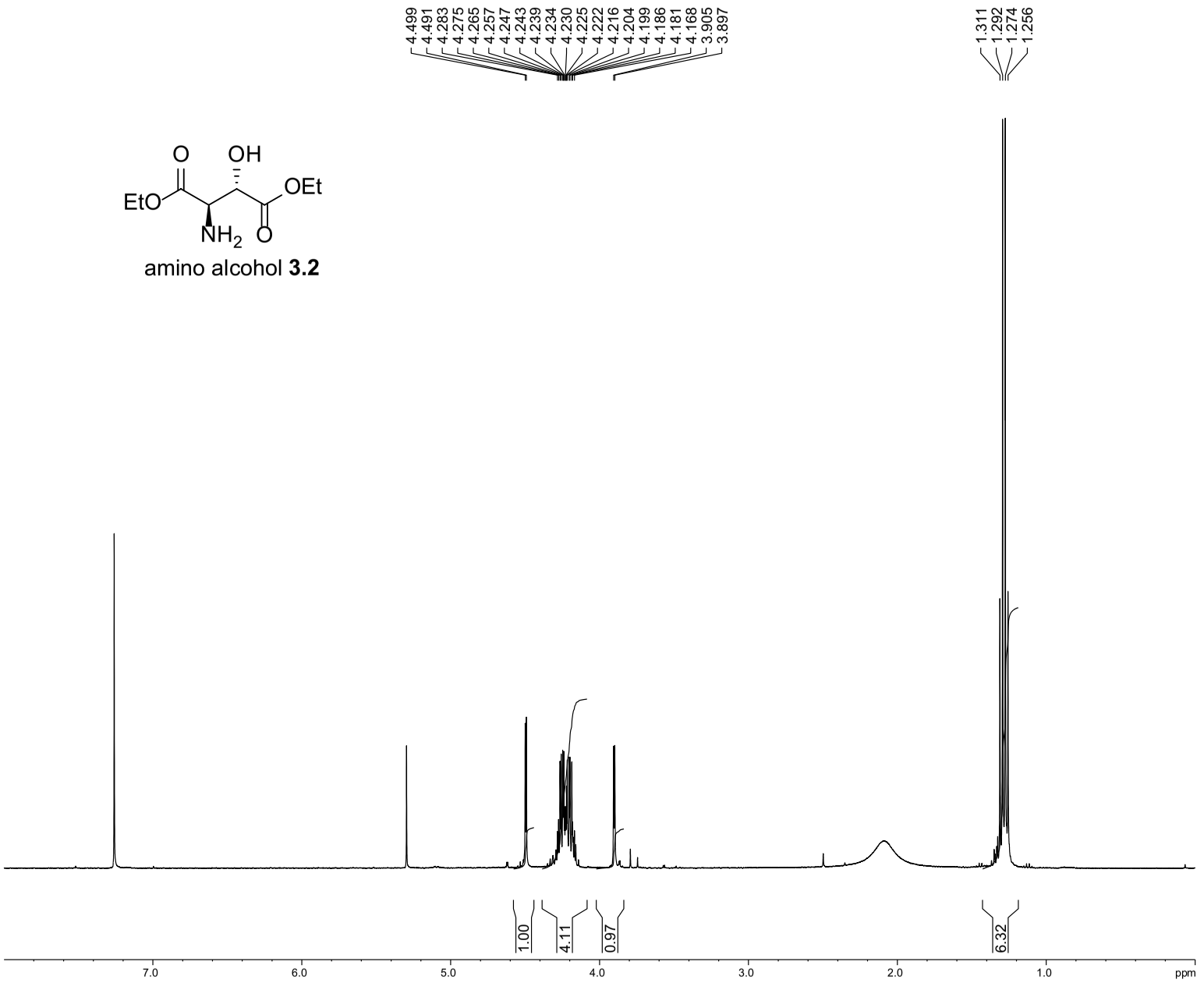

amino alcohol **3.2**

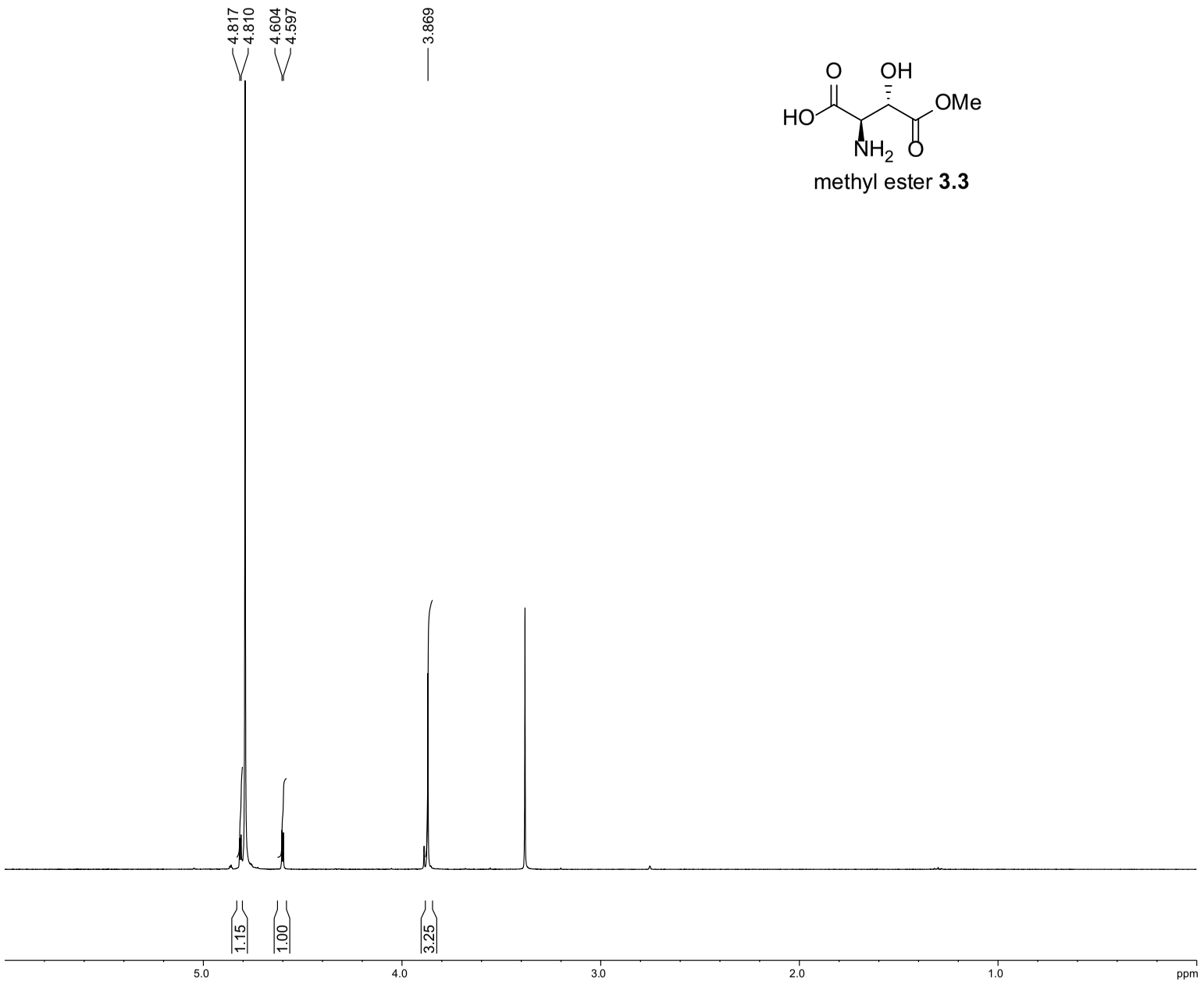
4.817
4.810
4.604
4.597
3.869
1.15
1.00
3.25
5.0
4.0
3.0
2.0
1.0
ppm
O
OH
HO
OMe
NH2
O
methyl ester 3.3

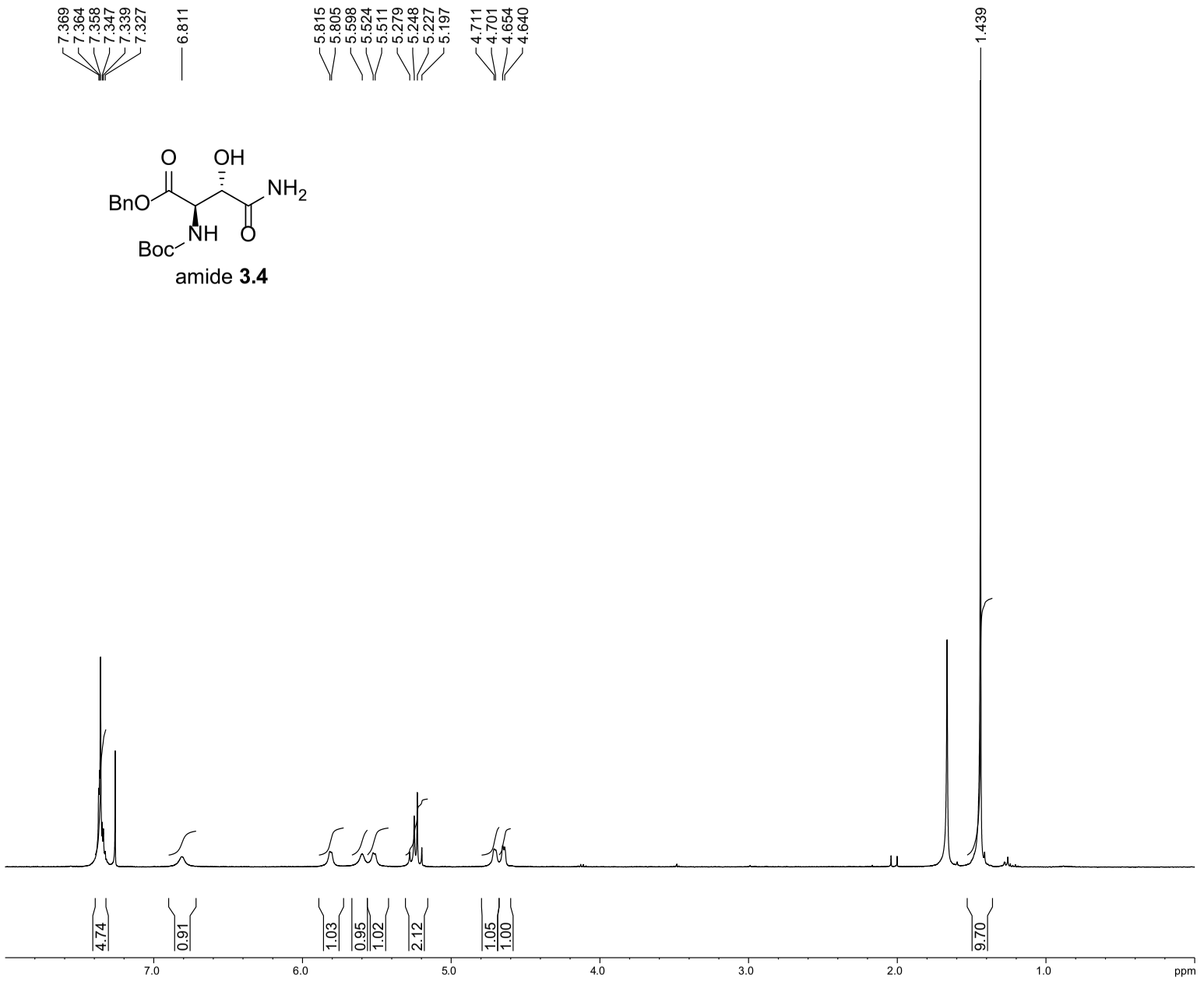
7.369
7.364
7.358
7.347
7.339
7.327
6.811
5.815
5.805
5.598
5.524
5.511
5.279
5.248
5.227
5.197
4.711
4.701
4.654
4.640
1.439
O
OH
BnO
NH2
NH
O
Boc
4.74
0.91
1.03
0.95
1.02
2.12
1.05
1.00
9.70
7.0
6.0
5.0
4.0
3.0
2.0
1.0
ppm

amide **3.4**

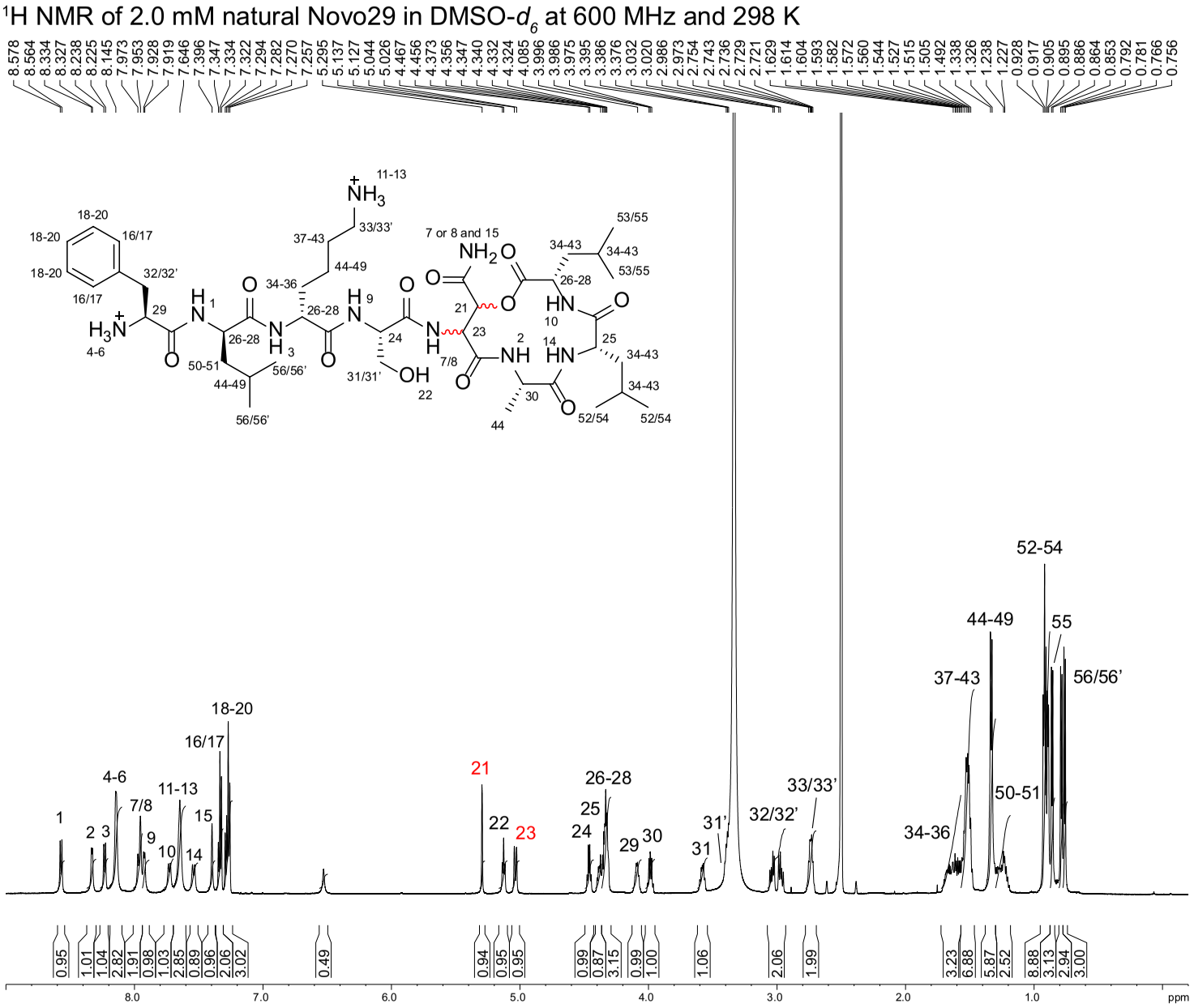
[1]H NMR of 2.0 mM natural Novo29 in DMSO-d6 at 600 MHz and 298 K
8.578 8.564 8.334 8.327 8.238 8.225 8.145 7.973 7.953 7.928 7.919 7.646 7.396 7.347 7.334 7.322 7.294 7.282 7.270 7.257 5.295 5.137 5.127 5.044 5.026 4.467 4.456 4.373 4.356 4.347 4.340 4.332 4.324 4.085 3.996 3.986 3.975 3.395 3.386 3.376 3.032 3.020 2.986 2.973 2.754 2.743 2.736 2.729 2.721 1.629 1.614 1.604 1.593 1.582 1.572 1.560 1.544 1.527 1.515 1.505 1.492 1.338 1.326 1.238 1.227 0.928 0.917 0.905 0.895 0.886 0.864 0.853 0.792 0.781 0.766 0.756
11-13
18-20
16/17
32/32'
29
4-6
1
26-28
50-51
56/56'
44-49
37-43
33/33'
34-36
31/31'
22
24
7/8
21
23
7 or 8 and 15
53/55
34-43
26-28
10
14
25
30
44
52/54
18-20
16/17
4-6
7/8
11-13
15
9
10
14
2 3
21
22
23
24
25
26-28
29
30
31
31'
32/32'
33/33'
34-36
37-43
44-49
50-51
52-54
55
56/56'
0.95 1.01 1.04 2.82 1.91 0.98 1.03 2.85 0.89 0.96 2.06 3.02 0.49 0.94 0.95 0.95 0.99 0.87 3.15 0.99 1.00 1.06 2.06 1.99 3.23 6.88 5.87 2.52 8.88 3.13 2.94 3.00
8.0 7.0 6.0 5.0 4.0 3.0 2.0 1.0 ppm

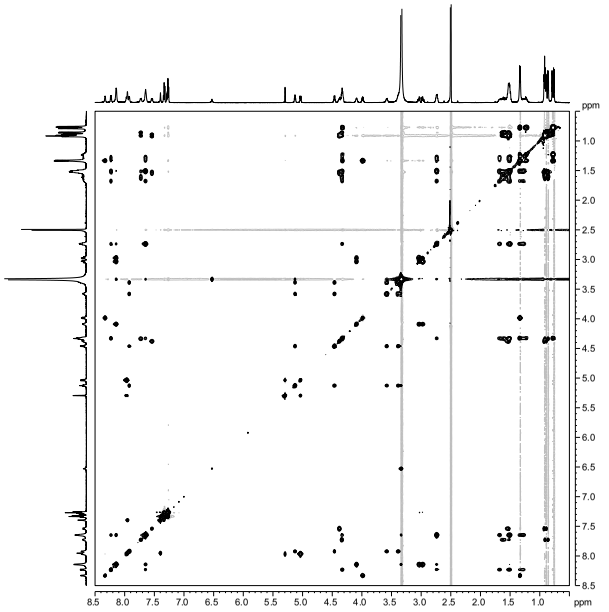

2.0 mM natural Novo29
in DMSO-d_6, 150-ms mixing time, 298 K
600 MHz TOCSY spectrum

Novo29

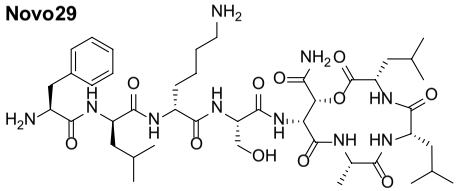

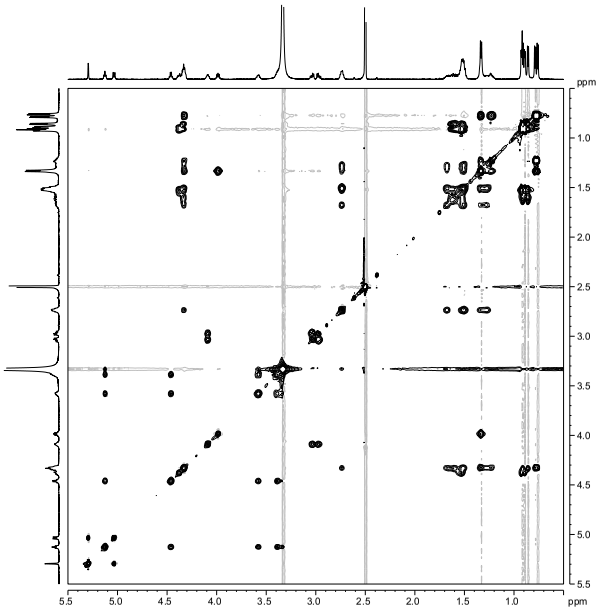

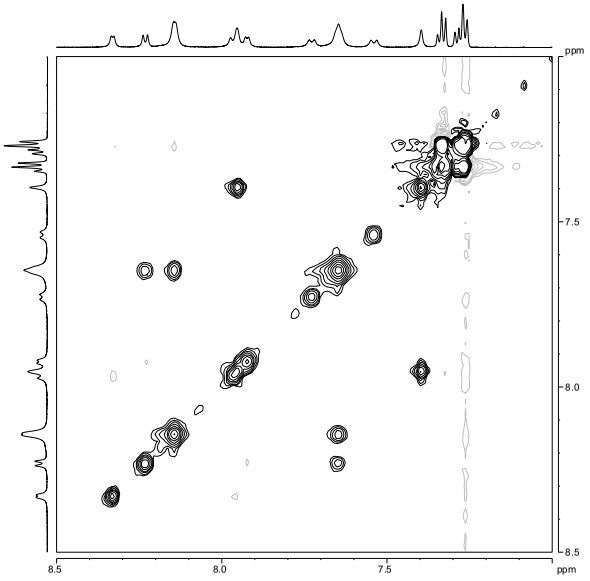

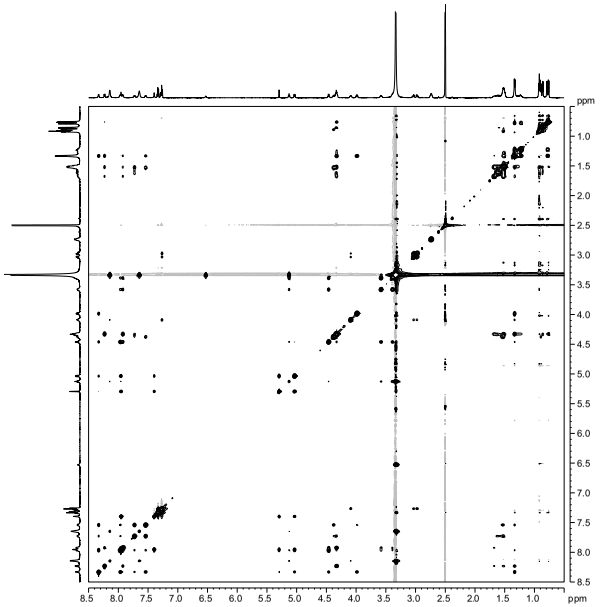

2.0 mM natural Novo29
in DMSO-d_6, 200-ms mixing time, 298 K
600 MHz NOESY spectrum

Novo29